

I. STRATIGRAPHIC CONSTRAINTS
ON THE NUMBER OF DISCRETE NEOPROTEROZOIC GLACIATIONS
AND THE RELATIONSHIP BETWEEN GLACIATION
AND EDIACARAN EVOLUTION

II. THE KWICHUP SPRING THRUST
IN THE NORTHWESTERN SPRING MOUNTAINS, NEVADA:
IMPLICATIONS FOR LARGE-MAGNITUDE EXTENSION
AND THE STRUCTURE OF THE CORDILLERAN THRUST BELT

Thesis by

Mark Joseph Abolins

In Partial Fulfillment of the Requirements

for the Degree of

Doctor of Philosophy

California Institute of Technology

Pasadena, California

1999

(Submitted July 28, 1998)

c 1999

Mark Joseph Abolins

All rights Reserved

ACKNOWLEDGMENTS

I would like to thank a number of people on both a personal and professional level. First and foremost, I would like to thank my parents Peter and Edith Abolins. The amount of effort that goes into parenting (particularly with a male child) is so colossal that I'm amazed anyone has children. I also thank my parents for instilling a love of nature. This passion for the wild is directly responsible for my pursuit of a career in natural science.

I also thank my "second set of parents" Albert and Susan Haldemann for unreserved support during my six years of graduate education. Our friendship survived the intense bouts of self-doubt and disillusionment that I experienced during the middle of my career as a graduate student. There are few things more valuable than a friendship that has been tested and found to be strong.

In large part, I survived graduate school because of the support of other members of the 1992 entering class. I've seen many graduate students come and go over the years, and the batch that came to the Division in 1992 is a particularly memorable bunch. I also thank the staff including (but not limited to) Jim O'Donnell, Donna Sackett, Cherylinn Rangel, and Tony Soeller. Without their aid (or should I say "complicity?") in various acts I could have never completed this thesis.

A number of other graduate students also deserve special mention for various kindnesses. These kindnesses may seem minor in isolation, but they added up. Martha Bowen provided sanity-boosting Jimmy Buffett tapes. Jeanne Hardebeck made a cake with an edible Triceratops for my 25th birthday. Emily Brodsky fed me many fine home-cooked meals. Mark Wanek was both a friend and an excellent field assistant, and John Holt spent many fine evenings with Mark and I under desert skies. I acknowledge my officemate Greg Holk as an all-around good guy.

I thank Arthur Dorough and Charlie Overfield for allowing me to map on their property. I thank Terry Pavlis, Laura Serpa, and the rest of the University of New Orleans crew for their hospitality and the use of their field station in Shoshone, CA.

On a professional level, interactions with a number of scientists were essential to my work on Neoproterozoic earth history. At Caltech, Dave Evans and Joe Kirschvink were an essential source of information. Outside Caltech, interactions with Nicholas Christie-Blick (Lamont), Martin Kennedy (UCLA), Whitey Hagadorn (USC), and Bruce Runnegar (UCLA) were essential. Their visits to my field area were invaluable. Ron Blom and Bob Crippen at NASA-JPL provided satellite and airborne imagery which was a real boon to this thesis.

The first part of my thesis contains data from a number of sources. Becky Charlton and Brian Wernicke provided measured stratigraphic sections from the Panamint and Resting Spring Ranges, respectively. In addition, Becky compiled stratigraphic information from the Death Valley region, prepared Appendix 2-A, and drafted early versions of some of the figures. Rob Ripperdan provided carbon isotope data.

During my first three years at Caltech, I was partially supported by an NSF Graduate Student Fellowship. I received this fellowship during my first year at Caltech when I was about to leave graduate school. I remained in graduate school at that time largely because I was too embarrassed to decline such a prestigious award.

Finally, I thank my thesis advisor Brian Wernicke for putting up with me (and continuing to pay me) for the last few years. We were a mismatched pair, so the fact that we survived working together (and even accomplished something) speaks well of both of us. I have much respect for Brian.

ABSTRACT

Stratigraphic and structural observations in the Death Valley region provide new insights into two topical problems. First, stratigraphic observations provide a better understanding of the number of discrete Neoproterozoic glaciations and the relationship between glaciation and the diversification of the first animals. Detailed stratigraphic investigations reveal incised valleys within the Neoproterozoic Johnnie Formation. The size (>150 m) and regional extent of the valleys, and the carbon isotope signature of underlying carbonates show that the valleys are probably glacioeustatic in origin. The incised valleys help to complete the Neoproterozoic glacial record in the western United States. The incised valleys and a pair of glacial diamictites in the underlying Kingston Peak Formation represent two to three discrete Neoproterozoic glaciations. This record of two to three glaciations matches the global Neoproterozoic glacial record. The incised valleys provide the youngest evidence for large-scale Neoproterozoic glaciation in the western United States. Correlation of the Johnnie valleys with incised valleys in the uppermost Caddy Canyon Formation of Idaho and Utah shows that this glaciation occurred before 580 Ma. These findings suggest that diverse Ediacaran faunas post-date the youngest major Neoproterozoic glaciation by tens of millions of years.

Second, structural and stratigraphic observations provide new constraints on the magnitude of extension in the Death Valley extended domain. These observations reveal a thrust fault in the northwestern Spring Mountains, NV. Correlation of this thrust fault with thrusts in other ranges constrains the translation of those ranges relative to the Spring Mountains. While these correlations are not unique, the most plausible correlations require large-magnitude extension in the Death Valley area and north of Las Vegas Valley.

Correlation of contractile structures in the northwestern Spring Mountains and Specter Range with Permo-Triassic structures in the Cottonwood Mountains may provide a link between the Permo-Triassic thrust belt in the Cottonwood Mountains and the Central

Nevada thrust belt. The Central Nevada thrust belt may be at least in part Permo-Triassic in age, and may represent a foreland fold and thrust belt which developed inboard of the Golconda allochthon during its emplacement.

TABLE OF CONTENTS

ACKNOWLEDGMENTS	iii
ABSTRACT	iv
TABLE OF CONTENTS	vi
CHAPTER 1: INTRODUCTION	1-1
REFERENCES	1-18
CHAPTER 2: PRE-580 MA INCISED VALLEYS IN THE CORDILLERAN MIOGEOCLINE: IMPLICATIONS FOR NEOPROTEROZOIC GLACIATION AND EDIACARAN EVOLUTION	
ABSTRACT	2-1
INTRODUCTION	2-2
GEOLOGIC SETTING	2-11
OBSERVATIONS	2-14
INTERPRETATION	2-23
DISCUSSION	2-27
FUTURE WORK	2-48
CONCLUSION	2-51
ACKNOWLEDGMENTS	2-51
APPENDIX 2-A	2-52
APPENDIX 2-B	2-69
APPENDIX 2-C	2-71
REFERENCES	2-74
CHAPTER 3: STRUCTURAL GEOLOGY OF THE NORTHWESTERN SPRING MOUNTAINS, NV	
INTRODUCTION	3-1
LITHOSTRATIGRAPHY	3-2
EXTENSIONAL STRUCTURES	3-9
CONTRACTILE STRUCTURES	3-47
AGE OF EXTENSIONAL STRUCTURES	3-81
AGE OF CONTRACTILE STRUCTURES	3-83
SUMMARY	3-85
APPENDIX 3-A	3-87
REFERENCES	3-88
CHAPTER 4: THE KWICHUP SPRING THRUST IN THE NORTHWESTERN SPRING MOUNTAINS, NEVADA: IMPLICATIONS FOR LARGE MAGNITUDE EXTENSION AND THE STRUCTURE OF THE CORDILLERAN THRUST BELT	
ABSTRACT	4-1
INTRODUCTION	4-2
OBSERVATIONS	4-21
DISCUSSION	4-74
FUTURE WORK	4-124
CONCLUSION	4-125
REFERENCES	4-126

CHAPTER 1

INTRODUCTION

This thesis uses new structural and stratigraphic observations in southern Nevada and southeastern California to better understand three topical problems: 1) the number of discrete Neoproterozoic glaciations and their relationship to the evolution of Ediacaran animals, 2) the amount of extension in the Death Valley extended domain, and 3) the development of the Cordilleran thrust belt in Nevada and southeastern California. The first of these three problems is of first-order significance to understanding the development of life on earth, and the other two problems are of first-order significance to understanding the development of the North American Cordillera.

NEOPROTEROZOIC GLACIATION

The second chapter is a topical examination of the relationship between Neoproterozoic glaciation and the evolution of the earliest animals. The Neoproterozoic was a time of enormous change in both the geosphere and biosphere. Climatically, the earth experienced glaciations of nearly global extent (Kirschvink, 1992; Schmidt and Williams, 1995; Park, 1997; Sohl, 1997). Tectonically, the supercontinent Rodinia fragmented (Hoffman, 1991). After the fragmentation of Rodinia, tectonic plates may have moved apart at anomalously high rates (Gurnis and Torsvik, 1994), or the entire planet may have experienced an episode of large-scale true polar wander (Kirschvink and others, 1997). Biologically, the appearance of the first animals (the Ediacarans) was followed by an enormous diversification of animals at the dawn of the Cambrian.

The stratigraphic record is one of the greatest resources for understanding Neoproterozoic earth history, and glaciation is one of the most prominent events within this record. Since Neoproterozoic glaciations were nearly global in extent, glacial diamictites associated with these glaciations are widespread. In areas where ice was not present,

glacioeustatic sea level change resulted in prominent incised valleys. In any Neoproterozoic section, some glaciations may be represented by diamictites while others are represented by incised valleys, so both must be examined to obtain a complete glacial history.

The Cordilleran miogeocline in the western United States provides an excellent opportunity to study the history of Neoproterozoic glaciation. The miogeocline contains a nearly complete Neoproterozoic record. In addition, sediments were deposited in a passive margin setting so the stratigraphy reflects eustatic rather than tectonic controls. As shown in Figure 1-1, two glaciations are recorded by a pair of glacial diamictites within the Perry Canyon Formation of Idaho and Utah and the Kingston Peak Formation of southeastern California, and Levy and others (1993) suggest that incised valleys in the uppermost Caddy Canyon Formation of Idaho and Utah may have formed during a third glaciation. The second chapter in this thesis examines incised valleys in the Neoproterozoic Johnnie Formation of southeastern California and southern Nevada, discusses their origin, and describes implications for Neoproterozoic glaciation and Ediacaran evolution.

LARGE-MAGNITUDE EXTENSION

The third and fourth chapters use new structural and stratigraphic observations in the northwestern Spring Mountains of southern Nevada to better understand the amount of Neogene extension in adjacent areas. During the last two decades, geologic studies in the Death Valley extended domain (Figure 1-2) have played a prominent role in our understanding of extensional tectonics. Reconstructions are based in large part on the correlation of pre-extension structural and stratigraphic markers (e.g., Wernicke and others, 1988; Snow, 1992; Snow and Wernicke, in press). The correlation of thrusts and other contractile structures between ranges has been particularly important in reconstructing the amount of extension in the Death Valley domain.

Figure 1-1. Diagram depicting evidence for late Neoproterozoic glaciation in the western U.S. Glacial diamictites in the Perry Canyon Formation from Link (1983). Glacial diamictites in the Kingston Peak Formation from Miller (1982) and Miller (1985). Incised valleys in the uppermost Caddy Canyon Formation from Levy and others (1994). Idaho and Utah formation names: GC, Geertsen Canyon Quartzite; BH, Browns Hole Fm.; M, Mutual Fm.; CC, Caddy Canyon Quartzite; KC, Kelley Canyon Fm.; MC, Maple Canyon Fm.; PC, Perry Canyon Fm. Nevada and California formation names: WC, Wood Canyon Fm.; SQ, Stirling Quartzite; JO, Johnnie Fm.; ND, Noonday Dolomite; KP, Kingston Peak Fm.; BS, Beck Spring Dolomite; CS, Crystal Spring Fm.

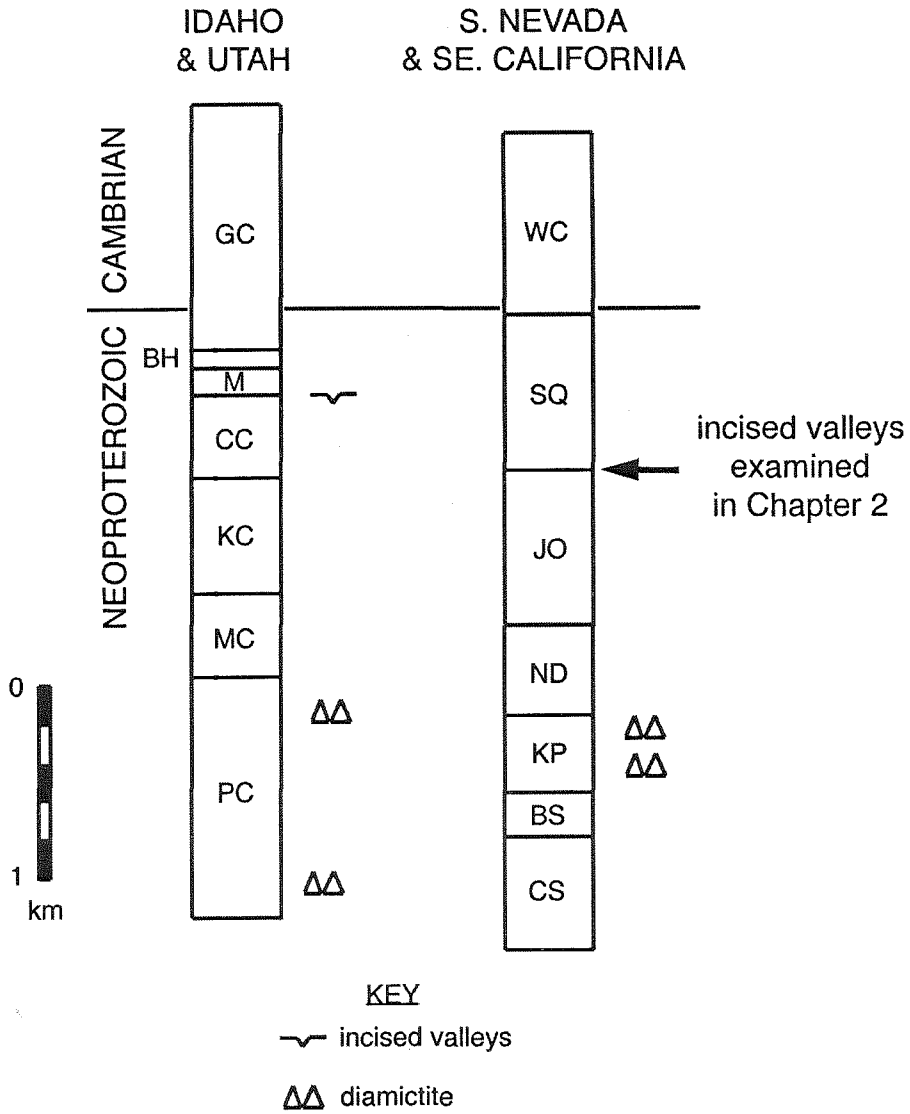
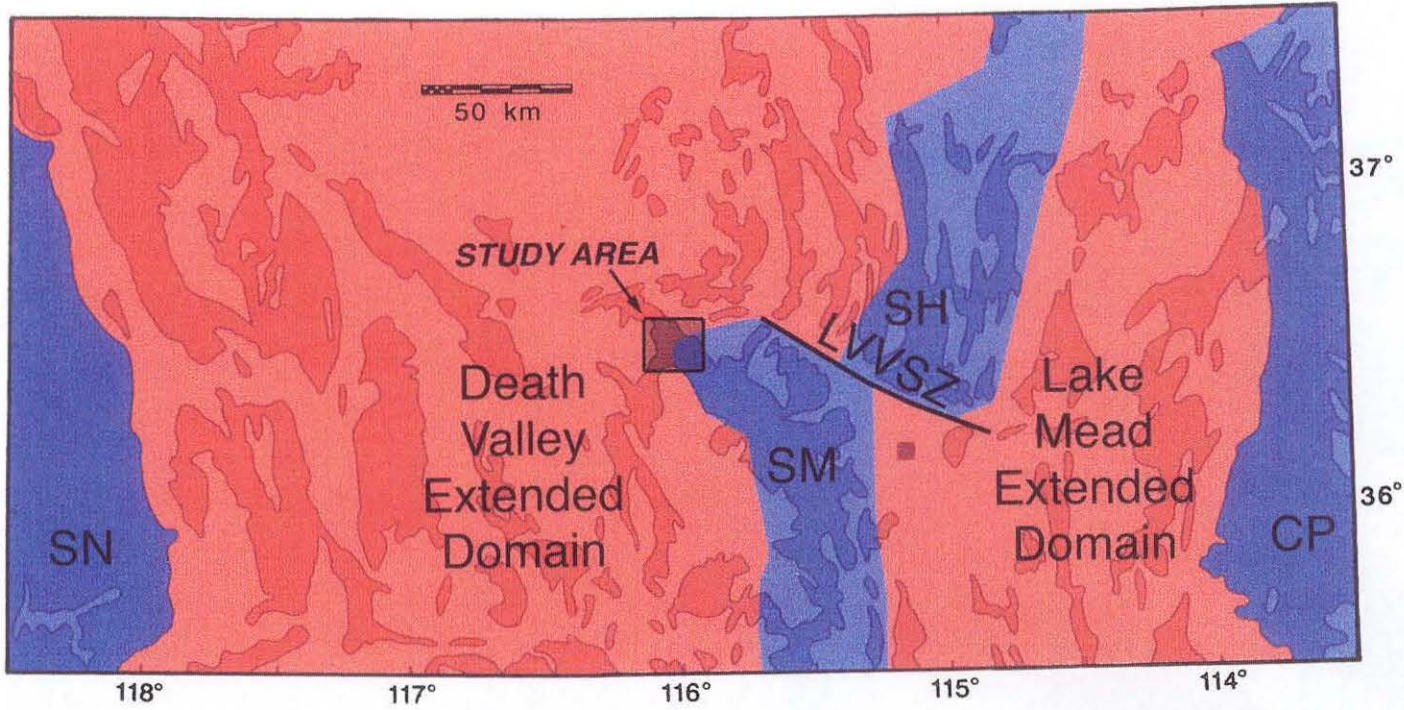


Figure 1-2. Map showing the location of the study area and the location of the Death Valley and Lake Mead extended domains in southern Nevada and southeastern California. The relatively unextended blocks which border the extended domains are the Sierra Nevada Mountains (SN), Spring Mountains (SM), Sheep Range (SH), and Colorado Plateau (CP). The Las Vegas Valley shear zone (LVVSZ) separates the Spring Mountains and Sheep Range.



-  extended domain
-  stable block

In southern Nevada and southeastern California, the thrust belt consists of about three dozen distinct contractile structures. Both normal and strike-slip faults disrupt the thrust belt. In addition, parts of the thrust belt are buried beneath alluviated basins or covered by volcanic rocks. As a result, contractile structures are not easily correlated between ranges.

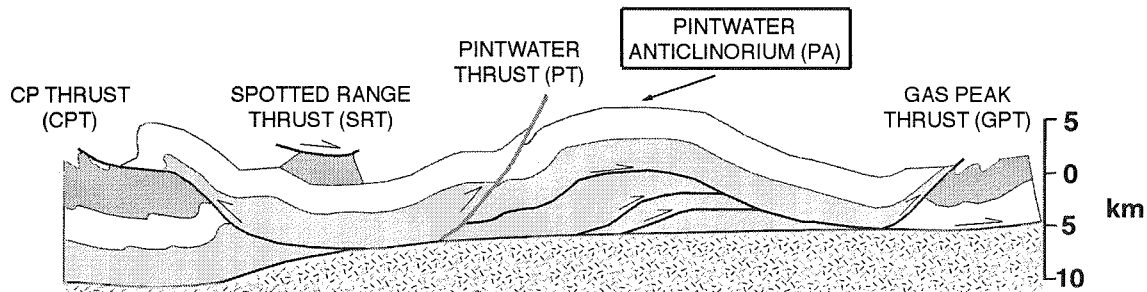
Wernicke and others (1988) and Snow (1992) suggested that the Cordilleran thrust belt in southern Nevada and southeastern California was narrow and laterally continuous before Neogene tectonism. They advanced a reconstruction in which the thrust belt originally consisted of five major contractile structures which were each continuous for over 200 kilometers along strike at the end of thrusting. A schematic cross section through their "narrow thrust belt" is shown in Figure 1-3. During the Neogene, large-magnitude extension fragmented this narrow thrust belt, and the distance between the Sierra Nevada Mountains and Colorado Plateau widened by 250-300 km.

The thrust correlations and magnitude of extension in their reconstruction have been hotly debated (e.g., Stevens and others, 1991; Serpa and Pavlis, 1996). Caskey and Schweickert (1992) presented the most comprehensive alternative. The Caskey and Schweickert interpretation of contractile structures north of Las Vegas Valley differs from that of Snow (1992). As a result, the thrust belt reconstructed by Caskey and Schweickert ("broad thrust belt" in Figure 1-3) is about twice as wide as that of Snow (1992). Consequently, Caskey and Schweickert advocate far less Neogene extension north of Las Vegas Valley.

The Snow (1992) and Caskey and Schweickert (1992) reconstructions are largely based on the geology of two different areas: the Cottonwood Mountains in southeastern California and the Test Site region in southern Nevada, respectively. As a result, it is possible that both are substantially correct and that the geometry of the Cordilleran thrust belt changes significantly between southern Nevada and southeastern California. A

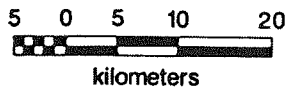
Figure 1-3. Two pre-extension reconstructions of the same part of the Cordilleran thrust belt. The “narrow thrust belt” reconstruction is largely based on work by Snow (1992) in the Cottonwood Mountains, CA and Burchfiel and others (1974) in the Spring Mountains, NV. The “broad thrust belt” reconstruction is based on work by Caskey and Schweickert (1992) north of Las Vegas Valley. Structures with names enclosed by boxes have been correlated with structures in the northwestern Spring Mountains, NV.

"BROAD THRUST BELT" Caskey and Schweickert, 1992

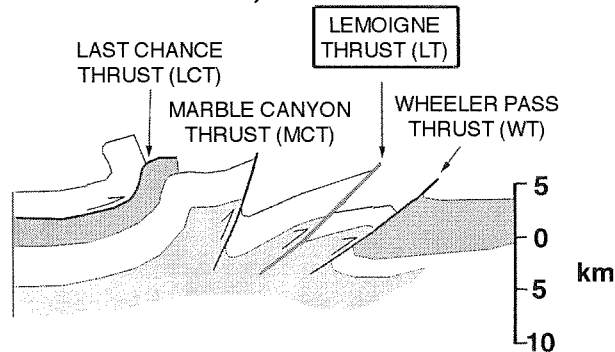


KEY

-  Paleozoic minus Cambrian
-  Cambrian
-  Precambrian



"NARROW THRUST BELT" Snow, 1992



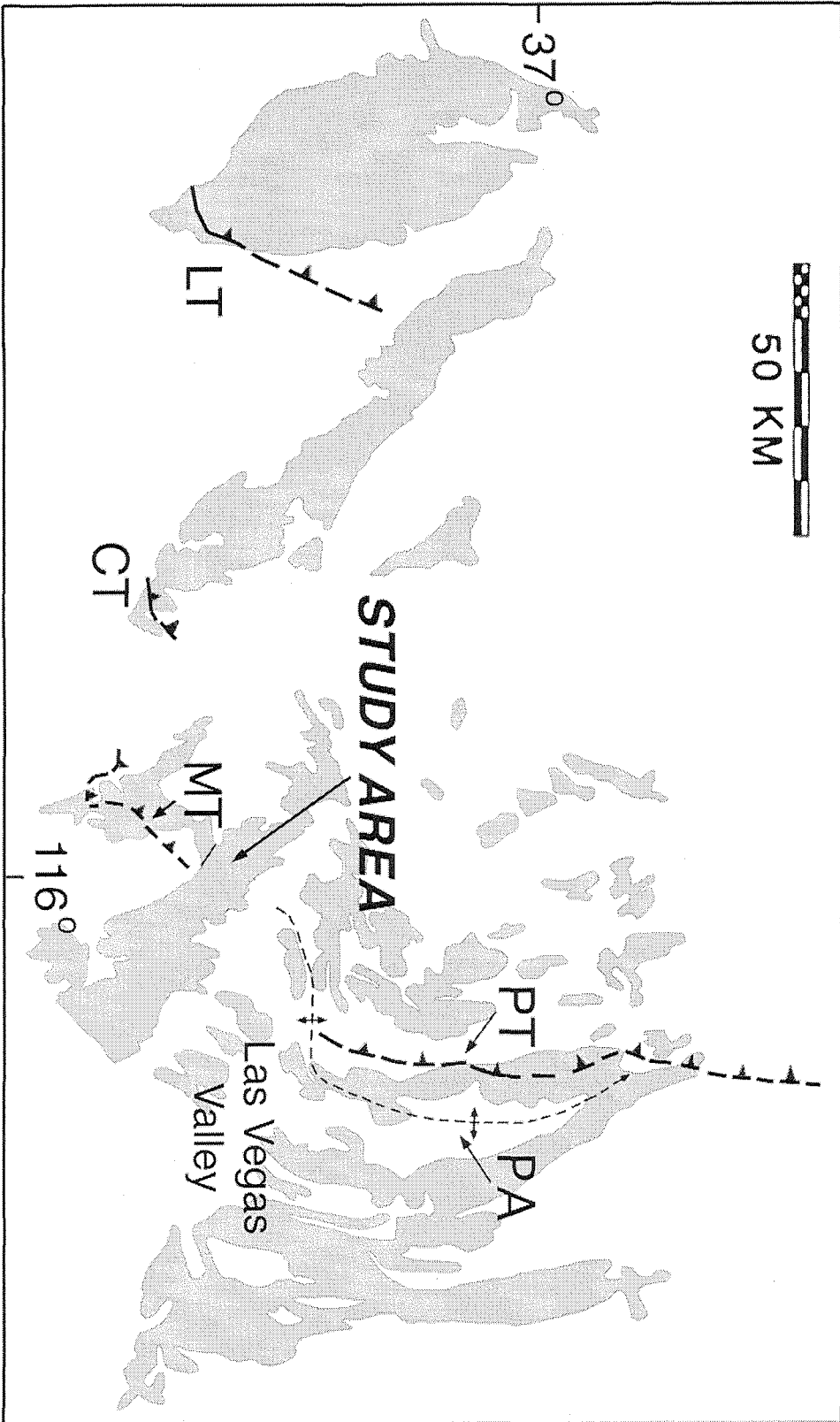
discontinuity separating the two segments of the thrust belt could occur in the California-Nevada border region and might be present in the northwestern Spring Mountains.

It is also possible that one or both reconstructions are seriously flawed. In that case, the Cordilleran thrust belt could be largely continuous throughout southern Nevada and southeastern California. This continuous thrust belt could either resemble one of the two reconstructions or a third distinctly different reconstruction.

The northwestern Spring Mountains in southern Nevada are one of the most problematic areas in both thrust belt reconstructions. Previous mapping (Burchfiel, 1965; Burchfiel and others, 1974; Burchfiel and others, 1983) showed that the northwestern Spring Mountains contains a complex suite of overturned folds and low-angle faults with normal-sense separation. As shown in Figure 1-4, these structures have been correlated with 1) the Lemoigne thrust in the Cottonwood Mountains, the Clery thrust in the Funeral Mountains, and the Pintwater thrust in the Pintwater Range (Snow, 1992; Snow and Wernicke, in press), 2) the Pintwater anticline north of Las Vegas Valley (Burchfiel and others, 1983; Caskey and Schweickert, 1992), and 3) the Montgomery thrust in the Montgomery Mountains (Burchfiel and others, 1983). The first of these correlations is an integral part of the "narrow thrust belt" reconstruction of Snow (1992), while the second correlation is part of the "broad thrust belt" reconstruction of Caskey and Schweickert (1992). The third correlation could require a thrust belt reconstruction which differs from both of these reconstructions.

The third and fourth chapters of this thesis describe new structural and stratigraphic investigations in the northwestern Spring Mountains of southern Nevada. Chapter 3 is primarily descriptive while Chapter 4 is topical and contains the principle conclusions of this study. Geologic investigations in the northwestern Spring Mountains lead to an improved understanding of the regional significance of contractile structures in the

Figure 1-4. Structures which may correlate with contractile structures in the study area in the northwestern Spring Mountains, NV. Correlative structures according to Snow (1992) and Snow and Wernicke (in press): Lemoigne thrust (LT) and Clery thrust (CT). Correlative structure according to Burchfiel and others (1983): Montgomery thrust (MT). Correlative structure according to Caskey and Schweickert (1992) and Burchfiel and others (1983): Pintwater anticline (PA).



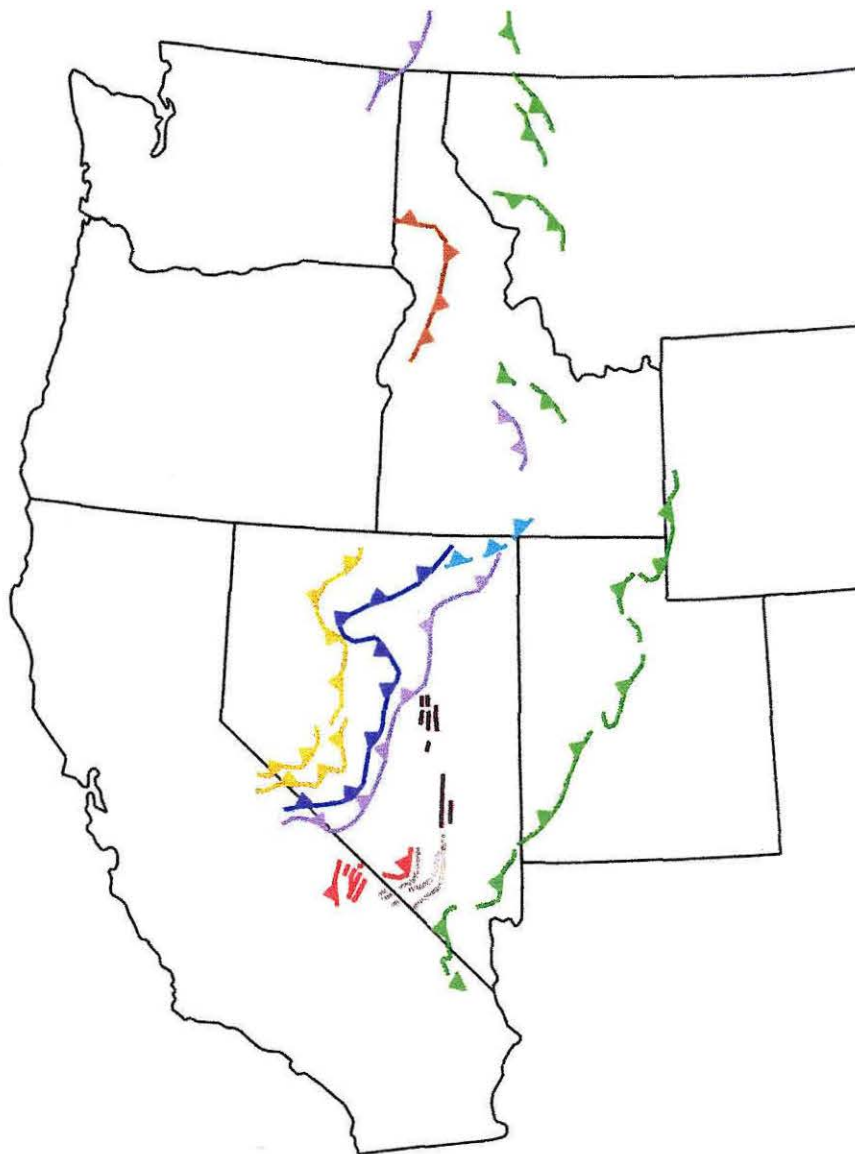
northwestern Spring Mountains. Implications for extension in both the Death Valley region and the ranges north of Las Vegas Valley are discussed in Chapter 4.

PERMO-TRIASSIC THRUSTING IN THE CORDILLERAN OROGEN

Understanding the relationship between Permo-Triassic contractile structures in the Cottonwood Mountains and contractile structures in the northwestern Spring Mountains and Specter Range is also critical to understanding the lateral extent of Permo-Triassic foreland thrusting. Along the length of the Cordillera, Permo-Triassic foreland thrusting is not widespread. Of all the collisional events experienced by the Cordillera, only Juro-Cretaceous convergence resulted in the development of an extensive foreland fold and thrust belt within the Cordilleran miogeocline. The late Jurassic and Cretaceous Sevier thrust belt (shown in green in Figure 1-5) stretches for thousands of kilometers from southeastern California to Canada. In Alberta along one of the best studied transects through the thrust belt (e.g., Price and Fermor, 1985), thrusting within the miogeocline is entirely late Jurassic and Cretaceous in age (Price, 1981). Older deformation is confined to the allochthonous terranes to the west (Smith and others, 1993). These allochthonous terranes include the Robert's Mountains allochthon (shown in purple on Figure 1-5) and the Golconda allochthon (shown in dark blue on Figure 1-5). Along the rest of the Cordillera in areas where age constraints exist, the timing and spatial distribution of deformation is similar.

In contrast, thrusts in the Cottonwood Mountains of southeastern California (shown in red in Figure 1-5) record Permo-Triassic deformation within the Cordilleran miogeocline. Permo-Triassic deformation is probably also present in other ranges in the Death Valley area (Snow, 1992) and in southern Nevada (Snow, 1992; Caskey and Schweickert, 1992). In addition, miogeoclinal strata were intruded and metamorphosed in the San Bernardino Mountains of southeastern California (Miller and Cameron, 1982). However, north of this

Figure 1-5. The Cordilleran thrust belt after Burchfiel and others (1992). The Central Nevada thrust belt is from Taylor and others (1993). Thrusts in the Cottonwood Mountains and adjacent ranges are from Snow (1992).



Age	Description
lt. J - K	eastern limit of Sevier thrust belt
J - ea. K	West Idaho suture zone
J	Elko thrust belt
J	Luning-Fencemaker thrust belt
?	Central Nevada thrust belt
?	structures of uncertain affinity
P - TR	Permo-Triassic foreland thrust belt
P - TR	Golconda thrust and equivalents
M	Roberts Mts thrust and equivalents

region, Permo-Triassic deformation is confined to the Golconda allochthon, and the miogeocline is not generally thought to have been deformed during Permo-Triassic time.

Is the Permo-Triassic thrust belt in southeastern California and southern Nevada a local phenomena or is it a small fragment of a thrust belt which, like the Sevier thrust belt, was once continuous along much of the Cordilleran margin? Saleeby and others (1992) suggest that Permo-Triassic miogeoclinal deformation in southeastern California and southern Nevada is a consequence of late Paleozoic or earliest Mesozoic truncation of the continental margin. This truncation resulted in the juxtaposition of younger compressive continental margin deformation across the miogeocline. In this context, the absence of Permo-Triassic deformation in the miogeocline of central Nevada is not surprising since central Nevada is far from the truncated margin. The Permo-Triassic thrust belt could end to the north before reaching central Nevada while the Central Nevada thrust belt could end to the south before reaching the Death Valley region.

Does the Permo-Triassic thrust belt in the Cottonwood Mountains terminate to the north or does it continue into central Nevada? The Central Nevada thrust belt of Taylor and others (1993) contains numerous poorly-dated contractile structures (shown in black on Figure 1-5), and some of these structures could be Permo-Triassic. However, Taylor and others (1993) suggest that the Central Nevada thrust belt is Jurassic to early Cretaceous in age based on its position south of the Jurassic Elko thrust belt (shown in light blue on Figure 1-5) and east of the Jurassic Luning-Fencemaker thrust belt (shown in gold on Figure 1-5). The Central Nevada thrust belt could also represent the easternmost part of the Sevier thrust belt as suggested by Stuart and Taylor (1997). Extension within the Death Valley extended domain obscures the relationship between the Permo-Triassic thrust belt in the Cottonwood Mountains and the Central Nevada thrust belt. Contractile structures in the northwestern Spring Mountains and Specter Range are part of a family of structures (shown in gray on Figure 1-5) which occupy an intermediate position between the Permo-

Triassic thrust belt in the Cottonwood Mountains and the Central Nevada thrust belt. The correlation of contractile structures in the northwestern Spring Mountains and Specter Range with contractile structures in the Cottonwood Mountains could link the two thrust belts. The possibility of such a connection and its implications for the development of the Cordilleran thrust belt are discussed at the end of Chapter 4.

REFERENCES

- Caskey, S. John, and Schweickert, Richard A., 1992, Mesozoic deformation in the Nevada Test Site and vicinity; implications for the structural framework of the Cordilleran fold and thrust belt and Tertiary extension north of Las Vegas Valley: *Tectonics*, v. 11, no 6, p. 1314-1331.
- Gurnis, Michael, and Torsvik, Trond H., 1994, Rapid drift of large continents during the late Precambrian and Paleozoic; paleomagnetic constraints and dynamic models: *Geology*, v. 22, no. 11, p. 1023-1026.
- Hoffman, Paul F., 1991, Did the breakout of Laurentia turn Gondwanaland inside-out? *Science*, v. 252, no. 5011, p. 1409-1412.
- Kirschvink, Joseph L., 1992, Late Proterozoic low-latitude global glaciation; the snowball Earth, *in* Schopf, J. William, and Klein, Cornelis, eds., *The Proterozoic biosphere; a multidisciplinary study*, p. 51-52.
- Kirschvink, Joseph L., Ripperdan, Robert L., and Evans, David A., 1997, Evidence for a large-scale reorganization of Early Cambrian continental masses by inertial interchange true polar wander: *Science*, v. 277, no. 5325, p. 541-545.
- Levy, Marjorie, Christie-Blick, Nicholas, and Link, Paul Karl, 1994, Neoproterozoic incised valleys of the eastern Great Basin, Utah and Idaho; fluvial response to changes in depositional base level, *in* Dalrymple, Robert W., Boyd, Ron, and Zaitlin, Brian

A., eds., Incised-valley systems; origin and sedimentary sequences: SEPM (Society for Sedimentary Geology) Special Publication 51, p. 369-382.

Miller, E. L., and Cameron, C. S., 1982, Late Precambrian to Late Cretaceous evolution of the southwestern Mojave Desert, California, *in* Cooper, John D., Troxel, Bennie W., and Wright, Lauren A., eds., Geology of selected areas in the San Bernardino Mountains, western Mojave Desert, and southern Great Basin, California, p. 21-34.

Park, John K., 1997, Paleomagnetic evidence for low-latitude glaciation during deposition of the Neoproterozoic Rapitan Group, Mackenzie Mountains, N.W.T., Canada: Canadian Journal of Earth Sciences, v. 34, no. 1, p. 34-49.

Price, R. A., 1981, The Cordilleran foreland thrust and fold belt in the southern Canadian Rocky Mountains, *in* McClay, K. R., and Price, N. J., eds., Thrust and nappe tectonics: Geological Society of London Special Publication, v. 9, p. 427-448.

Price, R. A., and Fermor, P. R., 1985, Structure section of the Cordilleran Foreland thrust and fold belt west of Calgary, Alberta: Geological Survey of Canada Paper 84-14.

Saleeby, Jason B., Busby-Spera, Cathy, Oldow, J. S., Dunne, G. C., Wright, J. E., Cowan, D. S., Walker, N., 1992, Early Mesozoic tectonic evolution of the Western U.S. Cordillera, *in* Burchfiel, B. C., Lipman, P. W., and Zoback, M. L., ed., The Cordilleran Orogen; conterminous U.S., p. 107-168.

- Schmidt, Phillip W., and Williams, George E., 1995, The Neoproterozoic climatic paradox; equatorial palaeolatitude for Marinoan Glaciation near sea level in South Australia: *Earth and Planetary Science Letters*, v. 134, no. 1-2, p. 107-124.
- Serpa, Laura, and Pavlis, Terry L., Three-dimensional model of the Cenozoic history of the Death Valley region, southeastern California: *Tectonics*, v. 15, no. 6, p. 1113-1128.
- Smith, Moira T., Dickinson, William R., and Gehrels, George E., 1993, Contractional nature of Devonian-Mississippian Antler tectonism along the North American continental margin: *Geology*, v. 21, no. 1, p. 21-24.
- Snow, J. Kent, 1992, Large-magnitude Permian shortening and continental margin tectonics in the southern Cordillera: *Geological Society of America Bulletin*, v. 104, no. 1, p. 80-105.
- Snow, J. Kent, and Wernicke, Brian P., in press, Cenozoic tectonism in the central Basin and Range: magnitude, rate, and distribution of upper crustal strain: *American Journal of Science*.
- Sohl, Linda E., 1997, Paleomagnetic and stratigraphic implications for the duration of low-latitude glaciation in the late Neoproterozoic of Australia: *Geological Society of America Abstracts*, v. 29, no. 6, p. 195.
- Stevens, Calvin H., Stone, Paul, and Belasky, Paul, Paleogeographic and structural significance of an Upper Mississippian facies boundary in southern Nevada and east-

central California; with Suppl. Data 91-14: Geological Society of America Bulletin, v. 103, no. 7, p. 876-885.

Stuart, Maureen A., and Taylor, Wanda J., 1997, Fragmentation of the Mesozoic Sevier orogenic belt, Utah by large-magnitude Cenozoic extension: Geological Society of America Abstracts, v. 29, no. 5, p. 67-68.

Taylor, Wanda J., Bartley, John M., Fryxell, Joan E., Schmitt, James G., and Vandervoort, Dirk S., 1993, Tectonic style and regional relations of the central Nevada thrust belt, *in* Lahren, Mary M., Trexler, James H., Jr., and Spinoso, Claude, ed., Crustal evolution of the Great Basin and the Sierra Nevada, p. 57-96.

Wernicke, Brian, Gary J. Axen, and J. Kent Snow, 1988, Basin and Range extensional tectonics at the latitude of Las Vegas, Nevada: Geological Society of America Bulletin, v. 100, no. 11, p. 1738-1757.

CHAPTER 2

PRE-580 MA INCISED VALLEYS IN THE CORDILLERAN MIOGEOCLINE: IMPLICATIONS FOR NEOPROTEROZOIC GLACIATION AND EDIACARAN EVOLUTION

Mark J. Abolins, Rebecca L. Charlton, and Brian P. Wernicke

Division of Geological and Planetary Sciences

California Institute of Technology, Pasadena, CA 91125

Robert L. Ripperdan

Department of Geology

University of Puerto Rico, Mayaguez, Puerto Rico 00681

ABSTRACT

Detailed stratigraphic investigations in southern Nevada and southeastern California reveal incised valleys within the Neoproterozoic Johnnie Formation. These valleys contain a distinctive conglomeratic lithofacies which is common in Neoproterozoic valley fill. The Johnnie valleys incise shallow marine sediments and were cut by subaerial erosion, indicating a fall in relative sea level. The size (>150 m) and regional extent of the Johnnie valleys imply a glacioeustatic origin. In addition, enriched carbon isotope values in underlying sediments are typical of carbon isotope values from carbonates which immediately underlie Neoproterozoic glacial deposits.

The Johnnie valleys provide the youngest evidence for large-scale Neoproterozoic glaciation in the western United States. Correlation of the Johnnie valleys with incised valleys in the uppermost Caddy Canyon Formation of Idaho and Utah suggests that this

glaciation occurred before 580 Ma. Our findings suggest that diverse Ediacaran faunas post-date the youngest major Neoproterozoic glaciation by tens of millions of years.

INTRODUCTION

Did Neoproterozoic ice ages effect the evolution of the earliest animals? The Neoproterozoic was a time of unusually severe ice ages which resulted in glaciations of nearly global extent (Harland, 1964; Kirschvink, 1992; Schmidt and Williams, 1995; Park, 1997; Sohl, 1997). Diverse Ediacaran faunas post-date the youngest glacial deposits, prompting speculation that Ediacarans diversified only after glaciation ceased and the earth's climate ameliorated (Glaessner, 1984; Sokolov and Fedonkin, 1986).

However, the age of the youngest Neoproterozoic glaciation and the timing of Ediacaran diversification are both poorly constrained. On one hand, U-Pb dating indicates that anywhere between 16 and 60 million years passed between the deposition of the youngest well-dated glacial diamictite (Thompson and others, 1996) and the appearance of a diverse Ediacaran fauna in Namibia (Grotzinger and others, 1995). On the other hand, one and possibly two glaciations occurred after the appearance of the first simple Ediacaran discs in northwestern Canada (Hofmann and others, 1990; Kaufman and others, 1997), but before the appearance of a diversified assemblage equivalent to that in Namibia.

These observations have resulted in two views of the relationship between glaciation and Ediacaran evolution. In one view, a diverse Ediacaran fauna appeared tens of millions of years after the youngest Neoproterozoic glaciation (Grotzinger and others, 1995). This view is largely based on U-Pb ages from Namibia and Newfoundland (Figure 2-1). Alternatively, two glaciations may have been intimately associated with Ediacaran diversification (Kaufman and others, 1997). The latter view is best supported by the Neoproterozoic section in the Mackenzie Mountains of northwestern Canada (Figure 2-2). Only simple Ediacaran discs are present below glacial diamictite of the Ice Brook Formation (Hofmann and others, 1990). The complex discs *Cyclomedusa* sp. and *Cyclomedusa*

Figure 2-1. Diagram showing U-Pb age constraints on the Ediacaran fauna and youngest radiometrically-dated glacial diamictite. Age constraints on Namibian Ediacaran fauna from (Grotzinger and others, 1995). Age of Ediacaran fronds in Newfoundland from Benus (1988). Age constraints on glacial diamictite in Newfoundland from Thompson and others (1996). An unpublished age from a volcanic ash in the White Sea region (not shown on figure) indicates that a diverse Ediacaran fauna similar to the one in Namibia may have lived as long ago as 555 Ma (Joseph Kirschvink, pers. comm.).

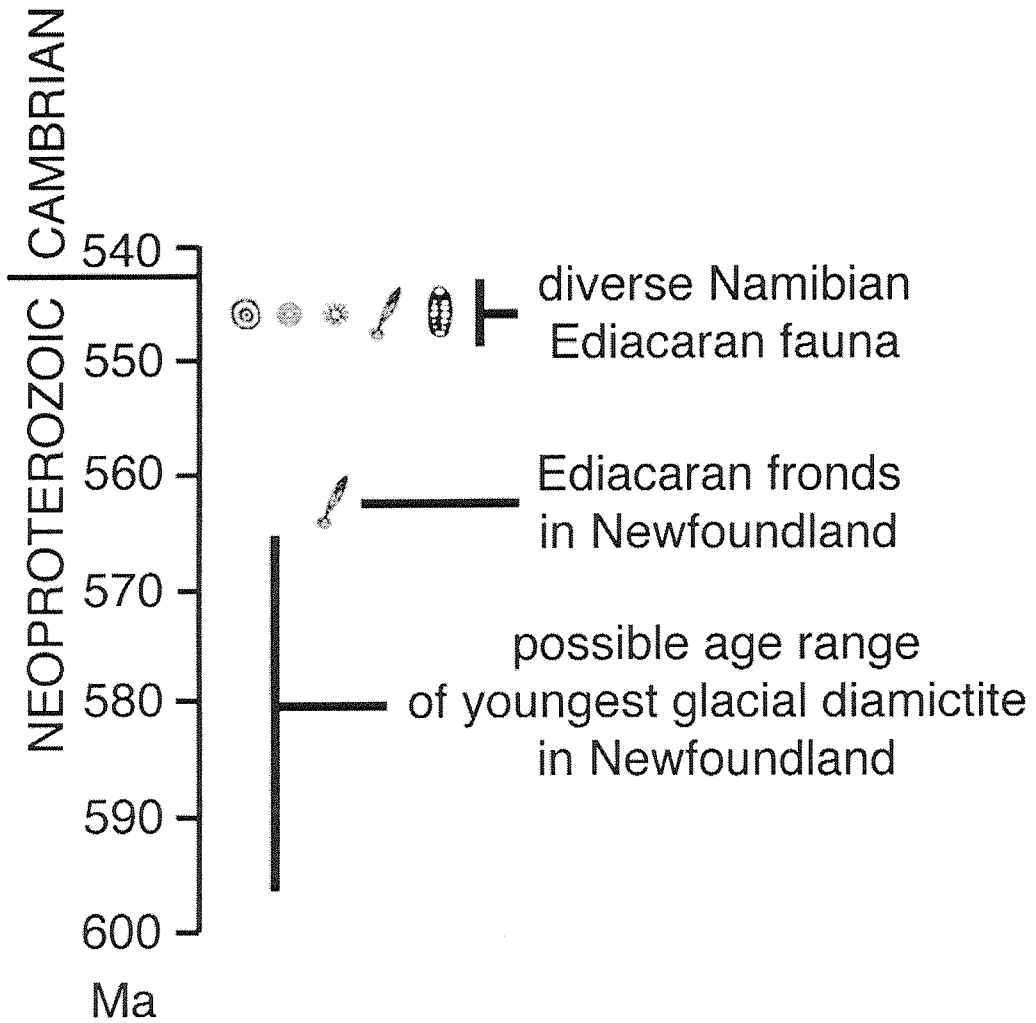
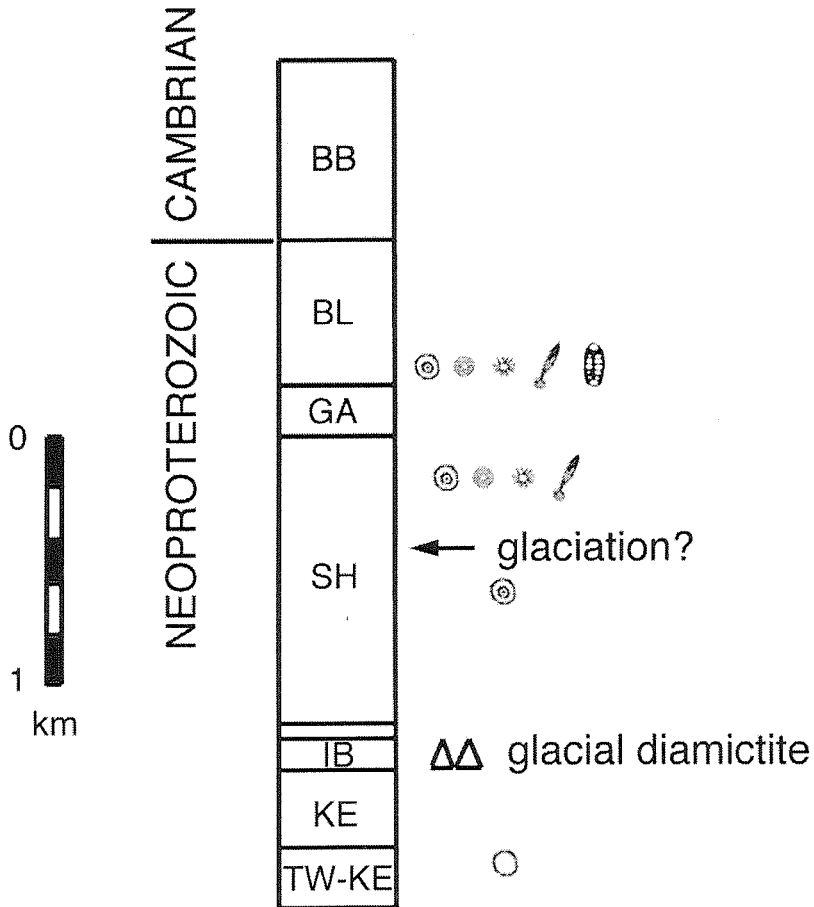


Figure 2-2. Diagram showing the stratigraphic relationship between Ediacaran fossils and glaciation in the Mackenzie Mountains of northwestern Canada. The stratigraphy is from Kaufman and others (1997). The youngest glaciation is inferred from carbon isotope data. The distribution of fossils is from Kaufman and others (1997) and Narbonne (1994). Formation names: BB, Backbone Range Fm.; BL, Blueflower Fm.; GA, Gametrail Fm.; SH, Sheepbed Fm.; IB, Ice Brook Fm.; Ke, Keele Fm.; TW-KE, Twitya-Keele Fm.

MACKENZIE MOUNTAINS



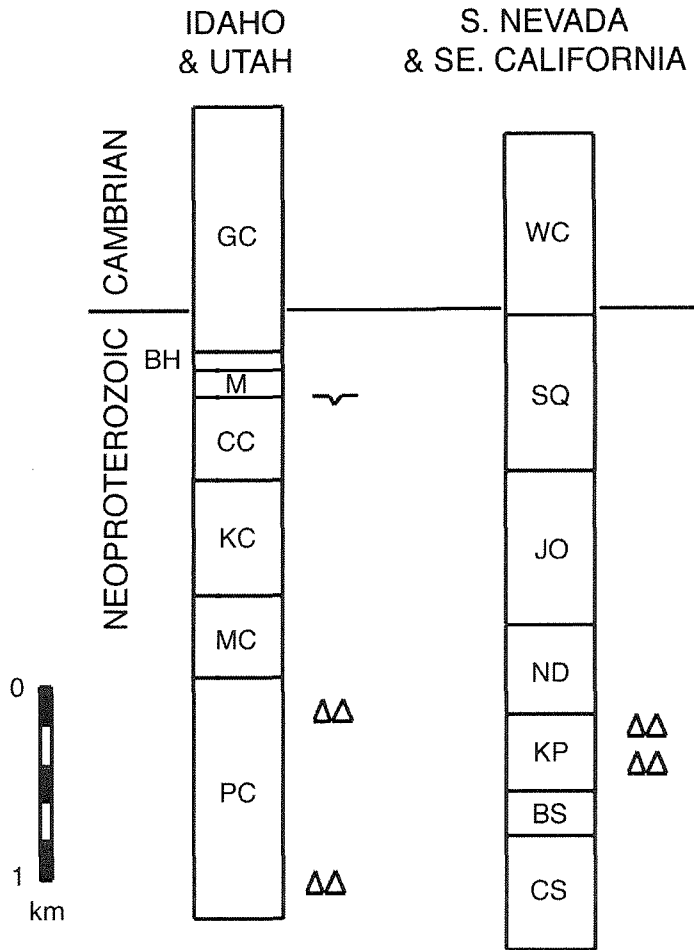
Fossils

-  segmented Ediacarans
-  Ediacaran fronds
-  tentaculate Ediacarans
-  annulate Ediacaran discs
-  complex Ediacaran discs
-  simple Ediacaran discs

plana appear above the diamictite (Narbonne, 1994). In strata that overlie the first complex discs, Kaufman and others (1997) infer another glaciation from carbon isotope data. After this inferred glaciation, additional complex discs, an annulate disc, a tentaculate disc, and a frond appear. Fronds and complex discs continue to diversify higher in the section, but segmented fossils are the only additional category of Ediacaran. Therefore, the diversification that immediately followed the inferred glaciation appears to be one of the most significant events in Ediacaran evolution. Views on glaciation and Ediacaran evolution differ in large part because of the uncertainty that surrounds the number, magnitude, and age of Neoproterozoic glaciations. No continuous Neoproterozoic section contains unequivocal evidence for more than two glaciations. As a result, Hambrey and Harland (1985) grouped Neoproterozoic glacial deposits into two glacial epochs: the Sturtian and the Varanger. Dateable material is scarce, but the Sturtian glacial epoch is generally thought to have happened at about 750 Ma, while the Varanger glacial epoch happened at about 590 Ma. In contrast, Kaufman and others (1997) suggest that the carbon isotope record indicates four discrete glacial epochs between 746 Ma and 549 Ma.

The Cordilleran miogeocline in the western United States is one of the best places to examine the history of Neoproterozoic glaciation. Sediments within the miogeocline provide a largely continuous record of the entire Neoproterozoic (Stewart, 1970). As shown in Figure 2-3, this record includes a pair of glacial diamictites within the Kingston Peak Formation of southeastern California (Miller, 1985) and within the Perry Canyon Formation of Idaho and Utah (Crittenden and others, 1971; Link, 1983). At least one additional glaciation may have occurred after deposition of the Perry Canyon Formation. Levy and others (1994) suggested that incised valleys in the uppermost Caddy Canyon Formation of Idaho and Utah were created by a large regional change in base level associated with glaciation. Together, these incised valleys and pair of diamictites show that the Cordilleran miogeocline may contain a record of at least three discrete glaciations.

Figure 2-3. Diagram depicting evidence for late Neoproterozoic glaciation in the western U.S. Glacial diamictites in the Perry Canyon Formation from Link (1983). Glacial diamictites in the Kingston Peak Formation from Miller (1982) and Miller (1985). Incised valleys in the uppermost Caddy Canyon Formation from Levy and others (1994). Idaho and Utah formation names: GC, Geertsen Canyon Quartzite; BH, Brown's Hole Fm.; M, Mutual Fm.; CC, Caddy Canyon Quartzite; KC, Kelley Canyon Fm.; MC, Maple Canyon Fm.; PC, Perry Canyon Fm. Nevada and California formation names: WC, Wood Canyon Fm.; SQ, Stirling Quartzite; JO, Johnnie Fm.; ND, Noonday Dolomite; KP, Kingston Peak Fm.; BS, Beck Spring Dolomite; CS, Crystal Spring Fm.



KEY

~ incised valleys

△△ diamictite

This paper focuses on the possible glacioeustatic origin of Neoproterozoic incised valleys in strata that overlie the Perry Canyon and Kingston Peak Formations. Valleys incised by glacioeustasy should meet three criteria. First, valleys formed by eustasy rather than tectonics should occur throughout a large region and lack any association with faulting. Second, valleys associated with a major glaciation should be of order 100 m in depth. Third, valleys formed through a change in sea level rather than a change in base level should incise shallow marine sediments and contain evidence for sub-aerial erosion.

Incised valleys that meet these criteria provide evidence for glaciation in stratigraphic sections geographically removed from direct glacial effects like the deposition of till and dropstones. As a result, the recognition of incised valleys associated with glacioeustasy is necessary for the correlation of glacial events between glaciated and ice-free regions. In addition, incised valleys associated with glacioeustasy provide an indirect measure of ice volume, and, therefore, of the magnitude of a glaciation, while till and dropstones only indicate the local presence of glaciers.

Incised valleys in the uppermost Caddy Canyon Formation are of sufficient depth (>150 m) to suggest glaciation, but do not unequivocally demonstrate a change in sea level. The Caddy Canyon valleys incise fluvial sediments which were deposited on a broad braid-plain (Levy and others, 1994). The published literature (e.g., Stewart, 1970) does not describe similar valleys in the broadly coeval shallow marine sediments of southern Nevada and southeastern California.

However, incised valleys have only recently gained widespread recognition as important stratigraphic phenomena (e.g., Posamentier and others, 1988; Christie-Blick and others, 1995), and could have been overlooked by earlier studies. Recent unpublished work by Catherine Summa (1993) in the Nopah Range indicates the need for a re-appraisal of shallow marine deposits in southern Nevada and southeastern California. In the Nopah Range, Summa observed a 75-150 m deep incised valley within the uppermost Johnnie

Formation. To better understand the regional extent and significance of these incised valleys, the authors investigated these units in the Panamint Range and Resting Spring Range in southeastern California and the northwestern Spring Mountains in southern Nevada.

GEOLOGIC SETTING

Miogeoclinal sediments in southern Nevada and southeastern California were deposited within a rift which formed when western North America separated from another continental landmass during the Proterozoic (Burchfiel and Davis, 1972; Stewart, 1972). Figure 2-4 summarizes the stratigraphy and paleontology of the miogeocline. The base of the miogeoclinal section rests on 1.75 Ga high-grade gneisses which are intruded by 1.4 Ga granitic plutons (Rb-Sr ages; Lanphere, 1964). The gneiss is nonconformably overlain by the Crystal Spring Formation which contains Baicalian stromatolites (Cloud and Semikhatov, 1969). These stromatolites are thought to have lived from 1.35 - .95 Ga, but their age range is poorly calibrated with radiometric dates and their morphology may reflect environment rather than taxonomy. The Crystal Spring Formation is intruded by 1.08 Ga diabase sills (U-Pb baddeleyite ages; Heaman and Grotzinger, 1992). Because the sills are abundant in the Crystal Spring Formation and underlying basement but do not intrude the uppermost Crystal Spring Formation and overlying strata, their age is generally taken as the time of deposition of the Crystal Spring Formation and the upper age limit for the superjacent Beck Spring Dolomite.

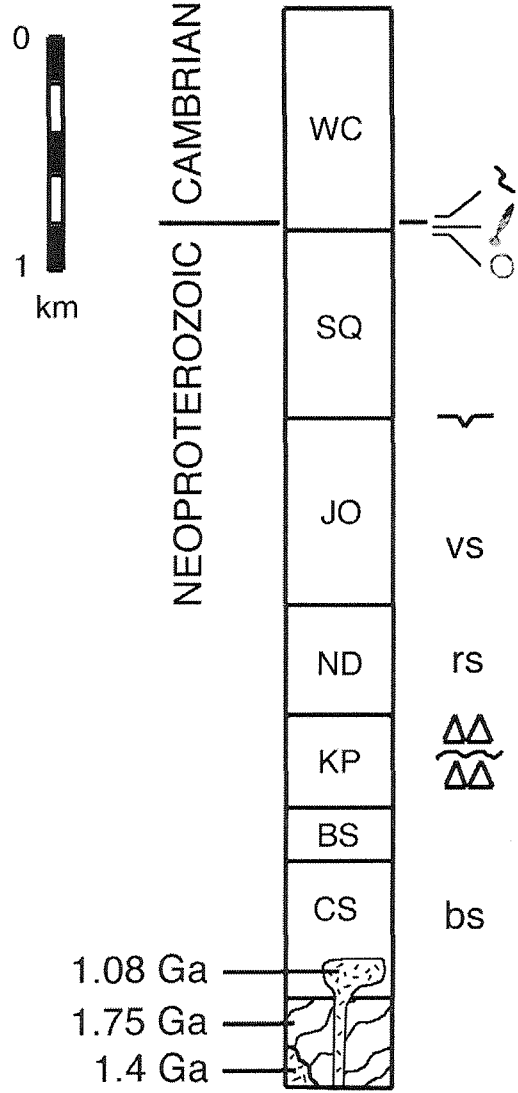
The Beck Spring Dolomite is overlain by the Kingston Peak Formation. The Kingston Peak Formation contains a record of both tectonism and glaciation. The lower part of the Kingston Peak Formation contains a glacial diamictite, and was involved in a tectonic event which involved both tight folding and normal faulting and may have occurred in a transcurrent setting (Walker and others, 1986). Rare dropstones and striated clasts within the Kingston Peak Formation support a glacial origin for the diamictite (Miller, 1982). As

Figure 2-4. Neoproterozoic physical stratigraphy and fossils from the Cordilleran miogeocline in southern Nevada and southeastern California. Physical stratigraphy: incised valley in uppermost Johnnie Formation from Summa (1983); glacial diamictites in Kingston Peak Fm. from Miller (1982) and Miller (1985); intra-Kingston Peak unconformity from Walker and others (1986). Ediacaran fossils from Waggoner and Hagadorn (1997). Vendian and Baicalian stromatolites from Cloud and Semikhatov (1969). Riphean stromatolites from Wright and others (1978). Formation names as in Figure 2-3.

S. NEVADA
& SE. CALIFORNIA

- KEY**
- Physical stratigraphy*
-  incised valleys
 -  diamictite
 -  angular unconformity

- Fossils*
-  *Phycodes pedum*
 -  Ediacaran fronds
 -  simple Ediacaran discs
 - vs Vendian stromatolites
 - rs Riphean stromatolites
 - bs Baicalian stromatolites



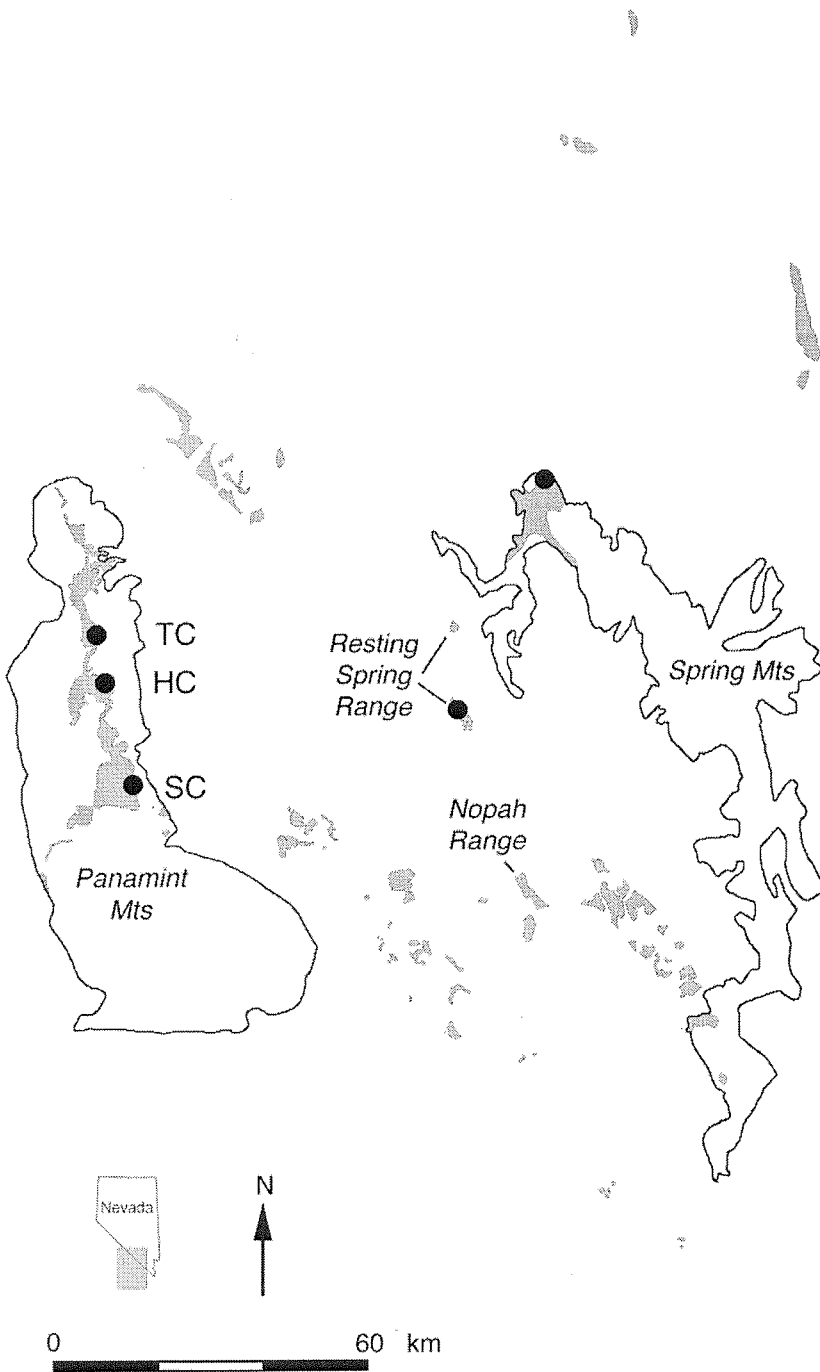
a result of tectonism, a major unconformity separates the lower and upper parts of the Kingston Peak Formation. A second glacial diamictite occurs above the unconformity within the upper part of the Kingston Peak Formation. The Kingston Peak Formation is unconformably overlain by the Noonday Dolomite which contains stromatolites that are thought to have lived before 700 Ma (Wright and others, 1978).

The Noonday Dolomite is overlain by the Johnnie Formation. The Johnnie Formation is exposed at scattered locations within a 25,000 km² area in southern Nevada and southeastern California. The formation consists predominantly of siltstone with lesser amounts of sandstone and carbonate. According to the detailed lithofacies analysis of Summa (1993), the Johnnie Formation is largely a shallow marine deposit with fluvial deposition at its base. The Johnnie Formation contains stromatolites which are thought to be younger than 700 Ma (Cloud and Semikhatov, 1969). The Stirling Quartzite overlies the Johnnie Formation. The uppermost Stirling Quartzite has yielded the simple disc *Nimbia* which is the oldest Ediacaran fossil found in the southwestern U.S. to date (Waggoner and Hagadorn, 1997). The Wood Canyon Formation overlies the Stirling Quartzite, and includes lower, middle, and upper members. The lower Wood Canyon Formation has yielded the frond *Ernieetta* (Horodyski, 1991) as well as an additional as-yet-undescribed frond (Waggoner and Hagadorn, 1997). Both of these fronds are also found in Namibia. The lowermost Wood Canyon Formation also contains the first appearance of *Phycodes pedum*, and, therefore, contains the Precambrian-Cambrian boundary. The upper member contains trilobite fossils, trilobite trace fossils, and *Skolithos* tubes.

OBSERVATIONS

In searching for incised valleys, the authors examined the Rainstorm member which is the uppermost member of the Johnnie Formation. The geographic distribution of the Johnnie Formation is shown in Figure 2-5 as are the locations of measured sections described below. The Rainstorm member is recognized within a large area in southern

Figure 2-5. Geographic distribution of the Johnnie Formation in southern Nevada and southeastern California, and measured sections described in text. TC, Trail Canyon; HC, Hanaupah Canyon; SC, Six Spring Canyon.



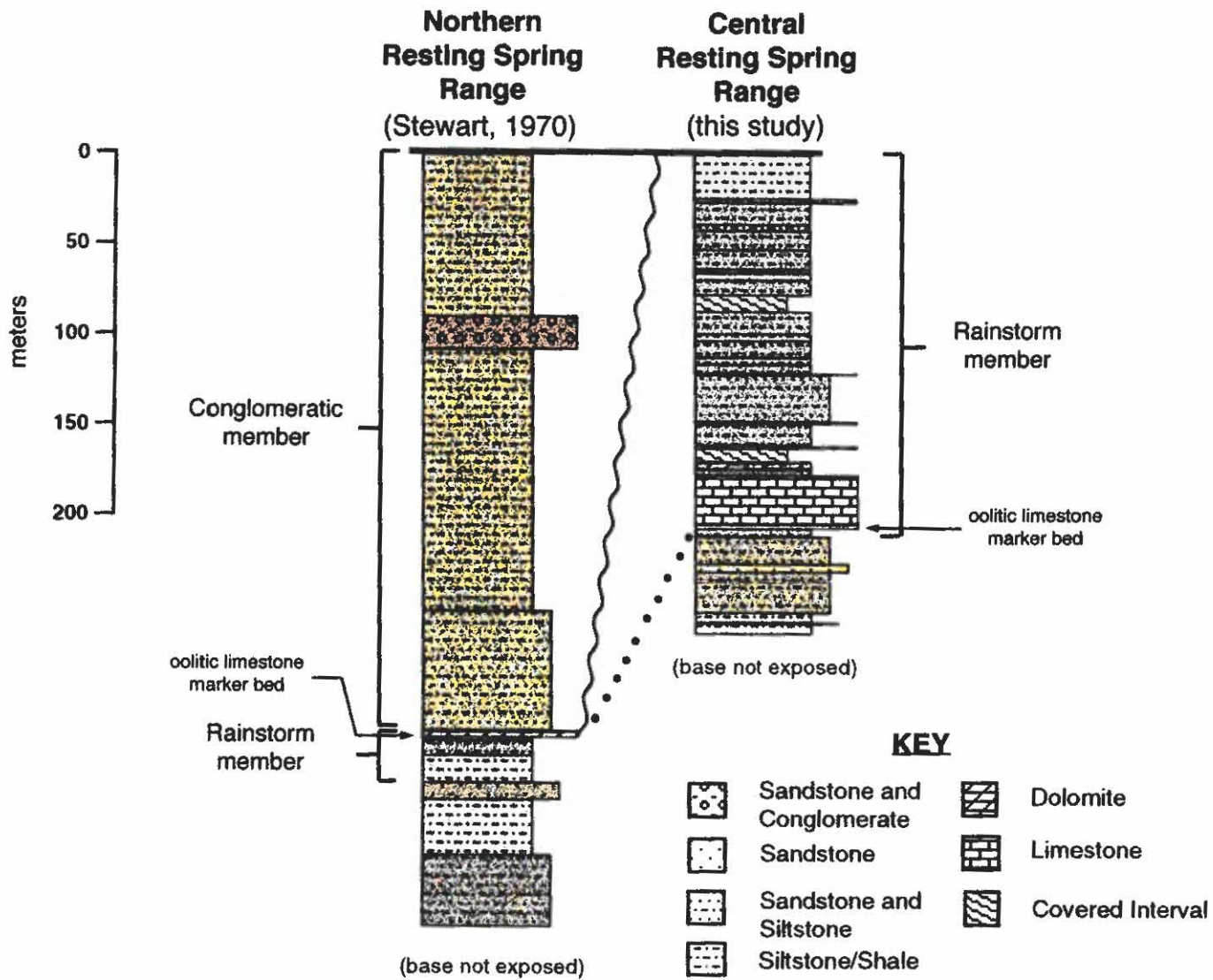
● measured section described in text

Nevada and southeastern California. Throughout most of this area, the Rainstorm member is predominantly siltstone and contains a distinctive suite of lithologies. These lithologies include a prominent 2-4 m thick grayish orange oolitic limestone marker bed near the base of the member and grayish purple siltstone and limestone. Ripple marks indicate shallow marine deposition (Stewart, 1970). Locally, the Rainstorm member is reduced in thickness or absent and a different suite of lithologies occur at the top of the Johnnie Formation. These distinctly different lithologies are assigned here to the informal Conglomeratic member, and include granular sandstone, conglomerate, olive gray siltstone, and, in the Panamint Range, diamictite. We observed the Conglomeratic member in the Resting Spring Range, Panamint Range, and northwestern Spring Mountains, and Summa (1993) observed similar lithologies at the same stratigraphic position in the Nopah Range. Thus, although the Conglomeratic member is only locally developed, it is observed at four locations scattered along a north-south distance of 80 kilometers. Very light gray and grayish purple coarse sandstone of the Stirling Quartzite overlies the Rainstorm and Conglomeratic members.

Resting Spring Range

The lateral transition between the Rainstorm and Conglomeratic members is best observed in the Resting Spring Range (Figure 2-6). The Rainstorm member is exposed in the central Resting Spring Range, and includes the oolitic limestone marker bed near its base as well as overlying pale red micritic limestones and grayish-purple siltstones. In the northern Resting Spring Range, the oolitic marker bed is present but the pale red micritic limestones and grayish-purple siltstones are absent. Instead, massive and parallel-laminated olive gray siltstone of the Conglomeratic member overlies the oolitic marker bed. Near the top of the Conglomeratic member, massive planar conglomerate beds are interstratified with granular sandstone. Granules and pebbles of vein quartz are common, and dolostone clasts up to 3 meters in diameter are present locally. The lateral transition

Figure 2-6. Measured sections of the upper part of the Johnnie Formation in the Resting Spring Range. See Figure 2-5 for location. See p. 53 in Appendix 2-A for Central Resting Spring Range measured section.



between the Rainstorm and Conglomeratic members occurs in an along-strike distance of about 300 m, but structural complexities obscure the contact between the two members.

Panamint Range

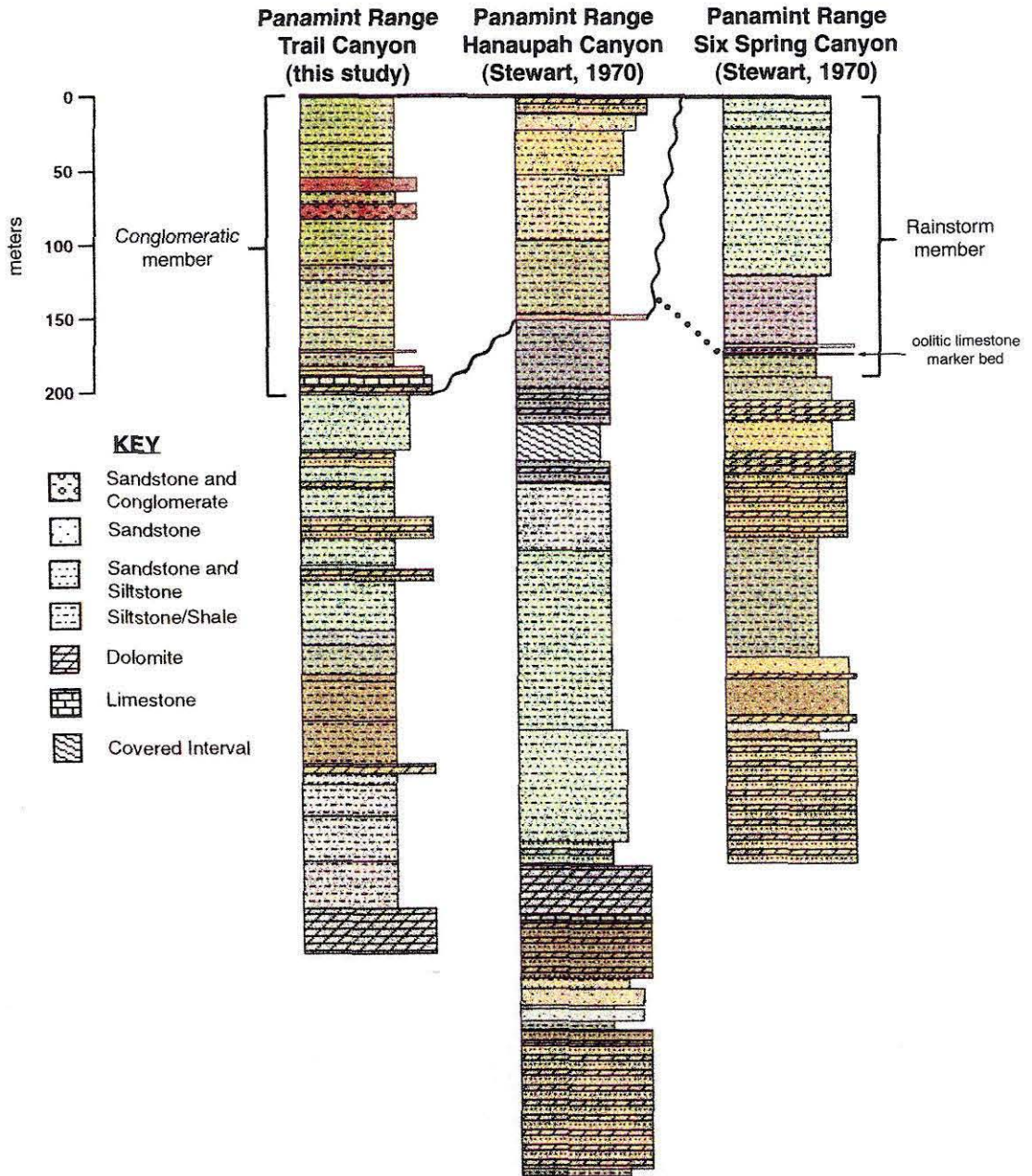
The Panamint Range also contains a lateral transition between the Rainstorm and Conglomeratic members as shown in Figure 2-7. The Rainstorm member is exposed at Johnson Canyon in the southern Panamint Range, but is absent at Trail Canyon and Tucki Mountain at the northern end of the range. As in the Resting Spring Range, the Conglomeratic member at Trail Canyon contains olive gray siltstone, granular sandstone, and pebble conglomerate. The sandstone and pebble conglomerate occurs in two 15 m intervals within the olive gray siltstone. As in the Resting Spring Range, pebbles of vein quartz are common, but rare granitic clasts are also present. A micritic limestone occurs at the base of the Conglomeratic member in Trail Canyon. This limestone rests on sub-Rainstorm Johnnie Formation siltstone.

At one location in the Trail Canyon area, the basal Conglomeratic member limestone is absent and about seven meters of diamictite are present instead. The diamictite contains meter-sized dolostone clasts, and is overlain by 2 m of olive gray siltstone and 15-20 m of carbonate breccia and conglomerate with clasts up to 250 cm in diameter.

To the north of Trail Canyon, the Conglomeratic member can be traced in continuous outcrop for 20 kilometers to Tucki Wash. In Tucki Wash, the Conglomeratic member contains thick, lenticular intervals of conglomerate and conglomeratic quartzite with a total thickness of at least 1000 m. The conglomerate includes pebbles of vein quartz as well as boulders of dolomitic quartz sandstone which are up to 10 m across.

In the Panamint Range, the lateral transition between the Rainstorm and Conglomeratic members occurs within an along-strike distance of 13.5 km in a structurally complex area between Johnson and Hanaupah canyons. In Hanaupah Canyon, clasts of the oolitic marker bed are found within a conglomerate which probably belongs to the Conglomeratic

Figure 2-7. Measured sections of the upper part of the Johnnie Formation in the Panamint Range. See Figure 2-5 for location. See p. 58 in Appendix 2-A for Trail Canyon measured section.



member.

Northwestern Spring Mountains

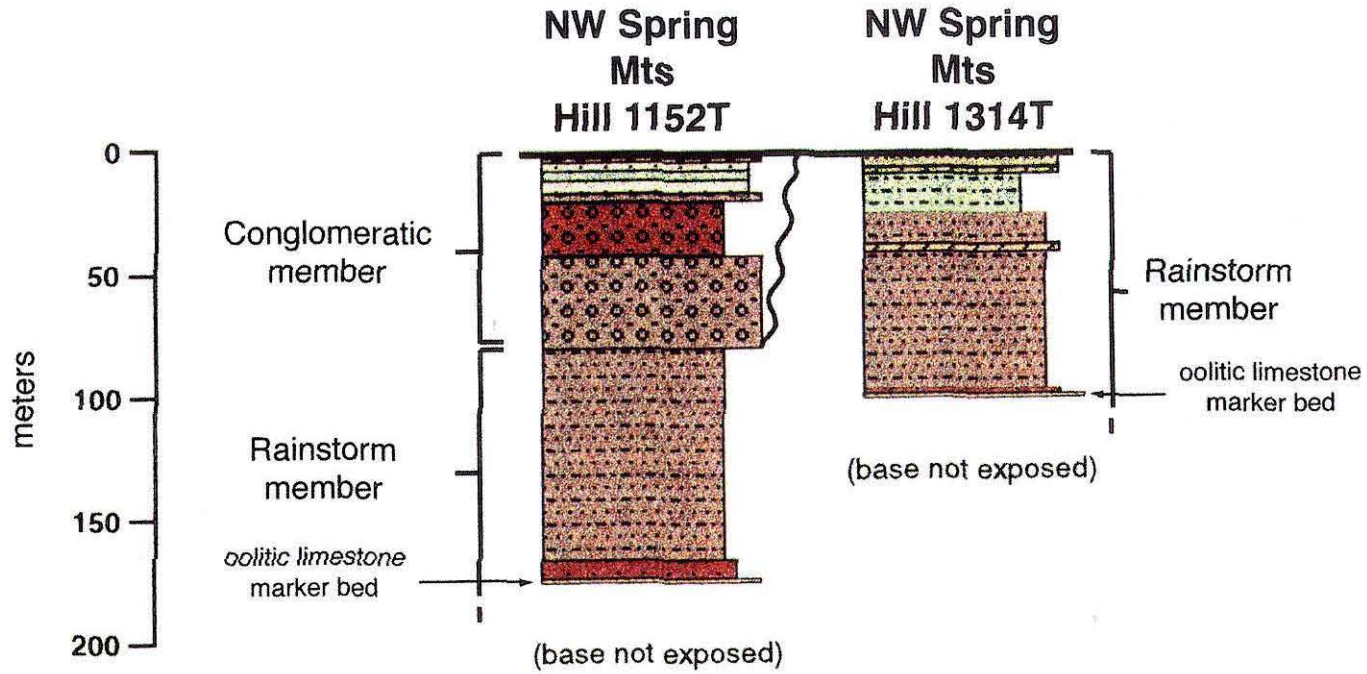
A lateral transition between the Rainstorm and Conglomeratic members also occurs in the northwestern Spring Mountains (Figure 2-8). At one location in the northwestern Spring Mountains, the Rainstorm member is about 150 m thick and is overlain by the Stirling Quartzite. About 3.6 km to the north-northeast, the thickness of the Rainstorm member has fallen to 90 m, and it is overlain by more than 80 m of conglomerate and olive gray siltstone of the Conglomeratic member. In outcrop, the base of the Conglomeratic member exhibits a few centimeters of erosional relief. Conglomerate occurs at the base of the Conglomeratic member and at a second horizon near the top of the member. Within the conglomerate, subtle size-grading and pebble alignment imparts a hint of bedding. Liver-colored siltstone occurs as lenses and intraclasts within the conglomerate, and some siltstone lenses contain flaser bedding. The lateral pinch-out of the Conglomeratic member in the northwestern Spring Mountains is obscured by structural complexities and alluvial cover.

INTERPRETATION

Origin of the Conglomeratic member as a valley fill

We interpret the Conglomeratic member as a valley fill which was deposited after valleys were incised into the Rainstorm member. Conglomerates within the Conglomeratic member are lithologically indistinguishable from conglomeratic fill within the Caddy Canyon valleys. The poorly developed bedding and siltstone lenses and intraclasts observed in the northwestern Spring Mountains are particularly diagnostic. Levy and others (1994) suggested a fluvial or fluvially-dominated marine origin for similar poorly bedded conglomerates in Idaho and Utah. Siltstone lenses within the conglomerates were deposited during times of reduced flow. During times of high flow, siltstone was ripped-up and clasts were incorporated in the conglomerates. Flaser bedding within some siltstone

Figure 2-8. Measured sections of the upper part of the Johnnie Formation in the northwestern Spring Mountains. See Figure 2-5 for location. See p. 65 in Appendix 2-A for Hill 1152T measured section and p. 67 for Hill 1314T measured section.



KEY

- | | | | |
|---|----------------------------|---|------------------|
|  | Sandstone and Conglomerate |  | Dolomite |
|  | Sandstone |  | Limestone |
|  | Sandstone and Siltstone |  | Covered Interval |
|  | Siltstone/Shale | | |

lenses in the northwestern Spring Mountains indicates intertidal conditions, and may suggest intermittent marine incursions. The lithologic similarity between conglomerates within the Conglomeratic member and fill within the Caddy Canyon valleys suggests that both deposits were formed by the same fluvial processes.

Other lithologies in the Conglomeratic member also fit into a valley-fill context. The micritic limestone at the base of the Conglomeratic member in the Panamint Range may have formed during rapid sea-level rise after valley incision. This micrite could be a cap carbonate like the carbonates observed above many glacial deposits around the world (Kennedy, 1996 and references therein). The micrite may have precipitated within valleys at other locations as well, but was removed by subsequent fluvial erosion. The diamictite in the Panamint Range is interpreted as a mass wasting deposit which formed through the collapse of a valley wall. A similar origin has been suggested for diamictite within valley-fill in the Neoproterozoic Wonoka Formation of Australia (Christie-Blick and others, 1995).

Erosional truncation of the Rainstorm member and sea level fall

Structural complexities preclude the direct observation of large-scale erosional truncation at the base of the Conglomeratic member, but the observed lateral transitions strongly suggest erosional truncation. In the Resting Spring Range, the short distance spanned by the transition suggests erosional truncation of the Rainstorm member and infilling by the Conglomeratic member rather than a lateral facies change. As suggested by Figure 2-6, erosional truncation in the Resting Spring Range could be as much as 150 m. Since the valleys incise shallow marine deposits and the valley-fill contains fluvial or fluvially-dominated marine deposits, the valleys were probably formed by sub-aerial rather than submarine erosion. Consequently, the amount of erosional truncation in the Resting Spring Range shows that sea level fell by at least 150 m.

DISCUSSION

Correlation of the Caddy Canyon and Johnnie valleys

The singularly large size of the Caddy Canyon and Johnnie valleys is the best argument for their correlation. The Caddy Canyon valleys and the Johnnie valleys are larger than any other incised valleys within the post-diamictite Neoproterozoic section in the western United States. In Idaho and Utah, the next largest incised valley is 60 m deep and occurs at the base of the Geertsen Canyon Quartzite (Levy and others, 1994). The base Geertsen Canyon incision has only been observed at one location in the Portneuf Range, and may be the result of local tectonic activity. Smaller incised valleys are present at multiple horizons within the Caddy Canyon Quartzite and Inkom Formation, but do not correlate between ranges in Idaho and Utah (Levy and others, 1994).

In southern Nevada and southeastern California, no incised valley elsewhere in the section approaches the size of the valley in the Resting Spring Range. Prominent unconformities occur at the base of the Johnnie Formation (Summa, 1993) and the base of the middle Wood Canyon Formation (Stewart, 1970; Runnegar and others, 1995), but neither unconformity is associated with substantial erosional relief. The Johnnie Formation contains several other sub-aerial unconformities (Summa, 1993), but none of these are associated with substantial erosional relief. When comparing the Neoproterozoic section in Idaho and Utah with the one in southern Nevada and southeastern California, the Johnnie valleys stand out as the only likely correlative of the Caddy Canyon valleys.

Glacioeustatic vs. tectonic origin of the Johnnie and Caddy Canyon valleys

Incision and filling of the Johnnie valleys requires a substantial drop in relative sea level followed by a substantial sea level rise. This fluctuation in sea level is most easily explained by a glacioeustatic mechanism in which the formation and melting of glaciers caused a dramatic sea level fluctuation over a relatively short time period. Sea level

oscillations are associated with many glacial deposits including both diamictites in the Kingston Peak Formation (Miller, 1985). Figure 2-9 depicts the regional extent of incised valleys in Idaho, Utah, southern Nevada, and southeastern California. If the Caddy Canyon valleys and Johnnie valleys are time correlative, base level changed along 700 km of the North American margin. A eustatic drop in sea level is the simplest explanation for a change in base level along this great length of the North American margin.

A regional tectonic event could have caused valley incision (Levy and others, 1994), but the Johnnie and Caddy Canyon Formations lack direct evidence for faulting. Structural and stratigraphic evidence for Neoproterozoic tectonism is largely confined to the lower Kingston Peak Formation (Walker and others, 1986) and the Perry Canyon Formation (Link, 1983). Evidence for younger tectonism is interpretive. Major thermal subsidence along the western U.S. margin began during the latest Neoproterozoic or early Cambrian (Levy and Christie-Blick, 1991), and may suggest a rifting event at that time. If subtle tectonism occurred during the intervening interval, it is entirely concealed by younger deformation and lack of exposure.

Carbon isotopes in the Noonday Dolomite and Johnnie Formation and Glaciation

As shown in Figure 2-10, carbon isotope values of up to +2.89 per mil occur in the upper four-fifths of the Johnnie Formation in the Nopah Range. These positive values are similar to isotope values which precede major Neoproterozoic glaciations. The positive carbon values are thought to reflect high rates of burial of organic carbon relative to total carbon (Kump, 1991). Burial of large amounts of organic carbon may have reduced atmospheric greenhouse capacity, and, in conjunction with 5-10% lower solar luminosity, lead to major glaciations (Hoffman and others, 1998).

The upper four-fifths of the Johnnie Formation also contains two clusters of negative carbon isotope values. Negative values within the uppermost Johnnie Formation and

Figure 2-9. Ranges containing incised valleys in the uppermost Caddy Canyon Formation (Idaho and Utah) and the uppermost Johnnie Formation (southern Nevada and southeastern California). Geographic distribution of incised valleys in the uppermost Caddy Canyon Formation from Levy and others (1994).

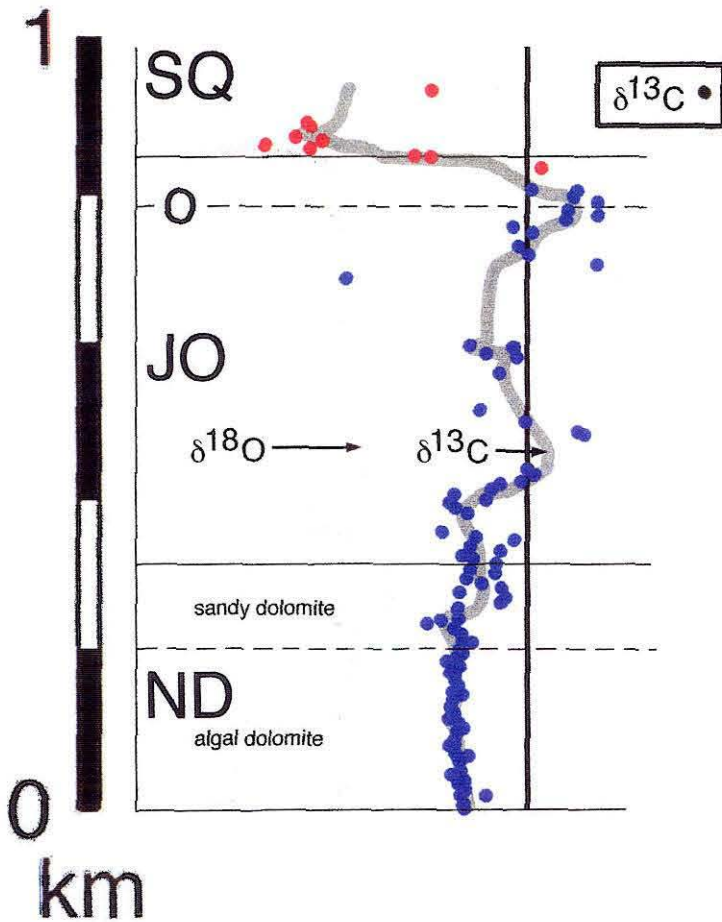


Figure 2-10. Carbon and oxygen isotope data for the Noonday-lowermost Stirling interval in the Nopah Range, southeastern California. Red dots indicate carbon isotope values which may be secondary (see text and Figure 2-11), and blue dots indicate carbon isotope values which are probably primary. See Appendix 2-B for description of analytical techniques and Appendix 2-C for table of isotope values. Formation names: SQ, Stirling Quartzite; JO, Johnnie Formation (o, oolitic limestone marker bed); ND, Noonday Dolomite.

NOPAH RANGE, CA

$\delta^{18}\text{O}$, $\delta^{13}\text{C}$

-15 -10 -5 0 5

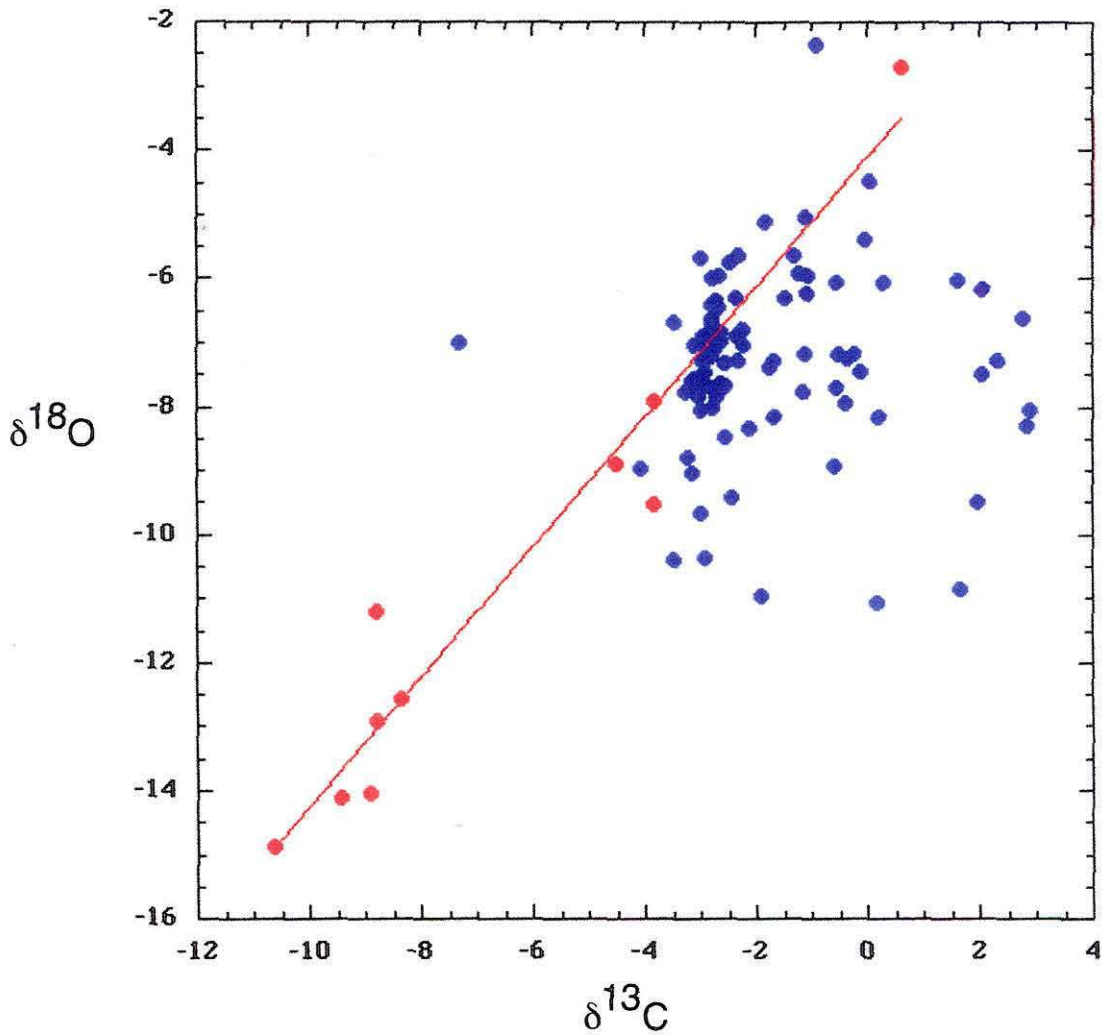


lowermost Stirling Quartzite are probably secondary for three reasons. First, the extremely negative carbon isotopic values (minimum of -10.65 per mil) are indicative of diagenetic alteration. The lowest primary carbon isotope values come from cap carbonates, and are generally between -5 and -1 per mil (Kennedy, 1996), although values as low as -7 per mil have been reported from the Tepee cap carbonate in northwestern Canada (Kaufman and others, 1997). Second, the correlation between oxygen and carbon isotope values ($r = .97$) is typical of carbonates which have undergone diagenesis. As shown in Figure 2-11, oxygen and carbon values near the Johnnie-Stirling contact form a linear trend (red dots) which includes the six samples which have the most depleted carbon and oxygen values. In contrast, samples from the Noonday Dolomite and lower 460 m of the Johnnie Formation (blue dots) show no correlation between carbon and oxygen values ($r = .3$). Third, the negative carbon and oxygen values coincide with the contact between the Johnnie Formation and Stirling Quartzite. The permeability contrast between Johnnie Formation siltstone and Stirling Quartzite probably resulted in considerable fluid flow along this contact.

Negative carbon isotope values in the middle of the Johnnie Formation may be primary or secondary. The minimum carbon value of -7.33 per mil looks like an outlier (the next lowest value is -2.33), but this value is similar to carbon isotope values from the Tepee cap carbonate in northwestern Canada. The poor correlation between oxygen and carbon isotopes in this interval suggests that the carbon values may be primary. If primary, could the negative carbon isotope values in this interval reflect glaciation? Summa (1993) documented changes in relative sea level within the Johnnie Formation which could have resulted from glacioeustasy, so this possibility could merit further study. However, mixed carbonate-siliciclastic rocks often yield disturbed carbon isotope values, and considerable fluid flow through this section seems likely. As a result, interpretation of these negative carbon isotope values should proceed with caution.

Figure 2-11. Relationship between carbon and oxygen isotope values for the Noonday-lowermost Stirling interval in the Nopah Range, southeastern California.

- lowermost Stirling Quartzite and uppermost 15 m of Johnnie Formation
- lower 460 m of Johnnie Formation and Noonday Dolomite



Carbon isotope values are uniformly negative in the Noonday Dolomite and lowest 50 m of the Johnnie Formation in the Nopah Range of southeastern California. Negative carbon isotope values occur through about 490 m of section above the Kingston Peak Formation, and are probably related to the youngest Kingston Peak glaciation. These low carbon isotope values are analogous to the low values associated with other Neoproterozoic glacial deposits.

In particular, Hoffman and others (1998) report similar carbon isotope values from the post-glacial Maiberg and Elandshoek Formations of Namibia. These formations overlie the Ghaub tillite within the Otavi Group. Carbon isotope values are uniformly negative throughout the lower 300 m of the formation, and then climb to 0 per mil between 300 and 500 m above the base of the Maiberg Formation.

Negative carbon isotope values are probably caused by two separate processes which operate on different timescales. On a timescale of millions of years, carbon isotope values in shallow marine carbonates are controlled by the ratio of organic carbon to total carbon in buried sediment (Kump, 1991). When this ratio is low, carbon isotope values are negative. The persistence of negative carbon isotope values through hundreds of meters of section suggests that shallow ocean waters were depleted for millions of years. Hoffman and others (1998) attribute this long-term negative isotopic shift to the extirpation of primary producers during global glaciation.

On a timescale of hundreds of thousands of years, carbon isotope values are influenced by transient phenomena like the upwelling of deep ocean water (Kump, 1991). Upwelling of depleted deep ocean water may be responsible for the thin isotopically negative (< -5 per mil) carbonates which cap many glacial diamictites (Kennedy and references therein, 1996).

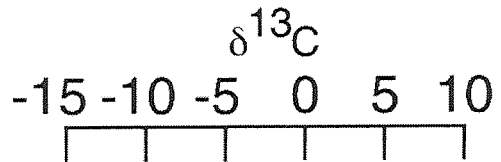
Carbon isotope data supports the correlation of incised valleys in the uppermost Johnnie Formation with incised valleys in the uppermost Caddy Canyon Quartzite. Figure

2-12 shows carbon isotope profiles from both the Nopah Range in southeastern California and the Bannock Range in Idaho (Smith and others, 1994). The Nopah Range profile does not traverse an incised valley, but the Johnnie-Stirling contact at this location probably correlates with the incised horizon nearby. In the Bannock Range, the incised horizon is at the top of the interval shown in Figure 2-12. The Bannock Range section is largely siliciclastic so carbon isotope sampling is sparse. However, carbon isotope values do not correlate with oxygen isotope values (Smith and others, 1994), so carbon values are probably primary.

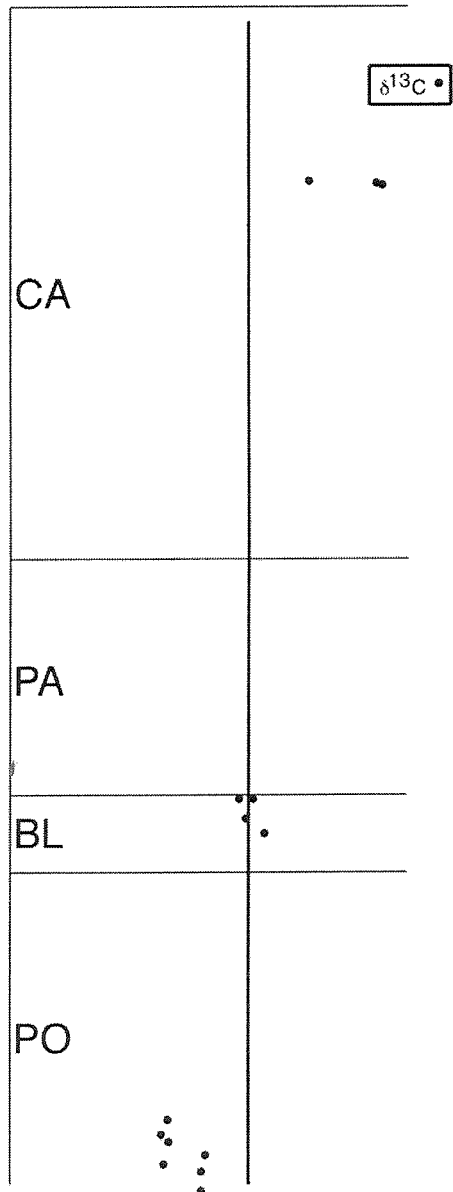
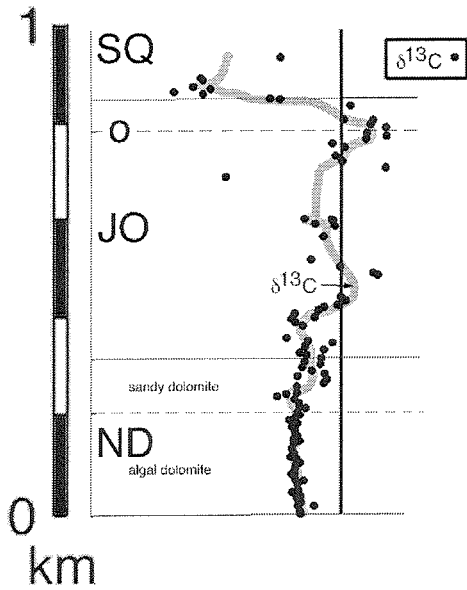
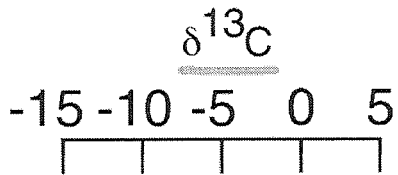
As in the Nopah Range, carbon isotope values in the Bannock Range change from negative to positive upsection. Negative values in the Pocatello Formation come from a carbonate which immediately overlies the uppermost glacial diamictite in the Idaho and Utah region. The stratigraphic position and carbon isotope values suggest that this carbonate correlates with the Noonday Dolomite. Carbon isotope values from the Blackrock Canyon Limestone record the transition from negative to positive values, so this unit may correlate with part of the Johnnie Formation. Carbon isotope values in the upper half of the Caddy Canyon Quartzite are positive like values in the stratigraphic interval that includes the Johnnie oolite in the Nopah Range, suggesting that these two intervals may be correlative. Carbon values in the Caddy Canyon Quartzite attain a maximum of +8.8 per mil. Similar extremely positive values are observed in the possibly correlative McCoy Creek Group of northeastern Nevada (Wickham and Peters, 1993), but are not observed in the Johnnie Formation. However, diagenetic alteration near the Johnnie-Stirling contact could mask extremely positive primary carbon values. In general, carbon isotope values from the Noonday-Johnnie interval match those from the upper Pocatello-Caddy Canyon interval.

Figure 2-12. Carbon isotope values in the Nopah Range, California, and Bannock Range, Idaho. California formations: SQ, Stirling Quartzite; JO, Johnnie Formation (o, oolitic limestone marker bed); ND, Noonday Dolomite. Idaho formations: CA, Caddy Canyon Quartzite; PA, Papoose Creek Formation; BL, Blackrock Canyon Limestone; PO, Pocatello Formation. The Papoose Creek Formation and Blackrock Canyon Limestone correlate with the Kelley Canyon and Maple Canyon Formations of Figure 2-3. The Pocatello Formation correlates with the Perry Canyon Formation in Figure 2-3.

BANNOCK RANGE, ID



NOPA H RANGE, CA



Implications for Neoproterozoic Glaciation

The age of the youngest Neoproterozoic glaciation

We interpret the Johnnie and Caddy Canyon valleys as the youngest Neoproterozoic glaciogenic features in the Cordilleran miogeocline of the western U.S. From Idaho to southeastern California, no glacial diamictites or large incised valleys occur between the Johnnie/Caddy Canyon valleys and the Precambrian-Cambrian boundary. Volcanic breccia of the Brown's Hole Formation occurs 200 m above the Caddy Canyon valleys, and has yielded an age of 580 \pm 7 Ma (Ar-Ar hornblende; Crittenden and Wallace, 1973). A straightforward interpretation of our findings shows that the youngest major Neoproterozoic glaciation occurred before 580 \pm 7 Ma.

In the Cordilleran miogeocline, the upper age limit for this glaciation is poorly constrained. In New England, the youngest Neoproterozoic glacial diamictite contains clasts of the 596 \pm 2 Ma Mattapan volcanic tuff (Thompson and others, 1996), and the youngest diamictite in Normandy probably post-dates the contact metamorphic aureole of the 584 \pm 4 Ma Coutances diorite (Guerrot and Peucat, 1990). A liberal interpretation of these age constraints suggests a 580 to 584 Ma age for the youngest major Neoproterozoic glaciation, while a conservative interpretation (using one sigma uncertainties and discounting the inferred age in Normandy) suggests a 573 to 598 Ma age range.

The number of discrete Neoproterozoic glaciations

Our findings indicate that the Cordilleran miogeocline in southern Nevada and southeastern California contains evidence for three distinct major Neoproterozoic glaciations within a largely continuous stratigraphic section. These three major glaciations are represented by the pair of glacial diamictites in the Kingston Peak and Perry Canyon Formations and the large incised valleys in the uppermost Johnnie and Caddy Canyon Formations. In the Kingston Peak Formation, substantial sea level changes associated with both diamictites (Miller, 1985) suggest that large volumes of ice were formed during these

glaciations. The Johnnie valleys demonstrate a fall in relative sea level of at least 150 m which is larger than the 120 m sea level fluctuations associated with Pleistocene glaciation (Benn and Evans, 1998). No other diamictites or large incised valleys are known to occur in Neoproterozoic sections in Idaho, Utah, southern Nevada, or southeastern California.

The lack of dateable material precludes an exact understanding of the temporal relationship between the two diamictites. The diamictite pairs in the Kingston Peak Formation and Perry Canyon Formation have been interpreted as Sturtian (Hambrey and Harland, 1985), and could represent a pair of glacial advances within a single glacial epoch. However, considerable time could have passed between deposition of the two Kingston Peak diamictites because a major angular unconformity separates the two deposits. This unconformity was formed by a substantial tectonic event which involved isoclinal folding, cleavage formation, and normal faulting (Walker and others, 1986). These observations leave open the possibility that the two Kingston Peak diamictites represent two glacial epochs which happened millions or tens of millions of years apart. For example, Prave (1998) suggested that the lower diamictite is Sturtian while the higher diamictite is Varanger.

The thickness of sediment between the top of the Kingston Peak Formation and the top of the Johnnie Formation suggests a substantial time gap between deposition of the highest Kingston Peak diamictite and incision of the Johnnie valleys. About 1.2 km of sediment was deposited in the Nopah Range during the intervening time. In the absence of direct evidence for faulting, we suggest that these sediments accumulated over tens of millions of years on a gradually subsiding continental shelf. The glacial epoch associated with incision in the uppermost Johnnie and Caddy Canyon Formations is probably distinct from the glacial epoch associated with deposition of the highest Kingston Peak diamictite.

The Neoproterozoic section in the western U.S. contains evidence for a discrete glacial epoch in the uppermost Johnnie and Caddy Canyon Formations and one or two glacial

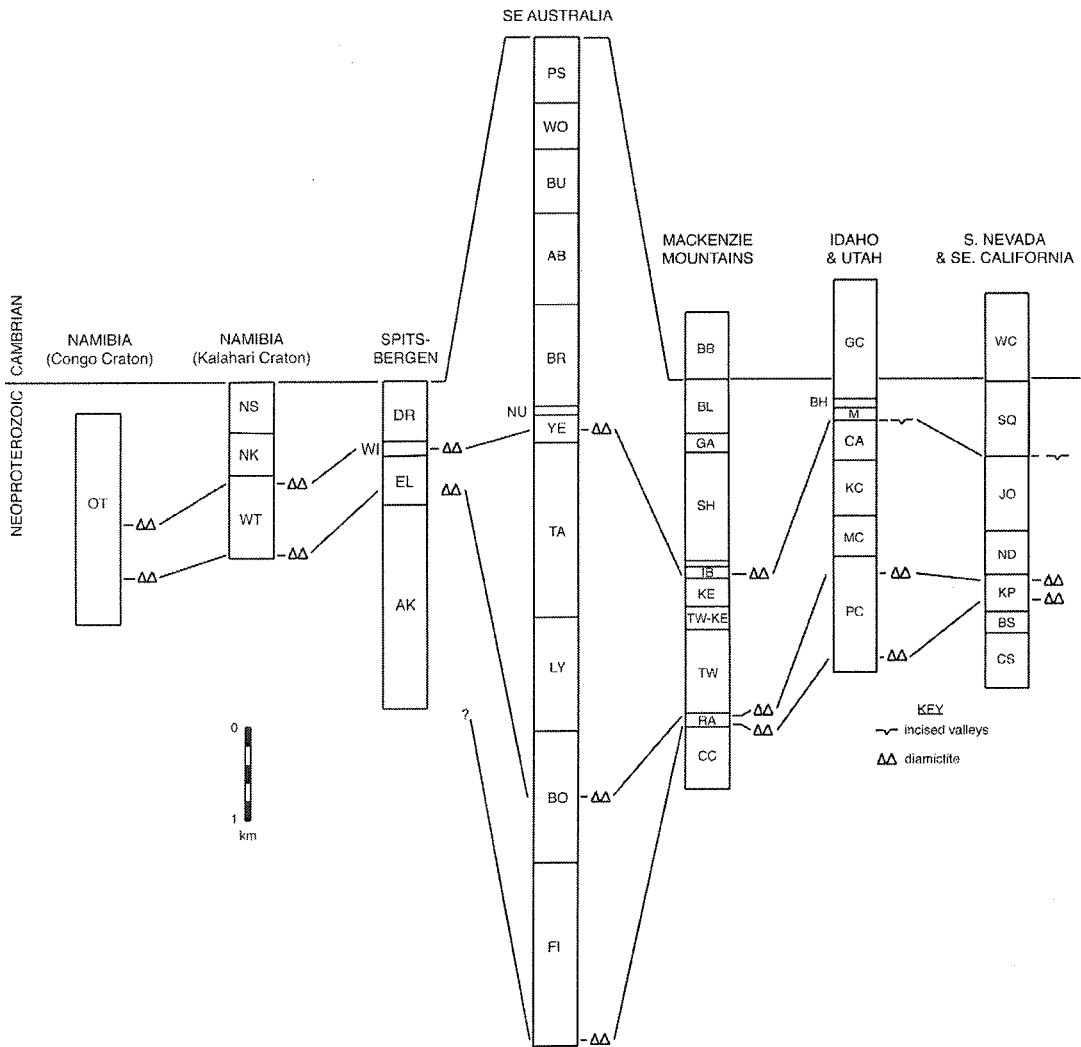
epochs in the Kingston Peak and Perry Canyon Formations. This record of two to three glacial epochs contrasts with the four or more Neoproterozoic glacial epochs envisioned by Kaufman and others (1997). In Figure 2-13 we offer alternative interpretations of Neoproterozoic sections described by Kaufman and others (1997), and suggest that their observations may fit into a framework which involves two to three glacial epochs.

Two to three glacial epochs in the Neoproterozoic of northwestern Canada

Like the Neoproterozoic section in the southwest U.S., the section in northwestern Canada contains lithologic evidence for two to three glacial epochs. The Canadian section includes a glacial diamictite in the Ice Brook Formation (Aitken, 1991), and a pair of glacial diamictites in the Rapitan Group (Eisbacher, 1985). We suggest that the Ice Brook diamictite was deposited during the youngest major Neoproterozoic glaciation, and correlates with the Johnnie and Caddy Canyon incised valleys. The unconformity at the base of the Ice Brook Formation involves about 120 m of local relief (Aitken, 1991), indicating a substantial drop in sea level during this glaciation. The pair of diamictites in the Rapitan Group probably correlate with the pair of diamictites in the Kingston Peak and Perry Canyon Formations. Like the Kingston Peak and Perry Canyon diamictites, the Rapitan diamictites either represent one or two glacial epochs.

The presence of glacial diamictite in the Ice Brook Formation and its absence in the Johnnie and Caddy Canyon Formations could reflect a difference in latitude between northwestern Canada and the southwest U.S. during the youngest glaciation. Paleomagnetic data from southern Nevada (Van Alstine and Gillett, 1979) indicates a paleolatitude of 1 ± 4 degrees during deposition of the Rainstorm member. While an equatorial location for the Caddy Canyon and Johnnie Formations seems to provide a simple explanation for the absence of glacial diamictite, this interpretation should be viewed with caution for two reasons. First, Neoproterozoic paleogeographic reconstructions (Hoffman, 1991; Dalziel, 1997) also place the Ice Brook diamictite near the equator during

Figure 2-13. Suggested correlation of diamictites and incised valleys in the western U.S. with Neoproterozoic sections elsewhere in the world. Stratigraphic relationships in Idaho and Utah from Levy and others (1994). Stratigraphic relationships in southeastern Australia from Young (1992). Other sections from Kaufman and others (1997). Names of units - **Nevada and California formation names:** WC, Wood Canyon Fm.; SQ, Stirling Quartzite; JO, Johnnie Fm.; ND, Noonday Dolomite; KP, Kingston Peak Fm.; BS, Beck Spring Dolomite; CS, Crystal Spring Fm; **Idaho and Utah formation names:** GC, Geertsen Canyon Quartzite; BH, Brown's Hole Fm.; M, Mutual Fm.; CC, Caddy Canyon Quartzite; KC, Kelley Canyon Fm.; MC, Maple Canyon Fm.; PC, Perry Canyon Fm.; **Mackenzie Mountains:** BB, Backbone Range Fm.; BL, Blueflower Fm.; GA, Gametrail Fm.; SH, Sheepbed Fm.; IB, Ice Brook Fm.; Ke, Keele Fm.; TW-KE, Twitya-Keele Fm.; **southeastern Australia:** PS, Pound Subgroup; WO, Wonoka Fm.; BU, Bunyeroo Fm.; AB, ABC Range Quartzite; BR, Brachina Fm.; NU, Nuccaleena Fm.; YE, Yerelina Subgroup; TA, Tapley Hill Fm.; LY, Lyndhurst Fm.; BO, Bolla Bollana Fm.; FI, Fitton Fm.; **Spitsbergen:** DR, Dracoisen Fm.; WI, Wilsonbreen Fm.; EL, Elbobreen Fm.; AK, Akademikerbreen Fm.; **Namibia (Kalahari Craton):** NS, Nama Group; NK, Kuibis Sub-group; WT, Witveli Group; **Namibia (Congo Craton):** OT, Otavi Group.



the late Neoproterozoic. Second, paleomagnetic data shows that the youngest glacial diamictite in southeastern Australia (Marinoan diamictite) was deposited within three degrees (Schmidt and Williams, 1995) to ten degrees (Sohl, 1997) of the equator.

Environmental controls on the geographic distribution of ice were probably complex.

Kaufman and others (1997) suggest that a carbon isotope excursion in the Canadian section indicates an additional glacial epoch. They interpret a carbon isotope excursion in the Sheepbed Formation as evidence for glaciation because similar isotope excursions are associated with glacial diamictites. While intriguing, their interpretation should be viewed with caution for four reasons. First, the carbon isotope measurements were made within a mixed carbonate-siliciclastic facies which is susceptible to diagenetic overprinting, and the observed carbon isotope excursion is consistent with diagenetic lowering of carbon isotope values. They did not publish oxygen isotope analyses which would help in the assessment of diagenetic effects. Second, excursions associated with glacial diamictites often reach $\delta^{13}\text{C}$ values of -5 per mil or less, while the lowest recorded values within the Sheepbed Formation are near 0 per mil. Third, the Sheepbed Formation lacks lithologic evidence for glaciation, although the formation was deposited on the continental slope where such evidence could be cryptic.

Fourth, while isotope excursions like the one in the middle Sheepbed Formation are often temporally associated with glaciation, other events can produce similar isotope excursions. For example, a carbon isotope excursion at the Cretaceous-Tertiary boundary is not associated with glaciation, but does coincide with a mass extinction and large physical perturbations which are probably related to bolide impact (Alvarez, 1980; Hildebrand and others, 1991) and/or large-scale volcanism (Courillot and others, 1996). A carbon isotope excursion at the Permo-Triassic boundary may be associated with short-lived high latitude glaciation (Knoll and others, 1996), but is also temporally associated

with a mass extinction and large-scale volcanism (Renne and others, 1995). By itself, a carbon isotope excursion does not provide unequivocal evidence for glaciation.

Two to three glacial epochs in southeastern Australia

As noted by Young (1992), the Neoproterozoic section in southeastern Australia is similar to the section in northwestern Canada. In both regions, three diamictites provide lithologic evidence for two to three glacial epochs. The Yerelina Sub-Group of the Wilpena Group contains the highest glacial diamictite, and may correlate with the Ice Brook Formation. The Bolla Bollana Formation and Hamilton Creek Member of the Fitton Formation each contain glacial diamictite and may correlate with the pair of diamictites in the Rapitan Group.

Two glacial epochs in the Neoproterozoic of Spitsbergen

Two glacial diamictites provide the only direct evidence for glaciation in the Spitsbergen Neoproterozoic section. Kaufman and others (1997) interpret carbon isotope excursions in the Akademikerbreen Group as evidence for two additional glacial epochs. However, many of the carbon isotope caveats from the preceding two paragraphs also apply to the Akademikerbreen carbon isotope data. In addition, the Akademikerbreen carbon isotope excursions were measured in organic carbon rather than calcite (Knoll and others, 1986), and organic carbon is particularly susceptible to diagenesis.

Two glacial epochs in the Neoproterozoic of Namibia

In Namibia, a pair of glacial diamictites occurs in the Otavi Group on the Congo Craton and another pair occurs in the Witveli Group on the Kalahari Craton. If the Otavi Group diamictites correlate with the diamictites in the Witveli Group, the Namibian section records two glacial epochs. In contrast, Kaufman and others (1997) suggest that the Otavi Group is entirely older than the Witveli Group, and that the two pairs of glacial diamictites formed during four separate glacial epochs. Existing radiometric constraints do not distinguish between these two interpretations.

Summary

The simplest interpretation of the Neoproterozoic stratigraphic record involves two to three glacial epochs. No continuous stratigraphic section contains physical evidence (glacial diamictite, incised valleys) for more than three glaciations. Carbon isotope excursions suggest avenues for future research, but, in the absence of corroborating physical stratigraphic evidence, are not unique indicators of glaciation.

Implications for Ediacaran Evolution

Glaciation and Ediacaran evolution

Our findings show that the youngest major Neoproterozoic glaciation pre-dates the diverse Ediacaran fauna in Namibia by at least 25 million years. Ediacaran diversification probably began after the glaciation which formed the Johnnie and Caddy Canyon valleys. The apparent diversification of Ediacarans within the Sheepbed Formation in northwestern Canada probably reflects intrinsic biological processes or a physical cause unrelated to glaciation.

The Ediacaran diversification and other biotic radiations

The time gap between the youngest glaciation and Ediacaran diversification is comparable to the timespan of most Phanerozoic biotic radiations. The spectacular Cambrian explosion occurred in about ten million years (Sepkoski and Schopf, 1992). The biotic radiation which post-dates the terminal Ordovician mass extinction took 5 to 7 million years (Sheehan and Watkins, 1995). Major biotic radiations followed the other four major Phanerozoic mass extinctions, and each took 10 to 20 million years (Sepkoski, 1995).

As often happened during the Phanerozoic, the Ediacaran biotic radiation may have followed an extinction event. A major glaciation probably caused the extinction of many species (Sokolov and Fedonkin, 1986) in a number of ways. Sea ice probably limited primary productivity (Hoffman and others, 1998), ocean currents probably changed, and large glacioeustatic sea level fall greatly reduced the inhabitable area of the continental

shelves. When glaciation ended and sea level rose, surviving organisms diversified quickly in a world with enormous geographic and ecological space for new species.

The diversity of planktonic microfossils provides evidence for an extinction event coincident with the youngest glaciation (Varanger glaciation) in Scandinavia and Russia. In that region, about 70% of plankters became extinct including virtually all complex acritarchs (Vidal and Knoll, 1982; Vidal and Moczydlowska-Vidal, 1997). Glacial sediments contain a low diversity fauna of morphologically simple plankters. Post-glacial sediments also contain a depauperate fauna even when the lithofacies match taxonomically-rich pre-glacial sediments (Vidal and Knoll, 1982). Planktonic diversity recovered before the Cambrian (Vidal and Moczydlowska-Vidal, 1997). Since plankton are at the base of the food chain, their extinction could have lead to the extinction of other organisms.

If the Ediacaran radiation is associated with extinction and global catastrophe, this radiation would most closely parallel the early Triassic and early Paleogene radiations. Both of these biotic radiations followed mass extinctions which were roughly coincident with global catastrophes. The early Triassic radiation followed a mass extinction which was associated with large-magnitude volcanism (Renne and others, 1995) and minor glaciation (Knoll and others, 1996), while the early Paleogene biotic radiation followed a mass extinction associated with a bolide impact (Alvarez, 1980; Hildebrand and others, 1991) and large-magnitude volcanism (Courtilot and others, 1996).

FUTURE WORK

Carbon isotopes and glaciation

As demonstrated by the preceding discussion, many questions about Neoproterozoic earth history remain unresolved. Could carbon isotope excursions in northwestern Canada and Spitsbergen indicate additional glacial epochs as suggested by Kaufman and others (1997)? To answer this question, these Neoproterozoic sections should be re-examined for (1) physical stratigraphic evidence for glacioeustacy and (2) oxygen isotopic evidence for

diagenesis. In particular, the Spitsbergen section is ripe for re-appraisal. The Akademikerbreen carbon isotope excursions occur in intertidal to shallow sub-tidal deposits (Knoll and others, 1986) which should have been sub-aerially exposed during any large glacioeustatic drop in sea level.

Incised valleys, sub-aerial unconformities, and global sea level

Could incised valleys which are deep and globally synchronous indicate additional glacial epochs as suggested by Charlton and others (1997)? Late Neoproterozoic sections in Australia, Namibia, the lesser Himalaya, and the southwestern U.S. each contain incised valleys or sub-aerial unconformities which may have formed in response to local changes in relative sea level or global eustatic changes in sea level. For each of these sections, prominent incised valleys or sub-aerial unconformities are discussed below.

Australia

In Australia, the Neoproterozoic Wonoka Formation is younger than the youngest (Marinoan = Varanger?) Australian glacial deposits, and contains incised valleys which cut into shallow marine sediments and which are up to 1 km deep (Christie-Blick, 1995). These valleys could have formed due to a large eustatic change in sea level or could have formed due to a combination of tectonic uplift and eustatic sea level fall. However, these valleys could also have formed during the desiccation of an enclosed basin in an event which was analogous to the Miocene Messinian event in the Mediterranean (Christie-Blick, 1997). As with incised valleys in the southwestern U.S., stable isotope measurements could aid in the interpretation of the Wonoka valleys. Unfortunately, existing carbon isotope values from the Wonoka Formation (Jenkins, 1995) are extremely negative (< -7 per mil), and are probably secondary (Kaufman and others, 1997).

Namibia

The Neoproterozoic Nama Group in Namibia is younger than the youngest glacial diamictite in Namibia, and contains incised valleys at four stratigraphic horizons (Grotzinger and others, 1995). Some of these incised valleys may have formed during eustatic changes in sea level. However, the Nama group was deposited in a foreland basin (Stanistreet and others, 1991), so some of the incised horizons may be tectonic in origin as are some incised horizons within the Cretaceous Sevier foreland basin in North America (Martinsen and others, 1993). Carbon isotope excursions are not associated with these incised valleys (Grotzinger and others, 1995), although parts of the section are sparsely sampled.

Lesser Himalaya and southwestern U.S.

In the Neoproterozoic Krol Formation of the lesser Himalaya, deposition of shallow marine carbonate was punctuated by the formation of three paleokarst surfaces (Jiang and others, 1997). Jiang and colleagues are currently investigating the physical stratigraphy and stable isotope profile of the Krol Formation in detail. The Neoproterozoic section in the western U.S. also contains sub-aerial unconformities at the base of and within the Johnnie Formation (Summa, 1993). In addition, the record of sea level change during deposition of the Stirling Quartzite is largely unknown. Some of the sub-aerial unconformities and incised valleys in the lesser Himalaya and southwest U.S. may reflect eustasy.

CONCLUSION

The Cordilleran miogeocline in the western U.S. preserves a largely continuous Neoproterozoic record. Like other Neoproterozoic sections, the one in the western U.S. contains physical stratigraphic evidence for two to three glacial epochs. Incised valleys in the uppermost Johnnie and Caddy Canyon Formations formed during one glacial epoch and a pair of glacial diamictites lower in the section formed during one or two additional glacial epochs.

In addition to the Johnnie and Caddy Canyon valleys, the Neoproterozoic section in the western U.S. contains lesser incised valleys and sub-aerial unconformities which may be of local, regional, or global significance. Other Neoproterozoic sections contain similar features, suggesting that some of these valleys and unconformities may correlate globally and reflect lesser eustatic fluctuations. Other incised valleys, like the Wonoka Canyons in Australia, may reflect intrabasin phenomena and may lack global correlatives.

Age constraints in Idaho and Utah show that the youngest major Neoproterozoic glaciation occurred before 580 Ma and preceded the diverse Ediacaran fauna by tens of millions of years. Ediacaran diversification is a largely post-glacial phenomena.

ACKNOWLEDGMENTS

This work benefited enormously from discussions with Nicholas Christie-Blick, Whitey Hagadorn, Martin Kennedy, Bruce Runnegar, and David Evans, although they may disagree with our conclusions. Stratigraphic studies in southern Nevada and southeastern California have also benefited from satellite and airborne images provided by Ronald Blom and Robert Crippen at the NASA Jet Propulsion Laboratory.

This research was partially supported by an NSF Graduate Student Fellowship to Mark Abolins.

APPENDIX 2 - A MEASURED SECTIONS

**CENTRAL RESTING SPRING RANGE
(upper) 2/97**

Stirling Quartzite - A Member

Unmeasured

Johhnie Formation - Rainstorm Member

FAULT AT TOP OF SECTION

Unit 14: Siltstone

Light greenish gray (5GY 8/1) and pale pink (5RP 8/2); weathers same. Somewhat mottled appearance; overall more of a greenish appearance at large scale than purplish siltstones below. Laminated siltstone. Some intervals near top similar to Unit 5. A few fine grained sandstone beds. Minor carbonate blebs and stringers.

24 m

Unit 13: Dolomitic sandstone:

Grayish orange pink (5YR 7/2); weathers grayish orange (10YR 7/4) and dark yellowish orange (10YR 6/6). Medium grained dolomitic sandstone. Medium bedded; planar and cross-stratification. Laminae at 20-30° in 5-10 cm sets.

2 m

Unit 12: Siltstone

Pale red purple (5RP 6/2) to grayish purple (5P 4/2); weathers same. Laminated siltstone; fissile. Contains 1-3 m lenses, blebs, and stringers of yellowish gray (5Y 8/1) to greenish gray (5GY 6/1) siltstone. Minor amounts of dolomitic siltstone or micrite; > 95% is "purple" siltstone.

26 m

Unit 11: Siltstone

Pale red purple (5RP 6/2) to grayish purple (5P 4/2); weathers same. Laminated siltstone; fissile. Contains 1-3 m lenses, blebs, and stringers of yellowish gray (5Y 8/1) to greenish gray (5GY 6/1) siltstone; about 5% of unit. Contains 30% pale red (10R 6/2); weathers pale yellowish brown (10YR 6/2); stringers and blebs of micritic limestone with blebs of siltstone. Dolomitic siltstone and dolomitic fine grained sandstone more abundant than in Units 9 and 10. Probably the same as Unit 10 or slightly higher in section.

11 ± 20-30 m

BREAK IN SECTION

Unit 10: Siltstone

Pale red purple (5RP 6/2) to grayish purple (5P 4/2); weathers same. Laminated siltstone; fissile. Contains 1-3 m lenses, blebs, and stringers of yellowish gray (5Y 8/1) to greenish gray (5GY 6/1) siltstone; about 5% of

unit. Contains minor (10-15%) pale red (10R 6/2); pale yellowish brown (10YR 6/2) weathering 2-3 cm thick beds of micritic limestone with blebs of siltstone.

14 m

COVERED INTERVAL

9 m

Unit 9: Siltstone

Pale red purple (5RP 6/2) to grayish purple (5P 4/2); weathers same. Laminated siltstone; fissile. Contains 1-3 cm lenses, blebs, and stringers of yellowish gray (5Y 8/1) to greenish gray (5GY 6/1) siltstone; about 5% of unit. Middle section of unit contains nodular appearing dolomitic siltstone and fine sandstone.

34 m

Unit 8: Dolomitic sandstone

Pale red purple (5RP 6/2) to grayish purple (5P 4/2); weathers moderate brown (5YR 4/4). Fine grained dolomitic sandstone. Laminated; moderately bedded.

0.5 m

Unit 7: Siltstone and sandstone

Pale red purple (5RP 6/2) to grayish purple (5P 4/2); weathers same. Laminated siltstone; fissile. Contains 1-3 m lenses, blebs, and stringers of yellowish gray (5Y 8/1) to greenish gray (5GY 6/1) siltstone. Also contains pale red (5R 6/2), brownish black (5R 2/1) to moderate brown (5YR 4/4) weathering fine-grained dolomitic siltstone.

26 m

Unit 6: Dolomitic sandstone

Pale red (5R 6/2); weathers brownish black (5R 2/1) to moderate brown (5YR 4/4). Fine-grained dolomitic sandstone. Contains several thin (5-10 cm) pale red (5R 6/2), moderate brown (5YR 4/4) sandstone. Sandstone contains symmetrical ripple marks.

1 m

Unit 5: Siltstone

Pale red purple (5RP 6/2) to grayish purple (5P 4/2); weathers same. Laminated siltstone; fissile. Contains 1-3 cm lenses, blebs, and stringers of yellowish gray (5Y 8/1) to greenish gray (5GY 6/1) siltstone; about 5% of unit.

12 m

Unit 4: Dolostone

Pale red (5R 6/2); weathers moderate yellowish brown (10YR 5/4). Very fine-grained dolostone; alternates between laminated to massive beds. Forms resistant unit within surrounding siltstones.

1 m

COVERED INTERVAL

7 m

Unit 3: Phyllitic Siltstone

Thinly interbedded phyllitic siltstone, micrite, and laminated silty carbonate. Phyllitic siltstone grayish

weathers moderate orange pink (10R 7/4) to grayish orange (10YR 7/4). Massive thin beds. Silty dolostone and limestone grayish red (5R 4/2); weathers same plus moderate yellowish brown (10YR 5/4). Thinly laminated; laminations locally truncated. At base, unit is 50% siltstone and 50% carbonate, grades upwards to 75% siltstone near top of unit.

7 m

Unit 2: Limestone

Pale red (10R 6/2) to grayish red (5R 4/2); weathers grayish orange pink (5YR 7/2) to light brown (5YR 6/4). Very fine-grained micrite. Thickly laminated to thinly bedded (1-10 cm) limestone and dolostone; siliceous partings on some bedding. Dolostone in continuous and discontinuous stringers. Possible HCS.

28 m

Unit 1: Limestone (Johnnie oolite)

Very pale orange (10YR 8/2); weathers grayish orange (10YR 7/4) to dark yellowish orange (10YR 6/6) oolitic dolostone. Coarse-grained ooids.

2 m

TOTAL THICKNESS OF MEASURED SECTION

297.5 ± 20 m

CENTRAL RESTING SPRING RANGE
(lower) 2/97

Johnnie Formation - Middle Member

Unit 10: Oolitic Dolomite (Johnnie Oolite)

Medium light gray (N6), weathers dark yellowish orange (10YR 6/6). Medium to coarse grained oolitic grainstone. Thickly bedded.

2 m

Unit 9: Siltstone

Medium gray (N5), weathers bluish gray (5B 5/1). Contains stringers of green siltstone throughout section.

4.5 m

Unit 8: Siltstone and Sandstone

Olive gray (5Y 4/1), weathers same plus moderate brown (5YR 3/4). Very fine grained sandstone (50%) and siltstone (50%). Siltstone laminated; moderately to thinly bedded. Contains some siltstone beds similar in appearance to Unit 1.

14.5 m

Unit 7: Sandstone

Medium light gray (N6), weathers light brownish gray (5YR 6/1). Medium grained sandstone. Medium bedded; beds generally parallel with low angle truncations.

4 m

Unit 6: Siltstone

Olive gray (5Y 4/1), weathers same plus moderate brown (5YR 3/4). Very fine grained sandstone (50%) and siltstone (50%). Siltstone laminated; moderately to thinly bedded. Contains some siltstone beds similar in appearance to Unit 1.

5 m

Unit 5: Sandstone

Medium gray (N5), weathers light brown (5YR 5/6). Fine grained sandstone. Contains a 20 cm bed of dolomitic sandstone that weathers in relief relative to surrounding beds.

0.5 m

Unit 4: Siltstone and Sandstone

Olive gray (5Y 4/1), weathers same plus moderate brown (5YR 3/4). Very fine grained sandstone (50%) and siltstone (50%). Siltstone laminated; moderately to thinly bedded. Contains some siltstone beds similar in appearance to Unit 1.

17.5 m

Unit 3: Siltstone and Sandstone

Greenish gray (5GY 6/1), weathers dark greenish gray (5GY 4/1) and grayish brown (5YR 3/2). Very coarse siltstone to very fine grained sandstone. Thin to medium bedded.

5 m

Unit 2: Sandstone

Medium gray (N5), weathers medium dark gray (N4). Very fine grained sandstone with silty partings. Some possible load structures.

1 m

Unit 1: Siltstone and Sandstone

Greenish gray (5GY 6/1), weathers dark greenish gray (5GY 4/1) and grayish brown (5YR 3/2). Very coarse siltstone to very fine grained sandstone. Thin to medium bedded.

5 m

**TOTAL THICKNESS
OF MEASURED SECTION (INCOMPLETE)**

59 m__

PANAMINT RANGE -TRAIL CANYON
(4/96)

Stirling Quartzite - A Member (unmeasured)

Unit 1: Quartzite

Quartzite, very pale orange (10YR 8/2) to yellowish gray (5Y 8/1); weathers same; very coarse grained, cemented with quartz overgrowths; massive, cliff former.

Unmeasured

Johnnie Formation - Unit 4

Unit 39: Quartzite

Quartzite, moderate reddish brown (10R 4/6); weathers same; moderately fissile, becomes much more fissile within 5 feet of contact with overlying Stirling; very fine grained quartz sand with ~20% silt. Unit as a whole weathers to form green slopes.

130 ft

Unit 38: Siltstone

Argillaceous siltstone, light olive gray (5Y 5/2) to olive gray (5Y 4/1); weathers same. Somewhat fissile, flaggy, becomes more fissile near top 15 feet of section.

100 ft

Unit 37: Phyllitic Siltstone

Phyllitic siltstone, grayish olive (10Y 4/2); weathers same plus light brown (5YR 5/6); platy to flaggy cleavage; breaks randomly; pyrite 1 mm or less common.

100 ft

Unit 36: Sandstone and Shale

Interstratified sandstone and shale, olive gray (5Y 4/1) to light brown (5YR 5/6); weathers same; Sandstone forms resistant ribs.

33 ft

Unit 35: Sandstone

Quartzite, moderate reddish brown (10R 4/6) and light brown (5YR 5/6); weathers same; very fine quartz sand with ~ 10% mafics. Forms more resistant layer within surrounding siltstone.

35 ft

Unit 34: Siltstone

Argillaceous siltstone; olive gray (5Y 4/1); weathers same plus light brown (5YR 5/6). Flaggy, cleaves along bedding planes. Ovals of Fe-discoloration surround 2-3 mm cubes of pyrite, ovals up to 23 cm long along b-axis.

100 ft

Unit 33: Phyllitic Siltstone

Phyllitic siltstone, light olive gray (5Y 5/2), weathers same; Thinly bedded, beds often up to 10 cm apart; fissile, slope former.

35.5 ft

Unit 32: Phyllitic Siltstone

Phyllitic siltstone, moderate brown (5YR 3/4), weathers same, .5 ft thick calcareous siltstone at 17.5 feet.

102 ft

Unit 31: Phyllitic Siltstone

Phyllitic siltstone. Medium dark gray (N4) to dark gray (N3); weathers same, plus moderate brown (5YR 4/4). Well-bedded; beds ~.5 cm thick; fissile, cleaves along bedding planes. Some Fe-discoloration; .5 mm pyrite cubes along more discolored beds. Slope former.

50 ft

Unit 30: Quartzite

Quartzite. Grayish orange (10YR 7/4); weathers same plus moderate brown (5YR 4/4) and grayish brown (5YR 3/2). Very fine-grained sand; siliceous cement. Minor tabular cross-bedding; thickly laminated; bedding somewhat convoluted. 2 mm pyrite cubes common. Forms resistant light colored ledge within darker shale.

5.5 ft

Unit 29: Shale

Argillaceous shale. Dark greenish gray (5GY 4/1) to olive gray (5Y 4/1); weathers same plus moderate olive brown (5Y 4/4) to moderate brown (5YR 4/4). Medium laminated to thinly bedded when visible; beds often widely separated, up to 25 cm. Fissile, cleaves along bedding planes. Fe-discoloration and pyrite cubes common in upper 20 feet. Less resistant than underlying limestone; slope-former.

30 ft

THICKNESS OF UNIT 4

821 ft

Johnnie Formation - Unit 3**Unit 28: Quartzite**

Phyllitic quartzite, light brown (5YR 5/6). Very fine sand. Contains some large clasts of underlying limestone (up to 3 cm), ~ 20% of rock. Unit as a whole weathers to form a shiny green slope with more resistant orange bands.

8.5 ft

Unit 27: Quartzite

Interbedded quartzite, moderate yellowish brown (10YR 5/4) and limestone, grayish red (10YR 7/4). Similar in characteristics to units 26 and 25.

12 ft

Unit 26: Dolomitic quartzite

Dolomitic quartzite. Moderate yellowish brown (10YR 5/4); weathers same. Very fine grained sand to coarse silt; very fissile, highly fractured; less resistant than limestone.

2.5 ft

Unit 25: Limestone

Limestone. Very pale orange (10YR 8/2) and grayish red (10YR 7/4); also medium gray (N5) to medium dark gray (N4); weathers same. Finely crystalline; thinly laminated to thinly bedded. Solution discoloration along fractures.

17 ft

Unit 24: Limestone breccia

Limestone breccia. Grayish red (10YR 7/4) and pale yellowish brown (10YR 6/2); weathers moderate yellowish brown (10YR 5/4) to dusky yellowish brown (10YR 2/2). Very fine to finely crystalline. Bottom .5 ft has angular clasts of limestone, Johnnie siltstone and chert, .5-5 cm long. Slight imbrication developed in clasts. Sandy calcareous cement. Highly fractured; hackly weathering. Forms a light colored ledge easily identifiable from a distance.

8 ft

Offset in section; Units 3 & 4 meas. 1 mile to north

Unit 23: Dolomitic sandstone

Dolomitic sandstone. Pale yellowish brown (10YR 6/2); weathers same plus moderate yellowish brown (10YR 5/4). Thinly bedded. Fissile, phyllitic cleavage, somewhat micaceous.

15.5 ft

Unit 22: Siltstone and Dolomitic Sandstone

Interstratified phyllitic siltstone, greenish gray (5GY 6/1) and dolomitic sandstone, pale reddish brown (10R 5/4). Interbeds a few inches thick every few feet. Siltstone very phyllitic; micaceous. Sandstone forms more resistant ribs.

122 ft

Unit 21: Phyllitic Siltstone

Phyllitic siltstone, greenish gray (5GY 6/1); weathers same; Fissile, micaceous.

37 ft

Unit 20: Phyllitic Siltstone

Phyllitic siltstone, greenish gray (5GY 6/1). 3 feet of dolostone; also 2 2-inch thick layers in base.

35 ft

Unit 19: Phyllitic Siltstone

Phyllitic siltstone. Moderate yellowish brown (10YR 5/4) to greenish gray (5GY 6/1) and pale olive (10Y 6/2); weathers same. Phyllitic cleavage well-developed, micaceous. Very small mafics (< .5 mm) throughout, probably goethite after pyrite. 10 feet of dolomitic sandstone.

14 ft

Unit 18: Phyllitic Siltstone

Phyllitic siltstone, greenish gray (5GY 6/1), fissile, micaceous. Some 1 cm thick pale reddish brown (10R 5/4) dolomitic quartzite layers near top of section.

65 ft

Unit 17: Dolomitic sandstone

Dolomitic sandstone, color grades from light brownish gray (5YR 6/1) at bottom of section to pale reddish brown (10R 5/4) at top of section. Fine grained quartz sand with ~ 10% mafics. Micaceous.

Unit 16: Dolomitic and Phyllitic Sandstone

Interbedded dolomitic sandstone and phyllitic sandstone; similar to unit 15; with a higher percentage sandstone.

47.5 ft

Unit 15: Phyllitic Siltstone and Dolomitic Sandstone

Interbedded phyllitic siltstone and dolomitic sandstone. Light olive gray (5Y 6/1); weathers grayish red (10YR 7/4) and dark yellowish red (10YR 6/6). Thinly bedded at top and thick at bottom.

60 ft

Unit 14: Phyllitic Siltstone

Phyllitic siltstone, greenish gray (5GY 6/1). Well-developed phyllitic cleavage; micaceous, fissile, poorly resistant.

9 ft

Unit 13: Dolomitic Quartzite

Dolomitic quartzite. Grayish red (10YR 7/4); weathers same plus minor amounts of dark yellowish red (10YR 6/6). Very fine grained quartz sand. Laminated to thinly bedded with some .5 ft intervals with no bedding. Top more fissile, breaks into tabular blocks along random planes. Generally more resistant than green siltstone, often forms resistant ribs. A few phyllitic units ~2 inches thick.

27 ft

THICKNESS OF UNIT 3

630 ft

Johnnie Formation - Unit 2**Unit 12: Phyllitic Siltstone**

Phyllitic siltstone. Light greenish gray (5GY 8/1); weathers greenish gray (5GY 6/1) to moderate brown (5YR 3/4). Fissile; well-developed phyllitic cleavage. .25-.5 mm pyrite common throughout, similar to unit 7. Unit as a whole weathers to form a dark brown slope.

110 ft

Unit 11: Phyllitic Siltstone

Phyllitic siltstone, medium gray (N5); weathers same. Fissile to blocky cleavage; more resistant than surrounding sections; small pyrite common throughout, similar to unit 7.

33.5 ft

Unit 10: Phyllitic Siltstone

Phyllitic siltstone, brownish gray (5YR 4/1); weathers same. Fissile, slope former, similar to unit 7.

65 ft

Unit 9: Phyllitic Siltstone

Phyllitic siltstone, medium gray (N5); weathers grayish brown (5YR 3/2). Fissile, slope former, similar to unit 7.

15 ft

Unit 8: Phyllitic Siltstone

Phyllitic siltstone, dark greenish gray (5GY 4/1); weathers grayish brown (5YR 3/2). Fissile, slope former, similar to unit 7.

90 ft

Unit 7: Phyllitic Siltstone

Phyllitic siltstone. Dark greenish gray (5GY 4/1) to moderate brown (5YR 4/4). Thinly laminated; beds often widely separated (~.3 m). Fissile to blocky fracture. Pyrite .3-1 mm common. Some thin shaley intervals; 1- 2 inches thick, more fissile than siltstone.

95.5 ft

THICKNESS OF UNIT 2

409 ft

Johnnie Formation - Unit 1**Unit 6: Dolomitic sandstone and Dolomite**

Dolomitic sandstone (65%) and dolomite (35%). Dolomitic sandstone medium gray (N5); weathers moderate yellowish brown (10YR 5/4). Very fine grained quartz sand. Dolomite medium gray (N5); weathers olive gray (5Y 4/1). Finely crystalline, hackly fracture. Forms a darker ledge within less resistant siltstone beds.

22 ft

Unit 5: Phyllitic Siltstone

Phyllitic siltstone. Medium gray (N5); weathers same plus medium yellowish brown (10YR 5/4). Very fissile; poorly resistant, slope former. 2-3 interbeds of moderate yellowish brown (10YR 5/4) dolostone; .3-.5 feet thick, near top of section.

25 ft

Unit 4: Phyllitic Siltstone

Phyllitic siltstone; greenish gray (5Y 6/1) interbedded with light greenish gray (5Y 8/1) and dusky brown (5YR 2/2)

layers; weathers same. Fissile, slope former.

70 ft

Unit 3: Phyllitic Siltstone

Phyllitic siltstone. Light greenish gray (5Y 8/1) and greenish gray (5Y 6/1); weathers same plus dusky brown (5YR 2/2) and dark yellowish red (10YR 5/6). Very fissile.

100 ft

Unit 2: Phyllitic Siltstone

Phyllitic siltstone. Light greenish gray (5Y 8/1); also bluish white (5B 9/1) and pale pink (5RP 8/2); weathers pale red (5R 6/2), moderate red (5R 5/4) and dark yellowish red (10YR 5/6). Bedding indistinct in outcrop; float with medium laminations found. Breaks randomly; poorly resistant, slope-former. Cast of pyrite (1 mm) common. Reddish beds less common in upper 25 feet.

105 ft

Unit 1: Dolostone and Siltstone

Interbedded dolomite (70%) and siltstone (30%). Dolostone medium gray (N5); weathers pale yellowish brown (10YR 6/2) to grayish red (10YR 6/4). Finely crystalline. Forms resistant ledges. Siltstone yellowish gray (5Y 7/2); weathers pale olive (10Y 6/2) and light brown (5 YR 5/6). Micaceous to mildly phyllitic; cleaves randomly. Weathers to form slope; poorly exposed.

100 ft

THICKNESS OF UNIT 1

422 ft

TOTAL THICKNESS OF JOHNNIE

2182 ft

Noonday Dolomite

Unit 4: Dolomite

Dolomite, medium light gray (N6) to medium gray (N5); weathers pale yellowish orange (10YR 8/6) plus same. Finely crystalline; indistinctly laminated, generally structureless. Hackly fracture; weathers to form prominent light-colored cliff. Lenses and stringers of quartz throughout.

305 ft

Unit 3: Dolomitic Siltstone

Dolomitic siltstone, yellowish gray (5Y 7/2) to pale olive (10Y 6/2); weathers same plus light brown (5YR 5/6). Micaceous, somewhat fissile, breaks randomly. Forms a less resistant darker band within the lighter colored dolomite.

3.5 ft

Unit 2: Dolomite

Dolomite, medium dark gray (N4), weathers same plus dark yellowish red (10YR 6/6) from Fe-discoloration. Thinly laminated, beds 1 mm or less in thickness; convoluted. Fissile near contact with siltstone; blocky; breaks randomly. 10% moderate yellowish brown (10YR 5/4) very fine grained dolomitic sandstone.

55 ft

Unit 1: Dolomite

unmeasured

**TOTAL THICKNESS OF NOONDAY DOLOMITE
(INCOMPLETE)**

363.5 ft

SPRING MOUNTAINS HILL 1152T
(4/96)

Stirling Quartzite - A Member (unmeasured)

Unit 1: Quartzite

Pale red (5R 6/2) coarse-grained quartzite, weathers pale red (10R 6/2). Medium to thickly bedded. Pebbles up to 3 cm occur locally.

Unmeasured

Johnnie Formation - Unit 4

Unit 8: Quartzite

Pale red (10R 6/2), weathers same or grayish red (10R 4/2). Interbedded coarse-grained sandstone and conglomerate. Beds 0.3 to 1.5 m thick; massive. Conglomerate contains granule to pebble size clasts up to 20 mm, including vein quartz (80-90%), lithics (feldspathic granitic rocks), jasper, and large purple shale rip-up clasts (less common higher in section).

3 m

FAULT IN SECTION

Unit 7: Quartzite

Interbedded quartzite and siltstone. Quartzite is white (N9) to very light gray (N8), weathers pinkish gray (5YR 8/1). Coarse-grained, form discontinuous beds. Similar in appearance to Unit 1 of overlying Stirling Quartzite. Siltstone is grayish green (5G 5/2), weathers grayish green (10G 4/2) to dark yellowish brown (10YR 4/2) (desert varnish). Fine to very fine grained sandstone is greenish gray (5GY 6/1), weathers dark greenish gray (5G 4/1). Contains asymmetrical ripple marks.

11 m

Unit 6: Quartzite

Pale red (10R 6/2), weathers same or grayish red (10R 4/2). Interbedded coarse-grained sandstone and conglomerate. Beds 0.3 to 1.5 m thick; massive. Conglomerate contains granule to pebble size clasts up to 20 mm, including vein quartz (80-90%), lithics (feldspathic granitic rocks), jasper, and large purple shale rip-up clasts (less common higher in section).

2 m

Unit 5: Quartzite

Interbedded fine grained sandstone and coarse siltstone. Grayish red purple (5RP 4/2); weathers grayish red (10R 4/2) with very dusky red desert varnish (10R 2/2). Several coarse sandstone beds similar in appearance to Unit 4.

21.5 m

Unit 4: Quartzite Conglomerate

Pale red (10R 6/2), weathers same or grayish red (10R 4/2). Interbedded coarse-grained sandstone and conglomerate. Beds 0.3 to 1.5 m thick; massive. Grading not apparent. Conglomerate contains granule to pebble size clasts up to 20 mm, including vein quartz (80-90%), lithics (feldspathic granitic rocks), jasper, and large purple shale rip-up clasts (less common higher in section).

37.5 m

Unit 3: Quartzite

Interbedded fine-grained sandstone and siltstone. Sandstone is grayish red (10R 4/2); weathers dark reddish brown (10R 3/4). Fine grained, moderate to thickly bedded; locally laminated within beds. Low angle truncations, load casts, rip-up mounds common. Siltstone is medium purple (5P 5/2); weathers grayish purple (5P 4/2). Parallel laminations. Beds become 50% sandstone 50% siltstone in upper 2/3 of unit. Fault in section; upper part of unit measured along strike 50 m across valley.

± 86 m

Unit 2: Quartzite

Grayish red (10R 4/2); weathers dark reddish brown (10R 3/4). Fine grained sandstone, moderate to thickly bedded. Locally laminated within beds.

7 m

Unit 1: Oolitic limestone (Johnnie Oolite)

Very pale orange (10YR 8/2), weathers grayish orange (10YR 7/4). Coarse grained (1 mm) oolitic grainstone. Thin, indistinct bedding. Pelletal material near base.

1.5 m

TOTAL THICKNESS OF UNIT 4

169.5 m

SPRING MOUNTAINS HILL 1314T
(2/97)

Stirling Quartzite - A Member (unmeasured)

Unit 1: Quartzite

Massive very light gray crystalline quartzite with 1.5 m of maroon and purple Stirling Quartzite bedded on a 1-3 cm scale at base.

Unmeasured

Johnnie Formation

Unit 11: Limestone and Siltstone

Orange limestone, some of it flat-pebble conglomerate, and siltstone. Upper 1 m is covered.

7.5 m

Unit 10: Siltstone

Brown laminated siltstone; brown, dark gray, and light gray siltstone at base; brown and light gray layers are fine while the dark gray layers contain silty quartzite; 2-10 mm laminations.

9 m

Unit 9: Siltstone

Blue fissile siltstone; fine grained with sub-millimeter dark spots (quartzose?); 2 mm parallel laminations; cm-scale partings; 15 cm layer of limestone flat-pebble conglomerate at top; fine pink quartzose siltstone weathering tan and heavily varnished at base.

7 m

Unit 8: Siltstone

Platy fissile purple siltstone capped by 50 cm yellow-brown siltstone and at least a few centimeters of thin-bedded pinkish limestone.

2 m

Unit 7: Limestone

Pink-purple platy limestone.

2 m

Unit 6: Siltstone and Fine Sandstone

Platy fissile purple siltstone and fine sandstone; at top, fine pink quartzose siltstone with fine parallel laminations and weathering maroon.

25.5 m

Unit 5: Limestone and Fine Sandstone

Purple limestone and fine sandstone with increasing fine sandstone upsection; 10-20 cm beds.

21 m

Unit 4: Fine Sandstone

Fine sandstone with parallel laminations; 35 cm layers.

1 m

Unit 3: Limestone

Foliated pink-purple limestone.

1 m

Unit 2: Fine Sandstone

Purple fine sandstone; some platy purple siltstone at top; 30 cm limestone layer 6 m above base; 15 cm pink-purple limestone layer 1.5 m above base.

9 m

Unit 1: Oolitic limestone (Johnnie Oolite)

Grayish orange oolitic limestone coarsening upward.

1.5 m

TOTAL MEASURED THICKNESS

97 m

APPENDIX 2 - B DESCRIPTION OF STABLE ISOTOPE DATA

One hundred and six core samples were collected from the Noonday Dolomite, Johnnie Formation, and basal Stirling Quartzite in the southern Nopah Range, California. Samples were collected at five to ten meter intervals through nine hundred and thirty-three meters of section. Carbonate whole rock isotopic analyses were performed using the conventional phosphoric acid method for generating CO₂ gas (McCrea, 1950). Samples were measured on a Varian MAT250 gas ionization mass spectrometer. Reproducibilities were better than 0.1‰ for δ¹³C and 0.2‰ for δ¹⁸O. Results were determined using standards calibrated against NBS-19 (δ¹³C=+1.92‰, δ¹⁸O=-2.20‰ vs. Peedee Belemnite (PDB); Coplen, Kendall & Hopple, 1983). Standard dissolution times were 24 h at 28 °C for samples with < 10 mol % dolomite, and 48 h for all others. Appendix 2-C lists measured δ¹³C and δ¹⁸O values relative to PDB, and Figure 2-10 shows carbon and oxygen isotope profiles from carbonate rocks.

Carbon isotope values ranged between -10.65‰ and +2.89‰ (vs. PDB). Values from the lower 201m of the section cluster tightly around a mean of -2.84‰ with a standard deviation of 0.28‰. These samples were collected in the informally defined algal dolomite member of the Noonday Formation (Hazard, 1937). Samples from the overlying sandy dolomite member (207.5-341.5 meters) and from the lower part of the Johnnie Formation (347.5-403.0 meters) range from -4.10‰ to -0.56‰, and stratigraphically adjacent samples vary by as much as 1‰. From 409 to 490 meters, δ¹³C values show a marked enrichment from -2.98‰ to +2.06‰. Overall, three positive and one negative sample were collected from a stratigraphic interval that spans 56m. The positive excursion is overlain by a 187m interval with δ¹³C values ranging from -2.33‰

to -0.10‰ with an outlier at -7.33‰ . Some stratigraphically adjacent values vary by as much as $1\text{-}2\text{‰}$. This negative interval is overlain by a 128m interval of generally positive values which range from -0.57‰ to $+2.89\text{‰}$. The stratigraphically lowest positive value in this interval occurs 72.5 meters below the oolitic marker bed in the Rainstorm Member, and the stratigraphically highest positive value occurs 55 meters above the marker bed. The maximum $\delta^{13}\text{C}$ value from the Noonday-Johnnie interval occurs 6m below the oolitic marker bed. The largely positive interval near the top of the Johnnie formation is overlain by a strongly negative interval which begins about 10m below the Johnnie-Stirling contact and includes at least the lower 75m of the Stirling Quartzite. $\delta^{13}\text{C}$ values in this interval range from -10.65 to -3.85 with a cluster of values from -9.44 to -8.36 in the lower 35m of the Stirling Quartzite.

$\delta^{18}\text{O}$ values ranged between -14.88‰ and -2.34‰ (vs. PDB). Values in the Noonday Formation generally increase from about -7.9‰ at the base to -5.5‰ about 75m below the top. Values decrease in overlying rocks to a low of about -9.5‰ about 60m above the base of the Johnnie Formation. In the interval of $\delta^{13}\text{C}$ enrichment from 409 to 490 meters, $\delta^{18}\text{O}$ values also increase to a maximum of -5.39‰ . In the remainder of the Johnnie Formation values range from -11.05 to -2.71 with stratigraphically adjacent values varying by as much as 5‰ . Near the Stirling-Johnnie contact, $\delta^{18}\text{O}$ values become markedly negative, correlate strongly with $\delta^{13}\text{C}$ ($r=.94$), and attain the minimum value for the traverse in the lowermost Stirling Quartzite.

APPENDIX 2 - C TABLE OF STABLE ISOTOPE DATA

SAMPLE#	height (ft)	$\delta^{13}\text{C}$	$\delta^{18}\text{O}$	COMMENTS
NRC 1	0	-2.56	-8.48	Base of Noonday Dolomite
NRC 2	20	-2.60	-7.70	
NRC 3	40	-1.76	-7.39	
NRC 4	60	-2.70	-7.85	
NRC 5	80	-2.57	-7.33	
NRC 6	100	-2.82	-8.00	
NRC 7	120	-2.57	-7.68	
NRC 8	140	-3.12	-7.75	
NRC 9	160	-2.77	-7.09	
NRC 10	180	-2.83	-6.88	
NRC 11	200	-2.80	-7.20	
NRC 12	220	-2.35	-6.91	
NRC 13	240	-2.93	-7.62	
NRC 14	260	-2.92	-7.02	
NRC 15	280	-3.14	-7.59	
NRC 16	280	-2.98	-7.56	
NRC 17	300	-2.97	-7.66	
NRC 18	320	-2.91	-7.45	
NRC 19	340	-2.65	-7.64	
NRC 20	360	-2.82	-7.70	
NRC 21	380	-3.22	-8.77	
NRC 22	400	-2.99	-8.06	
NRC 23	420	-3.13	-7.56	
NRC 24	440	-3.14	-7.68	
NRC 25	460	-3.03	-7.74	
NRC 26	480	-2.63	-6.83	
NRC 27	500	-3.04	-7.85	
NRC 28	520	-2.83	-7.19	
NRC 29	540	-2.94	-6.89	
NRC 30	560	-2.92	-7.29	
NRC 31	580	-3.13	-7.05	
NRC 32	600	-2.79	-6.73	
NRC 33	620	-3.30	-7.78	
NRC 34	640	-2.94	-7.29	
NRC 35	660	-2.68	-6.43	
NRC 36	680	-2.79	-7.15	Sandy dolomite marker bed
NRC 37	700	-2.25	-7.02	
NRC 38	720	-2.64	-6.98	
NRC 39	740	-2.70	-6.32	
NRC 40	760	-3.02	-5.67	
NRC 41	780	-4.10	-8.95	
NRC 42	800	-3.50	-6.67	

SAMPLE#	height (ft)	$\delta^{13}\text{C}$	$\delta^{18}\text{O}$	COMMENTS
NRC 43	820	-2.79	-6.63	
NRC 44	840	-2.75	-6.42	
NRC 45	860	-2.81	-5.99	
NRC 46	880	-1.12	-5.03	
NRC 47	900	-0.91	-2.34	
NRC 48	920	-2.79	-6.40	
NRC 49	940	-1.07	-5.96	
NRC 50	960	-1.84	-5.11	
NRC 51	980	-2.49	-5.74	
NRC 52	1000	-1.32	-5.64	
NRC 53	1020	-2.35	-6.29	
NRC 54	1040	-1.26	-5.91	Oölites
NRC 55	1060	-2.22	-6.79	
NRC 56	1080	-2.66	-5.94	
NRC 57	1100	-1.08	-6.22	
NRC 58	1120	-2.34	-5.65	
NRC 59	1140	-0.56	-6.07	Base of Johnnie Formation
NRC 60	1155	-2.11	-8.33	Sandy-dolomitic member of Johnnie Fm
NRC 61	1175	-3.46	-10.38	
NRC 62	1260	-2.44	-9.41	
NRC 63	1280	-2.92	-10.35	
NRC 64	1302	-3.16	-9.04	
NRC 65	1322	-1.68	-7.29	
NRC 66	1342	-2.98	-9.65	
NRC 67	1362	-1.46	-6.29	
NRC 68	1382	-1.10	-7.16	
NRC 69	1402	-0.23	-7.17	Quartzite member
NRC 70	1422	0.27	-6.07	
NRC 71	1442	-0.03	-5.39	
NRC 72	1597	2.33	-7.29	
NRC 73	1607	2.06	-7.48	
NRC 74	1657	-0.10	-7.45	
NRC 75	1697	-1.91	-10.94	
NRC 76	1857	-1.15	-7.76	
NRC 77	1927	-0.40	-7.93	
NRC 78	1947	-1.68	-8.15	
NRC 79	1960	-0.52	-7.19	
NRC 80	1965	-0.60	-8.91	
NRC 81	1975	-2.33	-7.27	Top of Quartzite member
NRC 82	2270	-7.33	-6.99	Rainstorm Member
NRC 83	2320	2.84	-8.29	
NRC 84	2368	0.06	-4.47	
NRC 85	2403	-0.35	-7.26	
NRC 86	2463	0.21	-8.16	
NRC 87	2483	-0.57	-7.69	
NRC 88	2518	1.60	-6.02	

SAMPLE#	height (ft)	$\delta^{13}\text{C}$	$\delta^{18}\text{O}$	COMMENTS
NRC 89	2538	2.89	-8.06	
NRC 90	2558	1.66	-10.84	
NRC 91	2593	2.77	-6.60	Johnnie Oölite
NRC 92	2613	1.95	-9.47	
NRC 93	2633	2.04	-6.16	
NRC 94	2653	0.16	-11.05	
NRC 96	2738	0.59	-2.71	
NRC 97	2783	-3.86	-7.90	Base of Stirling Quartzite
NRC 98	2788	-4.54	-8.90	
NRC 99	2818	-8.80	-11.20	
NRC 100	2833	-10.65	-14.88	
NRC 101	2853	-8.36	-12.56	
NRC 102	2866	-9.44	-14.12	
NRC 103	2916	-8.80	-12.91	
NRC 104	2931	-8.93	-14.03	
NRC 106	3061	-3.85	-9.52	

REFERENCES

- Aitken, J. D., 1991, Two late Proterozoic glaciations, Mackenzie Mountains, northwestern Canada: *Geology*, v. 19, no. 5, p. 445-448.
- Alvarez, L. W., Alvarez, W., Asaro, F., Michel, H.V., 1980, Extraterrestrial cause for the Cretaceous Tertiary extinction, *Science*, 208 (4448), p. 1095-1108.
- Benn, Douglas I., and Evans, David J.A., 1998, *Glaciers and Glaciation*: New York, John Wiley and Sons, Inc., 734 p.
- Benus, Alison P., 1988, Sedimentological context of a deep-water Ediacaran fauna (Mistaken Point Formation, Avalon Zone, eastern Newfoundland), *in* Landing, Ed, Narbonne, Guy M., Myrow, Paul Michael, eds., Trace fossils, small shelly fossils, and the Precambrian-Cambrian boundary: *Bulletin - New York State Museum*, v. 463, p. 8-9.
- Burchfiel, B. C., and Davis, Gregory A., 1972, Structural framework and evolution of the southern part of the Cordilleran orogen, western United States: *American Journal of Science*, v. 272, no. 2, p. 97-118.
- Charlton, Rebecca L., Wernicke, Brian P., and Abolins, Mark J., 1997, A major Neoproterozoic incision event in the Johnnie Formation, southwestern Great Basin: *Geological Society of America Abstracts*, v. 29, no. 6, p. 197.

Christie-Blick, Nicholas, 1997, Messinian-style drawdown model supported by new results from the Wonoka Canyons (terminal Proterozoic), south Australia: Geological Society of America Abstracts, v. 29, no. 6, p. 197.

Christie-Blick, Nicholas, Dyson, Ian A., von der Borch, C. C., 1995, Sequence stratigraphy and the interpretation of Neoproterozoic Earth history, *in* Knoll, Andrew H., and Walter, Malcolm, eds., Neoproterozoic stratigraphy and Earth history: Precambrian Research, v. 73 (1-4), p. 3-26.

Cloud, P. E., Jr., and Semikhatov, M. A., 1969, Proterozoic stromatolite zonation: American Journal of Science, v. 267 (9), p. 1017-1061.

Coplen, Tyler B., Kendall, Carol, and Hople, Jessica, 1983, Comparison of stable isotope reference samples: Nature, v. 302, no. 5905, p. 236-238.

Courtillot, V., Jaeger, J. J., Yang, Z., Feraud, G., and Hofmann, C., 1996, The influence of continental flood basalts on mass extinctions; where do we stand? *in* Ryder, Graham, Fastovsky, David, and Gartner, Stefan, eds., The Cretaceous-Tertiary event and other catastrophes in Earth history: Geological Society of America Special Paper 307, p. 513-525.

Crittenden, Max D., Jr., Schaeffer, Frederick E., Trimble, D. E., and Woodward, Lee A., 1971, Nomenclature and correlation of some upper Precambrian and basal Cambrian sequences in western Utah and southeastern Idaho: Geological Society of America Bulletin, v. 82, no. 3, p. 581-601.

- Crittenden, M.D., Jr., and Wallace, C.A., 1973, Possible equivalents of the Belt Supergroup in Utah, *in* Belt Symposium: Idaho Bureau of Mines and Geology Special Report 2-3, v. 1, p. 116-138.
- Dalziel, Ian W. D., 1997, Neoproterozoic-Paleozoic geography and tectonics; review, hypothesis, environmental speculation: Geological Society of America Bulletin, v. 109, no. 1, p. 16-42.
- Eisbacher, G. H., 1985, Late Proterozoic rifting, glacial sedimentation, and sedimentary cycles in the light of Windermere deposition, western Canada, *in* Deynoux, Max, ed., Glacial record: Palaeogeography, Palaeoclimatology, Palaeoecology, v. 51, no. 1-4, p. 231-254.
- Glaessner, Martin F., 1984, The dawn of animal life; a biohistorical study: Cambridge, Cambridge University Press, 244 p.
- Grotzinger, John P., Bowring, Samuel A., Saylor, Beverly Z., and Kaufman, Alan J., 1995, Biostratigraphic and geochronologic constraints on early animal evolution: Science, v. 270, no. 5236, p. 598-604.
- Guerrot, C., and Peucat, J. J., 1990, U-Pb geochronology of late Proterozoic Cadomian Orogeny in the northern Armorican Massif, France, D'Lemos, R. S., Strachan, R. A., and Topley, C. G., eds., The Cadomian Orogeny: Geological Society Special Publications 51, p. 13-26.

- Hambrey, Michael J., and Harland, W. B., 1985, The late Proterozoic glacial era, *in* Deynoux, Max, ed., *Glacial record: Palaeogeography, Palaeoclimatology, Palaeoecology*, v. 51, no. 1-4, p. 255-272.
- Harland, Walter Brian, 1964, Evidence of late Precambrian glaciation and its significance, *in* Nairn, A. E. M., ed., *Problems in palaeoclimatology*, p. 119-149.
- Hazzard, John C., 1937, Paleozoic section in the Nopah and Resting Springs Mountains, Inyo County, California: *California Journal of Mines and Geology*, v. 33, no. 4, p. 270-339.
- Heaman, L. M., and Grotzinger, J. P., 1992, 1.08 Ga diabase sills in the Pahrump Group, California; implications for development of the Cordilleran Miogeocline: *Geology*, v. 20, no. 7, p. 637-640.
- Hildebrand, Alan R., Penfield, Glen T., Kring, David A., Pilkington, Mark, Camargo Z., Antonio, Jacobsen, Stein B., and Boynton, William V., 1991, Chicxulub Crater; a possible Cretaceous/Tertiary boundary impact crater on the Yucatan Peninsula, Mexico: *Geology*, v. 19, no. 9, p. 867-871.
- Hoffman, Paul F., 1991, Did the breakout of Laurentia turn Gondwanaland inside-out? *Science*, v. 252, no. 5011, p. 1409-1412.
- Hoffman, Paul F., Halverson, Galen P., Kaufman, Alan J., and Soffer, Gaddy, 1998, Snowball Earth and Neoproterozoic Stratigraphy, *Eos*, v. 79, no. 17, p. 50.

- Hofmann, H. J., Narbonne, Guy M., Aitken, J. D., 1990, Ediacaran remains from intertillite beds in northwestern Canada: *Geology*, v. 18, no. 12, p. 1199-1202.
- Horodyski, Robert J., 1991, Late Proterozoic megafossils from southern Nevada: *Geological Society of America Abstracts*, v. 23, no. 6, p. 163.
- Kaufman, Alan J., Knoll, Andrew H., and Narbonne, Guy M., 1997, Isotopes, ice ages, and terminal Proterozoic earth history: *Proceedings of the National Academy of Sciences*, v. 94, p. 6600-6605.
- Kennedy, Martin J., 1996, Stratigraphy, sedimentology, and isotopic geochemistry of Australian Neoproterozoic postglacial cap dolostones; deglaciation, $\delta^{13}\text{C}$ excursions, and carbonate precipitation: *Journal of Sedimentary Research, Section B; Stratigraphy and Global Studies*, v. 66, no. 6, p. 1050-1064.
- Kimura, Hiroto, Matsumoto, Ryo, Kakuwa, Yoshitaka, Hamdi, Bahaeddin, and Zibaseresht, Hamid, 1997, The Vendian-Cambrian $\delta^{13}\text{C}$ record, North Iran; evidence for overturning of the ocean before the Cambrian explosion: *Earth and Planetary Science Letters*, v. 147, no. 1-4, p. E1-E7.
- Kirschvink, Joseph L., 1992, Late Proterozoic low-latitude global glaciation; the snowball Earth, *in* Schopf, J. William, and Klein, Cornelis, eds., *The Proterozoic biosphere; a multidisciplinary study*, p. 51-52.

Kirschvink, Joseph L., Ripperdan, Robert L., and Evans, David A., 1997, Evidence for a large-scale reorganization of Early Cambrian continental masses by inertial interchange true polar wander: *Science*, v. 277, no. 5325, p. 541-545.

Knoll, A. H., Bambach, R. K., Canfield, D. E., and Grotzinger, J. P., 1996, Comparative Earth history and Late Permian mass extinction: *Science*, v. 273, no. 5274, p. 452-457.

Knoll, Andrew H., Hayes, J. M., Kaufman, A. J., Swett, K., and Lambert, I. B., 1986, Secular variation in carbon isotope ratios from upper Proterozoic successions of Svalbard and East Greenland: *Nature*, v. 321, no. 6073, p. 832-838.

Kump, Lee R., 1991, Interpreting carbon-isotope excursions; Strangelove oceans: *Geology*, v. 19, no. 4, p. 299-302.

Lanphere, Marvin A., 1964, Geochronologic studies in the eastern Mojave Desert, California: *Journal of Geology*, v. 72, no. 4, p. 381-399.

Levy, Marjorie, and Christie-Blick, Nicholas, 1991, Tectonic subsidence of the early Paleozoic passive continental margin in eastern California and southern Nevada: *Geological Society of America Bulletin*, v. 103, no. 12, p. 1590-1606.

Levy, Marjorie, Christie-Blick, Nicholas, and Link, Paul Karl, 1994, Neoproterozoic incised valleys of the eastern Great Basin, Utah and Idaho; fluvial response to changes in depositional base level, *in* Dalrymple, Robert W., Boyd, Ron, and Zaitlin, Brian

A., eds., Incised-valley systems; origin and sedimentary sequences: SEPM (Society for Sedimentary Geology) Special Publication 51, p. 369-382.

Link, Paul Karl, 1983, Glacial and tectonically influenced sedimentation in the upper Proterozoic Pocatello Formation, southeastern Idaho, *in* Miller, David M., Todd, Victoria R., and Howard, Keith A., eds., Tectonic and stratigraphic studies in the eastern Great Basin: Geological Society of America Memoir 157, p. 165-181.

Martinsen, Ole J., Martinsen, Randi S., and Steidtmann, James R., 1993, Mesaverde Group (Upper Cretaceous), southeastern Wyoming; allostratigraphy versus sequence stratigraphy in a tectonically active area: American Association of Petroleum Geologists Bulletin, v. 77, no. 8, p. 1351-1373.

McCrea, J. M., 1950, On the isotopic chemistry of carbonate and a paleo-temperature scale: Journal of Chemical Physics, v. 18, p. 849-857.

Miller, Julia M. G., 1982, Kingston Peak Formation in the southern Panamint Range; a glacial interpretation, *in* Cooper, John D., Troxel, Bennie W., and Wright, Lauren A., eds., Geology of selected areas in the San Bernardino Mountains, western Mojave Desert, and southern Great Basin, California, p. 155-164.

Miller, Julia M. G., 1985, Glacial and syntectonic sedimentation; the upper Proterozoic Kingston Peak Formation, southern Panamint Range, eastern California: Geological Society of America Bulletin, v. 96, no. 12, p. 1537-1553.

- Miller, Julia M. G., 1987, Paleotectonic and stratigraphic implications of the Kingston Peak-Noonday contact in the Panamint Range, eastern California: *Journal of Geology*, v. 95, no. 1, p. 75-85.
- Narbonne, Guy M., 1994, New Ediacaran fossils from the Mackenzie Mountains, northwestern Canada: *Journal of Paleontology*, v. 68, no. 3, p. 411-416.
- Park, John K., 1997, Paleomagnetic evidence for low-latitude glaciation during deposition of the Neoproterozoic Rapitan Group, Mackenzie Mountains, N.W.T., Canada: *Canadian Journal of Earth Sciences*, v. 34, no. 1, p. 34-49.
- Posamentier, Henry W., Jervey, M. T., and Vail, Peter R., 1988, Eustatic controls on clastic deposition; I, Conceptual framework, *in* Wilgus, Cheryl K., Hastings, Bruce S., Ross, Charles A., Posamentier, Henry W., Van Wagoner, John, Kendall, and Christopher G. St. C., eds., *Sea-level changes; an integrated approach*: Society of Economic Paleontologists and Mineralogists Special Publication 42, p. 109-124.
- Renne, Paul R., Zhang Zichao, Richards, Mark A., Black, Michael T., and Basu, Asish R., 1995, Synchrony and causal relations between Permian-Triassic boundary crises and Siberian flood volcanism: *Science*, v. 269, no. 5229, p. 1413-1416.
- Runnegar, Bruce, Gehling, James G., Horodyski, Robert J., Jensen, Soren, and Knauth, L. Paul, 1995, Base of the Sauk Sequence is a global eustatic event that lies just above the Precambrian-Cambrian boundary: *Geological Society of America Abstracts*, v. 27, no. 6, p. 330.

- Schmidt, Phillip W., and Williams, George E., 1995, The Neoproterozoic climatic paradox; equatorial palaeolatitude for Marinoan Glaciation near sea level in South Australia: *Earth and Planetary Science Letters*, v. 134, no. 1-2, p. 107-124.
- Sepkoski, J. John, Jr., 1995, Recoveries of global biodiversity after mass extinctions: *Geological Society of America Abstracts*, v. 27, no. 6, p. 165.
- Sepkoski, J. John, Jr., and Schopf, J. William, 1992, Biotic diversity and rates of evolution during Proterozoic and earliest Phanerozoic time, *in* Schopf, J. William (editor), and Klein, Cornelis, eds., *The Proterozoic biosphere; a multidisciplinary study*, p. 521-565.
- Sheehan, Peter M., and Watkins, Rodney, 1995, Ecologic recovery from the Ordovician extinction and a discussion of the Lipps-Signor effect, *Geological Society of America Abstracts*, v. 27, no. 6, p. 163.
- Smith, L. H., Kaufman, A. J., Knoll, A. H., and Link, P. K., 1994, Chemostratigraphy of predominantly siliciclastic Neoproterozoic successions; a case study of the Pocatello Formation and lower Brigham Group, Idaho, USA: *Geological Magazine*, v. 131, no. 3, p. 301-314.
- Sohl, Linda E., 1997, Paleomagnetic and stratigraphic implications for the duration of low-latitude glaciation in the late Neoproterozoic of Australia: *Geological Society of America Abstracts*, v. 29, no. 6, p. 195.

- Sokolov, Boris S., and Fedonkin, Michael A., 1986, Global biological events in the late Precambrian, *in* Walliser, Otto H., ed., Global bio-events; a critical approach: Lecture notes in Earth sciences, v. 8, p. 105-108.
- Stanistreet, Ian G., Kukla, Peter A., and Henry, George, 1991, Sedimentary basinal responses to a late Precambrian Wilson Cycle; the Damara Orogen and Nama Foreland, Namibia, *in* Eriksson, P. G., Callaghan, C. C., and Zawada, P. K., eds., Precambrian sedimentary basins of Southern Africa, *Journal of African Earth Sciences*, v. 13, no. 1, p. 141-156.
- Stewart, John H., 1970, Upper Precambrian and Lower Cambrian strata in the southern Great Basin, California and Nevada: U. S. Geological Survey Professional Paper 620, 206 p.
- Stewart, John H., 1972, Initial Deposits in the Cordilleran Geosyncline; evidence of a Late Precambrian (<850 m.y.) Continental Separation: *Geological Society of America Bulletin*, v. 83, no. 5, p. 1345-1360.
- Summa, Catherine L., 1993, Sedimentologic, stratigraphic, and tectonic controls of a mixed carbonate-siliciclastic succession; Neoproterozoic Johnnie Formation, Southeast California, unpublished doctoral dissertation: Massachusetts Institute of Technology.
- Thompson, M. D., Davidek, K. L., and Bowring, S. A., 1996, New U-Pb zircon age constraint on Neoproterozoic Varanger glaciation from Squantum "Tillite," Quincy, Massachusetts: *Geological Society of America Abstracts*, v. 28, no. 7, p. 493.

- Van Alstine, D. R., and Gillett, S. L., 1979, Paleomagnetism of upper Precambrian sedimentary rocks from the Desert Range, Nevada: *Journal of Geophysical Research*, v. 84, no. B9, p. 4490-4500.
- Vidal, Gonzalo, and Knoll, Andrew H., 1982, Radiations and extinctions of plankton in the late Proterozoic and Early Cambrian: *Nature*, v. 297, no. 5861, p. 57-60.
- Vidal, Gonzalo, and Moczydlowska-Vidal, Malgorzata, 1997, Biodiversity, speciation, and extinction trends of Proterozoic and Cambrian phytoplankton: *Paleobiology*, v. 23, no. 2, p. 230-246.
- Waggoner, Benjamin M., and Hagadorn, James W., 1997, Ediacaran fossils from western North America; stratigraphic and paleogeographic implications: *Geological Society of America Abstracts*, v. 29, no. 6, p. 30.
- Walker, J. Douglas, Klepacki, David W., and Burchfiel, B. C., 1986, Late Precambrian tectonism in the Kingston Range, Southern California: *Geology*, v. 14, no. 1, p. 15-18.
- Wickham, Stephen M., and Peters, Mark T., High $\delta^{13}\text{C}$ Neoproterozoic carbonate rocks in western North America: *Geology*, v. 21, no. 2, p. 165-168.
- Wright, L., Williams, E. G., and Cloud, P., 1978, Algal and cryptalgal structures and platform environments of the late pre-Phanerozoic Noonday Dolomite, eastern California: *Geological Society of America Bulletin*, v. 89, no. 3, p. 321-333.

Young, Grant M., 1992, Late Proterozoic stratigraphy and the Canada-Australia connection: *Geology*, v. 20, no. 3, p. 215-218.

CHAPTER 3

STRUCTURAL GEOLOGY

OF THE NORTHWESTERN SPRING MOUNTAINS, NV

INTRODUCTION

The Spring Mountains in Nevada and the Cottonwood Mountains in southeastern California are two stable range-blocks within a highly extended region. Each of the two ranges contains a fragment of the Cordilleran thrust belt, but the relationship between contractile structures in the two ranges remains controversial. Previous mapping (Burchfiel, 1965; Burchfiel and others, 1974; Burchfiel and others, 1983) showed that contractile structures in the northwestern Spring Mountains include overturned folds and a minor thrust. However, the northwestern Spring Mountains also contain high- and low-angle normal faults. Overprinting of contractile structures by extensional structures obscures the geometry and size of the contractile structures. As a result, the comparison of contractile structures in the northwestern Spring Mountains with structures in adjacent ranges is difficult, and correlations are uncertain.

To better understand contractile structures in the northwestern Spring Mountains, 170 km² of new mapping was completed at scales of 1:7,500 to 1:12,000. New mapping focused on the possibility that contractile structures are related to a significant thrust fault that has been omitted by normal faults. This hypothetical thrust fault was dubbed the “Kwichup Spring thrust” by Snow (1992), and figures prominently in the correlation of thrusts in the Specter Range and northwestern Spring Mountains with thrusts in the Cottonwood Mountains. According to Snow (1992), the Kwichup Spring thrust has a throw of more than 1.5 km, but no thrust of this size appears on existing geologic maps (Burchfiel, 1965; Burchfiel and others, 1983). If the Kwichup Spring thrust exists, the

thrust has been excised by normal faults. The extensional reactivation and excision of thrust faults is a common phenomena in the Basin and Range. As a result, new mapping also examined extensional structures to evaluate the possible excision of the Kwichup Spring thrust.

Structures described in this chapter are located between a pair of northwest-striking high-angle faults called the Rock Spring and Grapevine faults. These structures are shown in detail on Plate 1. (Please note that the key to Plate 1 is on Plate 2.) Structures southwest of the Grapevine fault were described by Burchfiel and others (1983) in their paper on the structural geology of the Montgomery Mountains. The structural geology of the area east of the Rock Spring fault is shown on Plate 2, and is described in the "Observation" section of Chapter 4. The relationship between structures in all three of these areas is discussed in Chapter 4. The stratigraphy of the northwestern Spring Mountains is discussed briefly below.

LITHOSTRATIGRAPHY

The stratigraphy of the northwestern Spring Mountains was described by Burchfiel (1964) and Burchfiel and others (1974), and is shown in Figure 3-1. The lower 3 km of section consists largely of terrigenous detrital units while the upper 3.7 km is largely carbonate. Within the terrigenous section, the Johnnie Formation, Stirling Quartzite, and Wood Canyon Formation are particularly relevant to structures in the northwestern Spring Mountains.

Johnnie Formation

The Johnnie Formation (Zj) is the stratigraphically lowest unit in the northwestern Spring Mountains, and consists primarily of siltstone with lesser amounts of quartzite and dolostone. The base of the Johnnie Formation is not exposed. In this study, the Johnnie Formation is divided into four informal units. The stratigraphy of the Johnnie Formation is shown in detail in Figure 3-2.

Figure 3-1. Stratigraphy of the northwestern Spring Mountains from Burchfiel and others (1974).

KEY

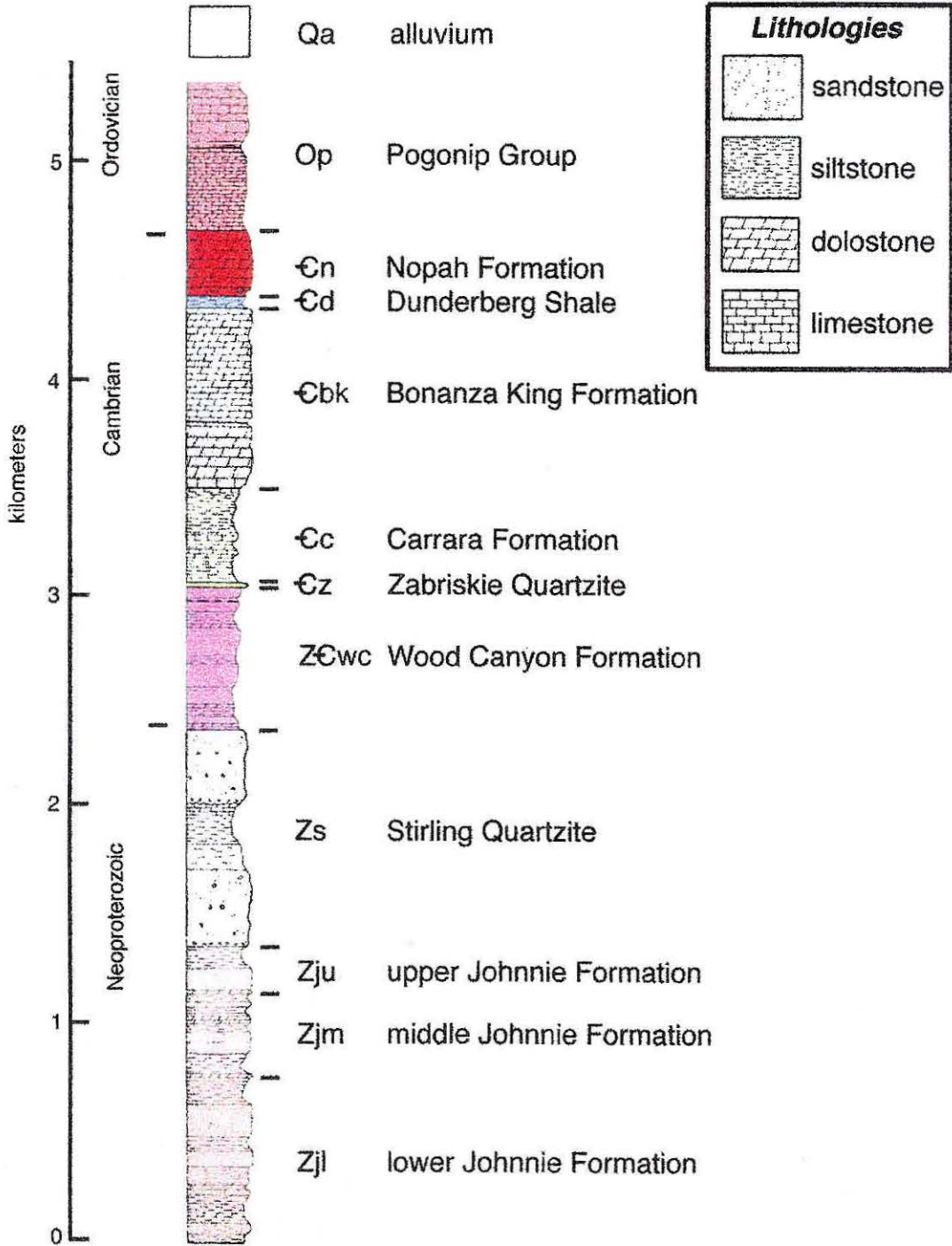
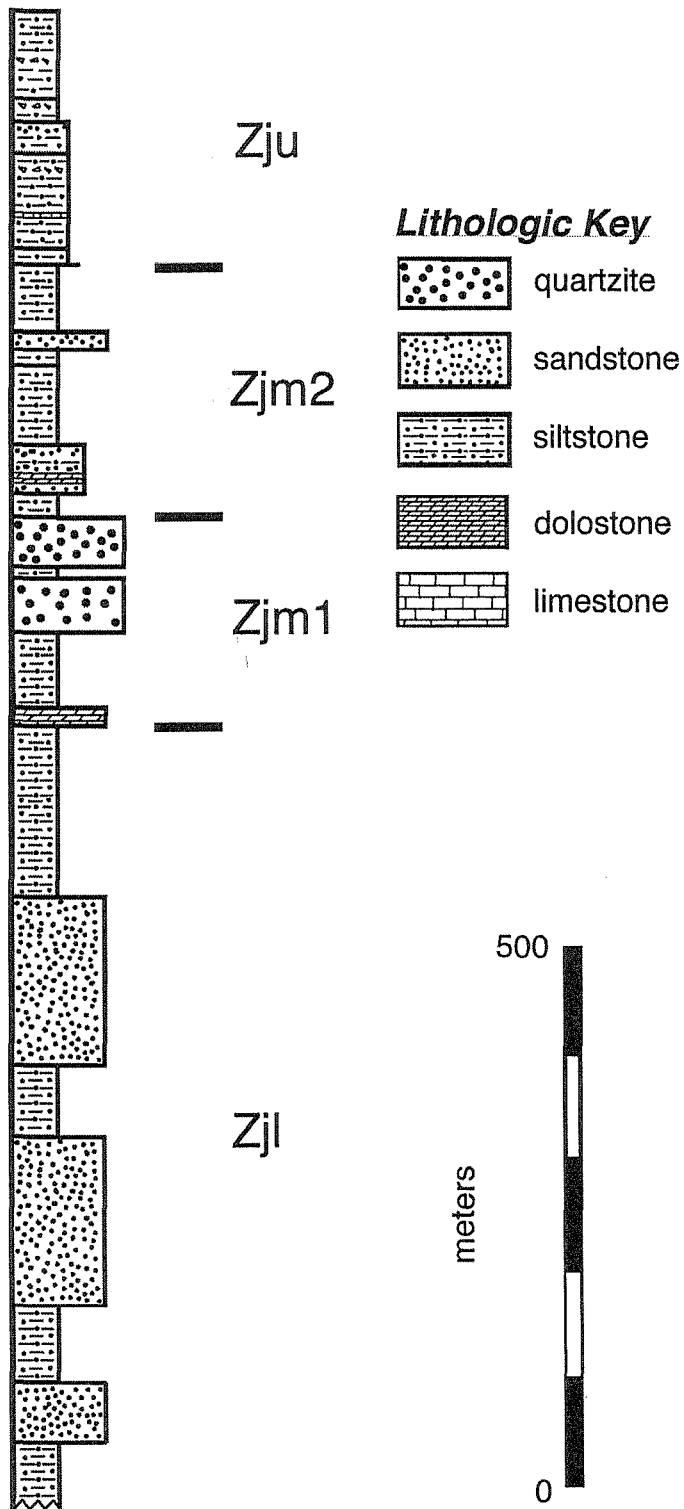


Figure 3-2. Stratigraphy of the Johnnie Formation. Units Zjl and Zjm1 adapted from Stewart (1970). Units Zjm2 and Zju from this study.



The lower Johnnie Formation (Zj1) consists of siltstone with lesser amounts of quartzite and sandstone, and is virtually free of carbonate. The contact between the lower and the middle Johnnie Formation is at the base of a distinctive 8 meter cherty dolostone which occurs throughout the northwestern Spring Mountains and Montgomery Mountains. The middle Johnnie Formation includes siltstone and thick intervals of quartzite at its base (Zjm1), and a mixture of siltstone, quartzite, and carbonate higher in the section (Zjm2). Medium quartzites in Zjm1 are lithologically almost indistinguishable from the Stirling Quartzite. The contact between Zjm1 and Zjm2 is placed at the top of the highest thick quartzite interval in Zjm1 and the lowest thick siltstone interval in Zjm2. Often, a layer or an interval of dolostone occurs near the base of Zjm2 within a few meters of the contact between Zjm1 and Zjm2. To better understand folding in the middle Johnnie Formation, Zjm1 and Zjm2 were each locally subdivided into five units: Zjm1a-e and Zjm2a-e.

The base of the upper Johnnie Formation is placed at the base of a distinctive grayish orange oolitic limestone marker bed. In most of the northwestern Spring Mountains, the marker bed is overlain by liver-colored fine sandstone and siltstone and limestone. Much of the limestone occurs as flat-pebble conglomerate. The liver-colored sediments are overlain by tan and light green siltstone just below the contact with the Stirling Quartzite. The upper Johnnie Formation thins from about 300 m in the southeastern part of the study area to about 100 m in northwestern exposures. In its most northerly exposures, the Johnnie Formation contains a conglomeratic unit (Zjc) which includes a lower conglomerate unit (Zjca) and an upper siltstone unit (Zjcb). Unit Zjc is probably an incised valley fill and correlates with the Conglomeratic member of Abolins and others (see Chapter 2).

Stirling Quartzite

Sub-units of the Stirling Quartzite were not mapped in this study. In the northwestern Spring Mountains, the Stirling Quartzite consists of upper and lower quartzitic units with a thin interval of siltstone, minor quartzite, and a layer of carbonate in between. The lower quartzitic unit consists of coarse very light gray and grayish purple quartzite, and probably correlates with the A member of Stewart (1970). The quartzite contrasts sharply with the underlying tan and light green siltstones of the upper Johnnie Formation. In much of the study area, a 2-meter interval of nearly white vitreous quartzite immediately overlies the Stirling-Johnnie contact. The lower part of the Stirling Quartzite contains isolated beds of dark dolomitic quartzite.

The middle part of the formation includes gray micaceous very fine-grained siltstone and fine quartzite and siltstone interbedded on the cm-scale. A single layer of carbonate occurs in the upper part of the silty interval. This interval probably corresponds to the B, C, and D members of Stewart (1970). The upper part of the formation includes very light gray quartzite which has a yellowish hue in places.

Wood Canyon Formation

The Wood Canyon Formation consists of silty lower and upper members with an interval of sandstone in between. The lower part of the formation includes two meter-thick dolostones as well as minor amounts of quartzite. The middle part of the formation includes coarse sandstone and conglomerate and the upper part of the formation also includes carbonate beds. Abundant fossil fragments in carbonates from the upper part of the formation allow them to be readily distinguished from the unfossiliferous carbonates in the lower part.

Zabriskie Quartzite

The Zabriskie Quartzite is readily distinguished from underlying siltstone of the upper Wood Canyon Formation and overlying siltstone and carbonate of the Carrara Formation.

In the study area, a 2 meter bed of skolithos piperock marks the base of the formation. The formation is almost entirely quartzitic, although some siltstone occurs in the middle.

Paleozoic Carbonates

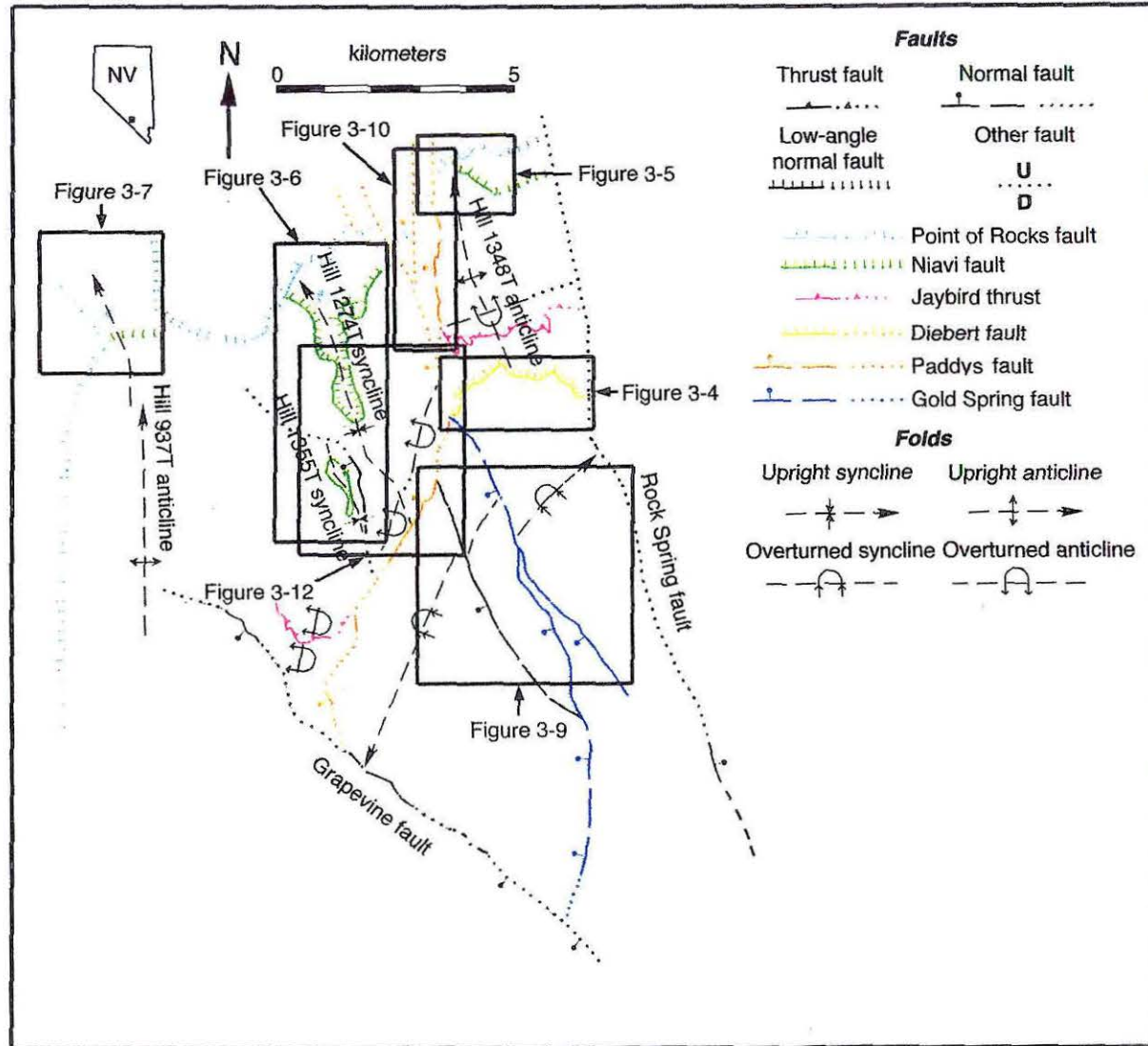
The primarily carbonate Paleozoic section includes the Carrara, Bonanza King, Nopah, and Pogonip Groups. The Carrara Formation is relatively recessive and consists largely of shale with interbedded limestone. The basal contact with the underlying Zabriskie Quartzite is sharp. In this study, the top of the formation was placed at the base of the first thick limestone interval in the Bonanza King Formation. The Bonanza King Formation is a cliff-forming unit which consists primarily of limestone with a thin shale interval in the middle. The Bonanza King Formation consists of cliff-forming dark gray dolostone with some dark gray limestone at its base. It is separated from the Bonanza King Formation by the Dunderberg Shale. This unit is a few tens of meters thick and includes brown siltstone with a gray limestone near its top. The Dunderberg Shale appears as a separate unit on the map. The Nopah Formation is overlain by the Pogonip Group. In the map area, the Pogonip Group consists of alternating resistant intervals of cherty carbonate (both limestone and dolostone) and less resistant silty limestone.

Paleozoic units overlying the Pogonip Group appear in the southeast quarter of Plate 2. Mapping in that area was adapted from Burchfiel and others (1974), and stratigraphic units are described in that paper.

EXTENSIONAL STRUCTURES

The principle extensional structures are shown on Figure 3-3. Extensional structures include high- and low-angle normal faults and broad upright folds. Low-angle normal faults include the Diebert, Niavi, and Point of Rocks faults. All of these faults have shallowly dipping fault planes ($< 30^\circ$). For reasons discussed in Chapter 4, the Diebert fault probably moved at a high-angle, and has been rotated to its current shallow dip. In contrast, the Niavi fault probably moved at a low angle. High-angle normal faults include

Figure 3-3. Map showing location of principle structures, and the location of figures showing principle extensional and extension-related structures.



the Gold Spring fault, Hill 5482 fault, Paddys fault, the Rock Spring fault, and the Grapevine fault. Broad upright folds include the Hill 1348T and 937T anticlines and the Hill 1274T syncline.

Low-angle normal faults

Diebert fault

The Diebert fault is exposed over an along-strike distance of 2.7 km. The fault is shown on Figure 3-4 and all locations and structures mentioned below are on this figure. The fault strikes west-southwest/east-northeast, and has a normal-sense separation, placing the lower quartzitic unit of the Stirling Quartzite on the lower Johnnie Formation. This relationship requires a stratigraphic throw of 1.4 km, using thicknesses for the Johnnie Formation and Stirling Quartzite reported in Burchfiel and others (1974). However, the normal fault may omit a thrust in which case the actual normal-sense separation is much greater. The fault dips 10-20° to the north-northwest. In general, the Stirling Quartzite in the hanging wall of the Diebert fault is upright and generally dips between 19 and 33°. Steeper dips are ascribed to localized small-scale folding. In the footwall, the Johnnie Formation immediately adjacent to the thrust is overturned and dips 38°. To the west, the Diebert fault terminates against the Gold Spring fault under alluvium immediately south of Hill 1328T. The fault is folded by the Hill 1348T anticline. The Diebert fault probably continued southward through the Spring Mountains, but has been omitted by dip-slip motion on Paddys fault.

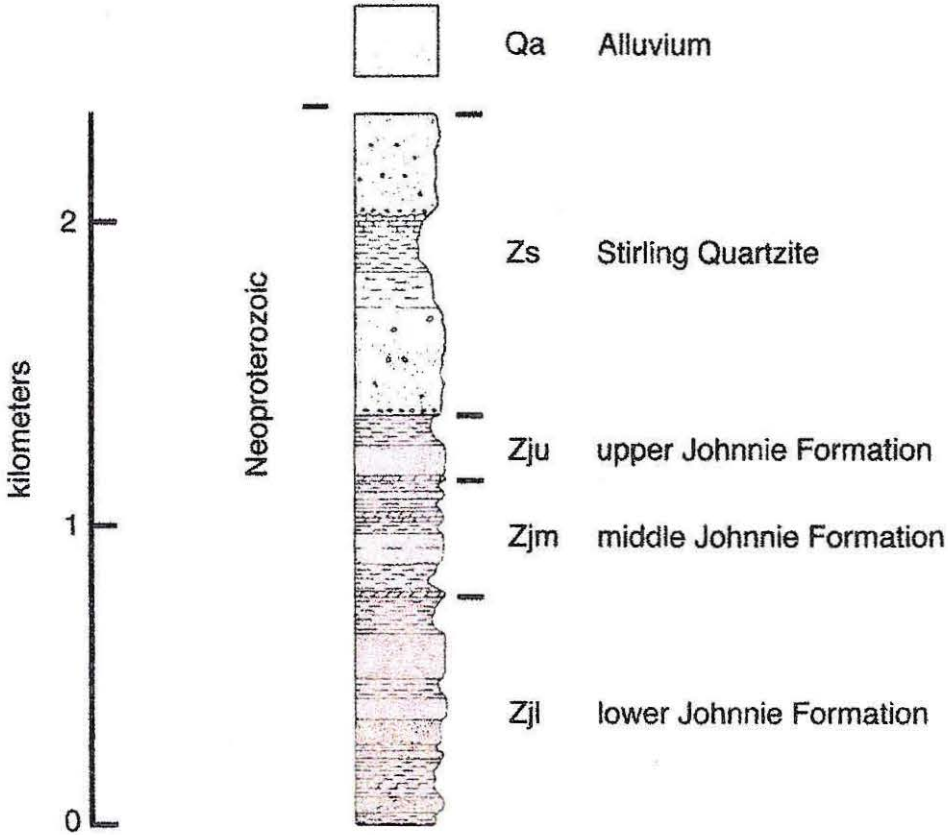
Previous work - Burchfiel (1965) and Burchfiel and others (1974) interpreted the Diebert fault as a thrust. Burchfiel and others (1983) interpreted the fault as a slide surface and the bedrock to the north as a "slide block."

Niavi fault

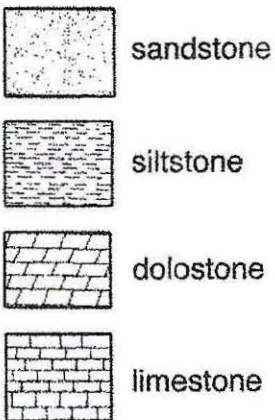
The Niavi fault is a currently low-angle structure with a younger-on-older relationship, and is shown in Figures 3-5, 3-6, and 3-7. The fault was folded and truncated by the

Figure 3-4. Geologic map of the Diebert fault. See Figure 3-3 for location of map. GSF stands for Gold Spring fault. In the area of this map, the Hill 1348T anticline is defined by folding of the Diebert fault surface. The Diebert fault generally dips in a northerly direction. However, the elevation of the fault surface is lower in the western and eastern parts of the map area than in the central part of the map area. The variations in elevation of the Diebert fault surface crudely define the Hill 1348T anticline.

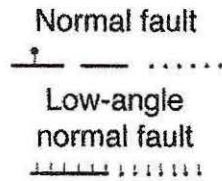
KEY



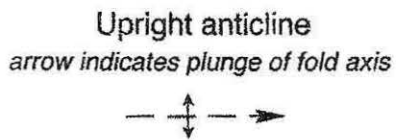
Lithology



Faults



Fold





3-15

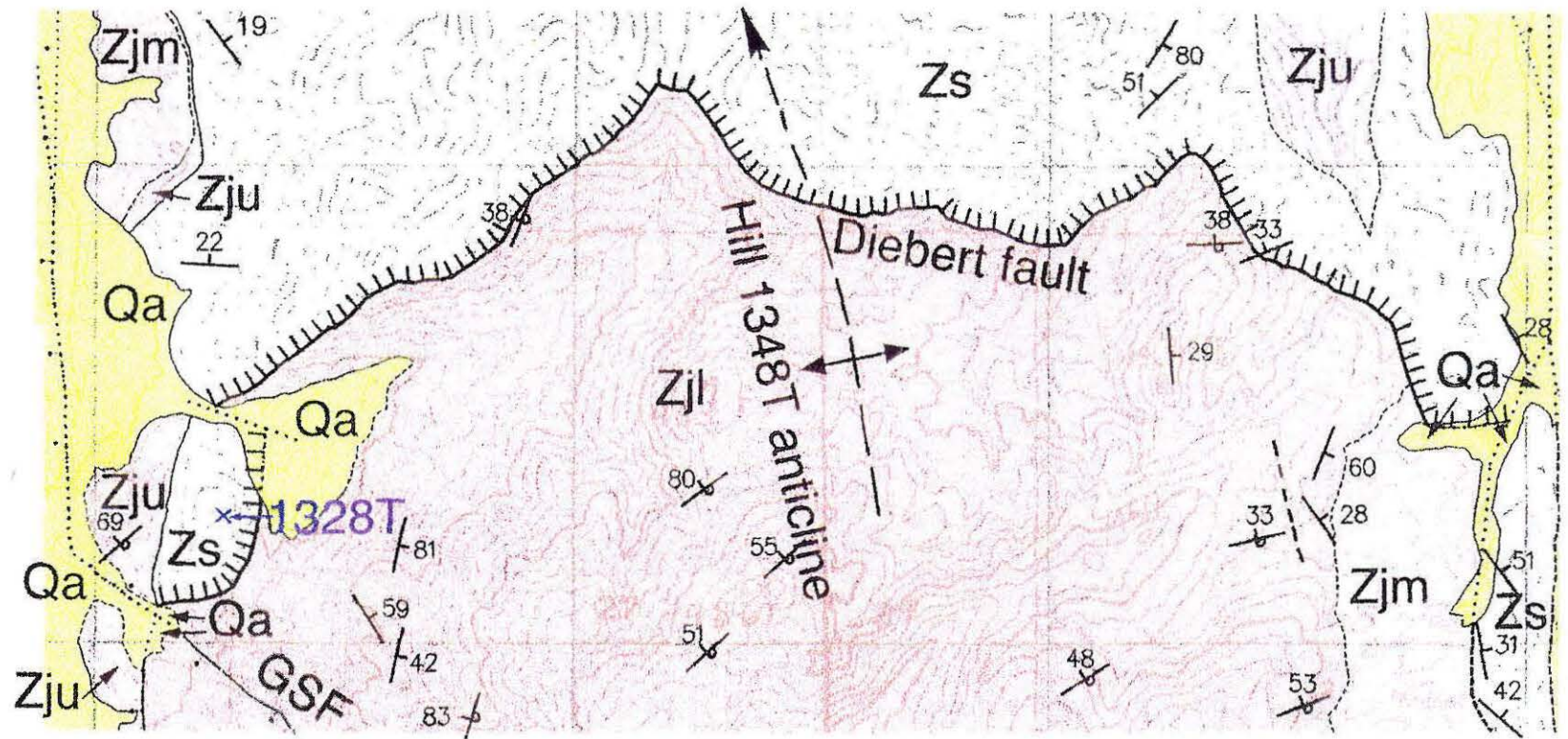
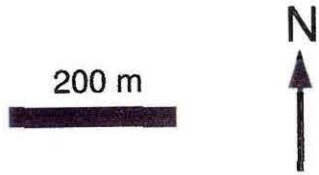


Figure 3-5. Map showing the relationship between the Niavi fault and cross-cutting structures in the northeastern part of the study area. See Figure 3-3 for location. In this map area, the Hill 1348T anticline is best defined by bedding dips in the Johnnie Formation. On the west limb of the anticline, bedding generally dips to the north-northwest (e.g., the attitudes with dips of 18, 25, and 35° located west of the axial trace). On the east limb of the anticline, bedding dips to the north-northeast (e.g., the attitudes with dips of 30, 32, 34, 35, and 39° located east of the axial trace).



Qa	alluvium
Cn	Nopah Formation
Zs	Stirling Quartzite
Zjcb	Conglomerate member - siltstone unit
Zjca	Conglomerate member - conglomerate unit
Zju	upper Johnnie Formation
Zjm	middle Johnnie Formation

Contact

Dashed where approximately located
Dotted where concealed

**Low-angle
normal fault**

Dashed where approximately located
Dotted where concealed

Normal Fault

Dashed where approximately located;
Dotted where concealed;
ball on downthrown side

3-18

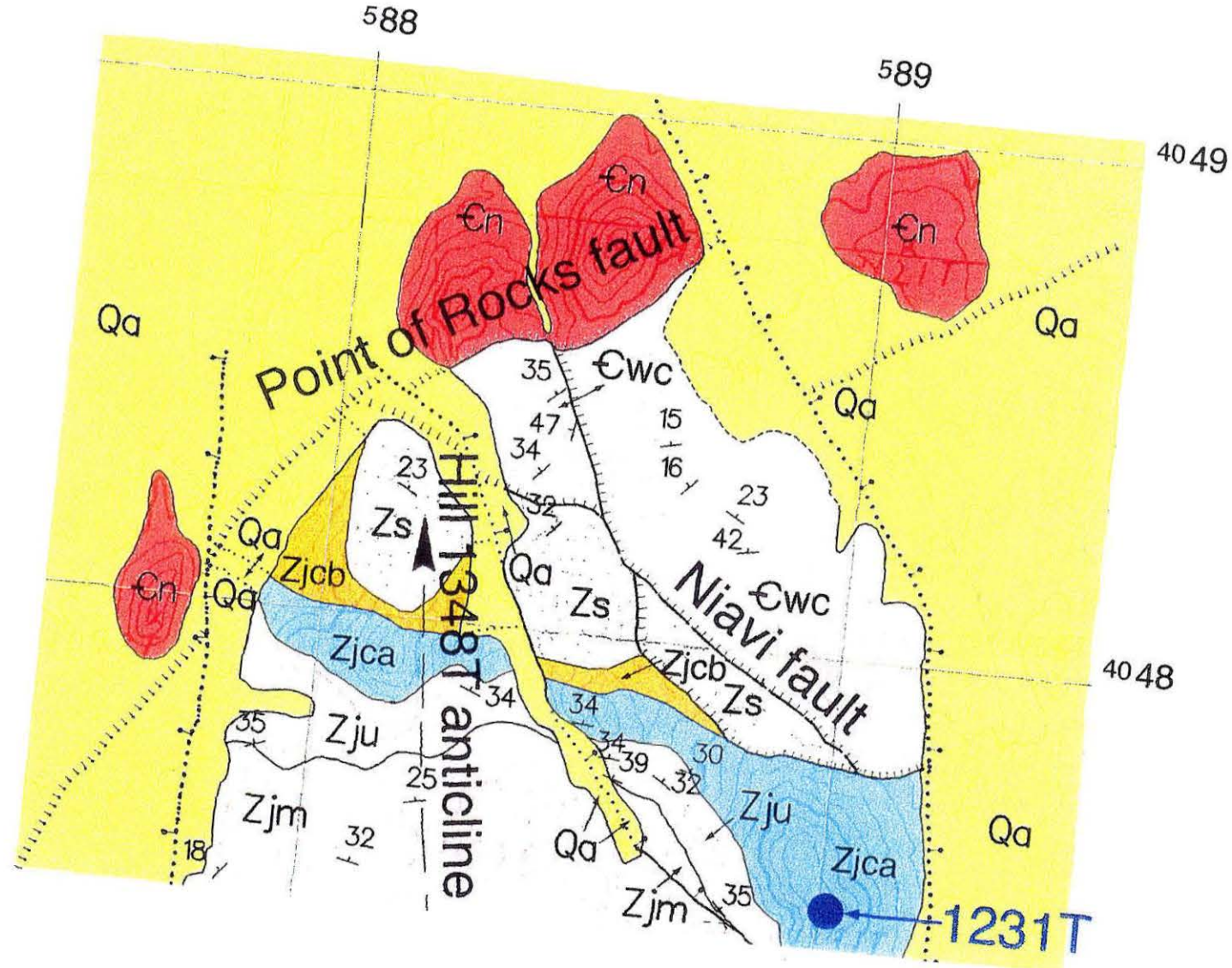
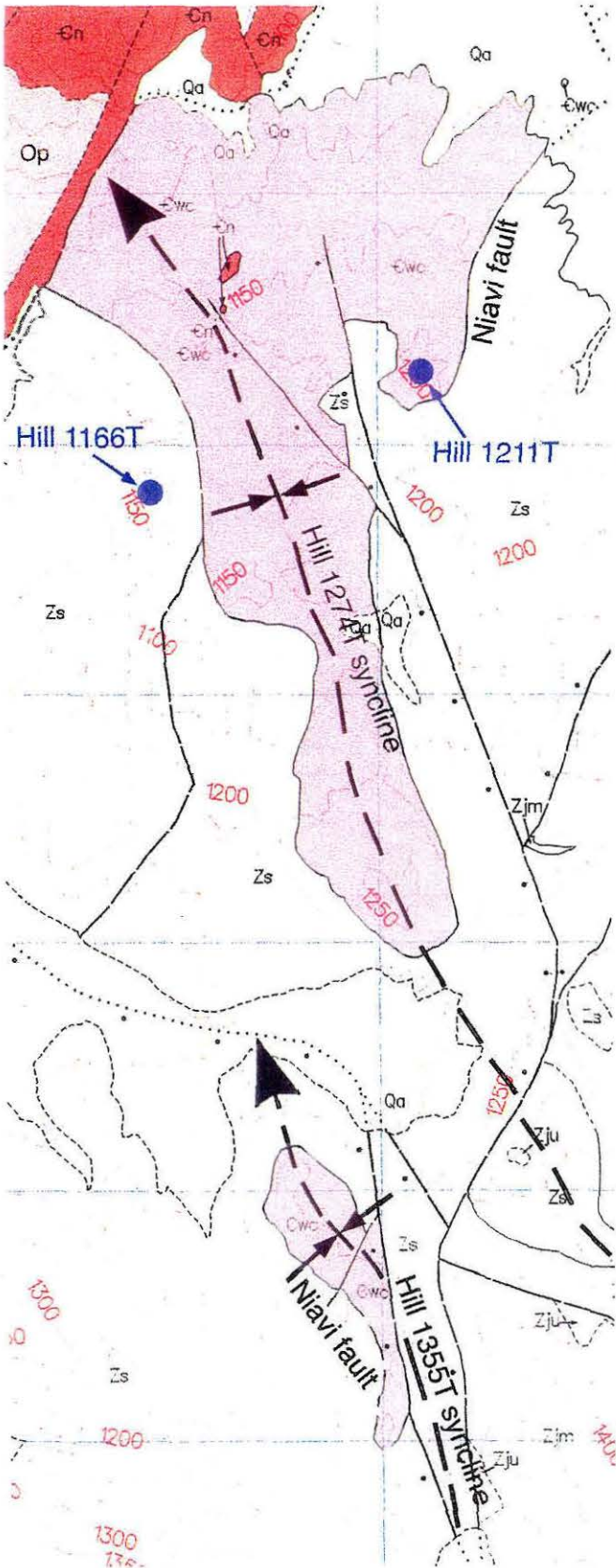


Figure 3-6. Map showing the Niavi fault and cross-cutting structures in the north-central part of the study area. See Figure 3-3 for location.



500 m

- Qa alluvium
- Op Pogonip Group
- En Nopah Formation
- Cwc Wood Canyon Formation
- Zs Stirling Quartzite
- Zju upper Johnnie Formation
- Zjm middle Johnnie Formation

Contact

Dashed where approximately located
Dotted where concealed

Fault

Dashed where approximately located;
Dotted where concealed

Normal Fault

Dashed where approximately located;
Dotted where concealed;
ball on downthrown side

Normal Fault

Dashed where approximately located;
Dotted where concealed;
ball on downthrown side

Figure 3-7. Map showing the Niavi fault and cross-cutting structures in the northwestern part of the study area. See Figure 3-3 for location.

Qa	alluvium
Tp	Tertiary playa deposits
Tg	Tertiary gravel
Tb	Tertiary carbonate breccia
En	Nopah Formation
Ebk	Bonanza King Formation
Cz	Zabriskie Quartzite
Ewc	Wood Canyon Formation
Zs	Stirling Quartzite
Zjm2	upper Johnnie Formation
Zjm1	middle Johnnie Formation

Contact

Dashed where approximately located
Dotted where concealed

Fault

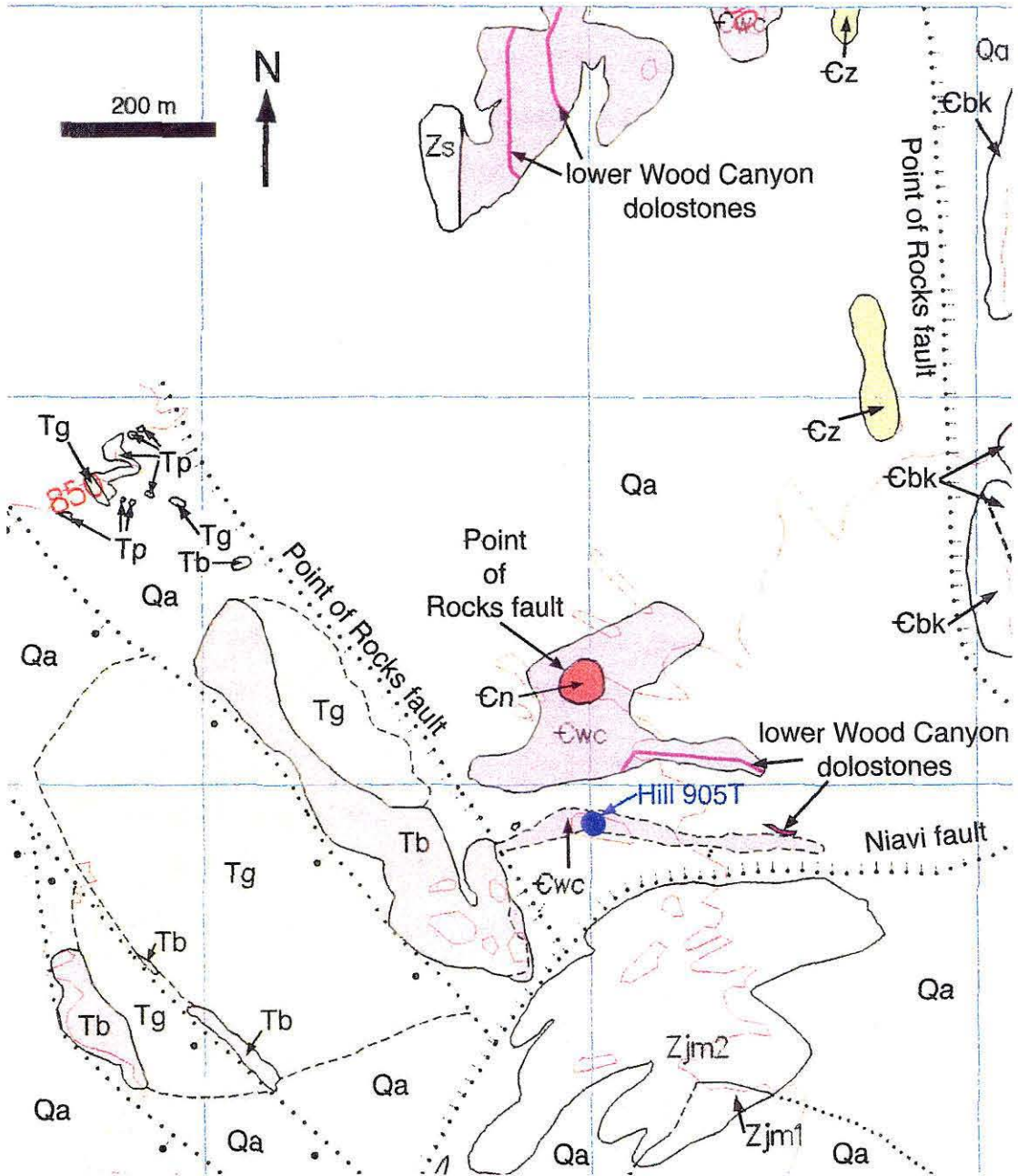
Dashed where approximately located;
Dotted where concealed

Normal Fault

Dashed where approximately located;
Dotted where concealed;
ball on downthrown side

Normal Fault

Dashed where approximately located;
Dotted where concealed;
ball on downthrown side



structurally higher Point of Rocks fault. The structurally highest exposures of the fault place quartzite of the lower Wood Canyon Formation on Stirling B siltstone, suggesting a stratigraphic throw of 575-760 m. Here the fault is a hanging wall flat or decollement, while in the footwall the fault cuts downsection to the west-northwest.

Previous work - Burchfiel (1965) interpreted the Niavi fault as a thrust. He did not extend the fault into the area northwest of Hill 1231T (Figure 3-5), presumably because he interpreted reddish fine quartzite assigned here to the middle Wood Canyon Formation as Stirling Quartzite.

This study - Bedding in the hanging wall of the Niavi fault intersects the fault surface at a low angle, and the fault cuts through little stratigraphic section in its hanging wall. A distinctive very light gray medium quartzite with sub-rounded grains sits atop the fault surface throughout the Hill 1274T syncline and in the northwestern part of the Hill 1355T syncline (folds shown on Figure 3-6). Throughout this area, a distinctive 2-meter-thick medium gray dolostone outcrops a few meters above the quartzite. A similar quartzite and dolostone also crop out within 50 m of the buried fault trace 4 km to the west of the syncline near Hill 905T (location on Figure 3-7). The stratigraphy above the fault is less clear in its easternmost exposures, but a potentially correlative dolostone was observed above the fault 280 m north-northwest of the summit of Hill 1231T (location on Figure 3-5). These observations suggest that bedding in the hanging wall of the Niavi fault is sub-parallel to the fault along a west-southwest/east-northeast distance of 8.8 km and a north-northwest/south-southeast distance of 4 km.

The Niavi hanging wall ramps through additional section in the northwesternmost part of the study area ("Highway 95 section," northern part of Figure 3-7). At least 80 and possibly as much as 180 m of additional section is exposed. More section may be buried beneath alluvium west of the Highway 95 exposure. Roughly 80 m of Stirling E Quartzite is present at the western end of the exposure, and up to 100 m of additional lower Wood

Canyon Formation is present above the quartzite. The amount of additional section in the lower Wood Canyon Formation depends on the correlation of dolostone marker beds between this location and the other figured locations. Two dolostones are present in the lower Wood Canyon Formation in the Highway 95 section and can be traced laterally for over 200 m. Farther south, only one dolostone is definitely present within the lower Wood Canyon Formation in the hanging wall. As a result, the hanging wall may pick up an additional dolostone and an additional 100 m of section to the north. The Highway 95 section is about 1.7 km north of the nearest hanging wall section in which the quartzitic marker sits atop the fault.

In contrast, the footwall of the fault ramps through 360-475 m of Stirling A and B and about 175 m of upper Johnnie Formation over an east-west distance of about 4.5 km. In the vicinity of Hill 1211T (location on Figure 3-6) where the fault involves 575-760 m of stratigraphic throw, the fault juxtaposes the quartzitic marker bed in the hanging wall with the silty middle unit of the Stirling Quartzite in the footwall. Although the contact is not well exposed, the Stirling B consists of two facies nearby: gray micaceous very fine-grained siltstone and fine quartzite and siltstone interbedded on the cm-scale.

Point of Rocks fault

The Point of Rocks fault is a low-angle fault which places Paleozoic carbonates on a folded footwall. Movement on the Point of Rocks fault post-dates folding of the Niavi fault. The low angle dip of the fault plane is most evident on Figures 3-6 and 3-7 where klippe of the hanging wall sit atop the Wood Canyon Formation. In the area shown on Figure 3-6, the fault dips 20-30°, while the fault is nearly flat under the klippe in Figure 3-7. In the northern part of Figure 3-7, the presence of Bonanza King Formation in the Point of Rocks hanging wall shows that hanging wall is ramping downward through additional section to the north or northwest. West of the klippe on Figure 3-7, the Niavi fault carries three tilted slices of Tertiary carbonate breccia (Tb) and conglomerate (Tg) in its hanging

wall. The age and significance of these deposits is discussed below under “Age of Extensional Structures.”

Broad upright folds

Three broad upright folds, the Hill 1348T and Hill 937T anticlines and the Hill 1274T syncline, are discussed in this section because cross-cutting relationships show that the folds formed during movement on the low-angle faults described in the preceding paragraphs. These three folds have north-northwest trending axes, have a wavelength of 3.25-4.25 km, and involve the entire stratigraphic section. All three of these folds are geomorphically expressed and resemble the turtleback folds of the Black Mountains (Holm and others, 1994) in their general shape and syn-extensional timing.

The Hill 1348T anticline (Figures 3-4 and 3-5) folds the Diebert and Niavi faults but is cut by the Point of Rocks fault. The anticline plunges 20-30° to the north, and has limb dips of about 20°. The axial trace of the anticline is nearly perpendicular to the strike of the Diebert and Jaybird faults and is sub-parallel to the strike of the Rock Spring fault. The Hill 937T anticline is similar to the Hill 1348T anticline, but may post-date the Point of Rocks fault because it provides a window into the lower plate of the fault in the northwestern corner of the study area.

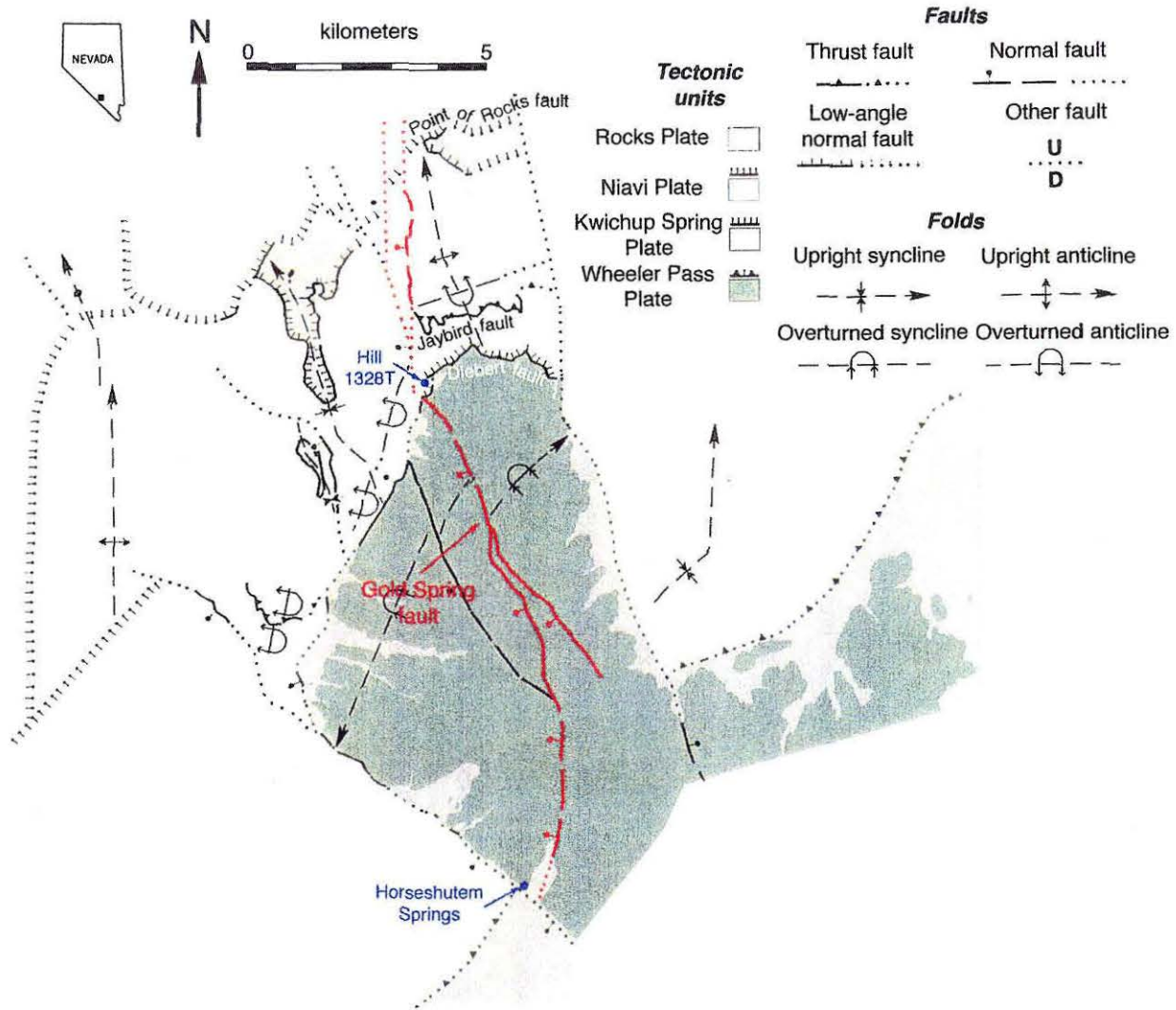
The Hill 1274T syncline (Figure 3-6) also folds the Niavi fault and is cut by the Rock Spring fault. The southern end of the syncline is offset by a moderately-dipping normal fault. The syncline has limb dips of 20-30°, and plunges to the north-northwest. The Hill 1355T segment of the syncline is offset by a normal fault with a moderate dip.

High-angle normal faults

Gold Spring fault

The Gold Spring fault is a high-angle west-side-down normal fault which cuts the Diebert, Jaybird, and Point of Rocks faults. The fault is highlighted on Figure 3-8, and was mapped for 11 km within the study area. As discussed below, the fault probably

Figure 3-8. The Gold Spring fault. Named structures are discussed in text. Note that the northern segment of the Gold Spring fault may have been reactivated as Paddys fault (discussed below), and is shown as a part of Paddys fault on Figure 3-3.



involves hundreds of meters of vertical separation. It is not topographically expressed in any obvious way.

Previous work - Burchfiel (1965) dashed the Gold Spring fault where it approaches the Diebert fault and did not indicate the continuity of the Gold Spring fault north of the Diebert fault. He inferred an east-side-down sense of displacement rather than the west-side-down displacement advocated in this chapter. The east-side-down sense of displacement is based on 950 m of apparent right-lateral horizontal separation on the axial trace of an overturned southeast-vergent syncline.

The Burchfiel and others (1974) compilation map of the Spring Mountains shows essentially the same geology as the 1965 map in the northwestern Spring Mountains. To the southeast, the mapped continuation of the Gold Spring fault is complex and apparently schematic. The only fault with large displacement is a west-side-down normal fault which traverses the range crest and terminates against the Grapevine fault at the Spring Mountains range front. This fault involves about 270 m of vertical separation on the Johnnie-Stirling contact northeast of Horseshutem Springs (location shown on Figure 3-8).

The Geologic Map of Nye County (Cornwall, 1972) shows the Gold Spring fault as a single continuous west-side-down structure which cuts the Diebert, Jaybird, and Point of Rocks faults in the northwest and terminates against the Grapevine fault near Horseshutem Springs in the southeast.

This study - New mapping supports Cornwall's interpretation. The Gold Spring fault offsets east and west dipping contacts with opposite separations, and, therefore, is predominantly dip-slip. The Gold Spring fault offsets the contact between the lower and middle Johnnie Formation by a horizontal distance of roughly 1.3 km in an apparent right-lateral sense (Figure 3-9). Since the contact dips east-southeast, the apparent right-lateral horizontal separation is consistent with southwest-side-down normal separation on the fault. Like Cornwall, I think the fault continues to the north and cuts the Diebert, Jaybird,

Figure 3-9. Map of the Gold Spring and Hill 5482 faults. See Figure 3-3 for location.
See Plate 1 for bedding attitudes.

Qa	alluvium
En	Nopah Formation
Zs	Stirling Quartzite
Zju	upper Johnnie Formation
Zjm	middle Johnnie Formation
Zjl	lower Johnnie Formation

Contact

Dashed where approximately located
Dotted where concealed

Fault

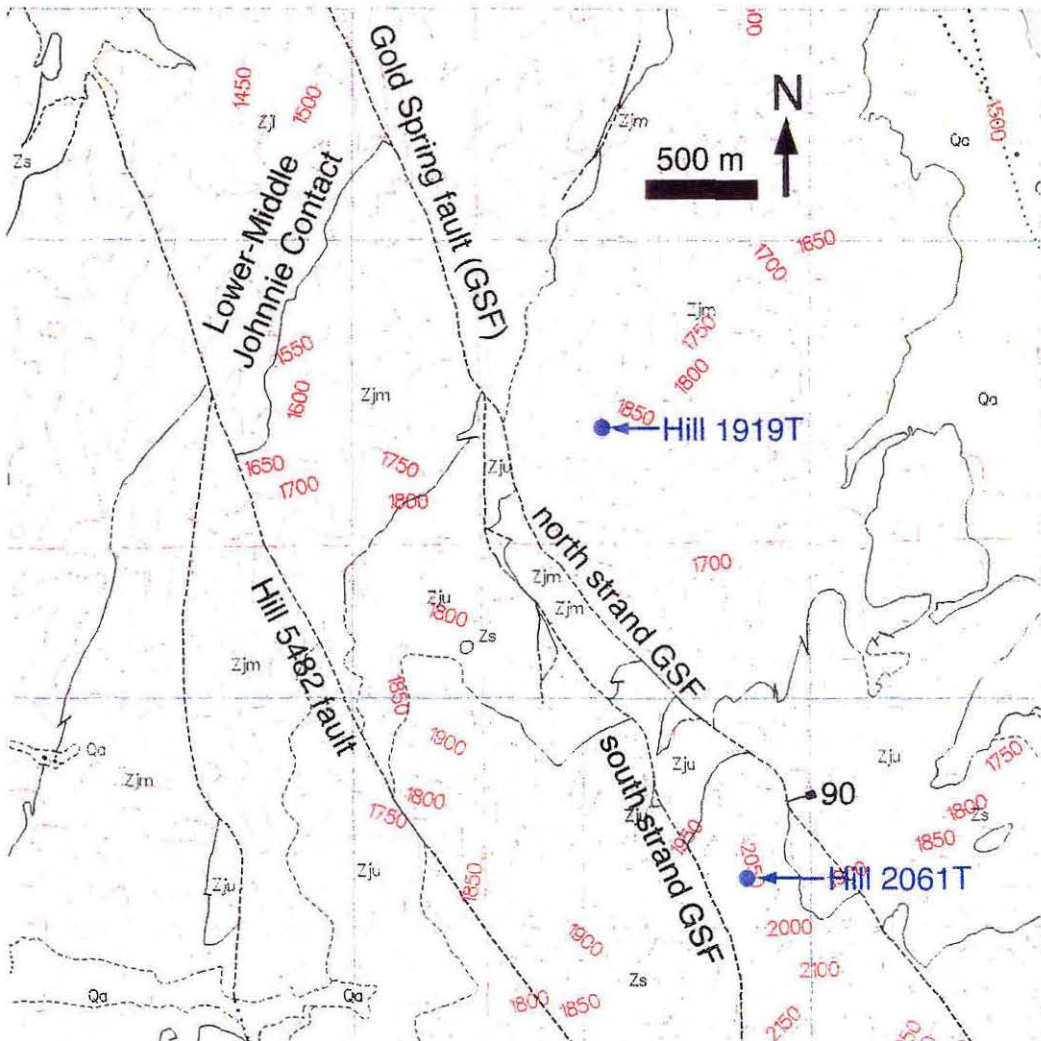
Dashed where approximately located;
Dotted where concealed

Normal Fault

Dashed where approximately located;
Dotted where concealed;
ball on downthrown side

Dip and Dip Direction of Fault

90
|

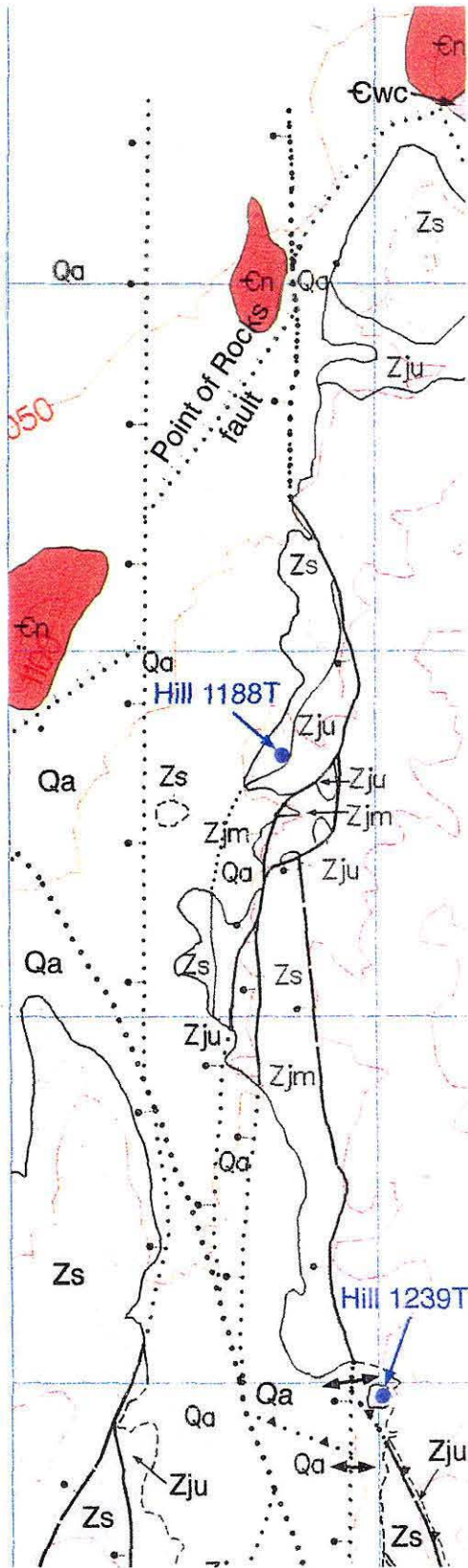


and Point of Rocks faults, although alluvium covers the key relationships. Mapping is consistent with apparent left-lateral horizontal separations on the Jaybird and Point of Rocks faults. Since these structures dip to the north-northwest, the apparent left-lateral separations are consistent with west-side-down slip on the Gold Spring fault. West-side-down slip is also indicated south of Hill 1188T (location on Figure 3-10) where the Gold Spring fault consists of anastomosing strands. One of the main strands is west-side-down and faults Stirling A Quartzite against the middle Johnnie Formation. Together, these observations strongly suggest that the Gold Spring Fault is a continuous west-side-down structure. The combination of apparent right-lateral and left-lateral separations is inconsistent with purely strike-slip motion although some component of strike-slip remains possible.

The estimated separation on the Gold Spring fault where it cuts the lower/middle Johnnie contact depends on the dip of the contact. The dip of the contact is complicated by folding within the Johnnie Formation (described in a separate section below). Folding of this contact was studied in detail about 5 km to the south. The base of the contact is marked by a prominent 8 m-thick dolostone. This dolostone is involved in folds with a wavelength and amplitude on the order of tens of meters. The fold envelope of these folds dips 42° to the east. If the dip of the fold envelope east of Kwichup Spring is taken as the dip of the lower/middle Johnnie Formation contact at the Gold Spring fault, the vertical slip on the fault is approximately 950 m.

This estimate is much larger than the vertical slip on the fault to the south near Horseshutem Springs and to the north where the fault cuts the Jaybird and Point of Rocks faults. Vertical slip could die out to both the north and south. Alternately, the fold envelope could dip more shallowly where the lower/middle Johnnie contact intersects the Gold Spring fault. A dip of 15° , for example, would imply about 430 m of vertical separation. This lower estimate of vertical separation is comparable to the vertical

Figure 3-10. Geologic map of the northern segment of the Gold Spring fault. See Figure 3-3 for location.



- Qa alluvium
- Cn Nopah Formation
- Zs Stirling Quartzite
- Zju upper Johnnie Formation
- Zjm middle Johnnie Formation

Contact
 Dashed where approximately located
 Dotted where concealed

Fault
 Dashed where approximately located;
 Dotted where concealed

Normal Fault
 Dashed where approximately located;
 Dotted where concealed;
 ball on downthrown side

Thrust Fault
 Dashed where approximately located;
 Dotted where concealed;
 teeth on hanging wall

separation on the fault near Horseshutem Springs given the large distance (7.5 km) between them. This lower estimate is also more consistent with the amount of apparent left-lateral separation on the Jaybird and Point of Rocks faults. The lower estimate of vertical separation requires 1.15 km of apparent horizontal left-lateral separation on the Jaybird fault, assuming it dips $\sim 20^\circ$, and is comparable to the minimum of 800 m required by mapped relationships.

The Gold Spring fault can be divided into three segments. The northernmost segment of the fault strikes north-south for about 5.3 km and is covered by alluvium except around Hill 1188T (location on Figure 3-10). The intersection between the fault and topography suggests a west dipping fault plane in this area. Two strands of the Gold Spring fault probably cut the Point of Rocks fault under alluvium. The fault also cuts the Jaybird fault under alluvium west of Hill 1239T (location on Figure 3-10). The largest vertical separation on the fault was observed south of Hill 1188T where the fault juxtaposes Stirling A Quartzite with the middle Johnnie Formation. A minor west-side-down strand of the fault was also mapped to the east of the main strand. About 360 m north-northwest of Hill 1239T (Figure 3-10), this minor strand offsets a prominent dolomitic marker bed by about 20 m. A minor east-side-down fault juxtaposes Stirling A Quartzite against the upper Johnnie Formation south of Hill 1188T. The fault was mapped over a distance of about 300 m and involves less than 20 m of throw. Under alluvium southwest of Hill 1328T (location on Figure 3-4), the strike of the fault changes to N23W. The central segment maintains this strike for about 3.27 km through the northwestern Spring Mountains.

To the west of Hill 1919T (location on Figure 3-9), the Gold Spring fault splits into two strands. These two strands comprise the southern segment of the fault. At the split, most of the slip is on the northern strand. This strand juxtaposes the upper Johnnie Formation with the uppermost lower Johnnie Formation. Displacement on this strand diminishes to the southeast. On the northwest flank of Hill 2061T (location on Figure 3-

9), this strand dips 49° and causes about 55 m of vertical offset on the base of the upper Johnnie Formation. On the northeast flank of Hill 2061T, the fault plane and slickensides on the fault surface are both vertical as shown on Figure 3-9. In contrast, the southern segment appears to pick up slip to the southeast. At the separation, the southern segment is entirely contained within the upper Johnnie Formation while the apparent offset of the Stirling-Johnnie contact by the southern segment west of Hill 2061T is considerable.

Hill 5482 fault

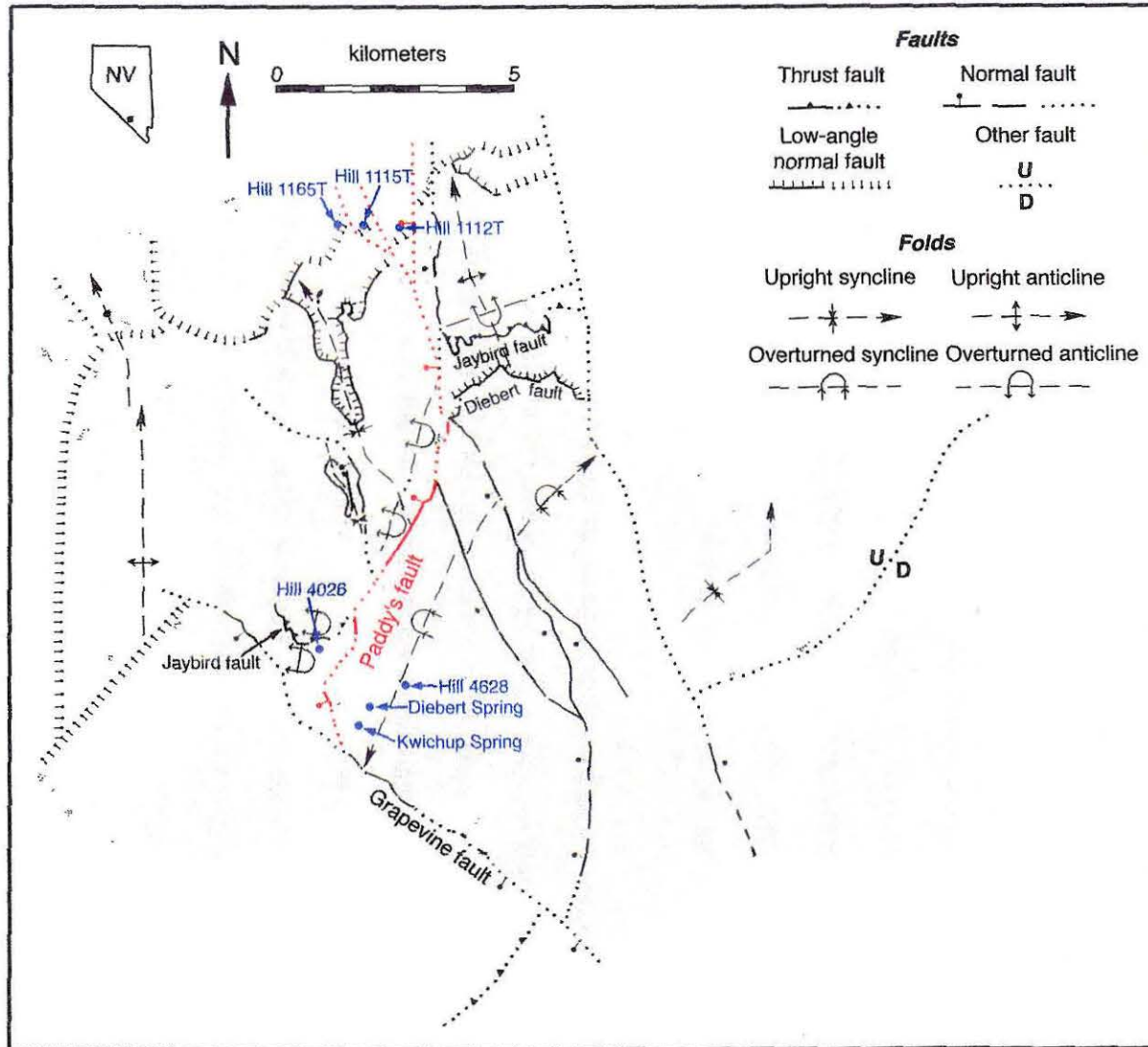
The Hill 5482 fault (shown on Figure 3-9) is similar to the Gold Spring fault and probably merges with the Gold Spring fault to the north and to the southeast outside the map area. The Hill 5482 fault offsets the lower/middle Johnnie Formation contact in an apparent right-lateral manner. The vertical separation involved is poorly constrained, but probably on the order of 130-342 m.

Paddys fault

Paddys fault (shown on Figure 3-11) is a high-angle normal fault with a west-side-down vertical displacement of at least 260 m and probably about 300 m. The fault consists of a number of segments which strike northwest, north, and northeast. In the southern part of the map area, the fault may consist of a single strand although alluvium may cover additional strands. The fault consists of a number of anastomosing strands in the central part of the map area. Strands of the fault cut the Niavi and Point of Rocks faults and probably cut the Diebert and Jaybird faults under alluvium. Paddys fault terminates to the south against the Grapevine fault. The continuation of the fault north of the central part of the map area is problematic and discussed below.

Previous work - Burchfiel (1965) mapped the central segment of Paddys fault, and the entire fault appears on the 1974 Spring Mountains compilation map (Burchfiel and others, 1974) and the 1983 map of the Montgomery Mountains and adjacent areas

Figure 3-11. Map showing Paddys fault. Named structures are discussed in the text.



(Burchfiel and others, 1983). Burchfiel and others (1983) suggested that Paddys fault was responsible for at least 1500 m of vertical separation on the Johnnie-Stirling contact.

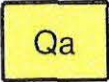
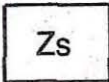
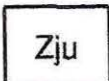
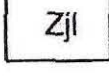
This study - I ascribe most of the vertical separation on this contact to movement on the Diebert fault, and suggest that Paddys fault is a younger structure of comparatively small throw which omits the Diebert fault. The minimum offset on Paddys fault is loosely constrained in the south by the position of the Jaybird fault and the projected position of the Diebert fault. The Diebert fault has been eroded but projects above exposures of the Johnnie Formation in the vicinity of Diebert and Kwichup Springs (locations on Figure 3-11). The Jaybird fault is located northwest of Hill 4026 (location on Figure 3-11). The Jaybird and Diebert faults are separated by a vertical distance of about 175 m to the north where they were both mapped. In the south, the juxtaposition of these two structures across Paddys fault requires at least 175 m of vertical separation. The actual amount of vertical separation is larger and depends on the projected elevation of the Diebert fault in the footwall.

In the central part of the map area, Paddys fault breaks into four major strands (Figure 3-12) involving at least 260 m of west-side-down vertical separation. Strand 1 divides into two strands that cut the Niavi fault (Figure 3-6). The Niavi fault dips shallowly to the northwest at this location. As shown on Figure 3-6, apparent right-lateral offsets of about 200 m on these strands probably indicate about 40 m of vertical slip on each strand.

Slip on strand 2 is best constrained on the southwest flank of Hill 1314T (location on Figure 3-12) where the Johnnie-Stirling contact is displaced by at least 92 m vertically on a fault that dips 56° to the west-northwest. This displacement estimate is a minimum because the Johnnie-Stirling contact is not exposed in the hanging wall.

Strand 3 omits about 80 m of the upper Johnnie Formation southeast of Hill 1349T (location on Figure 3-12). Finally, slip on strand 4 includes contributions from the Hill

Figure 3-12. Geologic map of Paddys fault in the central part of the study area. See Figure 3-3 for location. Numbered strands are discussed in the text. Strand 1 continues to the north and cuts the Niavi fault as shown on Figure 3-6.

	alluvium
	Wood Canyon Formation
	Stirling Quartzite
	upper Johnnie Formation
	middle Johnnie Formation
	lower Johnnie Formation

Contact

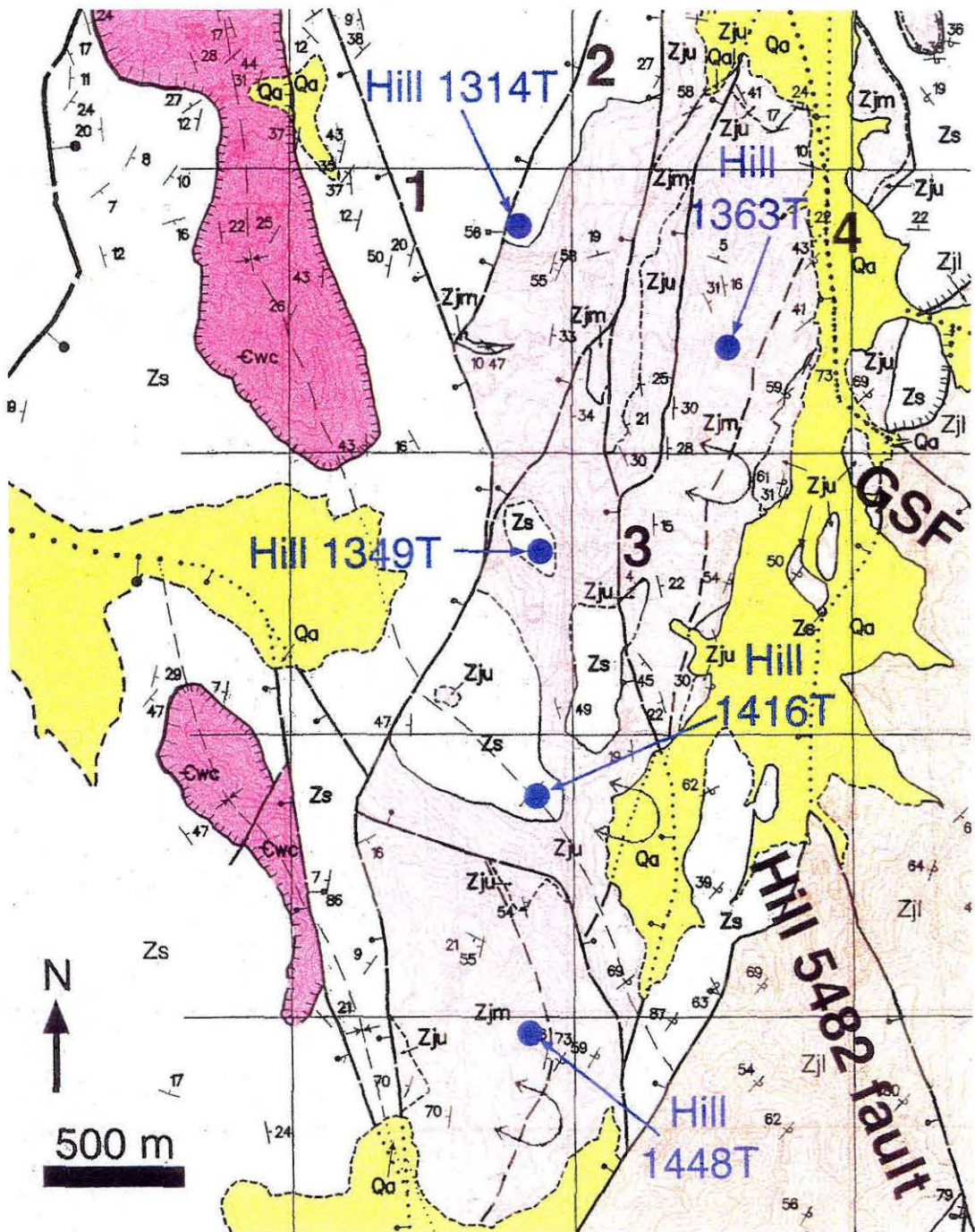
Dashed where approximately located
Dotted where concealed

Fault

Dashed where approximately located;
Dotted where concealed

Normal Fault

Dashed where approximately located;
Dotted where concealed;
ball on downthrown side



5482 and Gold Spring faults. The amount of slip contributed to this strand by Paddys fault may be small, and the total amount contributed by all three faults is unknown.

The continuation of Paddys fault to the north is uncertain. The fault may reactivate portions of the Gold Spring fault or it may terminate against two faults that cut the Point of Rocks fault under alluvium between Hill 1165T and Hill 1115T and between Hill 1115T and Hill 1112T (locations on Figure 3-11). These faults involve apparent right-lateral horizontal separations on the Point of Rocks fault. Since the Point of Rocks fault dips to the north, these faults either involve east-side-down or right-lateral strike-slip motion. In either case, these two faults probably join and bound the Specter Range on the east.

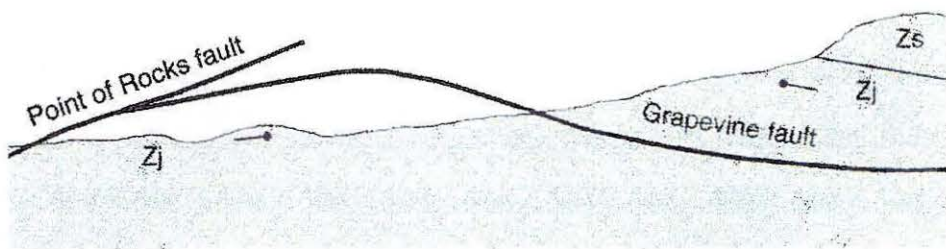
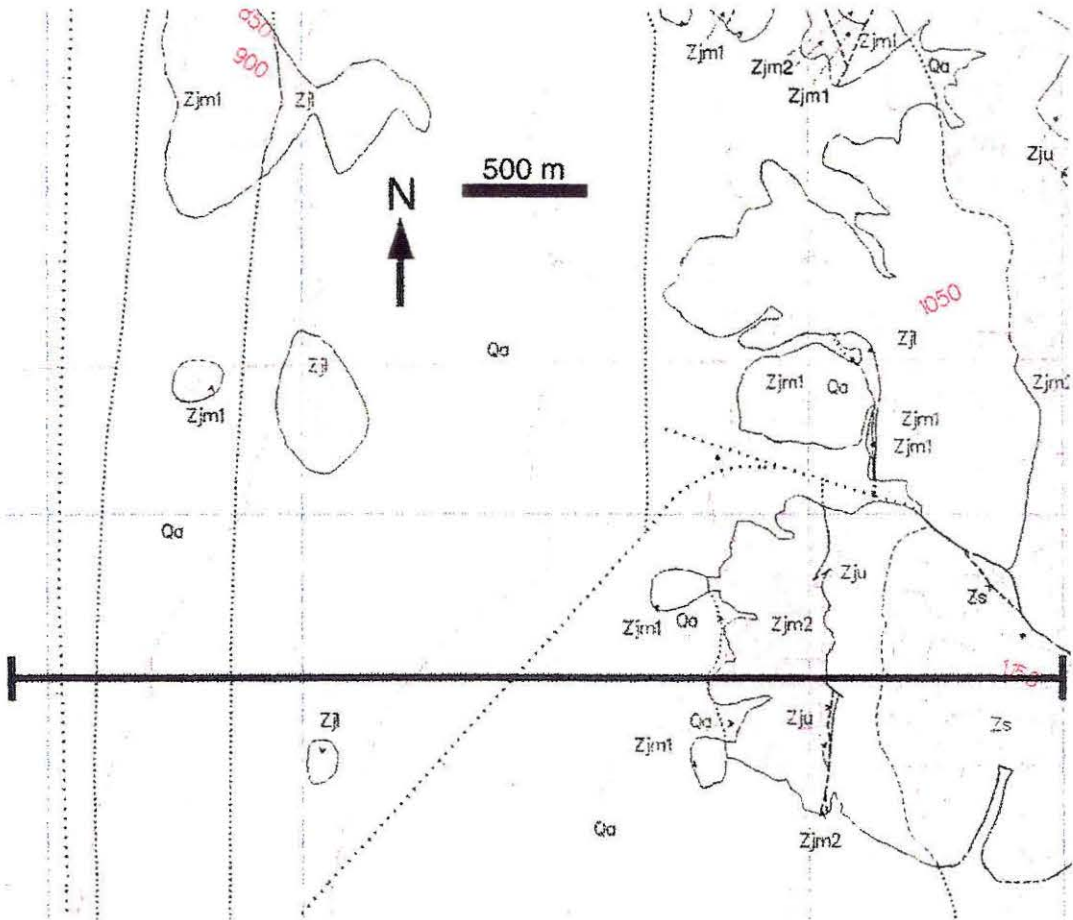
Grapevine fault

The Grapevine normal fault bounds the area described in this chapter on the southwest. As shown on Plate 1, the fault dips 75° S near its western end, and its southwest side is down-dropped. At its western end, the fault involves about 800 m of stratigraphic throw. The fault does not offset units on the west limb of the Hill 937T anticline (described below), indicating that the fault does not continue to the west. This observation is probably best explained by projecting the Grapevine fault as a low-angle structure *over* outcrops of the west limb of the Hill 937T anticline as shown schematically in Figure 3-13. To the southeast, the Grapevine fault involves a stratigraphic separation of at least 3.5 km, (apparently) accommodating uplift of the northwestern Spring Mountains with respect to the Montgomery Mountains.

Rock Spring fault

The east-side-down Rock Spring fault bounds the area described in this chapter on the east. As shown on Plate 1, the fault involves a stratigraphic throw of about 1.8 km where it juxtaposes the Zabriskie Quartzite and middle Johnnie Formation. The fault zone is silicified and the fault plane dips 61° NE at one location and 83° NE at a second location. To the southeast on Plate 2, the fault juxtaposes the upper part of the Carrara Formation

Figure 3-13. Map (A) and schematic profile view geometry (B) of the Grapevine fault at its western end. The Grapevine fault is depicted here as a low-angle structure. In this interpretation, the Grapevine fault has been omitted by a younger high-angle fault of small displacement where it passes through bedrock and separates the Stirling Quartzite from the Johnnie Formation.



with the lower part of the Stirling Quartzite with about the same stratigraphic throw. The fault dies out to the southeast on the Geologic Map of the Spring Mountains, Nevada (Burchfiel and others, 1974).

CONTRACTILE STRUCTURES

The principle contractile structures are the Jaybird fault and trains of folds in the Johnnie Formation (Figure 3-14).

Jaybird fault

The Jaybird fault places the upper Johnnie Formation on top of the lower quartzitic member of the Stirling Quartzite. The fault was mapped in the northern and southern parts of the study area. Strand 4 of Paddys fault omits the fault plane in the central part of the study area.

Previous work - Burchfiel (1965) mapped the Jaybird Fault in the northern part of the study area. The fault also appears in a summary figure in Burchfiel and others (1983). In the southern part of the study area, parts of the Jaybird fault were mapped by Hamill (1966) and Ivošević (1976) during thesis work. Neither geologist recognized the fault as a thrust, and it appears as a south-side-down normal fault on the map of Burchfiel and others (1983).

This study - In the northern part of the study area, the Jaybird fault strikes west-southwest/east-northeast for about 4.5 kilometers. Figure 3-15 depicts the Jaybird fault in the northern part of the study area, and locations mentioned in this paragraph and the next paragraph appear on Figure 3-15. The intersection of the fault plane with topography near Hill 1321T and Hill 1339AT indicates a dip of less than 20°. At Hill 1321T, the Jaybird fault cuts the Stirling Quartzite along an across-strike distance of 500 meters, suggesting at least one half kilometer of slip. Bedding is consistently overturned in both the Johnnie Formation and the Stirling A quartzite adjacent to the fault. On Hill 1321T, for example, beds in the upper Johnnie Formation are overturned and dip 39-46° to the north-northwest.

Figure 3-14. Map showing principle structures, and the locations of figures showing the principle contractile structures.

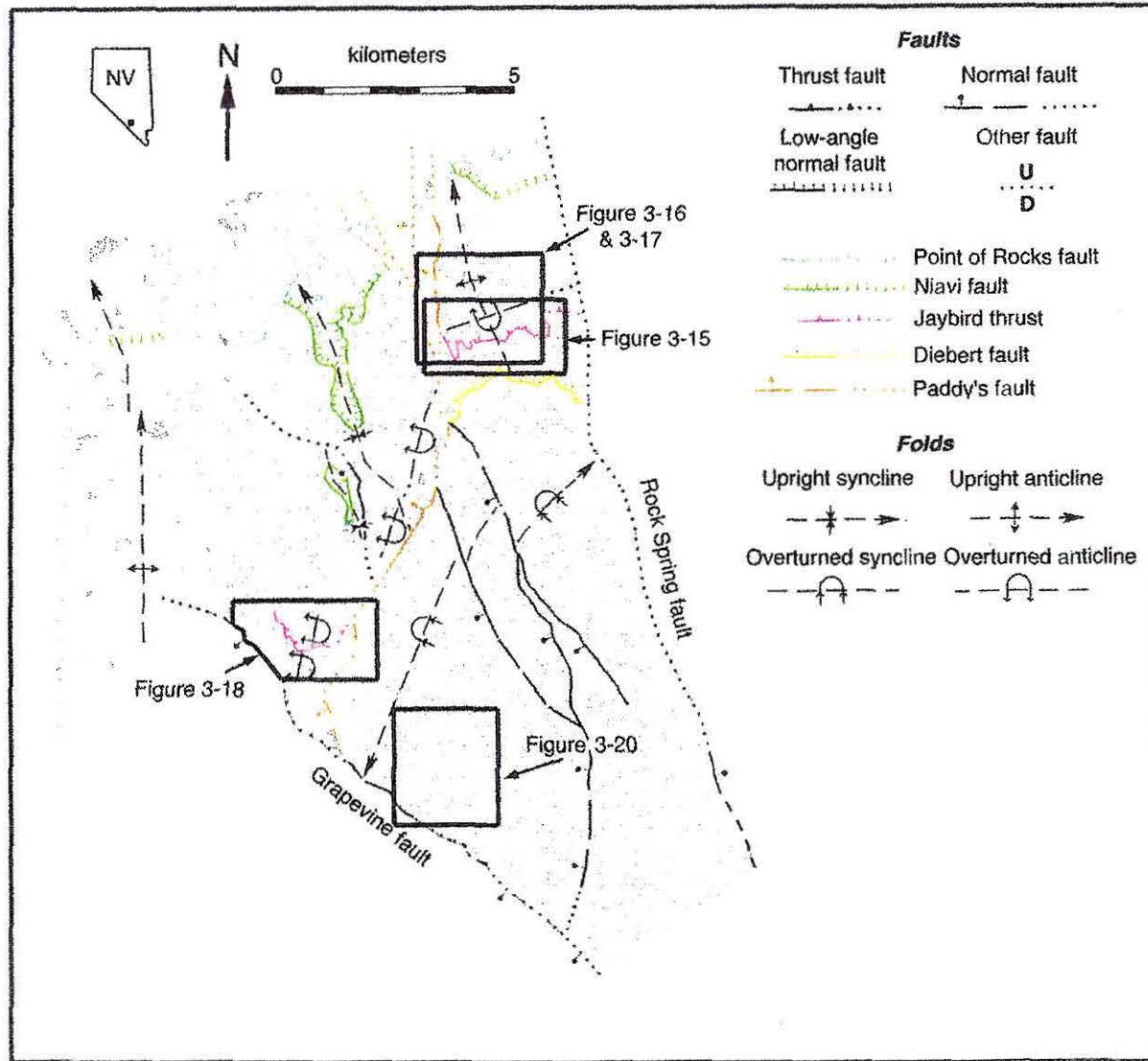
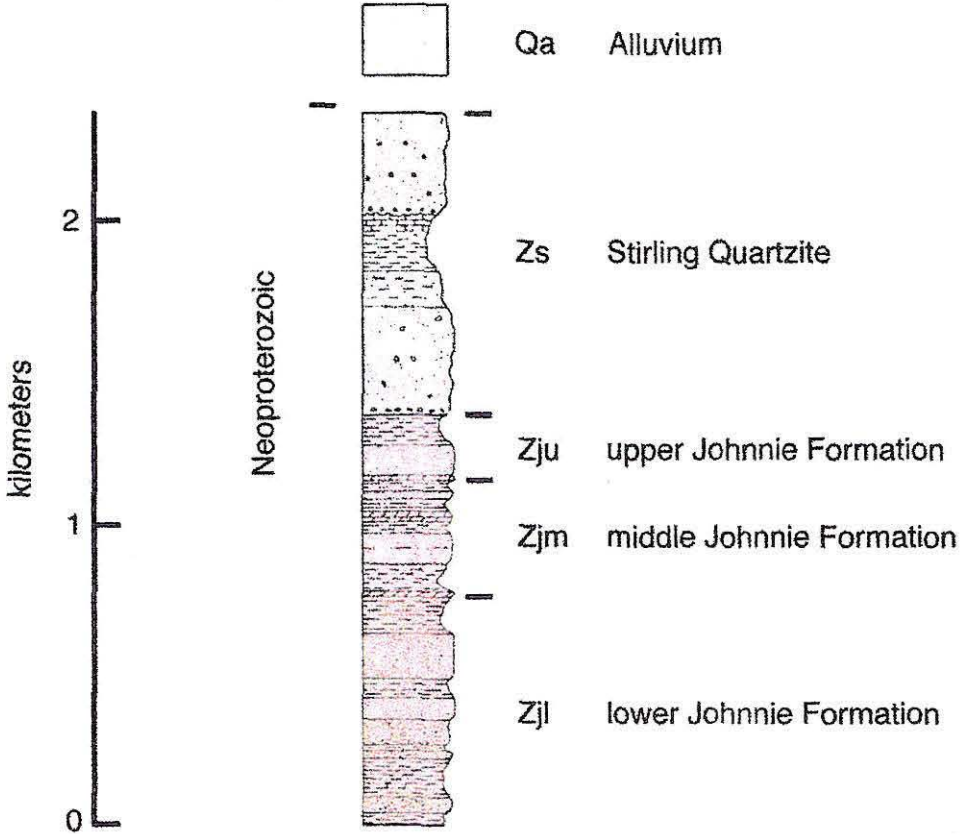
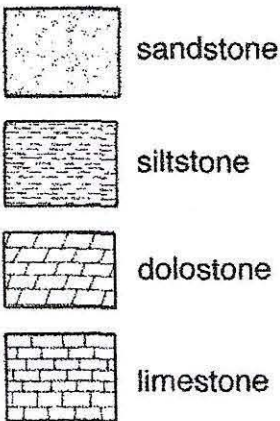


Figure 3-15. Geologic map of the Jaybird fault. See Figure 3-3 for location.

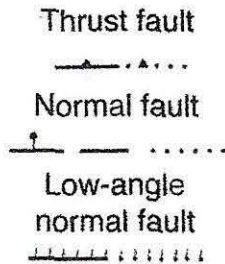
KEY



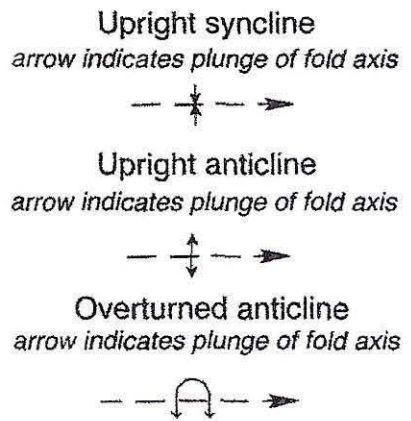
Lithology

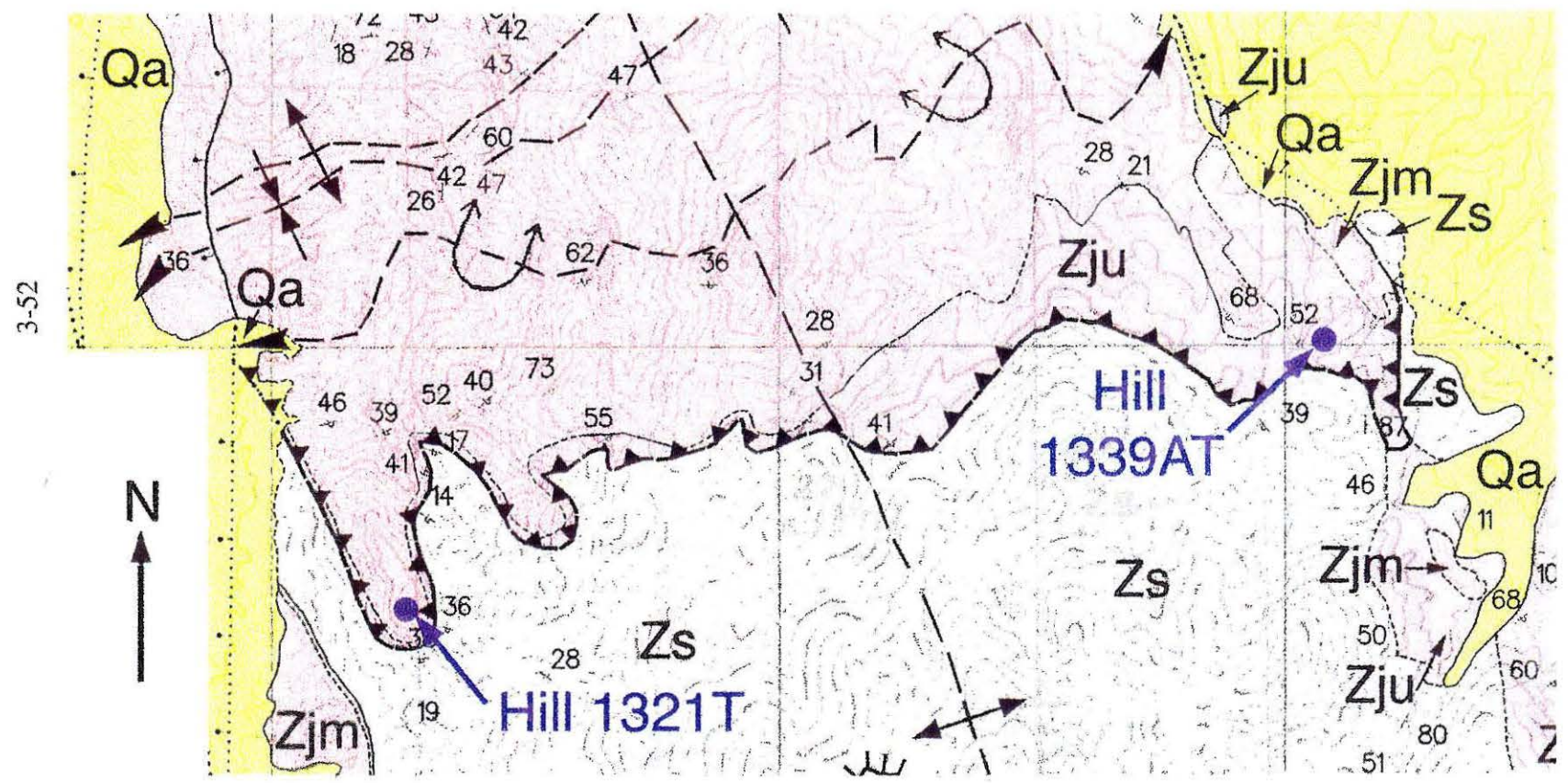


Faults



Folds





Dips outside this range (for example, an overturned attitude of 73° one kilometer to the northeast of Hill 1321T) are ascribed to small-scale folding. The axial plane of the hanging wall anticline dips more shallowly (30°) than other folds in the Johnnie Formation to the north. Bedding in the Stirling A quartzite is overturned and dips $36-38^\circ$. Since bedding in the Stirling Quartzite is upright less than 150 meters from the fault, folding in the Stirling Quartzite is probably confined to rocks immediately adjacent to the fault.

On Hill 1321T, about ten meters of upper Johnnie Formation purple fine sandstone occurs between the oolite and the fault plane. This thickness is substantially less than the thickness of the upper Johnnie Formation at Johnnie Wash (~ 303 meters) and in the area shown on Figure 3-12. However, the thickness of the upper Johnnie Formation does not provide a solid constraint on the throw of the fault. An unconformity at or below the base of the Stirling Quartzite may omit considerable section in the upper Johnnie Formation at Hill 1321T. Such an unconformity is present 3.1 kilometers to the northwest of Hill 1321T in the area shown on Figure 3-5. A pebble conglomerate below the fault at Hill 1321T may correlate with the conglomerate (Zjca) which overlies the unconformity on Figure 3-5. Structural and stratigraphic relationships near Hill 1339AT are similar to relationships at Hill 1321T. In other areas, the fault is obscured by talus from the lower quartzitic member of the Stirling Quartzite.

In the southern part of the study area, the Jaybird fault involves a little over 200 m of structural relief on the base of the Stirling Quartzite. Bedding in the Stirling Quartzite adjacent to the fault is steep and overturned, dipping 88° to the southwest. About 200 m to the south of the fault, bedding is upright and dips $35-46^\circ$ to the east-southeast. The upper Johnnie Formation in the hanging wall of the fault has been tectonically thickened by tight folds with a wavelength on the order of 5 m. Folding within the upper Johnnie Formation was not studied systematically. One fold has an overturned forelimb dipping 69° to the west and an upright backlimb dipping 35° to the west-northwest. The upper Johnnie

Formation is pervasively cleaved. The Jaybird fault cuts a fold train in the middle Johnnie Formation and offsets the axial surface of an overturned anticline by at least 350 m.

*Folds within the Johnnie Formation in the Hanging Wall
of Paddys fault*

The hanging wall of the Diebert fault and Paddys fault contains a train of buckle folds. These folds have a wavelength of about 500 m and a maximum amplitude of about 100 m. Folds die out upward within the upper Johnnie Formation. Folding of the base of the Stirling Quartzite is minor, and largely localized along the Jaybird fault (described above). In the southern part of the study area, the fold train is folded by the Hill 937T anticline and the Hill 1274T syncline.

Previous work - Nolan (1929) recognized folds within the Johnnie Formation but did not describe them in detail. Burchfiel schematically shows the folds as an overturned anticline on the Geologic Map of the Specter Range Quadrangle, Nevada (Burchfiel, 1965). Traces of fold axial surfaces were mapped by Hamill (1966) and Ivošević (1976) during thesis work. Generalized axial traces are depicted by Burchfiel and others (1983).

This study - Folds in the northern part of the study area were studied in reconnaissance with the aid of an AVIRIS image (see Appendix 3-A at the end of this chapter for processing information). As shown in Figure 3-16, AVIRIS image reveals a prominent dolostone marker bed in the middle Johnnie Formation. This dolostone is purple on the AVIRIS image, and reddish purple on the geologic map as shown in Figure 3-16. The schematic overturned anticline of Burchfiel (1965) actually consists of three folds. From north-northwest to south-southeast the three folds are (1) an upright anticline, (2) an upright syncline, and (3) an overturned anticline. The overturned anticline is adjacent to the Jaybird fault as mentioned above. The folds strike west-southwest/east-northeast. The Johnnie Formation to the north of the folds dips 9-39° with dip directions ranging from north-northwest to north-northeast. Much of the range in dip is due to small-scale folding.

Figure 3-16. AVIRIS image (top) and geologic map (bottom) of folds within the Johnnie Formation in the northeastern part of the study area.

Qa	alluvium
Zs	Stirling Quartzite
Zju	upper Johnnie Formation
Zjm ₂	middle Johnnie Formation (above marker bed)
	dolostone marker bed
Zjm ₁	middle Johnnie Formation (below marker bed)

Contact

Dashed where approximately located
Dotted where concealed

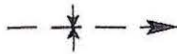
Fault

Dashed where approximately located;
Dotted where concealed

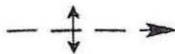
Normal Fault

Dashed where approximately located;
Dotted where concealed;
ball on downthrown side

Upright syncline

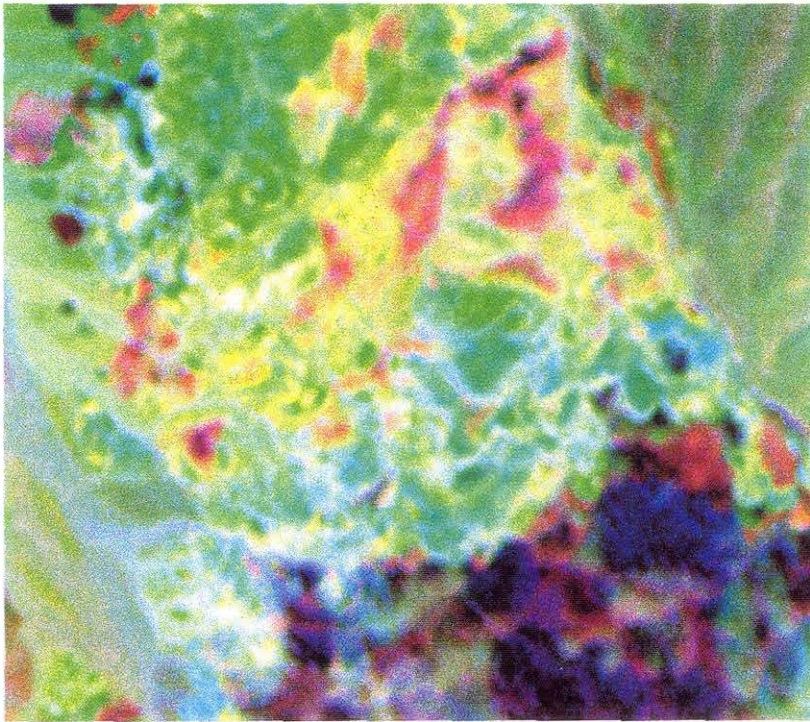


Upright anticline

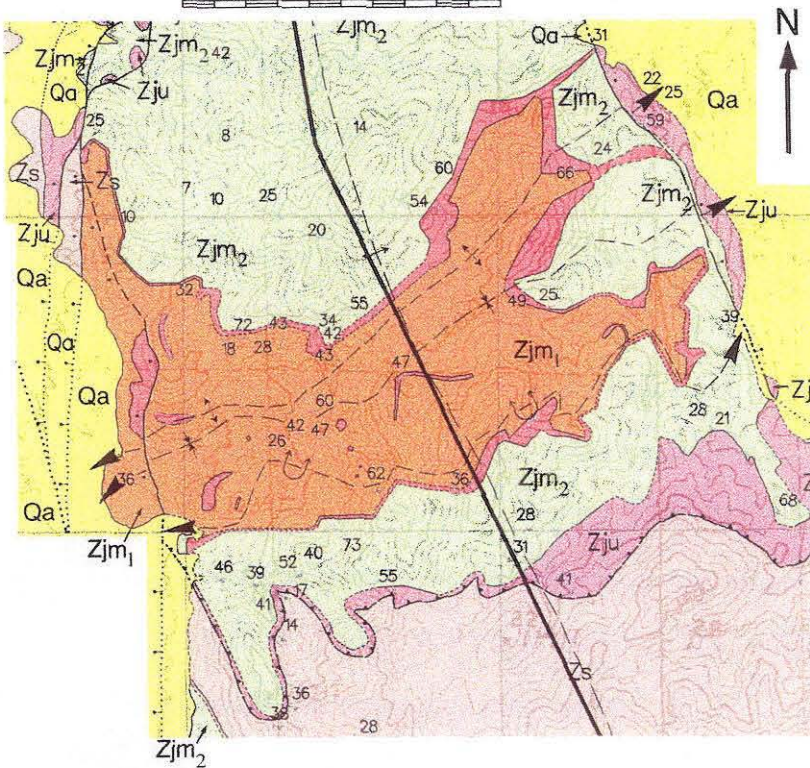


Overturned anticline





0 500 1000 METERS



The folds are shown on Figure 3-17 and all locations mentioned below are on that Figure. The upright anticline has a forelimb dipping $42-66^\circ$ and a backlimb dipping $32-60^\circ$. A single backlimb dip of 72° about 600 m southwest of Hill 1348T is ascribed to small-scale folding. The similar forelimb and backlimb dips suggest a steeply dipping axial plane. The amplitude of the fold is probably on the order of 75 m. The fold is best defined by dinosaur-spine-like outcrops of dolostone at the eastern base of Hill 1348T, along the crest of Hill 1277T, and along the eastern flank of Hill 1329T. These outcrops are clearly visible in purple on the AVIRIS image. An attitude from the hinge region of the fold suggests that the fold plunges to the east at about 24° . To the east of these hills, the axial trace of the fold is cut by a north-northwest/east-southeast striking, east-side-down high-angle normal fault. The continuation of the fold east of the fault is likely, but the location of the trace is unknown. To the west of these hills, the fold is less well-defined by the outcrop distribution of dolostone. A relatively flat-lying dolostone outcrop which caps a hill about 1 km southwest of Hill 1348T is probably a remnant of the fold hinge. To the west of this outcrop, the fold is cut by a north-south striking west-side-down high-angle normal fault.

Scant structural data from the upright syncline suggests a forelimb dip of $25-47^\circ$. Since the backlimb dips $42-66^\circ$, the syncline is asymmetric with a south-southeast vergence. Dolostone involved in the forelimb of the fold is best exposed south of Hill 1329T, on the hillside 500 m south-southwest of Hill 1348T, and on the north flank of Hill 1239T. Outcrops at the first two locations are readily apparent on the AVIRIS image (Figure 3-16).

The overturned anticline is adjacent to the Jaybird fault as mentioned above. The forelimb is overturned and dips $39-46^\circ$ to the north-northeast. The backlimb dips $25-47^\circ$, so the fold is roughly isoclinal and verges south-southeast.

Of the three folds in the northern part of the study area, only the overturned anticline can be followed to the south. The anticline is shown on Figure 3-12 and all locations in the

Figure 3-17. Geologic map showing folds within the Johnnie Formation in the northeastern part of the study area. See Figure 3-3 for location.

Qa	alluvium
Zs	Stirling Quartzite
Zju	upper Johnnie Formation
Zjm ₂	middle Johnnie Formation (above marker bed)
	dolostone marker bed
Zjm ₁	middle Johnnie Formation (below marker bed)

Contact

Dashed where approximately located
Dotted where concealed

Fault

Dashed where approximately located;
Dotted where concealed

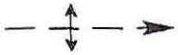
Normal Fault

Dashed where approximately located;
Dotted where concealed;
ball on downthrown side

Upright syncline

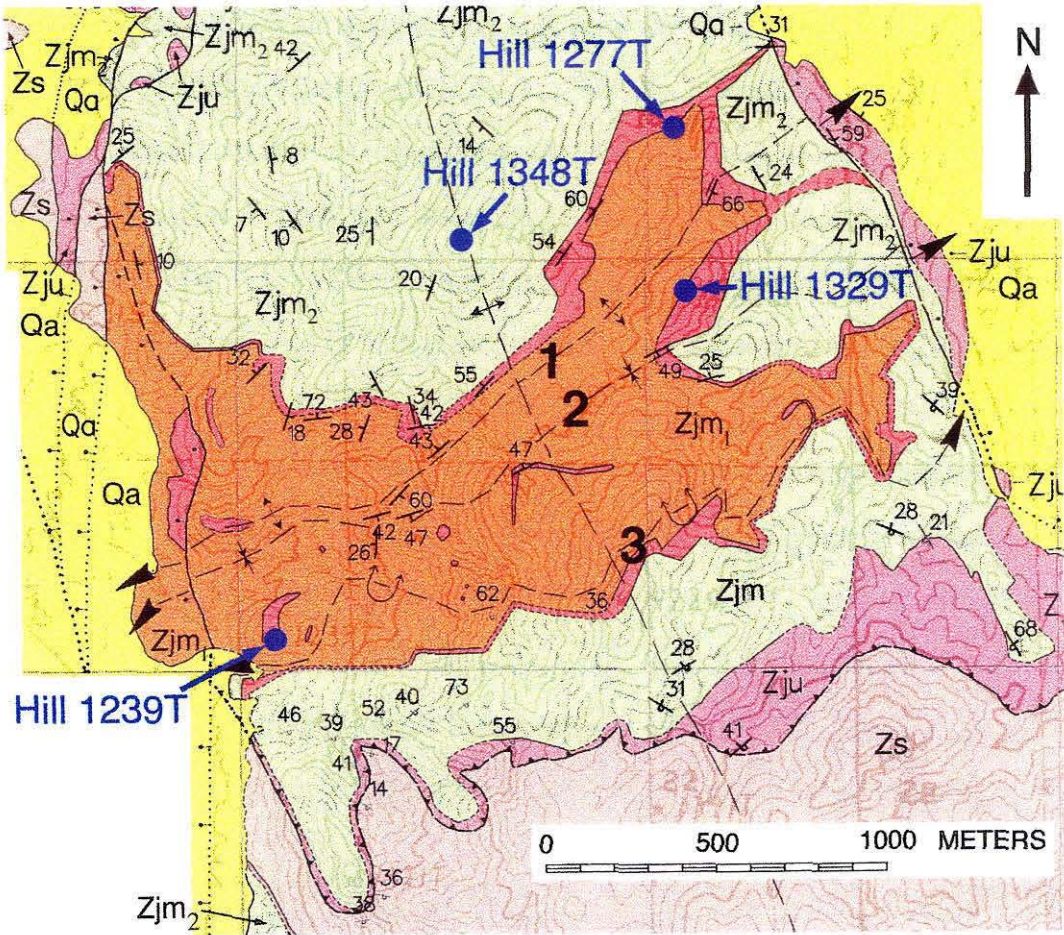


Upright anticline



Overtured anticline





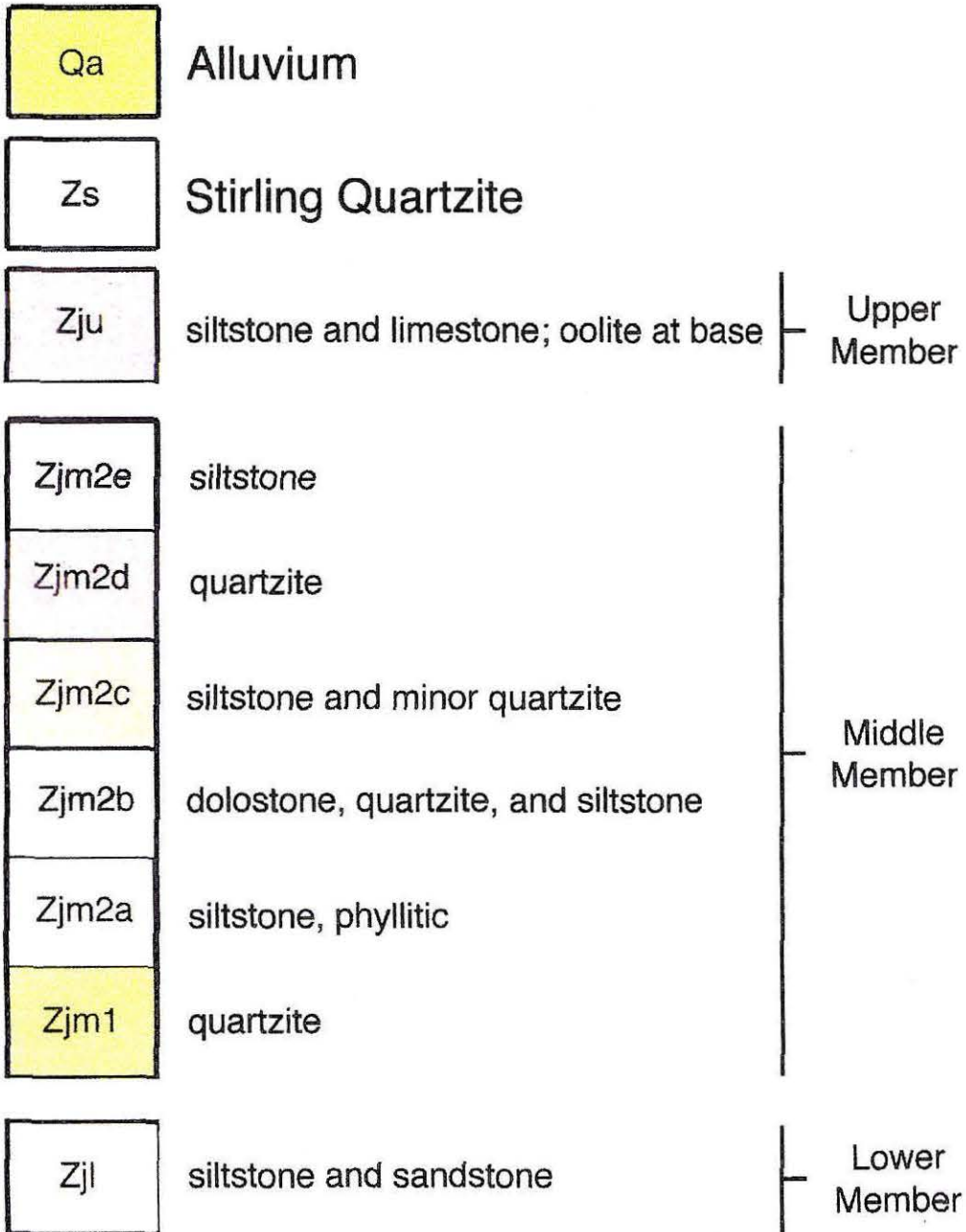
following two paragraphs refer to that figure. The anticline is disrupted by a number of high-angle normal faults. The strike of the anticline changes by about 70° from west-southwest/east-northeast in the north to south-southwest/north-northeast in the central part of the study area.

Broadly speaking, the anticline displays three categories of dips: backlimb, hinge, and forelimb. Backlimb dips are upright and range between 9 and 70° . Backlimb strike is generally north-northeast/south-southwest, but, like dip, ranges considerably. The variability in backlimb attitude suggests considerable small-scale folding within the Johnnie Formation. Small-scale folds were not studied in detail, but one small-scale syncline on the southeast flank of Hill 1314T strikes north-northeast/south-southwest and has upright backlimb and forelimb dips of 55 and 58° , respectively. Burchfiel (1965) observed two other small-scale folds in the Johnnie Formation within the central part of the study area. Most hinge dips are between 21 and 49° to the east-northeast. The hinge involves the Stirling Quartzite, as demonstrated by the outcrop distribution of quartzite northeast of Hill 1416T. The forelimb is overturned and dips between 30 and 73° . Involvement of the Stirling Quartzite in the overturned limb is uncertain. A 1.25 km long and 250 - 400 m wide block of overturned Stirling Quartzite is exposed east of Hill 1448T. This overturned block could belong to the overturned limb of the anticline or to the footwall syncline below the Jaybird fault.

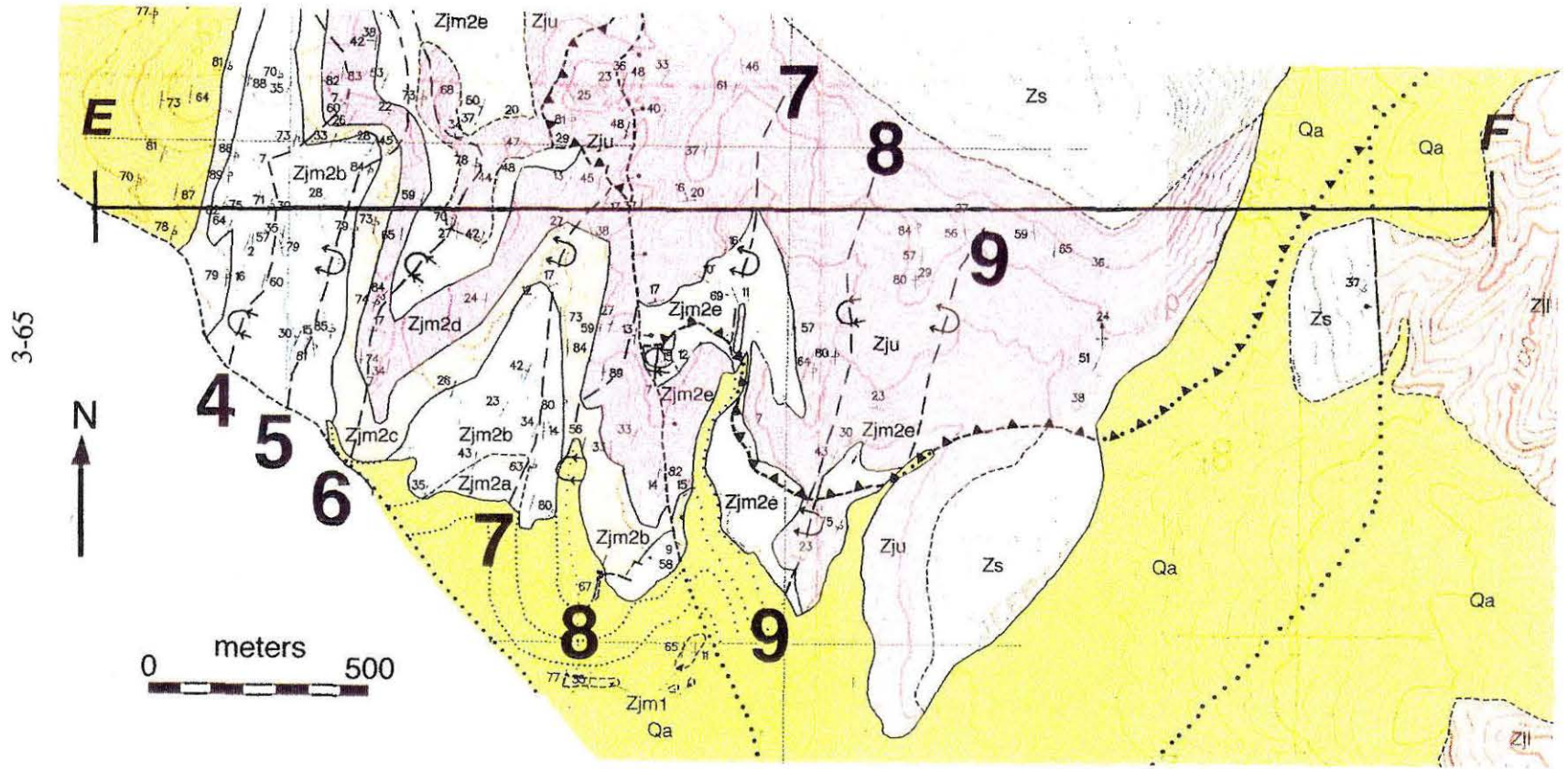
Folds were studied in the greatest detail in the southern part of the study area, and are shown on Figures 3-18 and 3-19. In this area, the hanging wall fold train involves seven major folds with a wavelength of roughly 350 m. These folds generally strike north-south, verge east, and plunge $\sim 20^\circ$ to the north based on hinge dips.

Fold 4 and Fold 5 have axial surfaces that dip 25 - 30° . These folds involve a competent quartzite interval as well as adjoining intervals of siltstone and an interval of mixed siltstone, quartzite, and carbonate. Both folds have relatively tight hinges. Fold 5 is nearly

Figure 3-18. Geologic map of fold train in the hanging wall of Paddys fault in the southern part of the study area.



Johnnie Formation



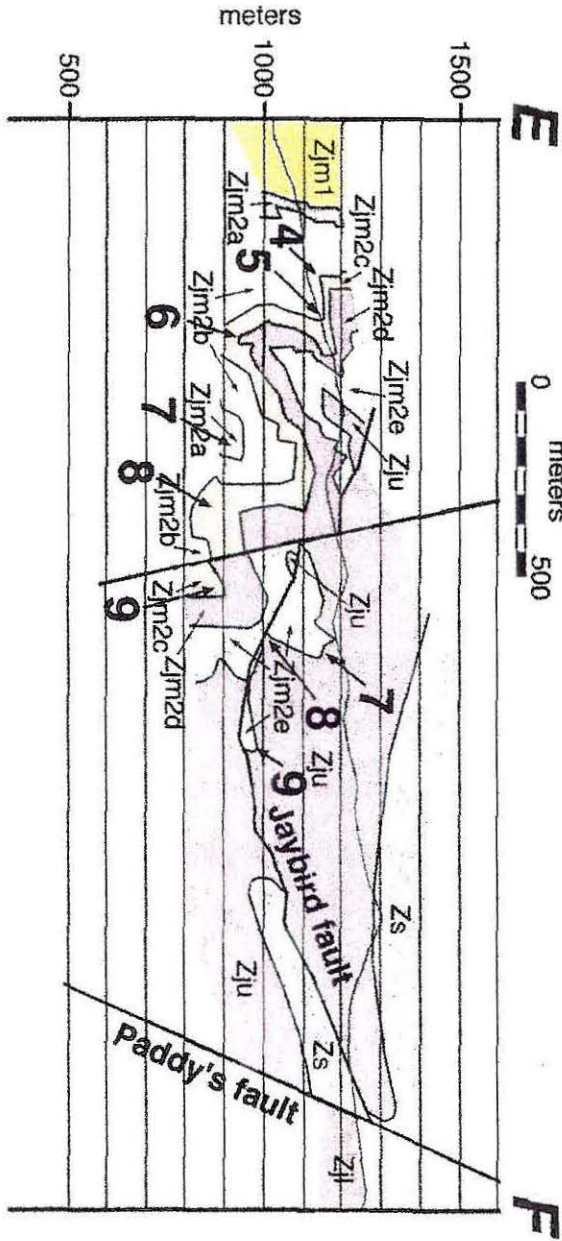


Figure 3-19. Cross section through folds shown in Figure 3-18.

isoclinal in its hinge region. The amplitude of Fold 4 is poorly constrained, but the amplitude of Fold 5 is about 75 m.

Fold 6 involves the same stratigraphic units. The fold has a steeper axial surface and a greater amplitude. The axial surface steepens downward from 38 to 65°, and the fold has an amplitude of about 100 m. The fold is relatively tight. In the quartzite interval, for example, dip changes from 34° west to 74° east in an across-strike distance of about 50 m. Where the fold involves the Johnnie oolite, the dip of the oolite changes from an upright 27° west to an overturned 70° west in an across-strike distance of about 10 m.

Fold 7 involves the same stratigraphic units as the three folds to the west of it. Like the syncline described in the preceding paragraph, the fold has a steep axial surface dipping roughly 60° and an amplitude of about 100 m. Fold 7 is not as tight as the preceding three folds. Mapping and limited structural data suggests a shallowly dipping hinge domain with an across-strike width of 100 to 200 m.

Faulting and lack of exposure preclude a detailed geometric understanding of the easternmost fold pair (Folds 8 and 9). However, these two folds are similar to the folds described above in several respects. The easternmost pair involves the same stratigraphic units. The folds plunge 17-23° to the north based on hinge dips. The forelimb of the anticline (Fold 9) is steep to moderately overturned. Neither of the easternmost folds appears to have the tightness or recumbent character of Folds 4 and 5.

*Folds within the Johnnie Formation in the Footwall
of Paddys fault*

A train of buckle folds also developed within the footwall of Paddys fault. Folding within the middle Johnnie Formation is similar in wavelength and amplitude to folds in the same part of the Johnnie Formation in the hanging wall. Axial surfaces generally dip more shallowly (15-40°). Folding in the lower Johnnie Formation is short wavelength and low amplitude.

Previous work - Burchfiel (1965) and Burchfiel and others (1983) schematically indicate an overturned syncline within the Johnnie Formation in the footwall of Paddys fault. During thesis work, Ivosevic (1976) discerned the complexity of folding in the Johnnie Wash area, but did not characterize fold geometry in detail.

This study - Folding within the footwall Johnnie Formation was studied in detail in the southern part of the study area with the aid of an AVIRIS image (Figure 3-20). As shown in Figure 3-21, folds generally consist of a limb that dips to the east at a shallow angle (10° - 30°), and a limb which dips steeply to the east (60° - 90°) or is overturned to the west. Folding is disharmonic, and the highest fold amplitude occurs in the upper part of the middle Johnnie Formation. Within that stratigraphic interval, folds achieve about 90% of the amplitude of the largest fold in the hanging wall. The base of the Stirling Quartzite is not folded.

Cleavage within the Johnnie Formation

The Johnnie Formation is cleaved throughout the field area, and this cleavage was studied in detail in the vicinity of the folds in the footwall of Paddys fault. As shown in Figure 3-22, cleavage generally dips to the west subparallel to the axial planes of the folds. Cleavage-bedding angles range between 60° and 90° with a median of 77° (Figure 3-23). As shown in Figure 3-24, cleavage-bedding angles between 60° and 77° are generally found in beds which dip 10° - 30° E and 60° - 90° E (i.e., in fold limbs). In contrast, cleavage-bedding angles between 77° and 90° are most abundant in beds dipping 30° - 60° E (i.e., in fold hinges).

The absence of low cleavage-bedding angles, and the relationships between cleavage-bedding angle and fold geometry, suggests the presence of a single early-formed cleavage in the Johnnie Formation. This cleavage probably developed at a high angle to bedding before folding. During folding, cleavage in incompetent units like siltstone rotated to lower cleavage-bedding angles due to flexural flow in fold limbs. In fold hinges, cleavage

Figure 3-20. AVIRIS image and geologic map of folds in the footwall of Paddys fault in the southern part of the study area.

Qa	Alluvium	
Zs	Stirling Quartzite	
Zju	siltstone and limestone; oolite at base	Upper Member
Zjm2e	siltstone	
Zjm2d	quartzite	Middle Member
Zjm2c	siltstone and minor quartzite	
Zjm2b	dolostone, quartzite, and siltstone	
Zjm2a	siltstone, phyllitic	
Zjm1e	quartzite	
Zjm1d	siltstone, phyllitic	
Zjm1c	quartzite	
Zjm1b	siltstone	
Zjm1a	cherty dolostone	
Zjl	siltstone and sandstone	

Johnnie Formation

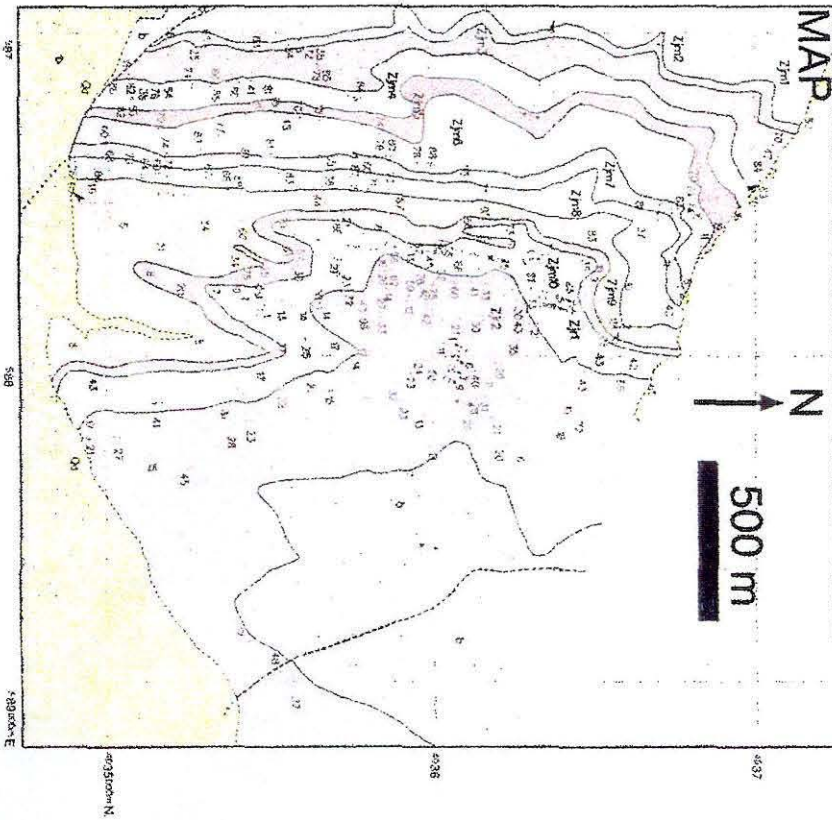


Figure 3-21. Cross section through folds in Figure 3-20.

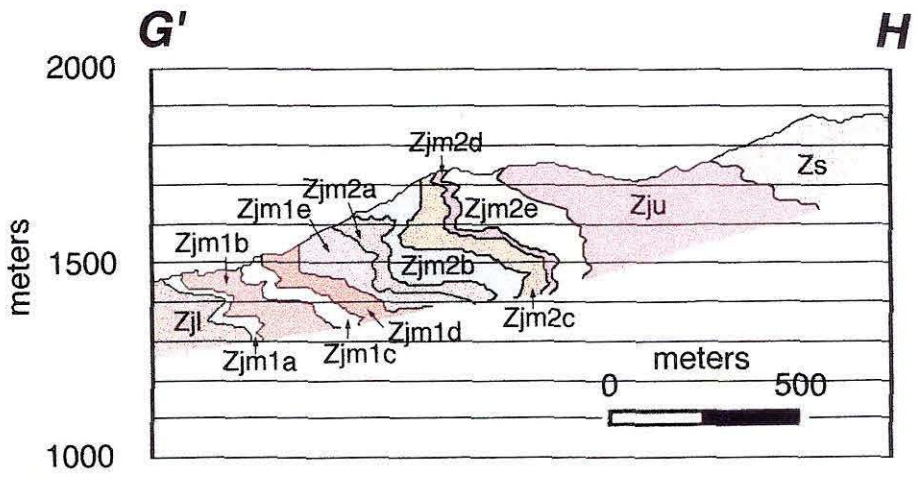
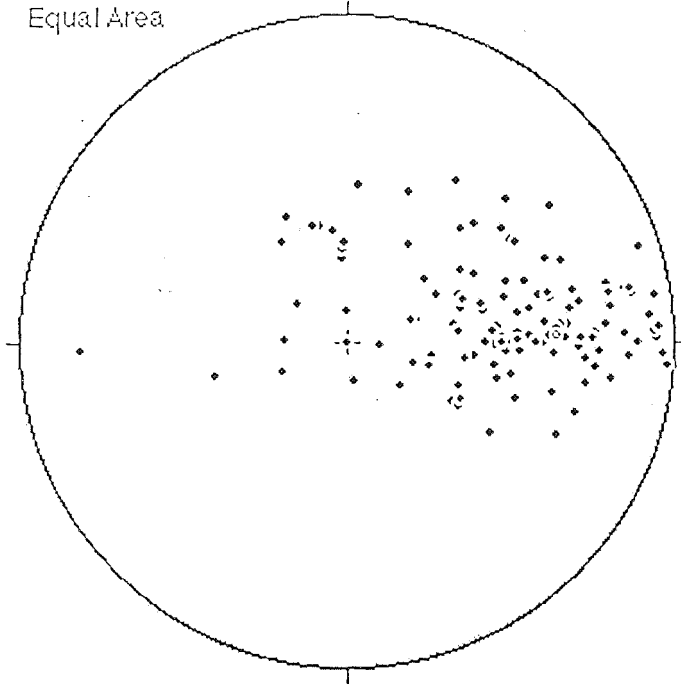
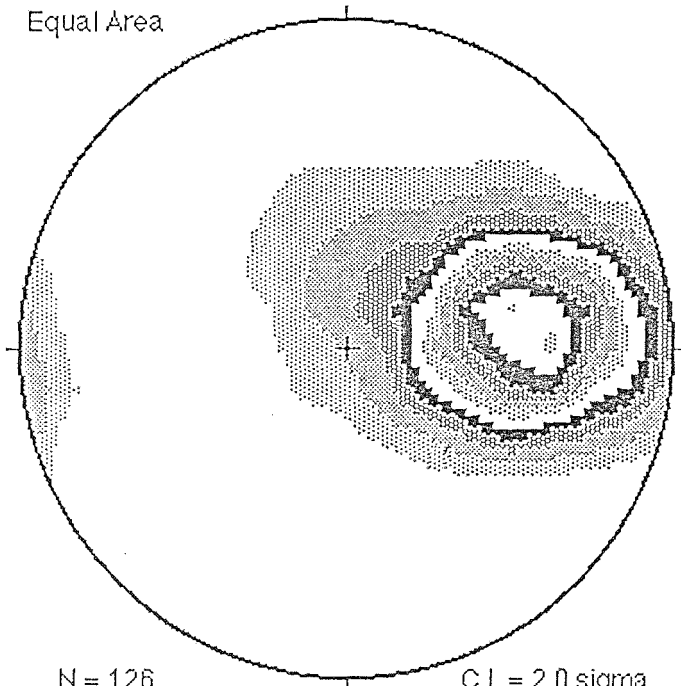


Figure 3-22. Lower hemisphere stereoplot of poles to cleavage in the Johnnie Formation.

Equal Area



Equal Area



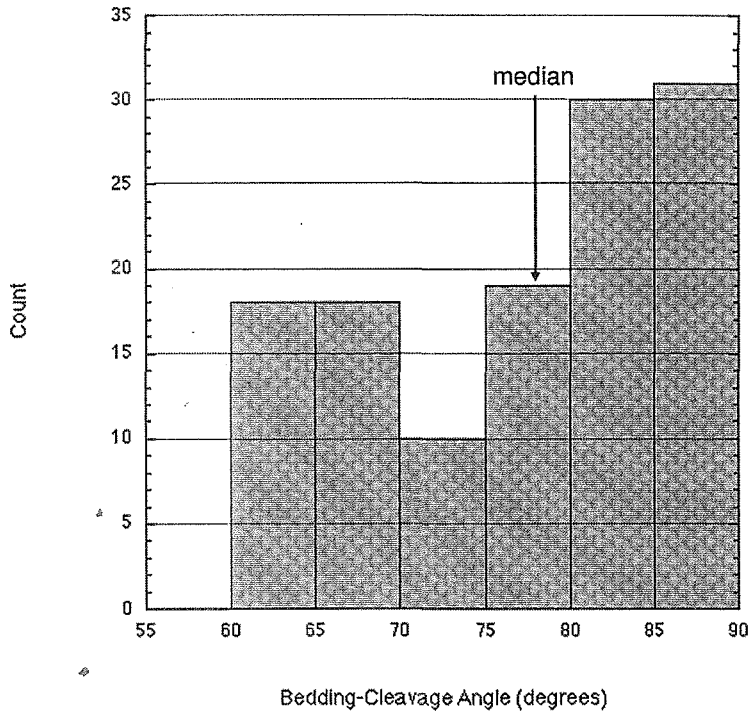
N = 126

C.I. = 2.0 sigma

Figure 3-23. Bedding-cleavage angle in the Johnnie Formation.

A

n = 126



B

n = 126

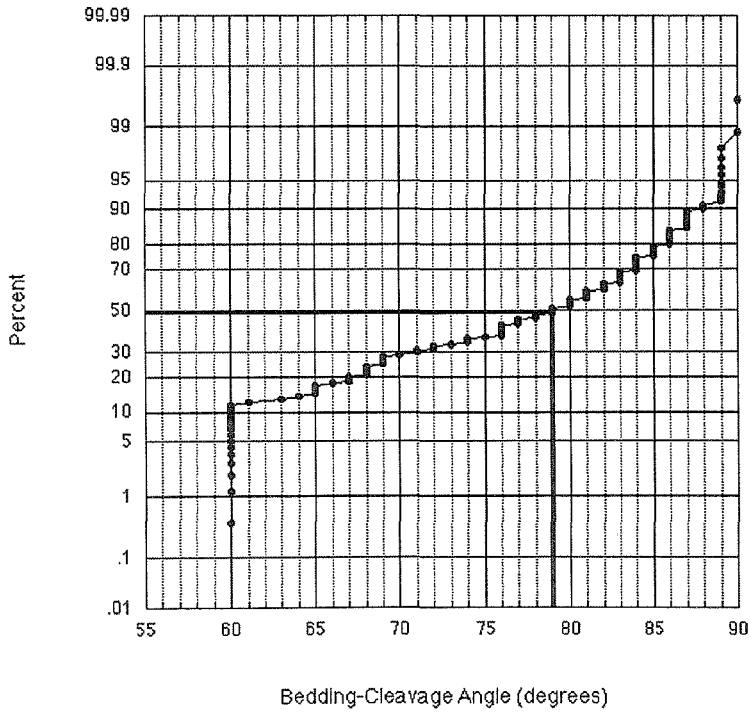
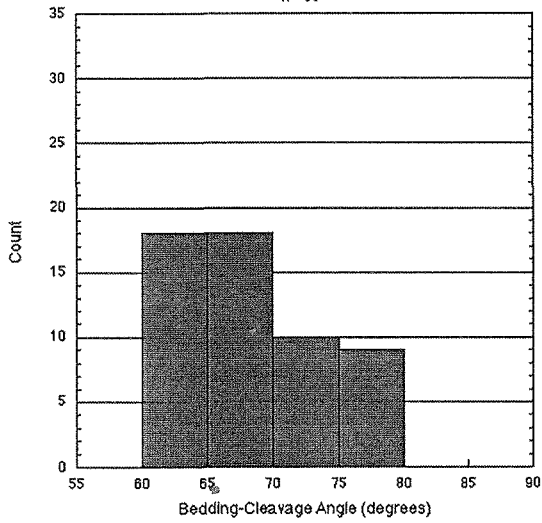
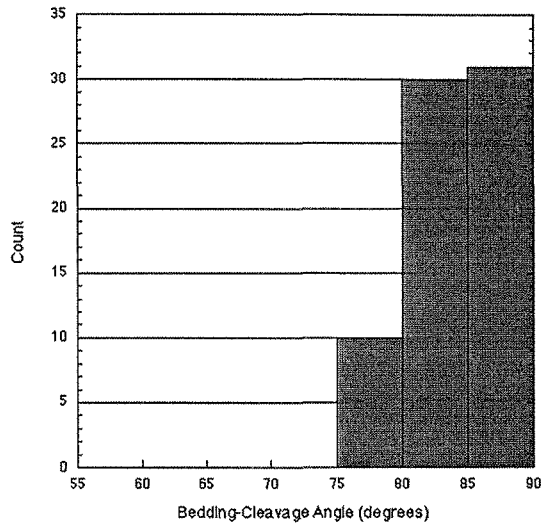


Figure 3-24. Dip histogram for beds with bedding-cleavage angle between 60 and 77° (left), and 77 and 90° (right).

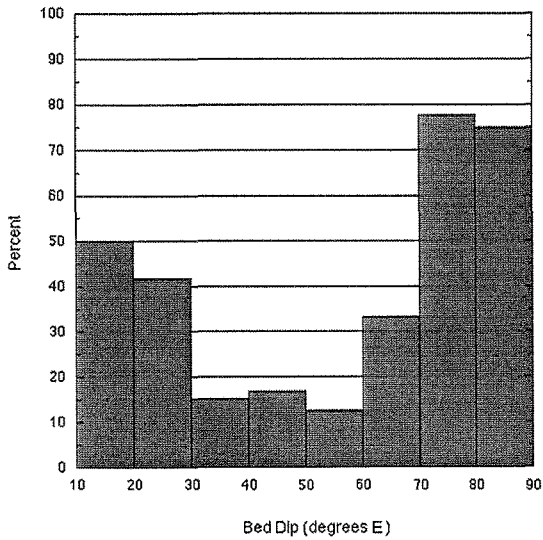
Histogram of Bedding-Cleavage Angle
 ($\beta = 60 - 77$)
 n = 55



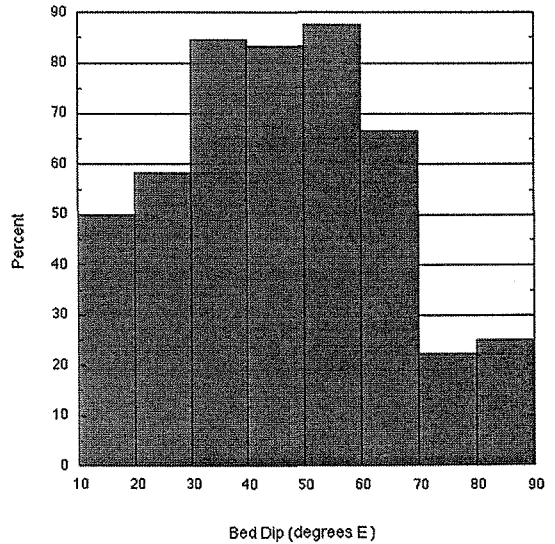
Histogram of Bedding-Cleavage Angle
 ($\beta = 77 - 90$)
 n = 71



Bed Dip Histogram for Cleaved Beds
 ($\beta = 60 - 77$)



Bed Dip Histogram for Cleaved Beds
 ($\beta = 77 - 90$)



remained at a high angle to bedding. In addition, competent units like quartzite did not experience flexural flow and preserve high cleavage-bedding angles regardless of position within a fold.

AGE OF EXTENSIONAL STRUCTURES

Ash beds from faulted and tilted conglomerate and breccia in the northwesternmost part of the study area provide the only direct age constraint on extensional structures in the northwestern Spring Mountains. The polymict conglomerate occurs above a carbonate breccia in three tilted fault slices. Biotite from interbedded ash deposits yielded K-Ar ages of 12.6 \pm .32, 13.3 \pm .33, and 13.5 \pm .34 Ma (Nakata in Zigler and Simonds, 1992). Miocene deposits were only mapped in reconnaissance in this study, but the presence of these deposits, including landslide breccias, in tilted fault slices suggests that the ages are syntectonic. In addition, the author located a pumaceous ash dated by Fleck (in Zigler and Simonds, 1992) and found that the bed has an attitude of N33W/20NE. This ash overlies the landslide breccia, and yielded plagioclase K-Ar ages of 10.9 and 12.0 Ma which are in general agreement with the biotite ages.

The ash beds probably date or post-date movement on the Point of Rocks fault, which is the youngest low-angle normal fault in the study area. The Tertiary deposits occur in the hanging wall of the Point of Rocks fault or in the hanging wall of a structurally higher fault that cuts the Point of Rocks fault along the northwestern margin of the study area.

Other age constraints on extensional structures are indirect. The Point of Rocks fault projects down-dip into a prominent, west-dipping low-angle reflection in the sub-surface of the Amargosa Desert (Brocher and others, 1993). This observation suggests that opening of the Amargosa Desert basin is probably linked to extension in the northwestern Spring Mountains. Widespread shallow sub-surface basalt flows of probable Miocene age provide an upper limit on the age of basin fill in the eastern Amargosa Desert. The flows cap 500 to 1000 m of Tertiary fill, and are overlain by 200 m or less of younger alluvium. The black

scoriaceous to dense basalt outcrops about 4.5 km northeast of the Fairbanks Hills (Swadley, 1983). The flows are chemically similar to 8.5 to 11 Ma flows on the Test Site (Crowe and others, 1986 in Brocher and others, 1993). Ash from alluvium overlying the basalt yielded a Miocene biotite K-Ar age (Swadley, 1983). Swadley thought the ash was altered and assigned a Quaternary age, but the Miocene K-Ar age may approximate the age of the ash and provide an upper limit on the age of the basalt. These findings suggest that the Amargosa Desert opened and was filled during the Miocene, and that extensional structures in the northwestern Spring Mountains may have been active at that time.

Miocene syn-extensional ages are common in the Death Valley region. Along the southern part of the Spring Mountains stable block, the Kingston Range/ Halloran Hills detachment moved at about the same time the syntectonic conglomerate was deposited in the northwestern part of the study area. The detachment cuts a hypabyssal felsic sill dated at 13.4 Ma (Fleck, K-Ar on hornblende, in Friedmann and others, 1996), and hanging wall sediments range in age from 13.1 \pm .2 Ma to 10.8 \pm .2 Ma (single grain laser fusion, Friedmann and others, 1996). Syntectonic deposits in the northwestern Spring Mountains are also time-correlative with the Eagle Mountain Formation of Niemi and others (in review). The Eagle Mountain Formation is exposed at Eagle Mountain and on the east side of the Resting Spring Range in Chicago Valley. Tephra within the Eagle Mountain Formation yielded laser-fusion Ar-Ar ages of 11.8, 12.8, and 14.7 Ma. The Spring Mountains syntectonic deposits may also time-correlate at least in part with the Navadu Formation of Snow and Lux (in review). The Navadu Formation outcrops in the Cottonwood Mountains, and contains the 12.1 Ma Tuff of Entrance Narrows. Both the Eagle Mountain and Navadu Formations have been interpreted as syn-extensional. Dips fan within the Navadu Formation, and the discordance across the basal unconformity is pronounced in many areas.

AGE OF CONTRACTILE STRUCTURES

The age of other contractile structures in the Death Valley region suggests that contractile structures in the northwestern Spring Mountains are probably Permo-Triassic or late Jurassic to Cretaceous in age. An apatite fission track age of 81.4 ± 8.5 Ma (Roy Dokka, pers. comm., 1996) may provide the only direct age constraint on Mesozoic tectonics in the study area. The sample was collected from the Stirling A quartzite about 5 km northwest of Paddys fault. This fission track age is the oldest apatite age from the Spring Mountains. Stirling A Quartzite yielded an apatite fission track age of 23.2 ± 3.3 Ma 17 km southeast of Paddys fault, and the Wood Canyon Formation yielded ages of 24.9 ± 15 Ma (only two grains counted) and 48.2 ± 6.6 Ma 11.25 km and 14 km southeast of the fault, respectively.

To understand the meaning of these ages, the apatite fission track ages must be placed within a regional geologic and geochronologic context. The apatite ages southeast of Paddys fault are older than much of the extension in the Death Valley extended domain. They are also older than syn-extensional deposits in the northwestern Spring Mountains (described in the preceding section) and syn-extensional basin deposits in Shadow Valley described by Friedmann and others (1996) along the southwestern border of the Spring Mountains structural block of Wernicke and others (1988). As a result, the apatite age may not directly date the uplift and unroofing of the Spring Mountains. Rather, the apatite may have resided in the apatite partial annealing zone for some time, so that the apatite age is older than the age of the Spring Mountains uplift.

The 81.4 Ma age northwest of Paddys fault suggests that the northwesternmost part of the range cooled before the rest of the Spring Mountains, and, in turn, that the area northwest of Paddys fault may have been structurally higher than the rest of the Spring Mountains since at least 81 Ma. Structural evidence supporting uplift of the area northwest of Paddys fault is described in Chapter 4. The apatite age does not necessarily date uplift

of the northwestern part of the range. Structural relief could have formed at an earlier time (e.g., Permo-Triassic), and the age could reflect Jura-Cretaceous uplift of the entire Wheeler Pass hanging wall. Jura-Cretaceous uplift along the Wheeler Pass thrust is supported by zircon fission track data from the area southeast of Paddys fault. Zircon ages define a fossil partial annealing zone that was quenched at 90-110 Ma (Wernicke and Dokka, in prep.).

Except for the apatite fission track data, no other direct evidence constrains the age of contractile structures in the northwestern Spring Mountains. As discussed in Chapter 4, contractile structures in the northwestern Spring Mountains may correlate with a number of other structures in the Death Valley region. Correlation of contractile structures in the northwestern Spring Mountains with the Lemoigne thrust in the Cottonwood Mountains (Snow, 1992) suggests a Permo-Triassic age. The Lemoigne thrust cuts strata containing early Permian fusulinids, and is overprinted by the contact metamorphic aureole of the Hunter Mountain batholith (Hall, 1971). The border phase of the batholith yielded a U-Pb age of 178 Ma on baddeleyite (Niemi and Saleeby in Niemi and others, in review), indicating that thrusting occurred between the early Permian and the Middle Jurassic. However, the proximity and structural similarity of the Lemoigne thrust to demonstrably Permo-Triassic structures in the Cottonwood Mountains, and the absence of other early to Middle Jurassic thrusts in the Death Valley region argues for a Permo-Triassic age.

As discussed in Chapter 4, contractile structures in the northwestern Spring Mountains could also correlate with the Cretaceous Panamint thrust in the Panamint Mountains. Cleavage associated with movement on the Panamint thrust cuts the 100 Ma Skidoo pluton (Wernicke and others, 1993).

In addition, structures in the northwestern Spring Mountains are along the southern projection of the Central Nevada thrust belt of Taylor and others (1993). They regarded the Central Nevada thrust belt as Jurassic or Cretaceous based on its central position with

respect to Jurassic thrusts in western and northeastern Nevada and Cretaceous thrusts in western Utah. However, as discussed in Chapter 4, the age of the Central Nevada thrust belt is poorly constrained.

SUMMARY

The table on the next page summarizes the sequence in which cleavage, faults, and folds developed in the northwestern Spring Mountains. Extensional structures and broad upright folds formed at or before 13.5 Ma. Regional relationships suggest that contractile structures are Permo-Triassic or late Jurassic to Cretaceous in age.

	Cleavage	Folding	Faulting
D1	cleavage formation at high angle to bedding		
D2	cleavage refraction	formation of overturned folds in Johnnie Formation	
D3			Jaybird fault
D4			Diebert fault Niavi fault
D5		Hill 1348T anticline Hill 1274T syncline	
D6			Point of Rocks fault
D7		Hill 937T anticline	
D8			Gold Spring fault Hill 5482 fault Paddys fault

APPENDIX 3 - A AVIRIS IMAGES

AVIRIS is an airborne scanner which acquires radiometric data in 224 channels in the visible and near infrared between .4 and 2.45 microns. The images used in this study have a spatial resolution of 20 m.

For easy interpretation, the images were processed to mimic Landsat Thematic Mapper band ratio images. This involved:

- 1.) Summing the AVIRIS channels which correspond to each Landsat band.

For example, $TMBAND1 = \text{SUM}(\text{CHANNEL}10:\text{CHANNEL}24)$, for each pixel.

- 2.) Correcting for haze by subtracting the minimum value in the scene.

For example, $TMBAND1CORR = TMBAND1 - \text{MINIMUM}(TMBAND1)$,
for each pixel.

- 3.) Assigning a commonly used band ratio to each primary color:

$RED = TMBAND5CORR/TMBAND7CORR$

$GREEN = TMBAND5CORR/TMBAND4CORR$

$BLUE = TMBAND3CORR/TMBAND1CORR$

- 4.) Multiplying each primary color by a band average:

For example,

$RED' = RED * (TMBAND1CORR + TMBAND2CORR + TMBAND3CORR +$
 $TMBAND4CORR + TMBAND5CORR + TMBAND7CORR) / 6$

- 5.) Applying a linear contrast enhancement for easy viewing.

Step 3 enhances lithologic differences while step 4 adds shadows to the image. The shadows provide geographic reference points for the eyes.

REFERENCES

- Brocher, Thomas M., Carr, Michael D., Fox, Kenneth F., Jr., and Hart, Patrick E., 1993, Seismic reflection profiling across Tertiary extensional structures in the eastern Amargosa Desert, southern Nevada, Basin and Range Province: Geological Society of America Bulletin, v. 105, no. 1, p. 30-46.
- Burchfiel, B. C., 1964, Precambrian and Paleozoic stratigraphy of Specter Range Quadrangle, Nye County, Nevada: Bulletin of the American Association of Petroleum Geologists, v. 48, no. 1, p. 40-56.
- Burchfiel, B. C., 1965, Structural geology of the Specter Range Quadrangle, Nevada, and its regional significance: Geological Society of America Bulletin, v. 76, no. 2, p. 175-191.
- Burchfiel, B. C., Fleck, R. J., Secor, D. T., Vincelette, R. R., and Davis, G. A., 1974, Geology of the Spring Mountains, Nevada: Geological Society of America Bulletin, v. 85, no. 7, p. 1013-1022.
- Burchfiel, B.C., Hamill IV, G.S., and Wilhelms, D.E., 1983, Structural geology of the Montgomery Mountains, and the northern half of the Nopah and Resting Spring Ranges, Nevada and California: Geological Society of America Bulletin, v. 94, no. 11, p. 1359-1376.
- Cornwall, Henry R., 1972, Geology and mineral deposits of southern Nye County, Nevada: Nevada Bureau of Mines and Geology Bulletin, v. 77, 45 p.

Friedmann, S. Julio, Davis, Gregory A., and Fowler, T. Kenneth, Geometry, paleodrainage, and geologic rates from the Miocene Shallow Valley supradetachment basin, eastern Mojave Desert, California, *in* Beratan, Kathi K., ed., *Reconstructing the history of Basin and Range extension using sedimentology and stratigraphy*: Geological Society of America Special Paper 303, p. 85-105.

Hall, Wayne E., 1971, *Geology of the Panamint Butte Quadrangle, Inyo County, California*: U. S. Geological Survey Bulletin, v. 1299, 67 p.

Hamill, Gilmore S., III, 1966, *Structure and stratigraphy of the Mount Schader quadrangle*, unpublished doctoral dissertation: Rice University.

Holm, Daniel K., Fleck, Robert J., and Lux, Daniel R., 1994, The Death Valley turtlebacks reinterpreted as Miocene-Pliocene folds of a major detachment surface: *Journal of Geology*, v. 102, no. 6, p. 718-727.

Ivosevic, Stanley Wayne, *Geology and ore deposits of the Johnnie District, Nye County, Nevada*, unpublished master's thesis: University of Nevada, Reno, 193 p.

Niemi, N.A., Wernicke, B.P., Brady, R.J., Saleeby, J.B., and Dunne, G.C., in review, *Distribution and provenance of the middle Miocene Eagle Mountain Formation, and implications for the tectonic development of the Death Valley extended terrane, California*: Geological Society of America Bulletin.

Snow, J. Kent, and Lux, Daniel R., in review, Tectono-sequence stratigraphy of Tertiary rocks in the Cottonwood Mountains and northern Death Valley area, California, and Nevada, *in* Wright, L.A., and Troxel, B.W., eds., Tertiary basins and volcanism in the Death Valley region; Their tectonic significance: Geological Society of America Special Paper.

Stewart, John H., 1970, Upper Precambrian and Lower Cambrian strata in the southern Great Basin, California and Nevada: U. S. Geological Survey Professional Paper 620, 206 p.

Swadley, W. C., 1983, Map showing surficial geology of the Lathrop Wells Quadrangle, Nye County, Nevada, U.S. Geological Survey Miscellaneous Investigations Series, I-1361.

Taylor, Wanda J., Bartley, John M., Fryxell, Joan E., Schmitt, James G., and Vandervoort, Dirk S., 1993, Tectonic style and regional relations of the central Nevada thrust belt, *in* Lahren, Mary M., Trexler, James H., Jr., and Spinosa, Claude, ed., Crustal evolution of the Great Basin and the Sierra Nevada, p. 57-96.

Wernicke, Brian, Snow, J. Kent, Hodges, Kip V., and Walker, J. Douglas, 1993, Structural constraints on Neogene tectonism in the southern Great Basin, *in* Lahren, Mary M., Trexler, James H., Jr., and Spinosa, Claude, ed., Crustal evolution of the Great Basin and the Sierra Nevada, p. 453-479.

Zigler, Jan L., and Simonds, F. William, 1992, A preliminary evaluation of the Point of Rocks fault, *in* Characterization of detachment faults in the Yucca Mountain region, U.S. Geological Survey Administrative Report 3GTD500M.

CHAPTER 4**THE KWICHUP SPRING THRUST
IN THE NORTHWESTERN SPRING MOUNTAINS, NEVADA:
IMPLICATIONS FOR LARGE-MAGNITUDE EXTENSION
AND THE STRUCTURE OF THE CORDILLERAN THRUST BELT****ABSTRACT**

Approximately 170 km² of new mapping in the northwestern Spring Mountains reveals contractile structures related to a regional thrust fault called the Kwichup Spring thrust. The Kwichup Spring thrust involves at least 1.4 km of stratigraphic throw. Along much of its length, the Kwichup Spring thrust has been reactivated or excised by a normal fault.

Stratigraphic and structural evidence suggests that the Kwichup Spring thrust correlates with the Montgomery thrust in the Montgomery Mountains. Correlation of these two thrusts requires a reappraisal of the geometry of the Cordilleran thrust belt in Nevada and southeastern California. The Kwichup Spring - Montgomery thrust probably correlates with either the Clery thrust in the Funeral Mountains or the Panamint thrust in the Panamint Mountains. Both possible correlations require large (>115 km) west-northwest translation of the Panamint and Cottonwood Mountains with respect to the Spring Mountains during Neogene extension.

Before this large-scale translation, the Panamint and Cottonwood Mountains were positioned along the southern projection of the Central Nevada thrust belt of Taylor and others (1993). Since contractile structures in the Cottonwood Mountains are Permo-Triassic, the Central Nevada thrust belt may be at least in part Permo-Triassic.

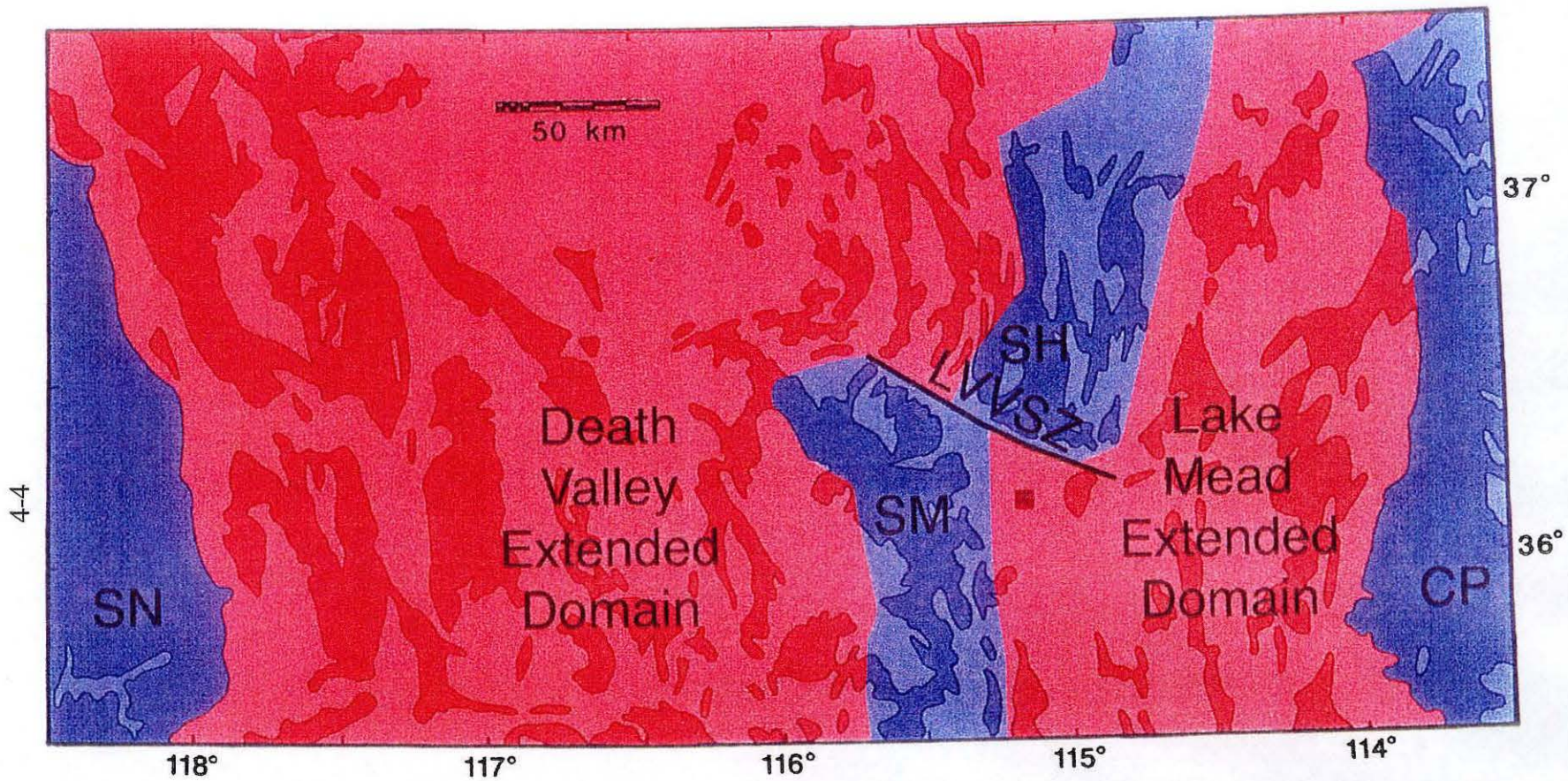
INTRODUCTION

During the last thirty years, the study of offset bedrock features and Tertiary basin deposits in southern Nevada and southeastern California has greatly improved our understanding of extensional tectonics. These studies resulted in the dramatic but controversial suggestion that the crust in this region may have extended by over 250 km since the Miocene (Snow and Wernicke, 1994; Snow and Wernicke, in press). This large amount of extension vastly exceeds earlier regional estimates of 10-35% (Stewart, 1978). Large-magnitude extension within the Basin and Range province may have been an important component of Pacific - North America plate motion during the Miocene and Pliocene (Dickinson and Wernicke, 1997).

According to Wernicke and others (1988), the distance between the Sierra Nevada Mountains and the Colorado Plateau widened by about 247 +/- 56 km along a vector of N73W +/- 12°. The crust extended within two domains, the Death Valley and Lake Mead extended domains, which are separated by the relatively unextended Spring Mountains and Sheep Range (Figure 4-1). In the Death Valley extended domain, abundant pre-extensional structural and stratigraphic markers and Tertiary basin deposits facilitate detailed tectonic reconstructions (e.g., Wernicke and others, 1988; Snow, 1992; Snow and Wernicke, in press).

The correlation of thrust faults in different ranges is critical to understanding the displacement of range blocks. Figure 4-2 shows the location of some of the major ranges between the Sierra Nevada and Spring Mountains. In the Death Valley domain, the correlation of the Panamint thrust in the Panamint Mountains with the Wheeler Pass thrust in the Spring Mountains constrains about 75% of the extension proposed by Wernicke and others (1988). Correlation of these two thrusts requires the westward translation of the Panamint and Cottonwood Mountains by over 125 km as shown in Figure 4-3. As the Panamint and Cottonwood Mountains moved away from the Spring Mountains, two

Figure 4-1. Map showing the location of the Death Valley and Lake Mead extended domains in southern Nevada and southeastern California. The relatively unextended blocks which border the extended domains are the Sierra Nevada Mountains (SN), Spring Mountains (SM), Sheep Range (SH), and Colorado Plateau (CP). The Las Vegas Valley shear zone (LVVSZ) separates the Spring Mountains and Sheep Range.



- extended domain
- stable block

Figure 4-2. Location map showing the study area and ranges mentioned in the text.

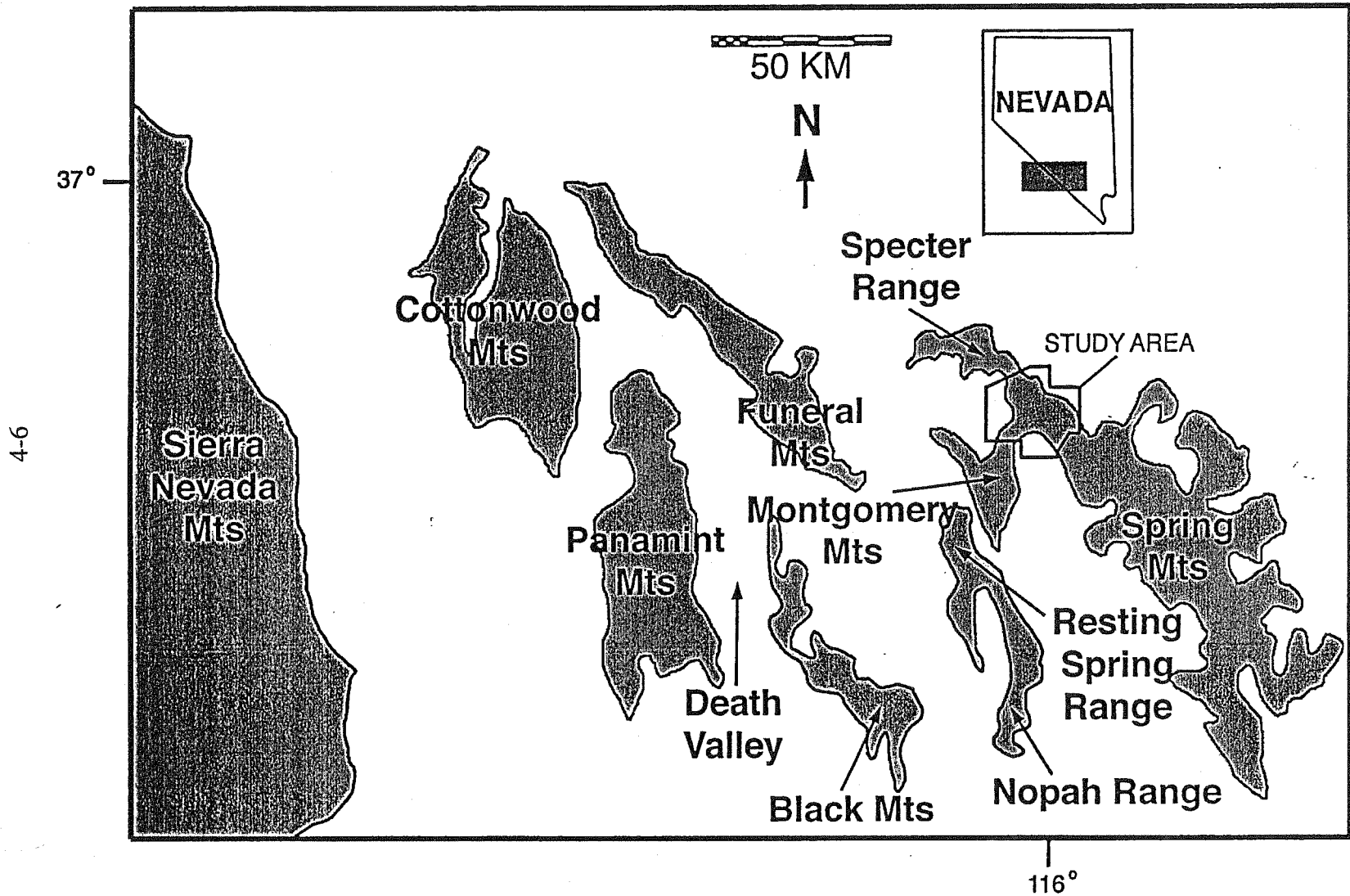
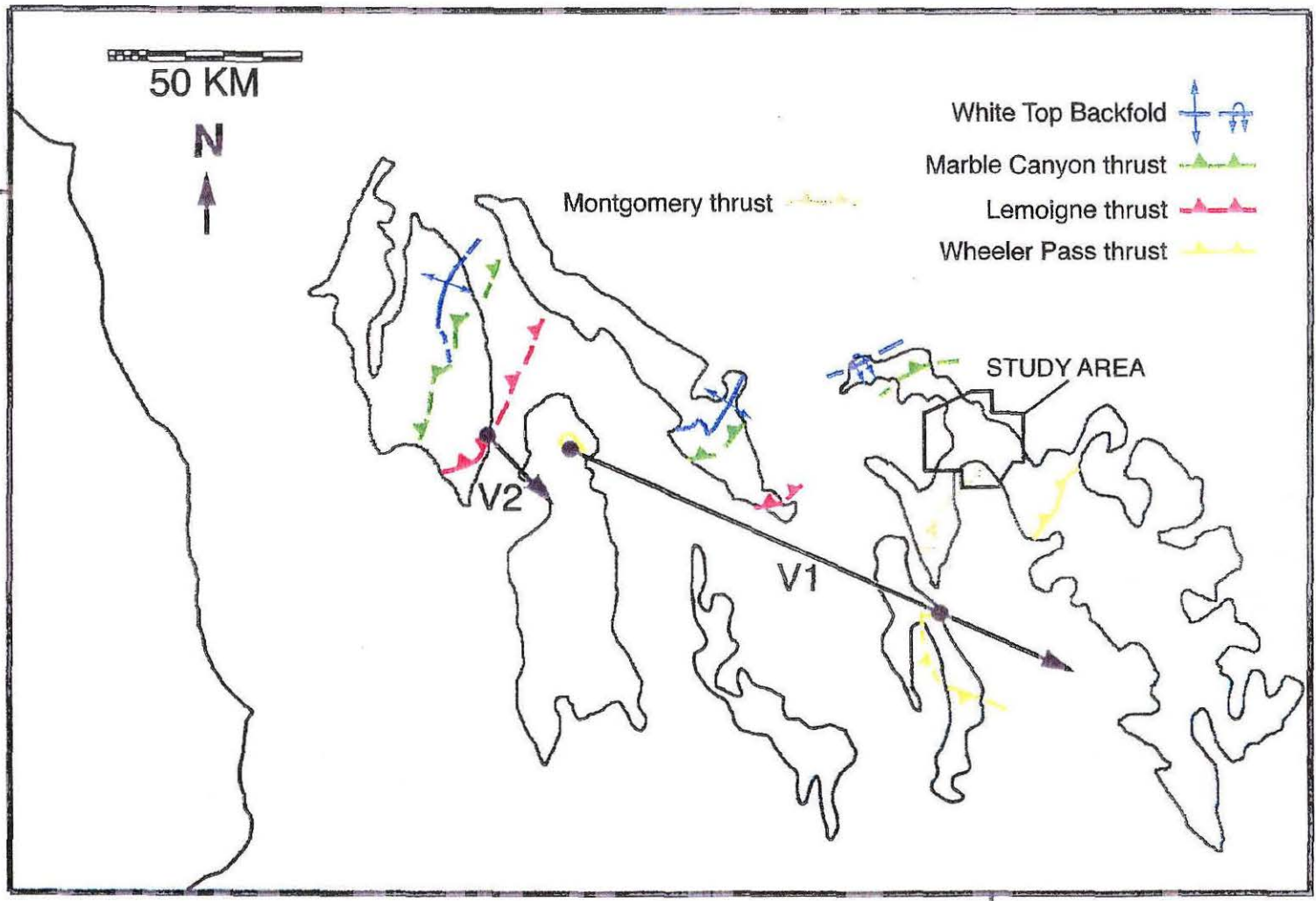


Figure 4-3. Map depicting the westward displacement of the Cottonwood and Panamint Mountains with respect to the Spring Mountains. Displacement vectors (V1 and V2) are from Wernicke and others (1988) and contractile structures are from Snow (1992). The structural affinity of the Montgomery thrust (shown in tan) is uncertain. V1 is based on the correlation of the Panamint thrust in the Panamint Mountains with the Wheeler Pass thrust in the Spring Mountains. V2 depicts the displacement on the Emigrant normal fault system as described by Hodges and others (1987).

37°



50 KM



- White Top Backfold 
- Marble Canyon thrust 
- Lemoigne thrust 
- Wheeler Pass thrust 

Montgomery thrust

STUDY AREA

V2

V1

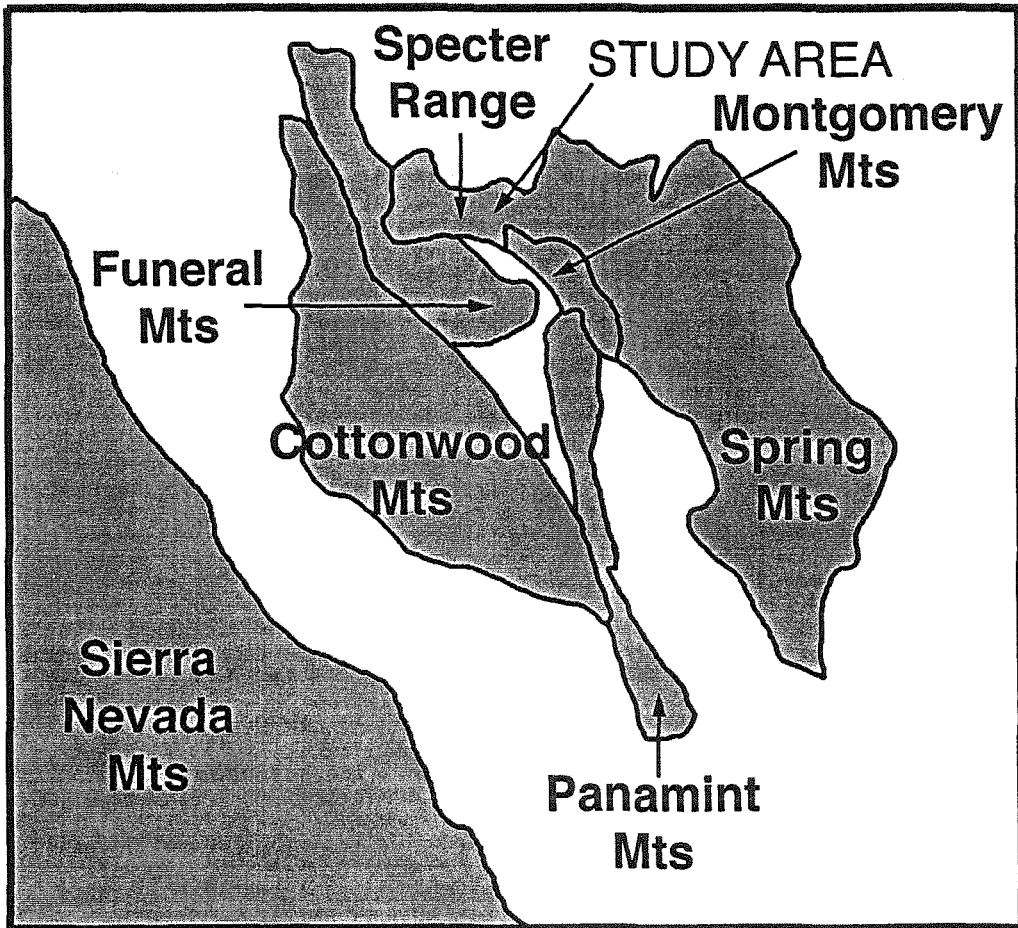
116°

fragments, the Nopah and Resting Spring Ranges, were left behind (Wernicke and others, 1988; Wernicke and others, 1993). According to Wernicke and others (1988), the Chicago Pass thrust in the Nopah - Resting Spring Range correlates with the Panamint and Wheeler Pass thrusts. During the westward translation of the Panamint and Cottonwood Mountains, crystalline rocks in the Black Mountains were unroofed and Death Valley opened (Holm and Wernicke, 1990).

The hypothesis of large-magnitude extension outlined in the preceding paragraph has been hotly debated. The scenario envisioned by Wernicke and others (1988) and Snow and Wernicke (in press) involves about 500% extension between the Panamint and Nopah-Resting Spring Range. In contrast, Wright and Troxel (1973) advocate 30-50% extension across the same area. Serpa and Pavlis (1996) suggest up to 200% extension across the same area, but place much of the extension between the Black Mountains and Nopah-Resting Spring Range rather than in Death Valley. Both of these alternative scenarios suggest that much of the displacement between range blocks has occurred on strike-slip faults with extension occurring at left-steps or releasing bends in these faults. The Serpa and Pavlis (1996) reconstruction requires alternative thrust correlations.

The correlation of contractile structures in different ranges is one of the best ways to evaluate the large amount of extension proposed by Wernicke and others (1988) and Snow and Wernicke (in press). As envisioned by Snow and Wernicke (in press), the restoration of the Panamint and Cottonwood Mountains to their pre-extension position places these two ranges south of the Specter Range and northwestern Spring Mountains. Figure 4-4 depicts the pre-extension configuration of these ranges and the adjacent Funeral Mountains and Montgomery Mountains. The Nopah - Resting Spring Range is omitted from Figure 4-4 for clarity but restores to a position below and to the east of the Panamint Mountains. The Snow and Wernicke reconstruction accounts for the translation (Wernicke and others,

Figure 4-4. Palinspastic map showing the study area and the ranges shown in Figure 4-2 prior to extension as reconstructed by Snow and Wernicke (in press).



1988), rotation (Snow and others, 1993; Snow and Wernicke, in press), and internal deformation of each range block.

According to the reconstruction shown in Figure 4-4, three major contractile structures in the Cottonwood Mountains project northward toward the Specter Range and northwestern Spring Mountains. The Funeral Mountains occupy an intervening position between the Cottonwood Mountains and the Specter Range - northwestern Spring Mountains, and contain plausible equivalents of all three major contractile structures (Wernicke and others, 1988; Snow and Wernicke, 1989). The correlation of major contractile structures between the Cottonwood Mountains and Specter Range - northwestern Spring Mountains would provide a robust pre-extension link between these two areas. As shown by Snow and Wernicke (1989), the probability that the thrust belt would duplicate by chance the size, order, spacing, and vergence of three contractile structures in two unrelated places is exceedingly small ($<10^{-4}$).

Two of the major contractile structures in the Cottonwood Mountains have plausible equivalents in the Specter Range. The west-vergent White Top backfold in the Cottonwood Mountains probably correlates with a west-vergent backfold at the northwestern end of the Specter Range (blue line on Figure 4-5), and the east-vergent Marble Canyon thrust in the Cottonwood Mountains probably correlates with the east-vergent Specter Range thrust (green line on Figure 4-5). However, the east-vergent Lemoigne thrust in the Cottonwood Mountains (red line on Figure 4-5) has no obvious equivalent in the northwestern Spring Mountains. The lack of an obviously correlative structure is a major weakness in the reconstruction shown in Figures 4-4 and 4-5.

Figure 4-5. Palinspastic map showing the study area and major contractile structures from Figure 4-3 prior to extension. Correlation of contractile structures in different ranges are from Snow (1992) and Snow and Wernicke (in press).



50 KM

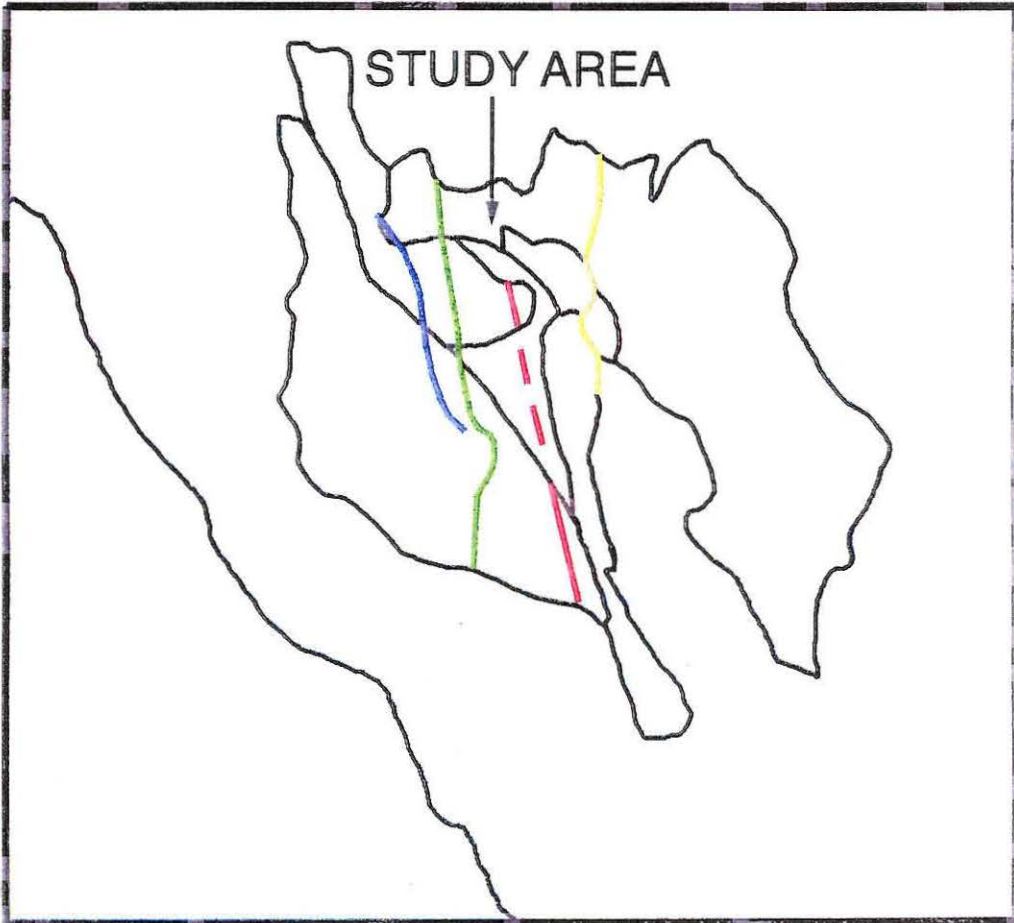
Montgomery thrust

White Top Backfold

Marble Canyon thrust

Lemoigne thrust

Wheeler Pass thrust

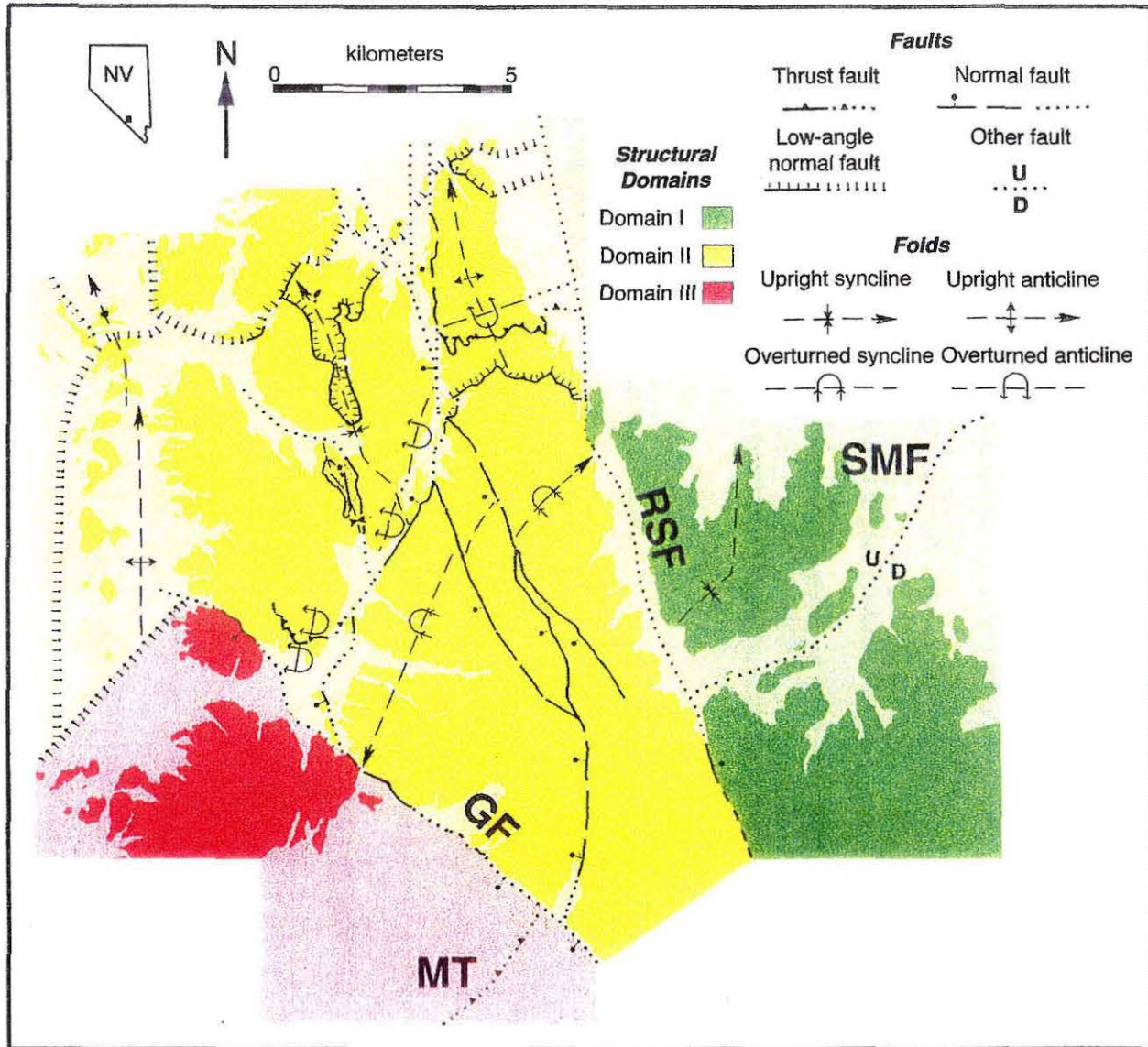


In the Snow and Wernicke reconstruction, the Lemoigne thrust projects into a structurally complex area in the northwestern Spring Mountains. The Lemoigne thrust is a ramp in both footwall and hanging wall and involves 3.0 +/- .3 km of stratigraphic throw (Snow, 1992). Previous mapping in the northwestern Spring Mountains revealed a minor thrust (Burchfiel, 1965) and overturned folds (Burchfiel, 1965; Burchfiel and others, 1974; Burchfiel and others, 1983). Contractile structures in the northwestern Spring Mountains are heavily overprinted by normal faults, so the original geometry and size of the contractile structures is not readily apparent. However, no previously mapped structure bares an obvious resemblance to the Lemoigne thrust. Snow (1992) suggested that the complex structural relationships in the northwestern Spring Mountains conceal a major thrust fault with at least 1.5 km of throw. He dubbed this hypothetical thrust the "Kwichup Spring thrust," and suggested that the Kwichup Spring thrust correlates with the Lemoigne thrust.

This paper examines the geology of the northwestern Spring Mountains to determine the regional significance of contractile structures and to evaluate the relationship between those structures and the Lemoigne thrust. As shown in Figure 4-6, the northwestern Spring Mountains and northern Montgomery Mountains are divided into three structural domains by the Rock Spring and Grapevine faults. Each domain contains structures which do not continue into adjacent domains in any obvious way. An understanding of the relationship between structures in adjacent domains is the first step toward understanding the regional significance of those structures.

To examine the relationship between structures in domains I and II, new mapping was completed at scales of 1:7500 to 1:12000. In domain I, new mapping focused on the Stirling Mine fault (SMF on Figure 4-6) and on a syncline northwest of the fault. Mapping in domain II focused on low-angle faults in the northern part of the domain and on folds in the southern part of the domain. Together, these new maps and associated cross sections

Figure 4-6. Structural domains in the study area. Each domain contains structures which do not continue into adjacent domains in any obvious way. Structures are generalized from Burchfiel (1965), Cornwall (1972), Burchfiel and others (1974), Burchfiel and others (1983), and mapping by the author. The Rock Spring fault (RSF) separates domains I and II, and the Grapevine fault separates domains II and III. The Stirling Mine fault (SMF) is the principle fault in domain I. The Montgomery thrust (MT) is the principle fault in domain III.



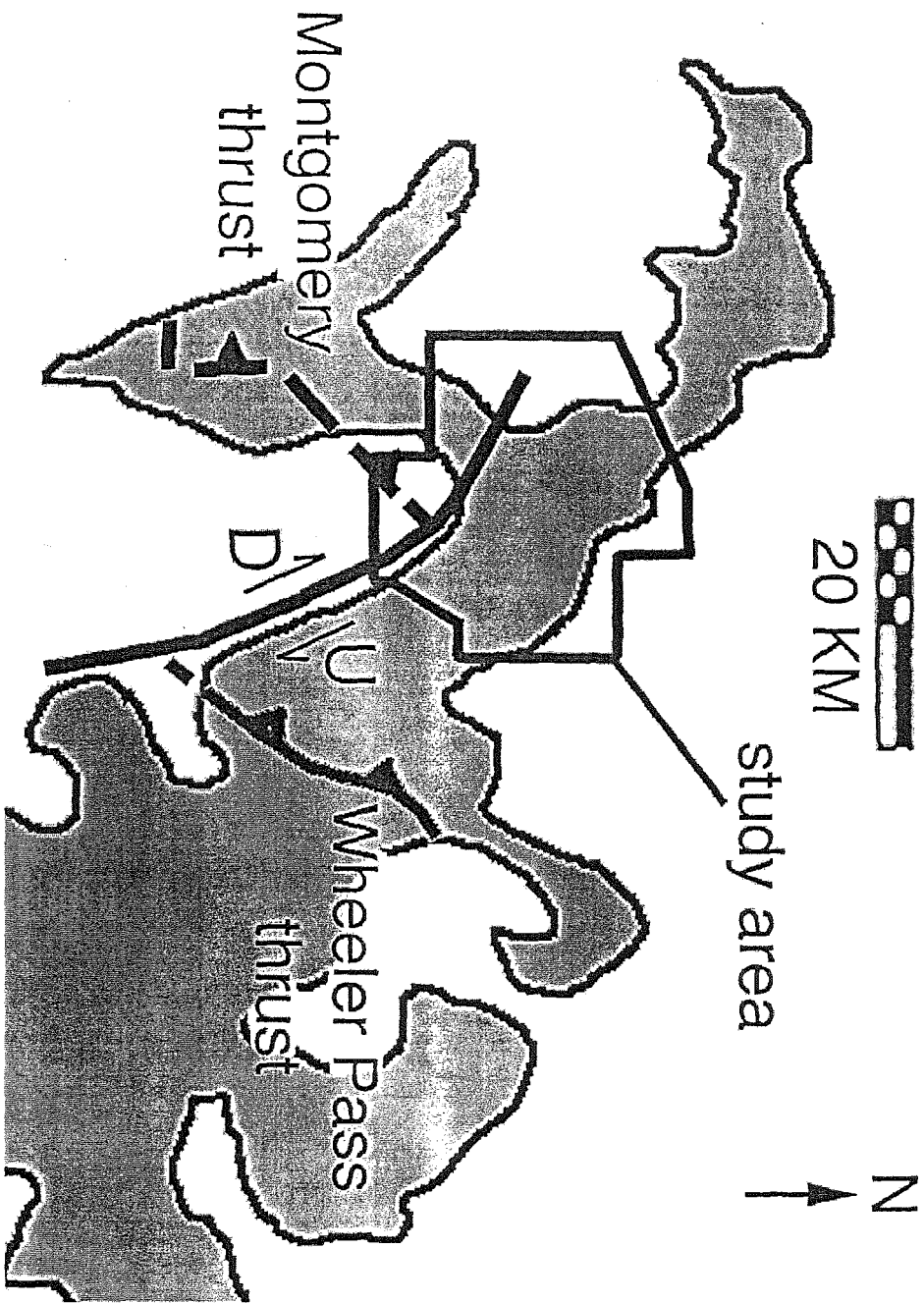
lead to an improved understanding of the possible connection between the Stirling Mine fault in domain I and the faults and folds in domain II.

Previous studies present two distinctly different views of the relationship between structures in domains II and III. These two views are rooted in different interpretations of the Montgomery thrust in the Montgomery Mountains. The Montgomery thrust is the principle contractile structure in the Montgomery Mountains (Burchfiel and others, 1983), and has a stratigraphic throw of at least 5 km. The thrust projects under alluvium (MT in Figure 4-6) toward a homocline in the Spring Mountains (Burchfiel and others, 1974). The abrupt lateral termination of this large thrust is problematic.

Burchfiel and others (1983) resolve this problem by suggesting that the Montgomery thrust continues into domain II where it dies out as asymmetric folds or is omitted by a normal fault. In contrast, Snow (1992) and Snow and Wernicke (in press) suggest that the Montgomery thrust has no equivalent in the northwestern Spring Mountains, and correlate the Montgomery thrust with the Wheeler Pass thrust. This correlation requires 20 km of right-lateral displacement between the Montgomery Mountains and Spring Mountains as shown in Figure 4-7.

The comparison of stratigraphic units in domains II and III is the best way to constrain the amount of lateral translation between the two domains. On one hand, correlation of the Montgomery thrust with the overturned folds in domain II suggests that the two domains share the same stratigraphy. On the other hand, a large amount of lateral translation between the two domains should juxtapose contrasting facies. To distinguish between these two possibilities, the Johnnie Formation was examined in detail at six locations in the two domains.

Figure 4-7. Proposed strike-slip displacement of the Montgomery Mountains and Montgomery thrust along the Spring Mountains range front.



OBSERVATIONS

Overview

The study area is divided into three structural domains by the Rock Spring fault and Grapevine fault. Each domain contains at least one major structure which is not found in the other domains. Domain I includes the area east of the Rock Spring fault. As shown in Figure 4-6, the Stirling Mine fault is the principle fault in Domain I. The fault terminates against the Rock Spring fault to the west and disappears under Las Vegas Valley to the east.

Domain II includes the area between the Grapevine and Rock Spring faults and is shown in Figure 4-8. Domain II contains four low-angle faults. From structurally lowest to highest, these faults are the Diebert fault, Jaybird fault, Niavi fault, and Point of Rocks faults. The Diebert, Niavi, and Point of Rocks faults have normal-sense separations, while the Jaybird fault is a thrust. The Diebert fault is only exposed for 2.85 km in the northern part of domain II. A high-angle normal fault called Paddy's fault occupies the same structural position through the rest of the domain.

Domain II also contains two categories of folds. One category includes trains of east-vergent overturned folds which are shown schematically as an overturned anticline and an overturned syncline on Figure 4-8. These folds are confined to the Johnnie Formation. The second category includes broad upright folds which involve the entire stratigraphic section.

Domain III includes the area southwest of the Grapevine fault. Structures in this domain were described previously by Burchfiel and others (1983), and the area was not re-mapped in detail. To investigate the amount of lateral translation between domains II and III, a total of 1.4 km of section was examined in the Johnnie Formation at six locations in the two domains.

Figure 4-9 shows the location of detailed maps which are discussed in this paper.

Figure 4-8. Map showing major faults and folds in domain II.

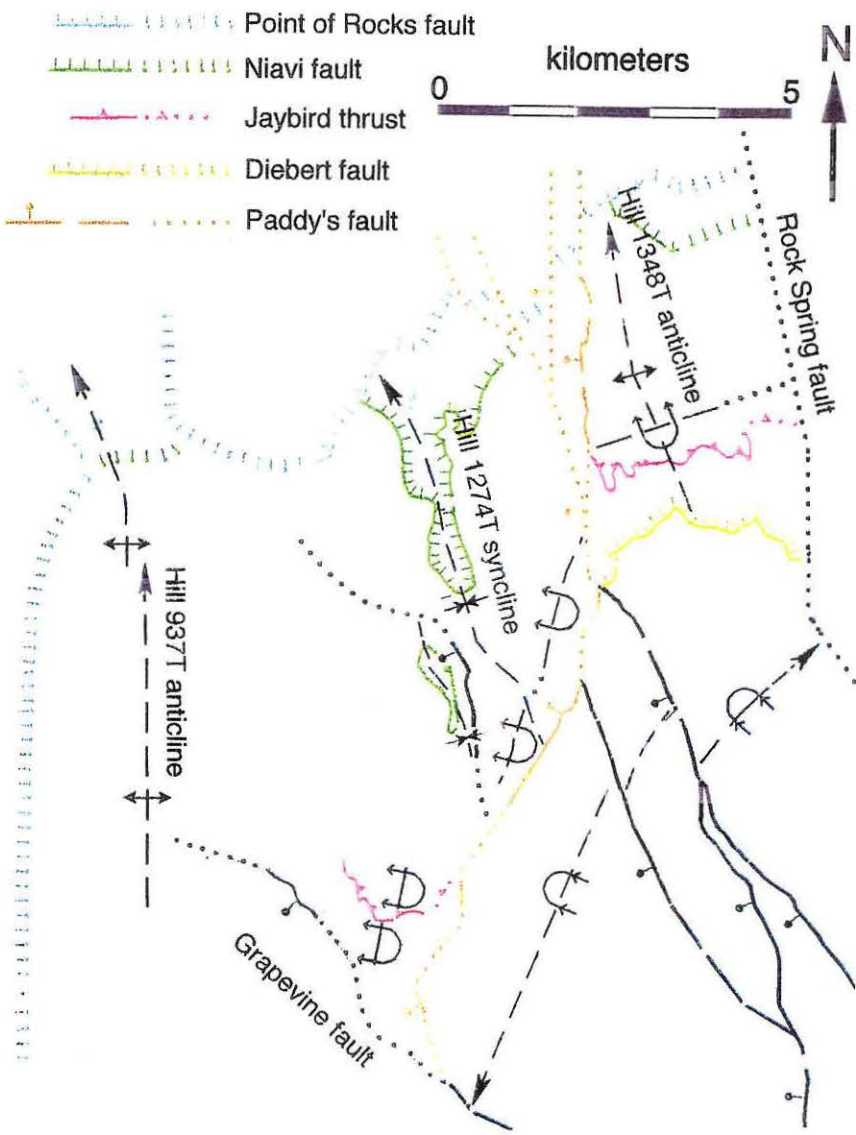
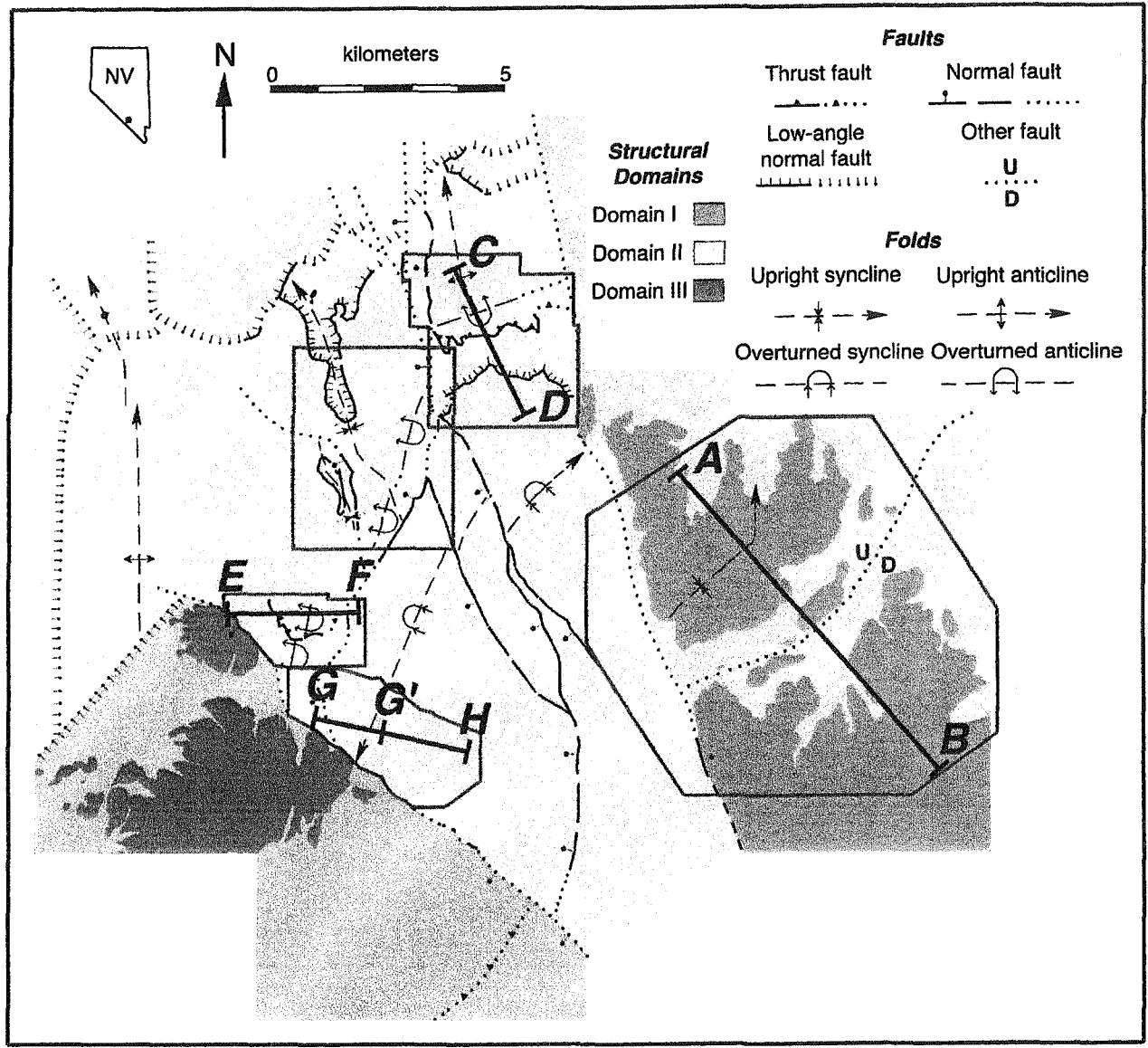


Figure 4-9. Map showing the location of areas described in detail in the Observation section.



Domain I

Geologic mapping in domain I focused on the Stirling Mine fault and an upright syncline to the northwest of the fault which is herein named the Stirling Mine syncline. The geologic map is shown in Figure 4-10.

Stirling Mine fault

The Stirling mine fault is a northwest-side-up structure which is covered by alluvium along its entire length. To the west, the fault terminates against the Rock Spring fault. To the northeast, the fault disappears under Las Vegas Valley. In the intervening 6 km, the location of the Stirling Mine fault is relatively well constrained by outcrops of the up-thrown (NW) and down-thrown (SE) blocks. Apparent stratigraphic throw varies along the fault. Where throw is greatest, the thrust juxtaposes the Cambrian Carrara Formation and Ordovician Pogonip Group. This represents about 1.5 km of stratigraphic throw according to unit thicknesses for the northwestern Spring Mountains from Burchfiel and others (1974).

The Stirling Mine fault is shown on Figure 4-10 as a northwest-side-up thrust but could also be a southeast-side-down normal fault. Observations relevant to the interpretation of the Stirling Mine fault are presented in the next two paragraphs and are discussed in a subsequent section.

Minor thrust

The upthrown block on the northwest side of the Stirling Mine fault contains two significant contractile structures. The first structure is a minor thrust about 150 m from the fault trace. On Figure 4-10, the thrust is located near the intersection between cross section line AB and the Stirling Mine fault. Figure 4-11 is an enlargement of the minor thrust and surrounding area. This thrust displays an apparent displacement of about 35 m. A minor anticline occurs in the hanging wall of the minor thrust and a minor syncline occurs in the footwall. The steepest measured dip in the footwall syncline is 71°, and bedding appears to

Figure 4-10. Geologic map of the Stirling Mine fault and surrounding area.

KEY

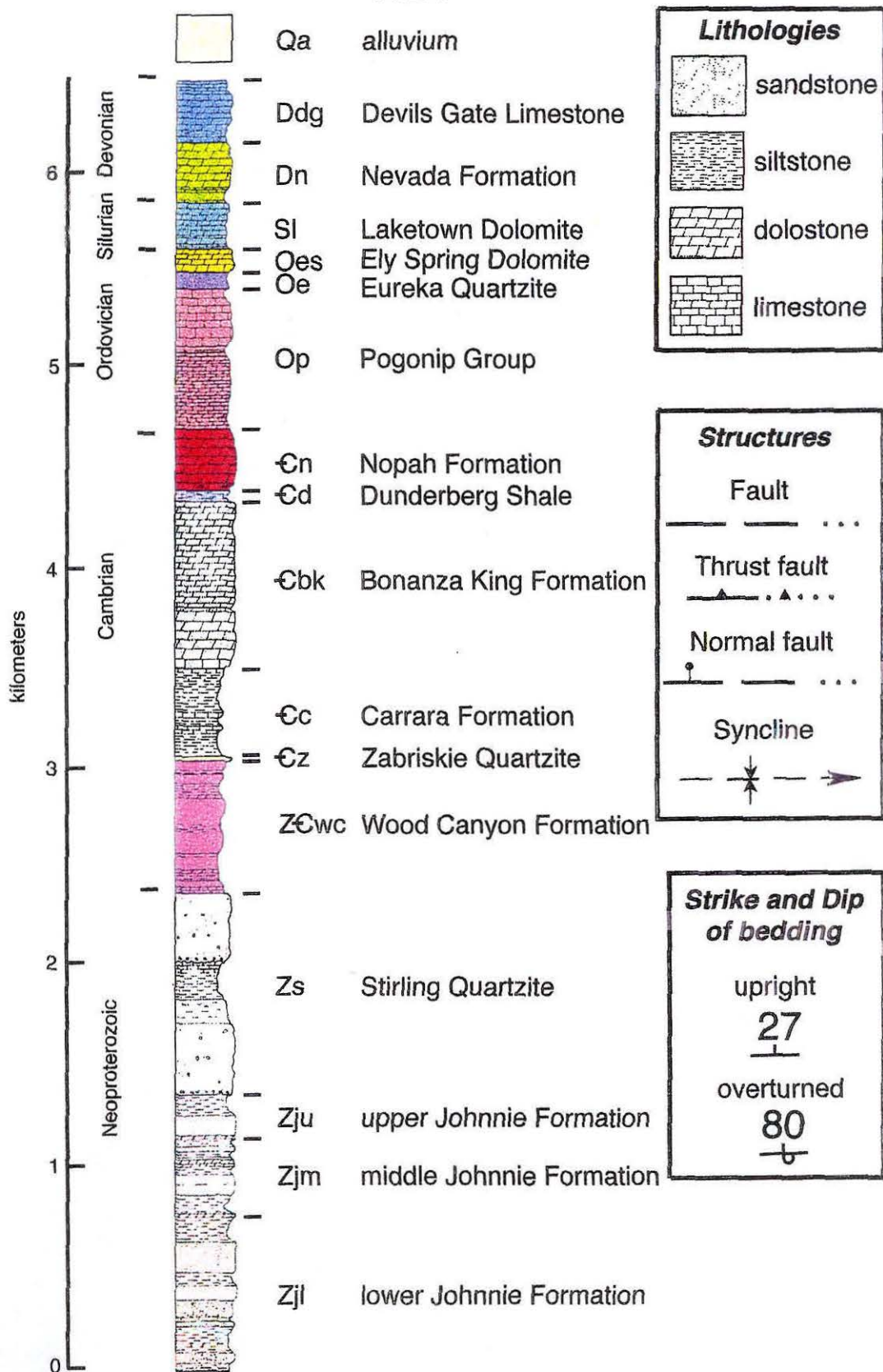
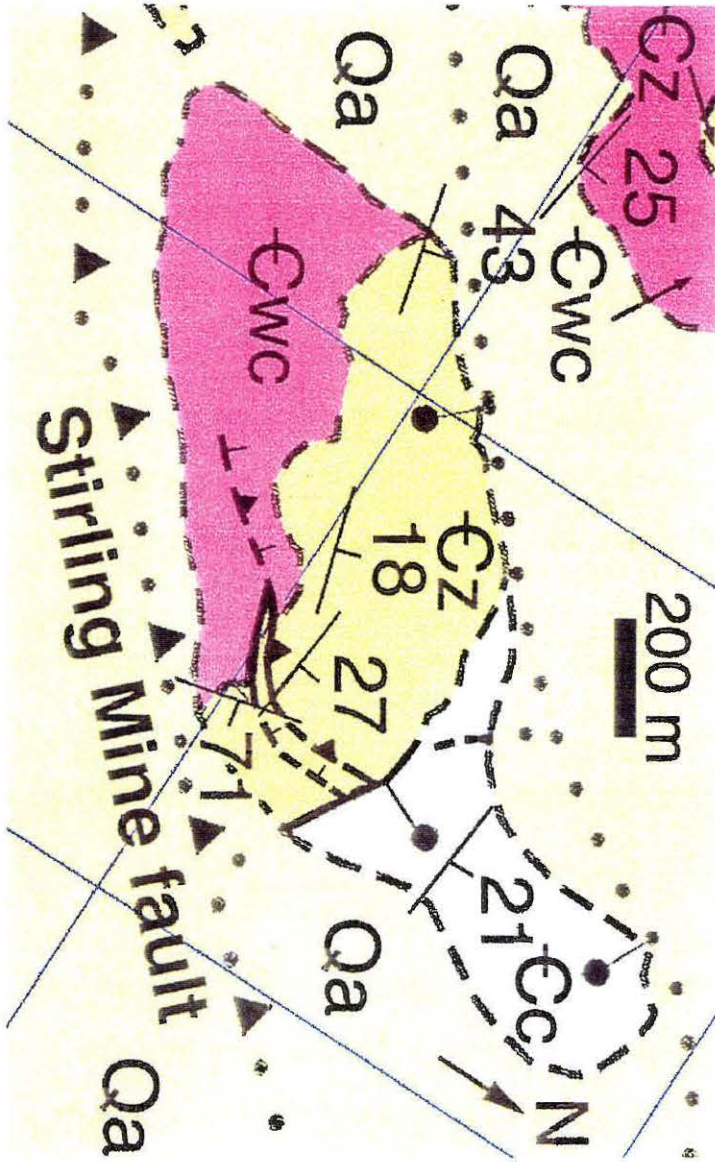


Figure 4-11. Map showing the minor thrust northwest of the Stirling Mine fault. See Figure 4-9 for location of map area.



overturn immediately below the fault (attitude not shown on map due to lack of access).

No other minor thrusts were observed in domain I, and the 71° dip in the footwall syncline is the steepest dip in domain I on Figure 4-10.

Stirling Mine syncline

The second structure is the Stirling Mine syncline (Figure 4-10). The syncline strikes southwest-northeast at its southwestern end and strikes nearly north-south at its northern end. At its southwestern end, the syncline terminates against the Rock Spring fault under alluvium. To the north, the syncline disappears beneath Las Vegas Valley. The syncline plunges 25-30° to the north. Both fold limbs dip moderately (25-40°).

Figure 4-12 presents a cross section through the Stirling Mine syncline and other structures shown on Figure 4-10 along line AB. Most fault dips are poorly constrained. The Stirling Mine fault is shown as a thrust which dips to the northwest. This interpretation is justified in the discussion section.

Domain II

Geologic mapping in domain II focused on the geometry of two low-angle faults (the Diebert and Jaybird faults on Figure 4-8), and the geometry of overturned folds within the Johnnie Formation. Other structures are also described because they provide critical cross-cutting relationships.

Diebert fault

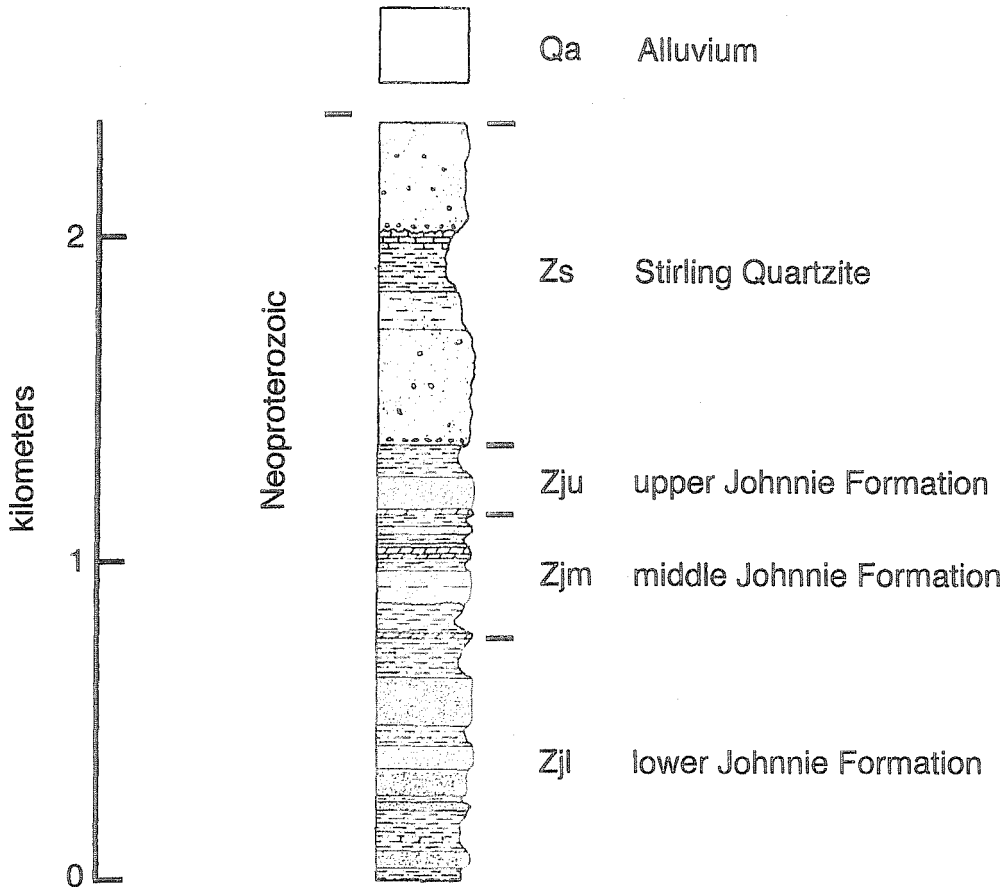
The Diebert fault is the structurally lowest of the four low-angle faults in domain II. The fault is shown in map-view on Figure 4-13, and in cross section on Figure 4-14. The fault strikes west-southwest/east-northeast over an exposed along-strike distance of 2.8 km. As shown on the cross section, the fault dips 10-20° to the north-northwest. The Diebert fault places the lowest member of the Stirling Quartzite on the lower Johnnie Formation for an apparent stratigraphic throw of 1.4 km. To the east, the continuation of the fault under alluvium is uncertain. To the west, a high-angle normal fault called Paddy's

Figure 4-12. Cross section AB through the Stirling Mine fault and Stirling Mine syncline.

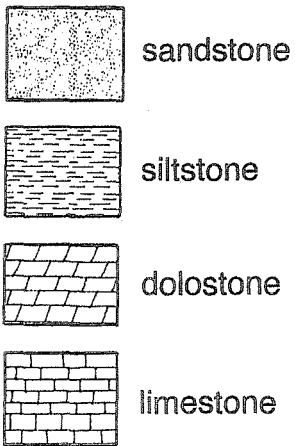
See Figure 4-11 for location of the section line.

Figure 4-13. Map of the Diebert fault, Jaybird fault, and folds in the hanging wall of the Jaybird fault. See Figure 4-9 for location of map area.

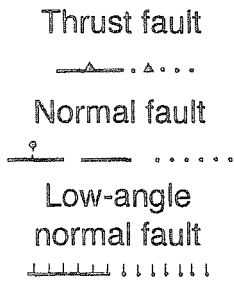
KEY



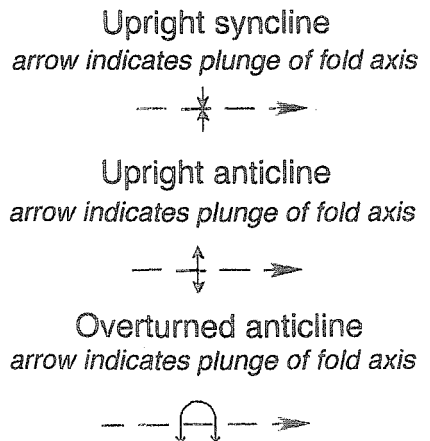
Lithology



Faults



Folds



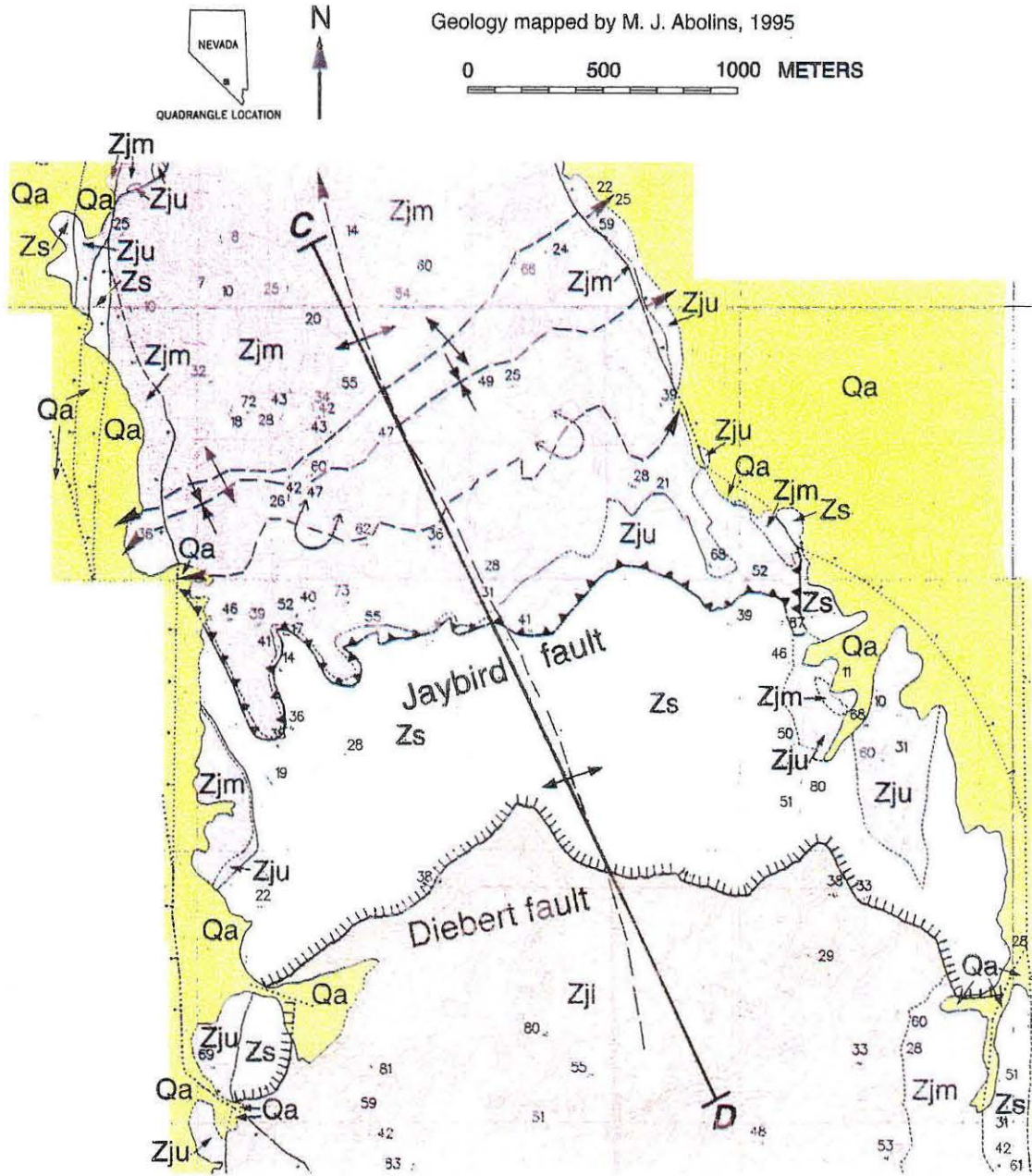
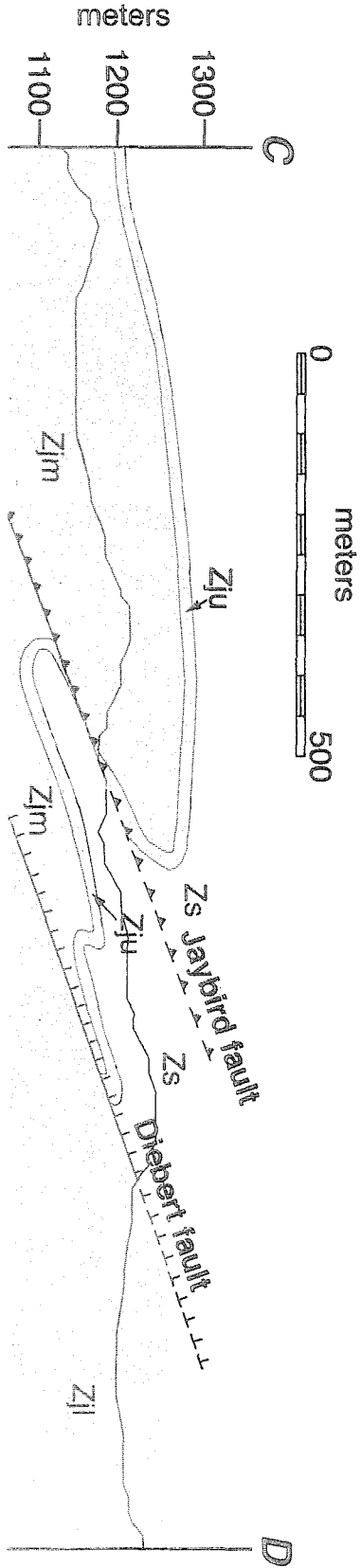


Figure 4-14. Cross section CD through the Jaybird and Diebert faults. See Figure 4-13 for location of section line.



fault (described below) occupies the same structural position as the Diebert fault. The Diebert fault is folded by a broad upright fold called the Hill 1348T anticline (described below).

Jaybird fault

The Jaybird fault is the only substantial thrust fault exposed in domain II. The Jaybird fault thrusts the upper Johnnie Formation over the lowest member of the Stirling Quartzite. In the northern part of the domain (Figures 4-13 and 4-14), the thrust dips less than 20°. In the southern part of the domain, the thrust offsets the axial surface of an overturned anticline by at least 350 m as shown in Figures 4-15 and 4-16. The thrust surface is folded by a pair of broad upright folds called the Hill 937T anticline and the Hill 1274T syncline (described below).

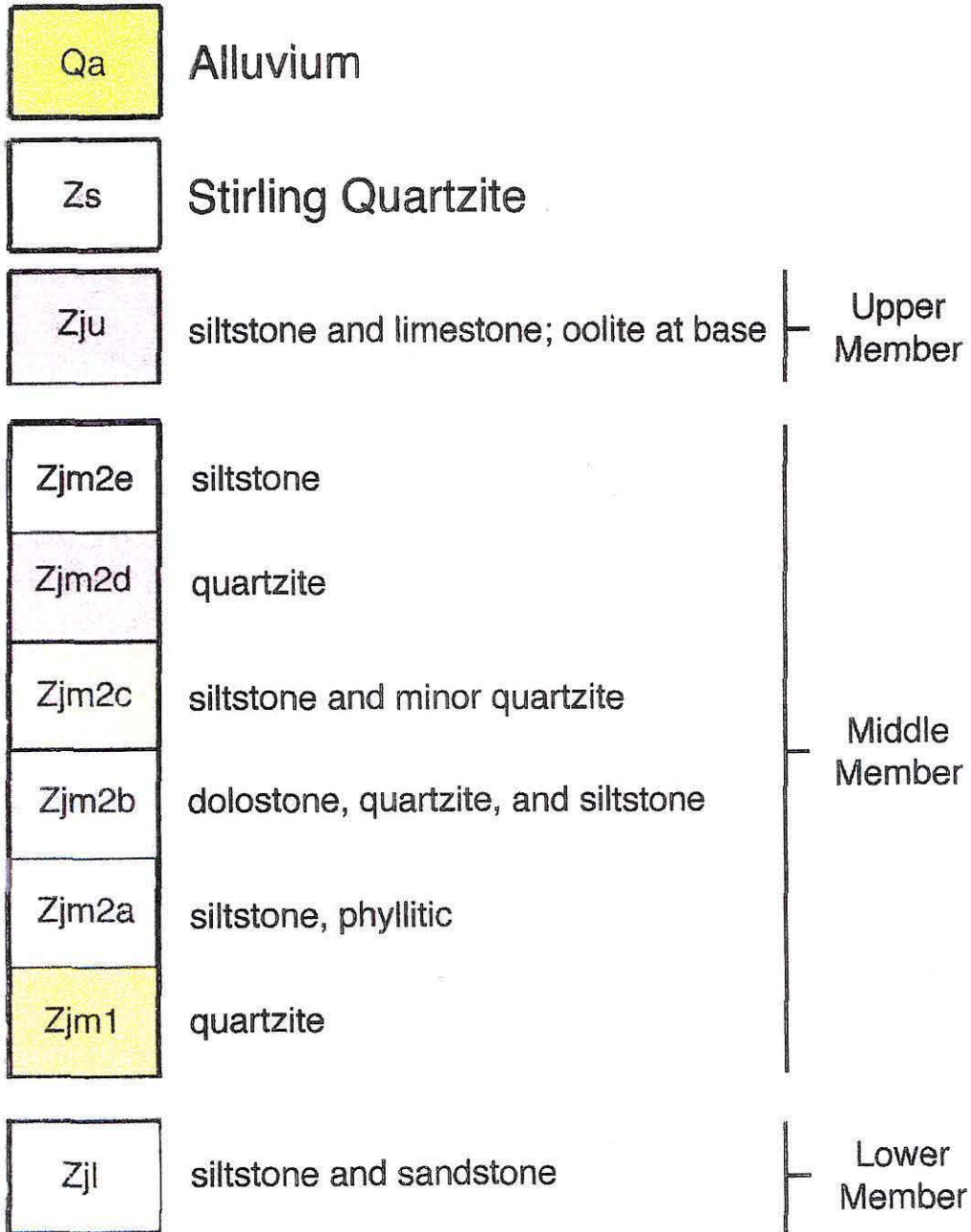
Paddy's fault

Paddy's fault is a high-angle normal fault with a northwest-side-down sense of displacement. The fault is shown in tan on Figure 4-8. It terminates against the Grapevine fault at its southern end and disappears under alluvium at its northern end. The fault plane is exposed at a single location where it dips 56° W. Like the Diebert fault, Paddy's fault juxtaposes the lowest member of the Stirling Quartzite in its hanging wall against the lower Johnnie Formation in its footwall.

Niavi fault

The Niavi fault is a low-angle normal fault which is structurally higher than the Jaybird fault. The fault is shown in green on Figure 4-8, and a segment of the fault is shown on Figure 4-17. The fault places quartzite of the lower Wood Canyon Formation on Stirling B siltstone for a stratigraphic throw of 575-760 m. The Niavi fault is folded by the Hill 1348T anticline and the Hill 1274T syncline.

Figure 4-15. Geologic map depicting the Jaybird fault, Paddy's fault, and overturned folds west of Paddy's fault. See Figure 4-9 for location of map area.



Johnnie Formation

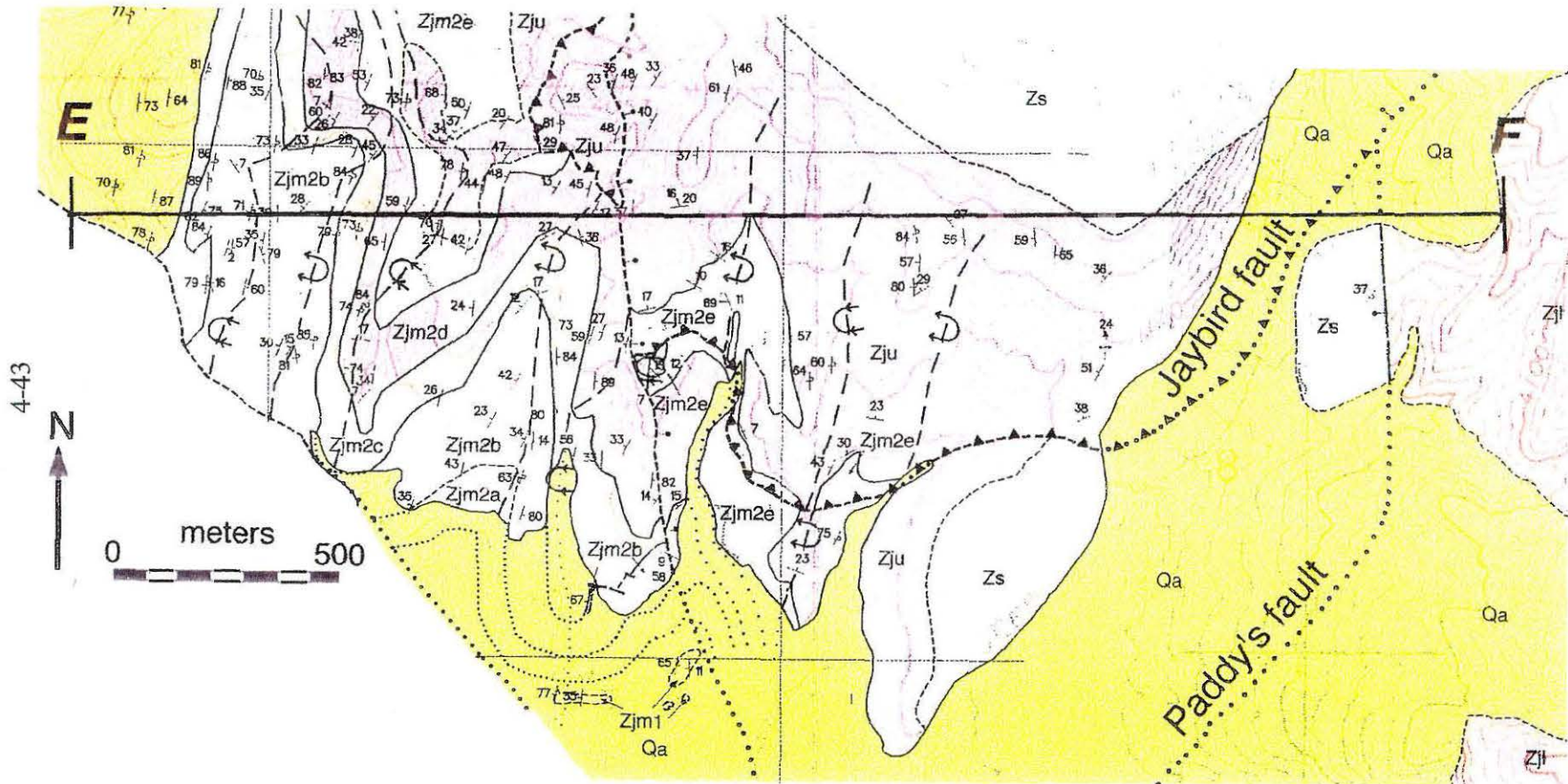


Figure 4-16. Cross section EF through Jaybird fault, Paddy's fault, and the overturned folds west of Paddy's fault. See Figure 4-15 for location of section line.

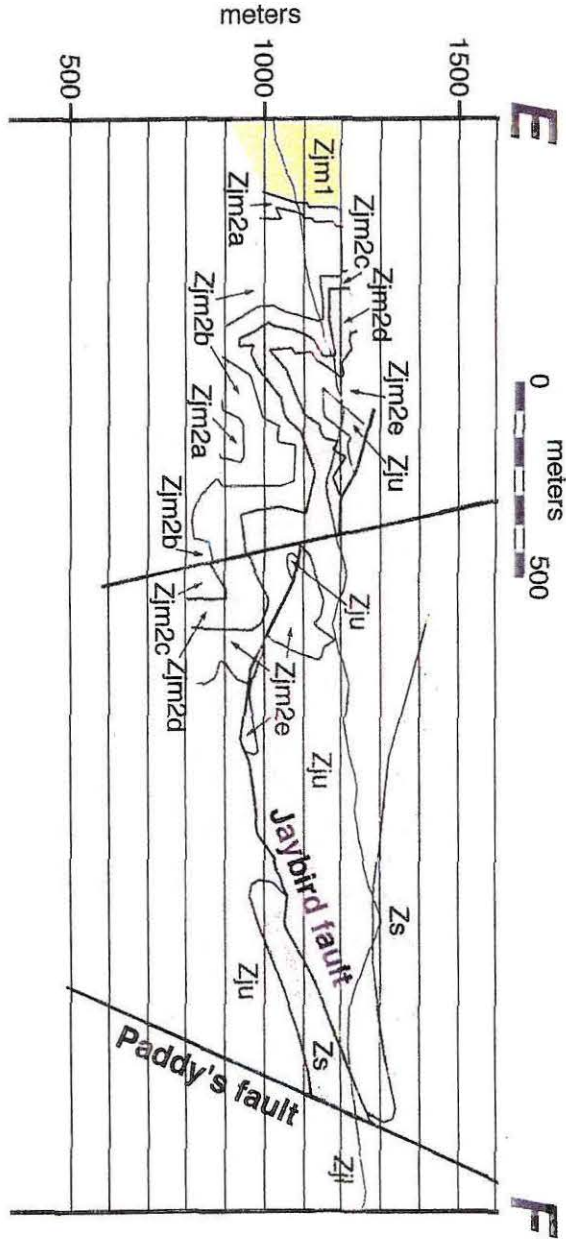
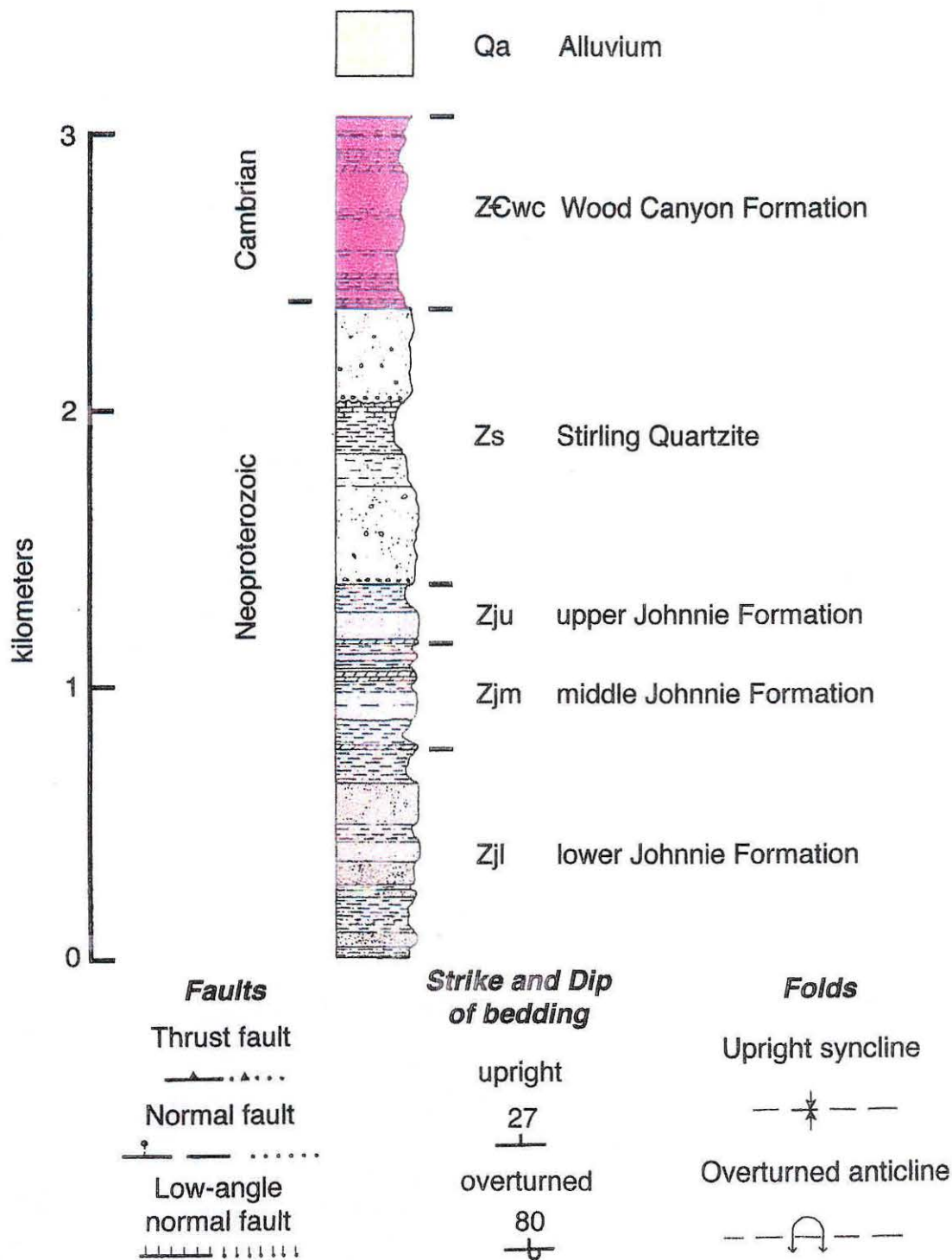
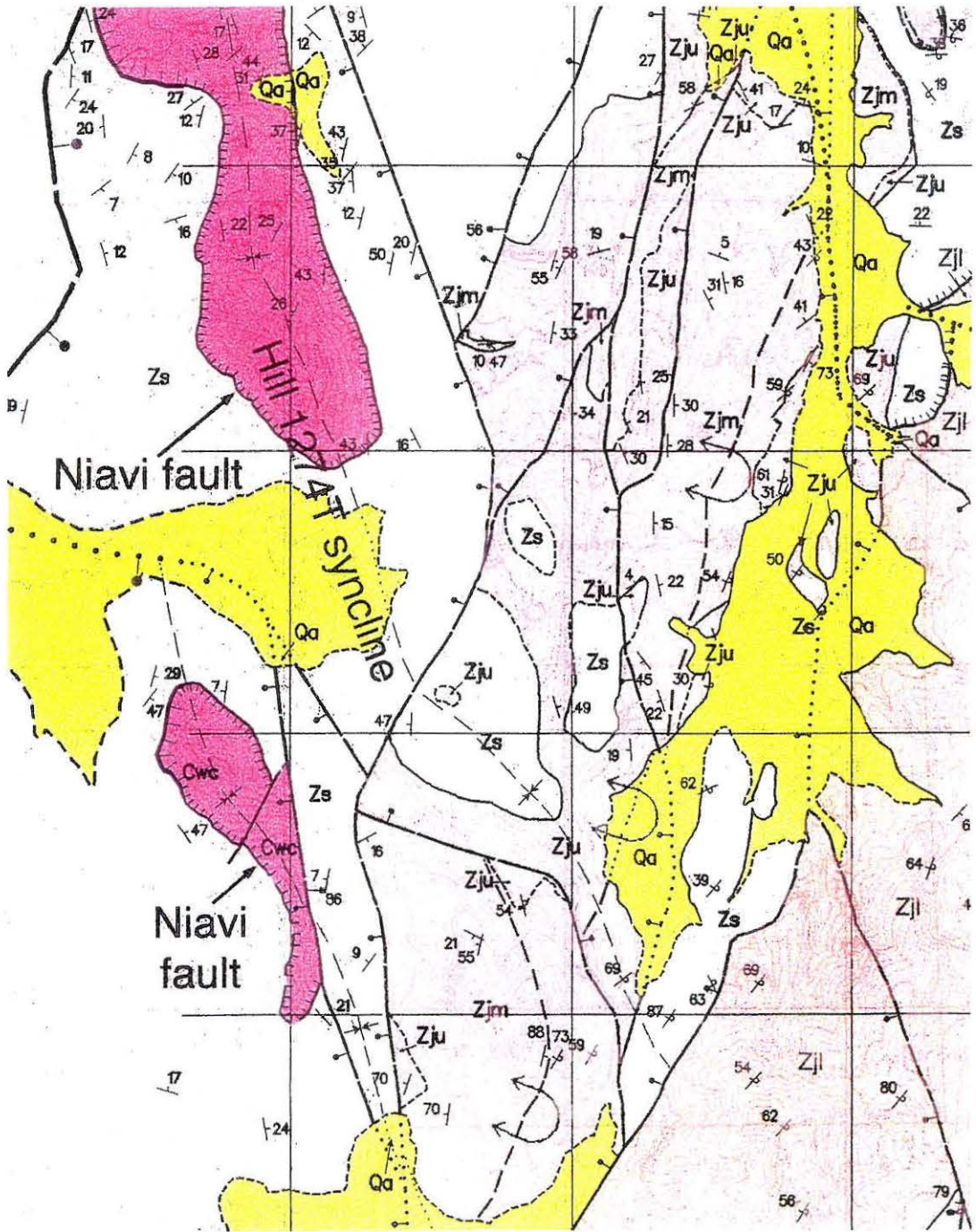


Figure 4-17. Geologic map depicting the Niavi fault, an overturned anticline in the Johnnie Formation, and Paddy's fault. See Figure 4-9 for location of map area.

KEY





Point of Rocks fault

The Point of Rocks fault is the structurally highest low-angle normal fault in the northwestern Spring Mountains. The fault is shown in blue on Figure 4-8. The fault places the Dundenberg Shale on a folded footwall. The Point of Rocks fault post-dates the Hill 1348T and Hill 1274T folds, and cuts the Niavi fault.

Broad upright folds

The Hill 1348T and Hill 937T anticlines and the Hill 1274T syncline are broad upright folds which involve the entire stratigraphic section. These three folds are shown on Figure 4-8. The folds plunge 25° to the north-northwest, and have a wavelength of 3.25-4.25 km. The fold limbs generally dip $25-40^{\circ}$. These structures fold the Diebert, Jaybird, and Niavi faults, but are cut by the Point of Rocks fault.

Overtured folds west of the Diebert fault and Paddy's fault

To determine the geometry of overturned folds west of Paddy's fault, a four square kilometer area was mapped in the southern part of domain II (Figure 4-15). Six informal units were mapped within the middle Johnnie Formation in that area. New mapping showed that the schematic overturned anticline of Burchfiel and others (1983) consists of six distinct east-vergent folds. These folds die out within the upper Johnnie Formation and do not involve the Stirling Quartzite. At least three of the folds are cut by the Jaybird fault. Hinge dips show that the folds plunge $\sim 20^{\circ}$ to the north-northeast. Mapped contacts were projected along the strike and plunge of the folds onto cross section EF (Figure 4-16). This cross section shows that the folds have a wavelength of roughly 500 m and a maximum amplitude of about 100 m.

Folds in the northern and central parts of domain II are similar in wavelength and amplitude to folds in the southern part of the domain, but do not correlate in detail. In the northern part of domain II (Figure 4-13), a single overturned fold occurs in the hanging wall of the Jaybird fault, and an upright syncline-anticline pair occurs to the northwest of

this fold. The overturned anticline can be traced southward into the central part of domain II on Figure 4-17, but the other two folds were not observed in the central part of the domain.

Overturned folds east of the Diebert fault and Paddy's fault

Folding in the Johnnie Formation east of Paddy's fault was studied in detail in the southern part of domain II. As in Figure 4-8, this structure has the general form of an east-vergent overturned syncline. Overturned west dips cluster along the west side of the structure (red dots in Figure 4-18) while shallow upright east dips characterize the east side of the structure (blue dots in Figure 4-18). As shown in Figure 4-19, the rocks contain a west-dipping axial planar cleavage which is consistent with the east-vergence of the folds. A stereoplot of bedding (Figure 4-20) shows that the structure strikes N5E and plunges 3° to the south. Bedding-cleavage intersections suggest a similar strike (Figure 4-21 and Figure 4-22), but a slightly steeper plunge (Figure 4-22).

The dip map suggests that, as with the "overturned anticline" west of Paddy's fault, the geometry of the overturned syncline is complex in detail. For example, Figure 4-18 reveals a prominent cluster of overturned attitudes within the upright limb of the overturned syncline. To better understand the geometry of the structure, nine informal units were mapped in the middle Johnnie Formation (Figure 4-23). The average strike and plunge were used to project contacts onto cross section G'H (Figure 4-24). The cross section shows that, as with the overturned anticline west of Paddy's fault, the overturned syncline consists of a fold train. The wavelength and maximum amplitude of the fold train east of Paddy's fault are similar to those of the fold train west of the fault.

Domain III

The Montgomery thrust is the principle structure in domain III, and the possible relationship between the Montgomery thrust and structures in domains I and II is examined

Figure 4-18. Map showing bedding attitudes in the Johnnie Formation east of Paddy's fault. See Figure 4-9 for location of map area.

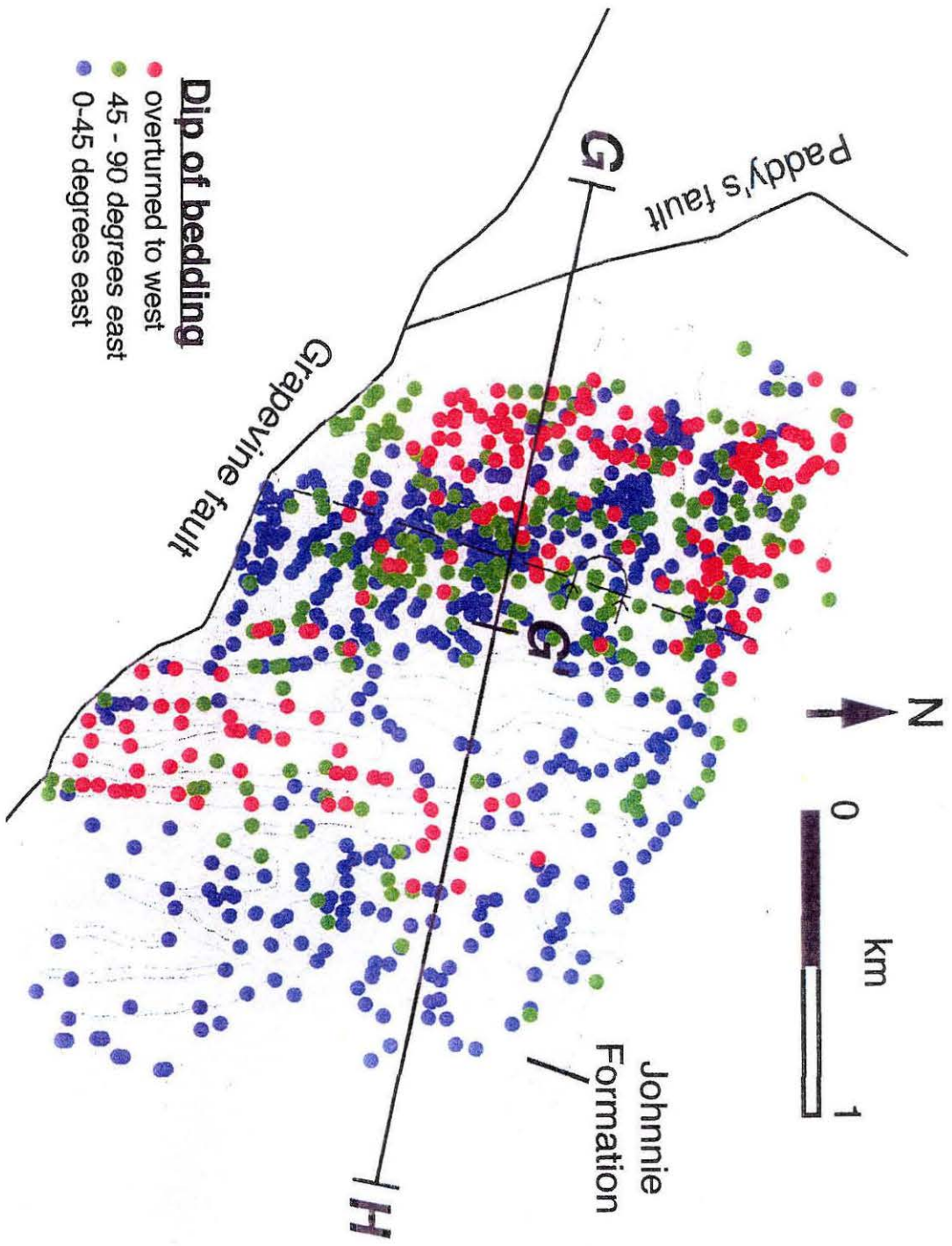
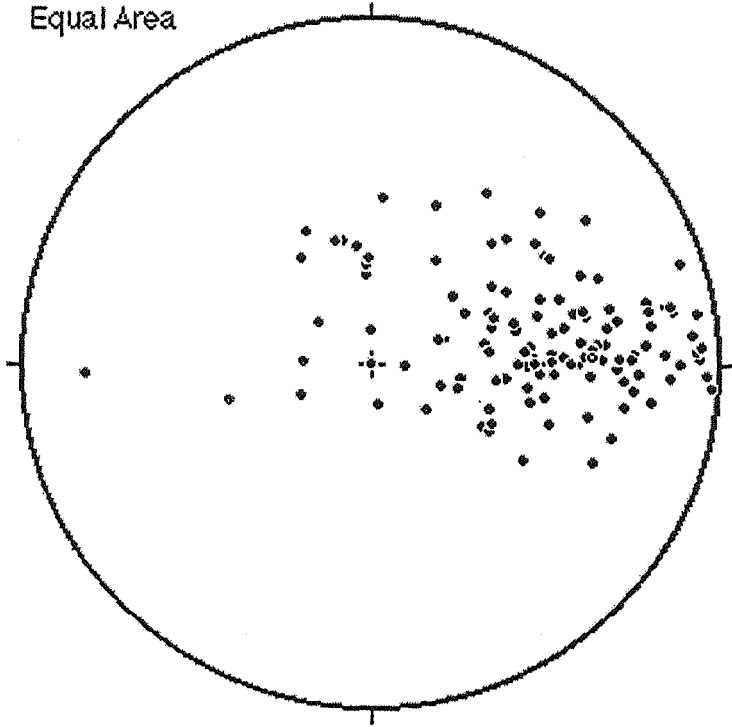
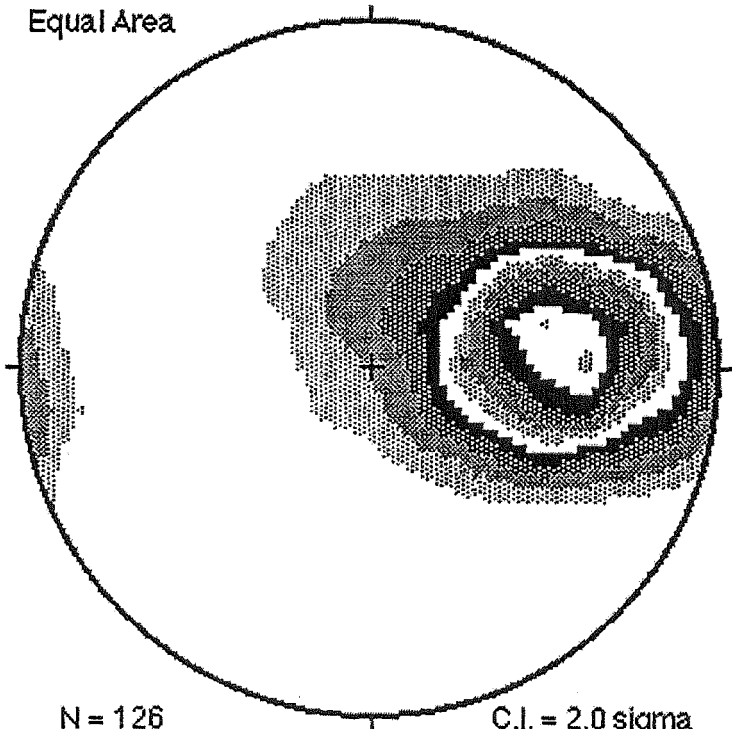


Figure 4-19. Lower hemisphere stereoplot of poles to cleavage in the Johnnie Formation within the map area shown in Figure 4-18.

Equal Area



Equal Area

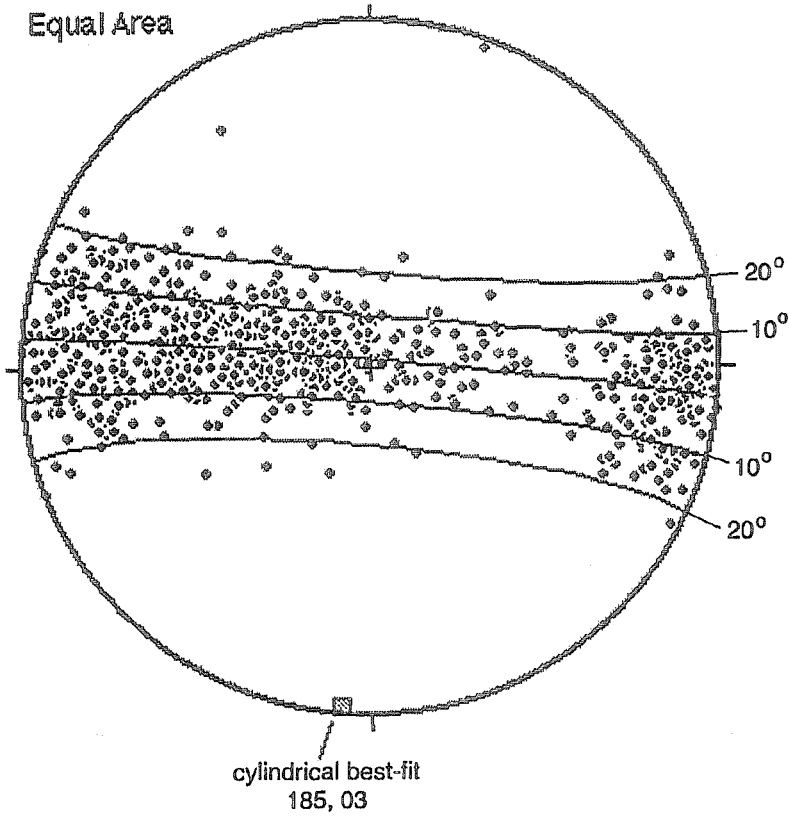


N = 126

C.I. = 2.0 sigma

Figure 4-20. Lower hemisphere stereoplot of poles to bedding in the Johnnie Formation within the map area shown in Figure 4-18.

Equal Area



Equal Area

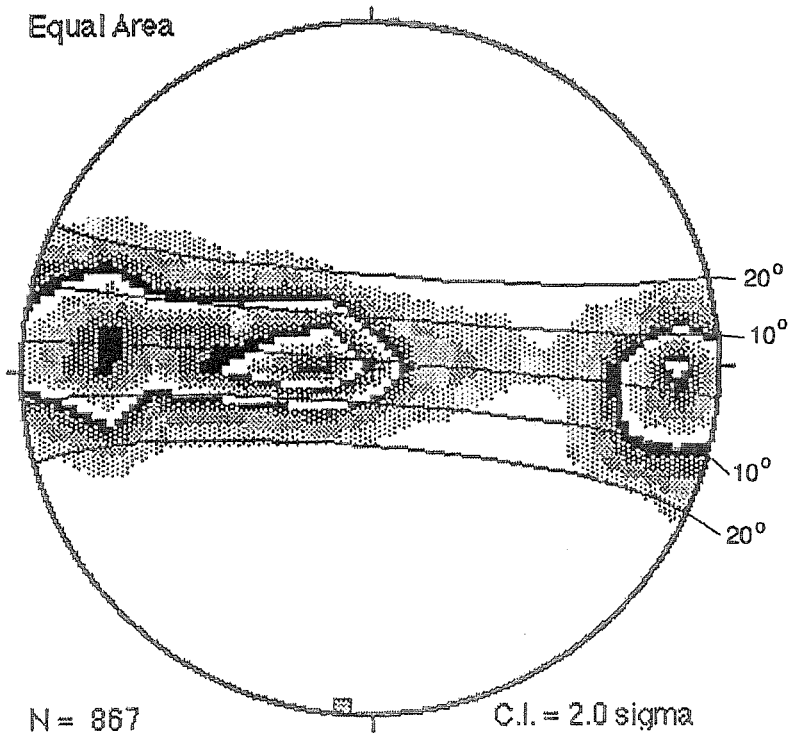
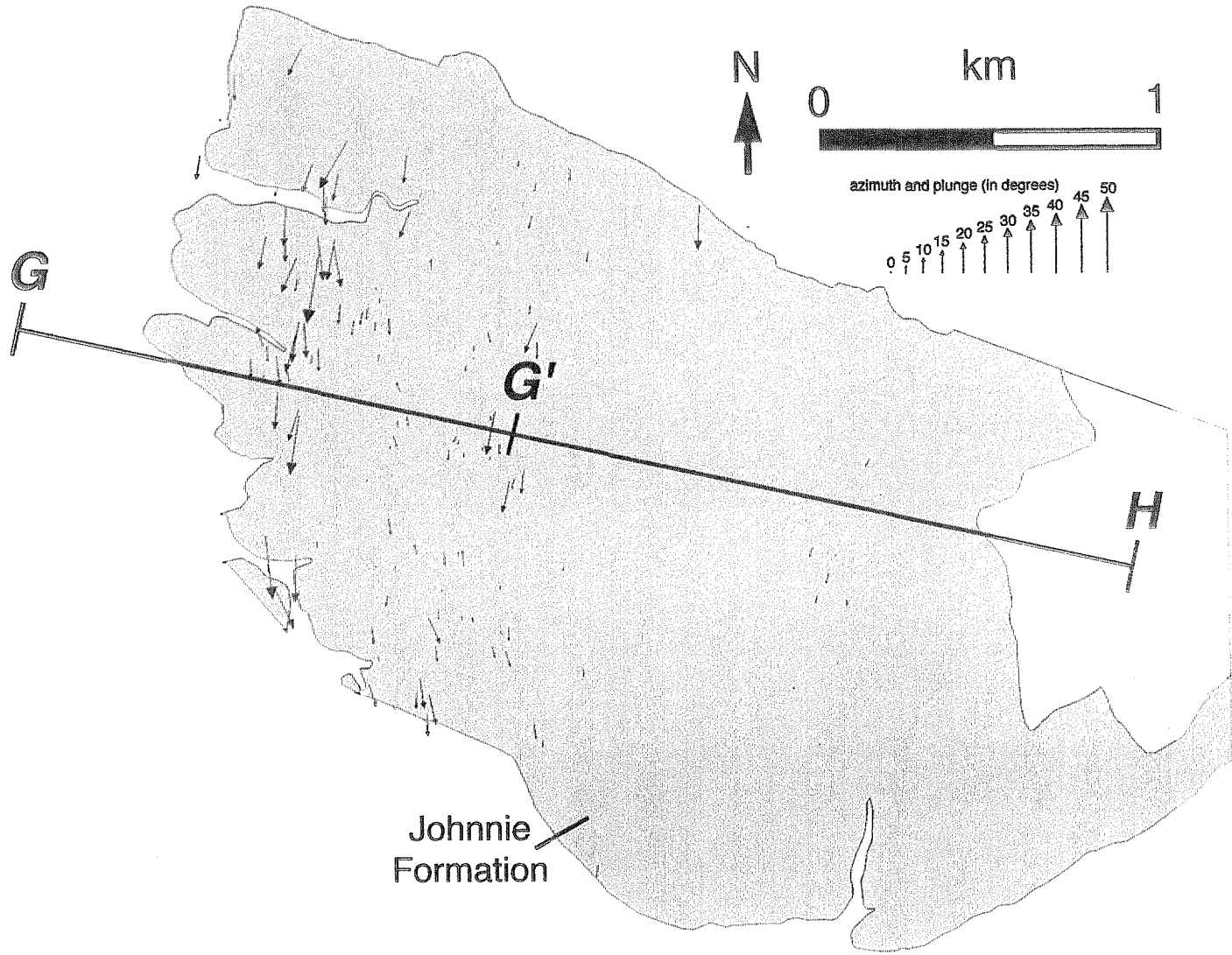


Figure 4-21. Map of bedding-cleavage intersections in the Johnnie Formation. See Figure 4-9 for location of map area.

4-58



Johnnie
Formation

Figure 4-22. Lower hemisphere stereoplot of bedding-cleavage intersections in the Johnnie Formation within the map area shown in Figure 4-21.

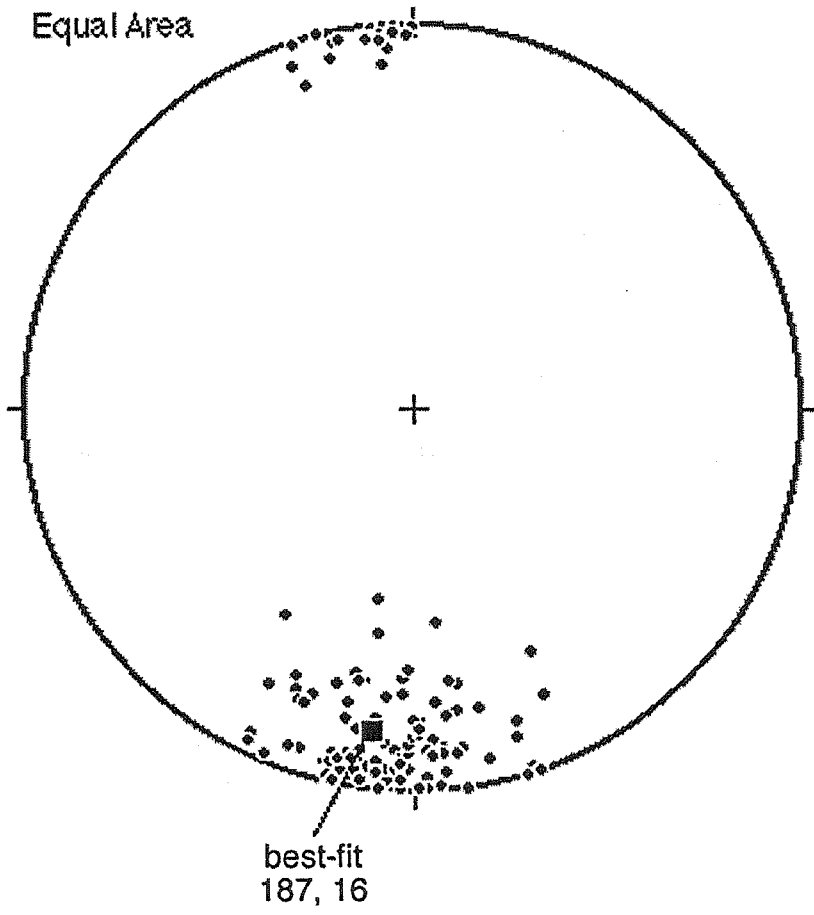
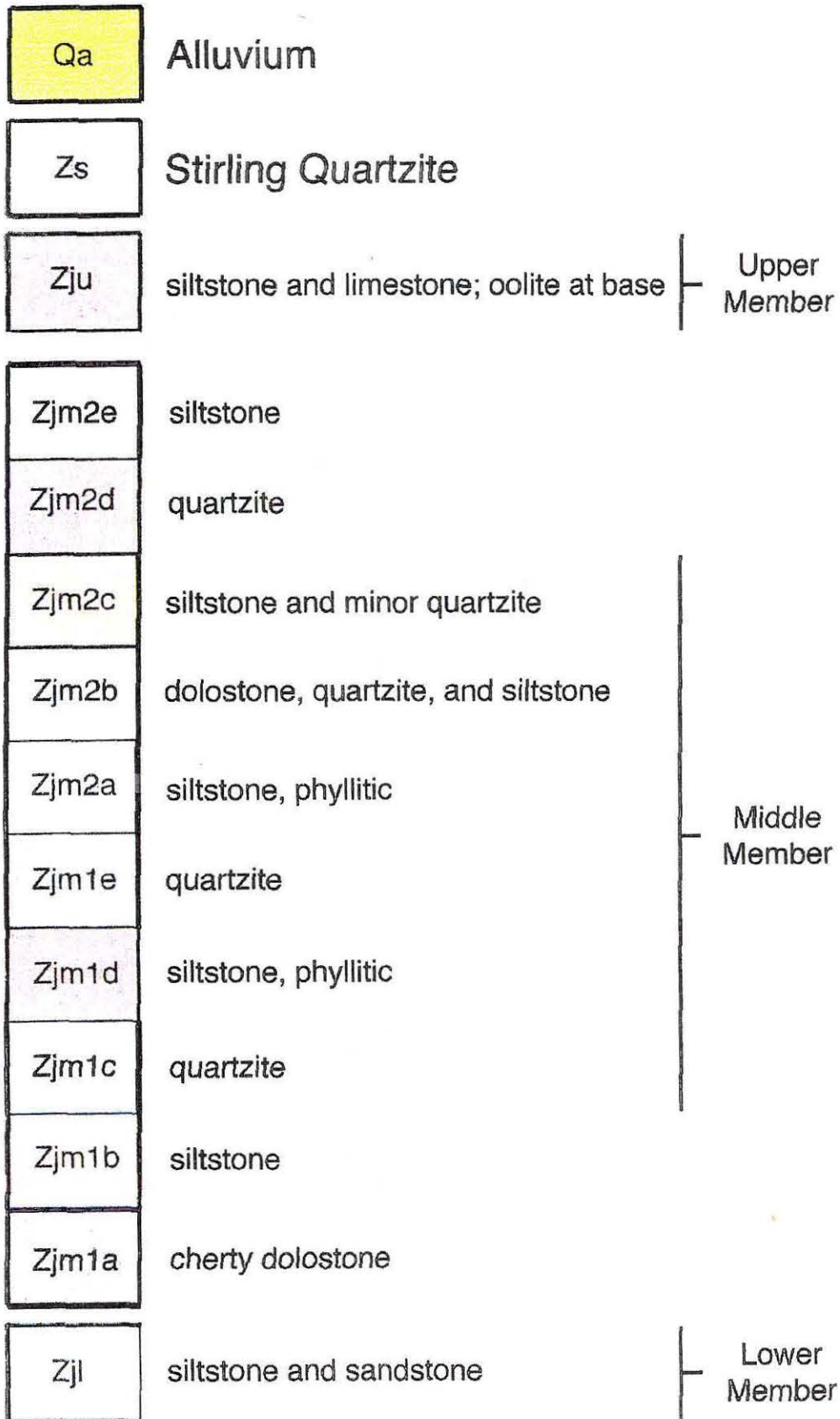


Figure 4-23. Geologic map of the middle and upper Johnnie Formation east of Paddy's fault.



Johnnie Formation

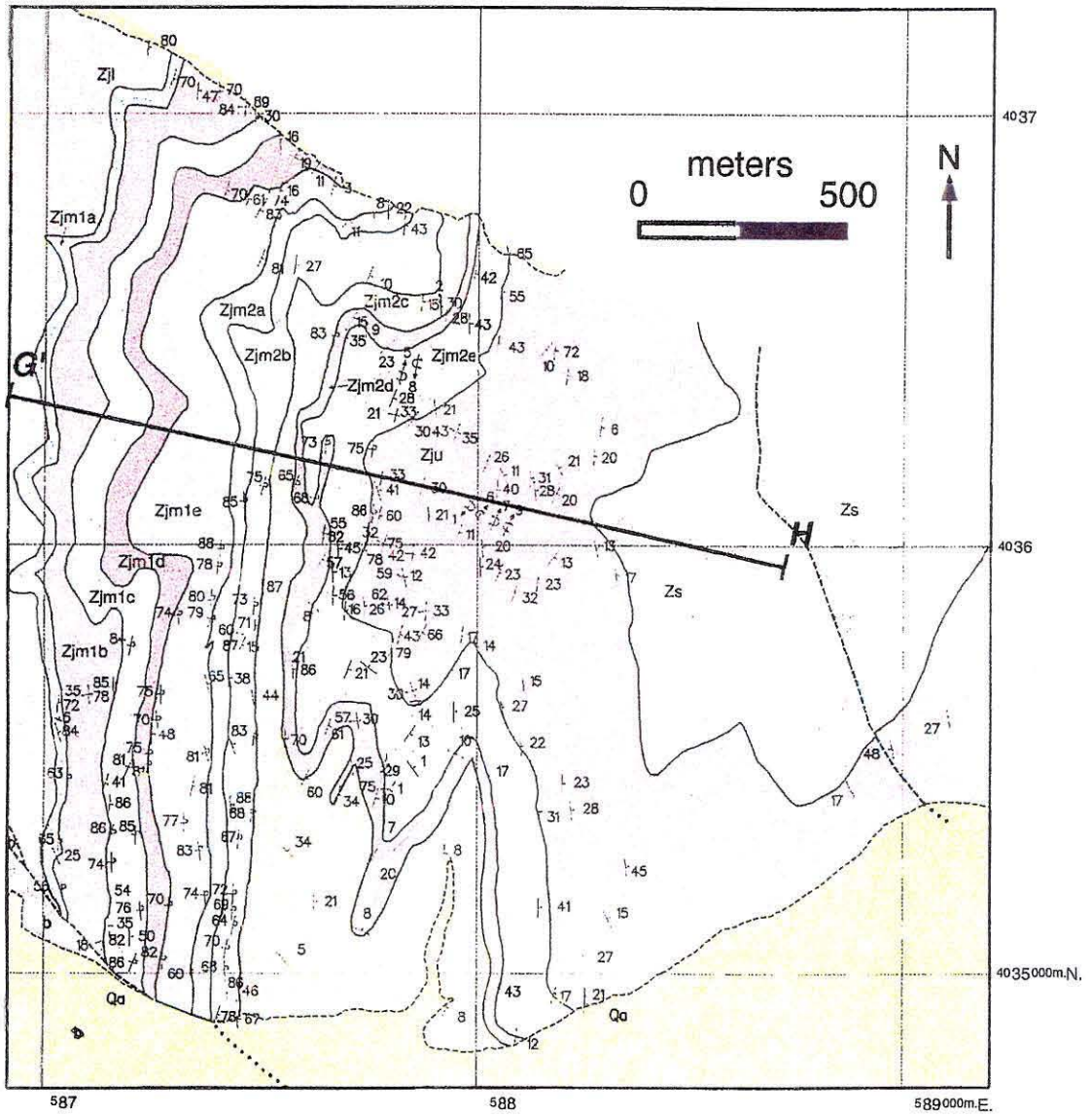
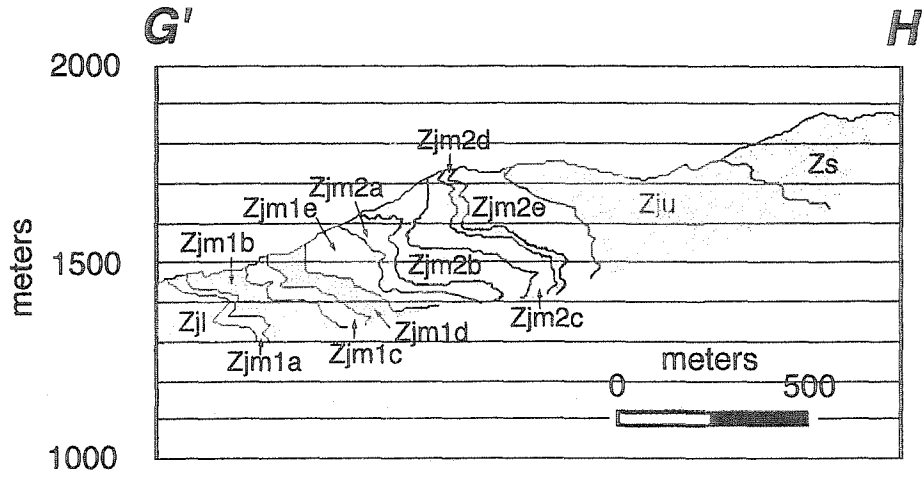


Figure 4-24. Cross section G'H through folds in the middle and upper Johnnie Formation east of Paddy's fault. See Figure 4-23 for location of section line.



below in the “Discussion.” The geology of domain III was previously described by Burchfiel and others (1983).

Stratigraphy of the middle Johnnie Formation in Domains II and III

Introduction

To constrain the amount of lateral translation between domains II and III, the Johnnie Formation was examined in both domains. As shown in Figure 4-25, five sections were measured in domain II and one section was measured in domain III. In domain II, both along-strike and across-strike lithologic variations were examined. In this region, isopachs and facies trends in the miogeocline are generally sub-parallel to the strike of contractile structures (Snow, 1992). As a result facies generally vary across strike more than they vary along strike. S-1 and S-2 constitute an “eastern” group of along-strike locations, and S-3, S-4, and S-5 constitute a “western” group of locations. Strictly speaking, the western locations are not precisely oriented along strike, but they are oriented at a low-angle to the strike of overturned folds in the Johnnie Formation. The along-strike distance between S-1 and S-2 is about 4.5 km and the along-strike distance between S-3 and S-5 is about 3.25 km. The two groups of along-strike locations are separated by an across-strike distance of about 5.5 km.

Method

Out of the entire stratigraphic section, a stratigraphic interval in the middle of the Johnnie Formation contains the most informative lateral facies changes. This interval is both lithologically variable (Stewart, 1970; Summa, 1993) and readily identifiable throughout southern Nevada and southeastern California. In addition, thesis work by Summa (1993) showed that this interval is bracketed by a pair of regional sequence stratigraphic boundaries as shown in Figure 4-26. At every location, sediments deposited between these two boundaries are roughly the same age, so lateral facies changes are readily apparent.

Figure 4-25. Map depicting the location of measured sections described in domains II and III.

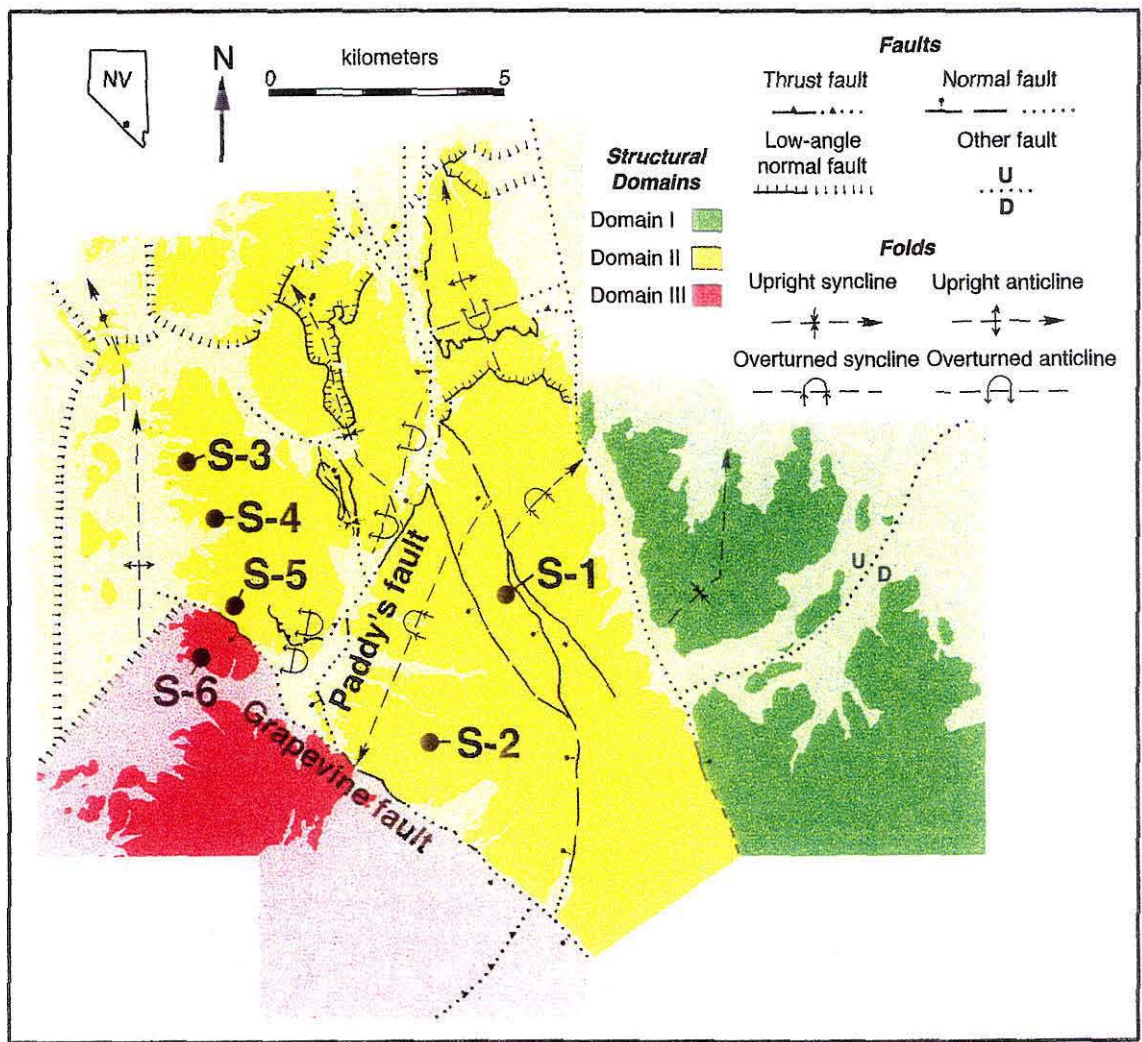
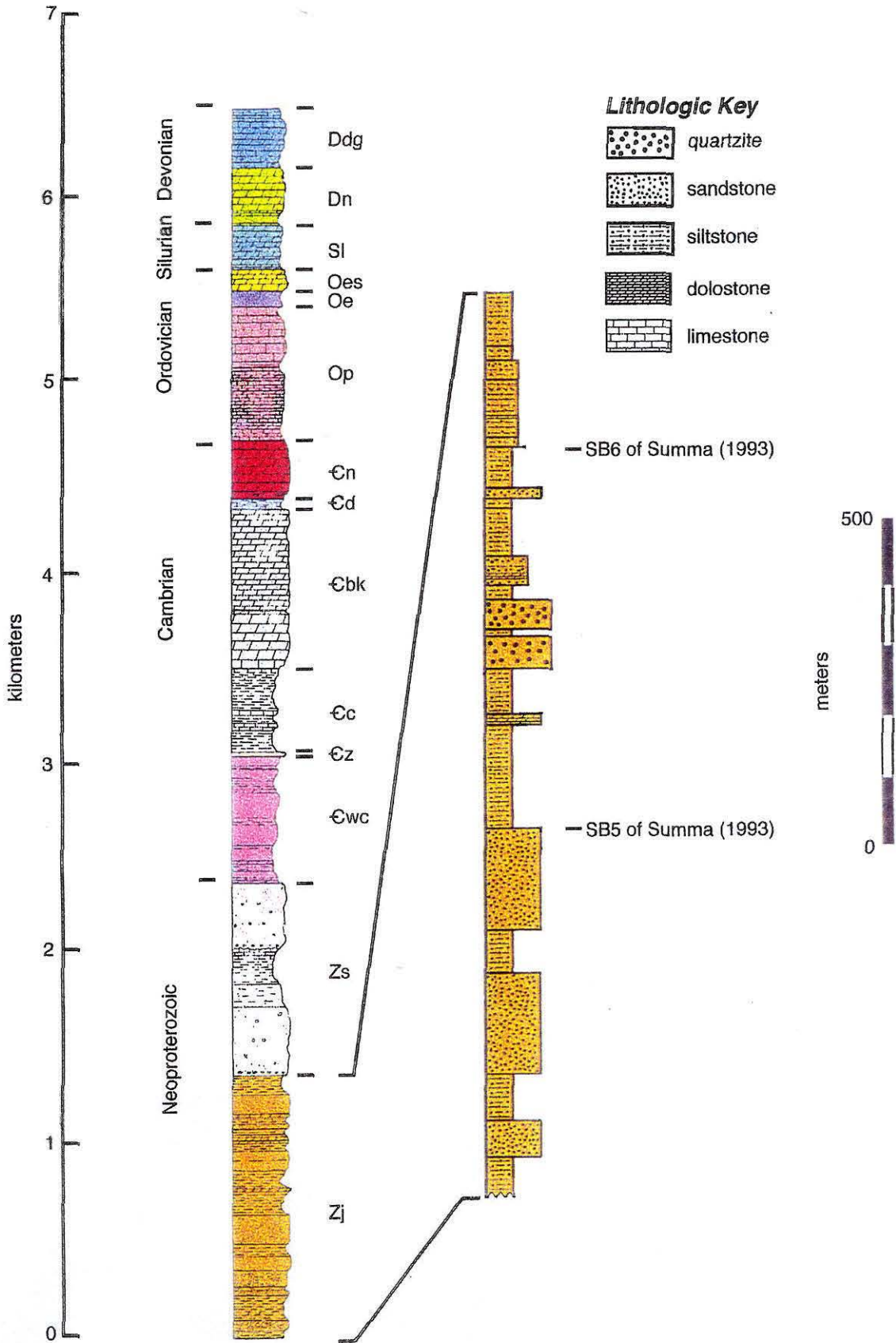


Figure 4-26. Stratigraphic interval used in comparison of Johnnie Formation between domains II and III.



Both sequence boundaries are easily recognized in the field. The higher of the two sequence boundaries (sequence boundary six of Summa, 1993) occurs at the base of a regionally persistent grayish orange oolitic limestone marker bed. The lower sequence boundary (sequence boundary five of Summa, 1993) is generally underlain by several meters of quartzite and is overlain by tens of meters of siltstone. The siltstone is usually capped by about 5 meters of cherty dolostone.

In the northwestern Spring Mountains, the interval bounded by the two sequence boundaries includes a series of thick siltstone and quartzite units at its base. These units are included here in the informal unit Zjm1, and were not investigated in detail because the quartzites are lithologically monotonous and experience substantial structurally-controlled variations in thickness. About 275 m of section separates the top of unit Zjm1 from the prominent grayish orange oolitic limestone marker bed above the upper sequence boundary. This 275 meter thick package is the focus of this investigation and is informally designated unit Zjm2. Unit Zjm2 includes a geographically variable package of siltstone, dolostone, dolomitic sandstone, and quartzite.

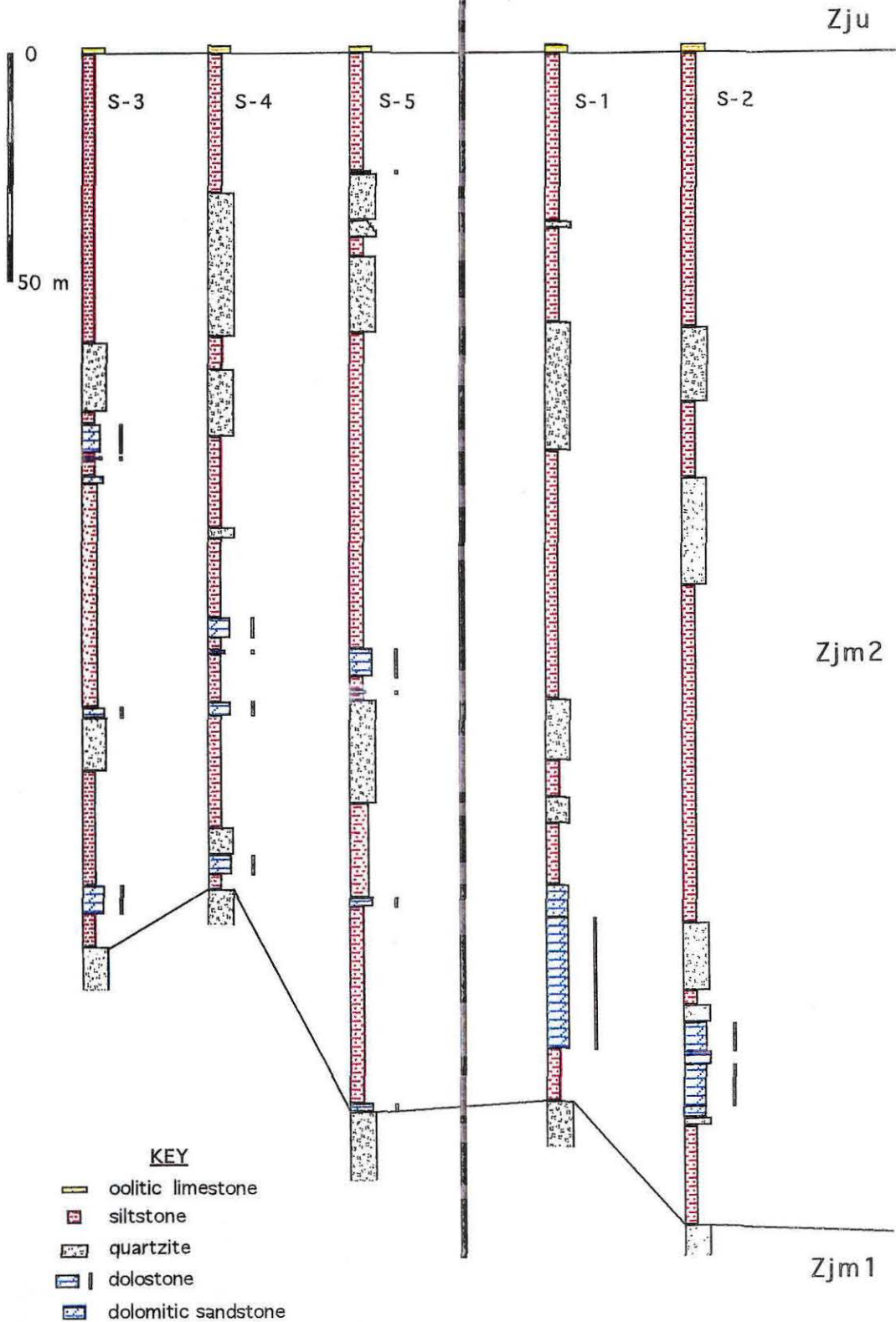
Observations

As shown in Figure 4-27, the number of dolomitic horizons within Zjm2 and their stratigraphic position is relatively constant along strike, but varies across strike. At S-1 and S-2, dolostone is confined to a single relatively thick interval near the base of Zjm2. The dolomitic interval is 30 meters thick at S-1. At S-2, the dolomitic interval is 18 meters thick and is interrupted by a thin interval of quartzite and dolomitic sandstone. In contrast, at S-3, S-4, and S-5, dolostone occurs at four distinct horizons, and no dolomitic interval exceeds 6.5 meters in thickness. A thin fifth dolomitic horizon occurs high in Zjm2 at S-5. In general, dolostones vary in thickness and color in the three western sections. However, all three sections share a distinctive thin light brown dolostone in the middle third of Zjm2.

Figure 4-27. Measured sections east and west of Paddy's fault. See Figure 4-25 for section locations. Black vertical line to right of section indicates dolostone.

West of Paddy's fault

East of Paddy's fault



In all three sections, this light brown dolostone occurs 1-2 meters below a 4.5-6.5 meter thick laminated dolostone.

In all five sections, significant variations in the thickness of siltstone intervals are probably structural. Variations in the thickness of quartzite intervals are probably also partially structural. No geographic trends in the overall percentage of dolostone, siltstone, and quartzite were observed.

As shown in Figure 4-28, Zjm2 at location S-6 in the hanging wall of the Grapevine fault most closely resembles Zjm2 at the three western footwall locations. As at those three locations, Zjm2 in the hanging wall contains four distinct dolomitic horizons. A thin light brown dolostone is also present in the middle third of Zjm2 at S-6. In particular, the lower half of Zjm2 at S-6 most resembles the lower half of Zjm2 at the nearest footwall location (S-5). The lower part of sections at both S-5 and S-6 are shown in Figure 4-29, and contain the same series of siltstone, dolostone, and quartzite intervals. The upper half of Zjm2 at S-6 contains 28 m of dolomitic sandstone. This thick interval of dolomitic sandstone was not observed at any of the other locations, but a thin dolostone occurs in about the same stratigraphic position at S-5.

DISCUSSION

Evidence for thrust motion on the Stirling Mine fault (domain I)

Two observations show that the Stirling Mine fault is probably a thrust. First, the minor thrust 150 m north-northwest of the buried fault trace is consistent with thrust motion on the main fault. This minor thrust is unique in domain I.

Second, the Stirling Mine syncline 1.7 km northwest of the Stirling Mine fault resembles a syncline in the hanging wall of the Montgomery thrust (Burchfiel and others, 1983) and a syncline in the hanging wall of the Wheeler Pass thrust (Burchfiel and others, 1974). Each of these synclines is probably a fault-bend-fold which formed as the hanging wall of the thrust moved up a thrust plane which steepens toward the surface. Cordilleran

Figure 4-28. Measured sections north (domain II) and south (domain III) of the Grapevine fault. Black vertical line to right of section indicates dolostone.

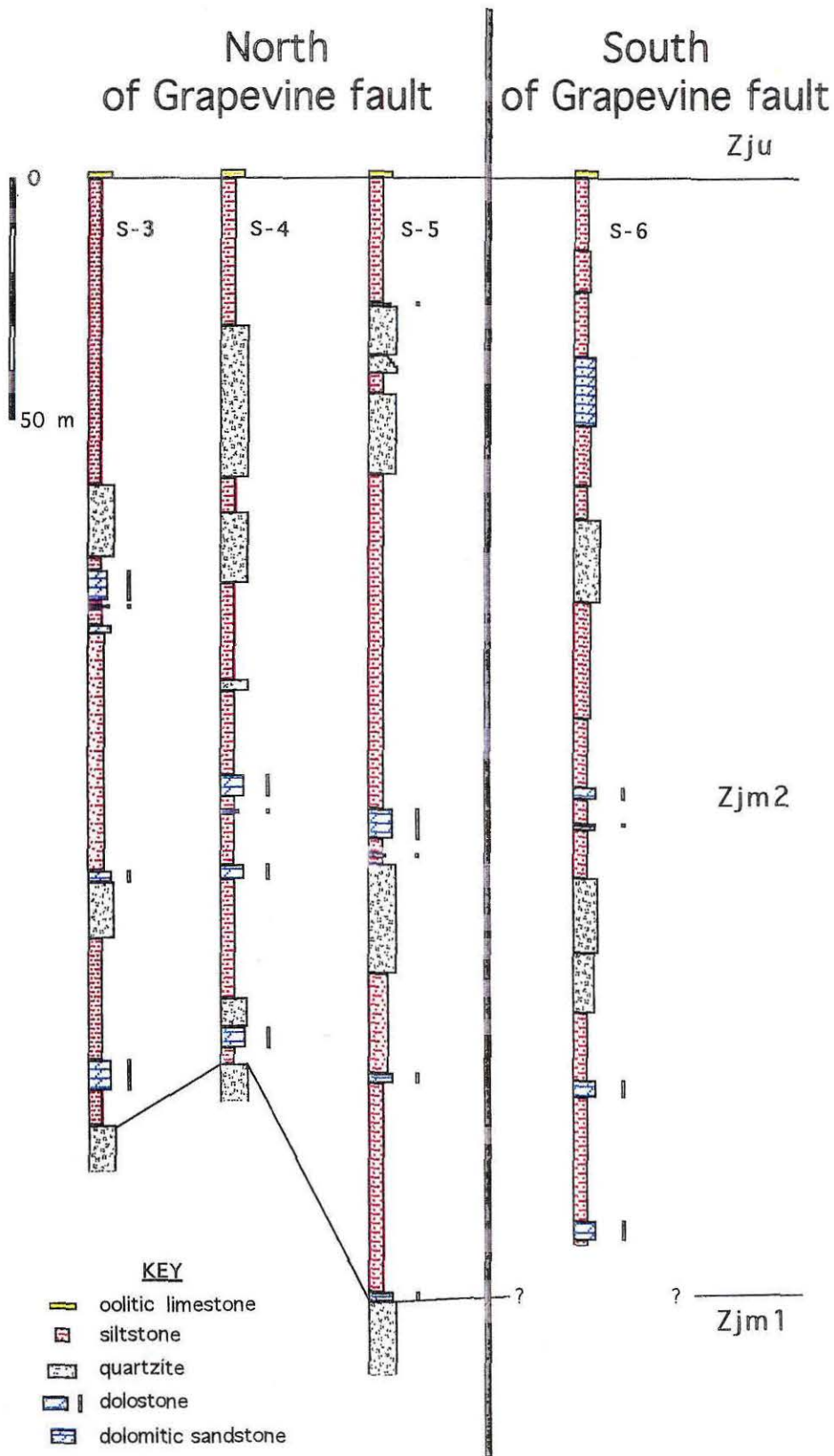
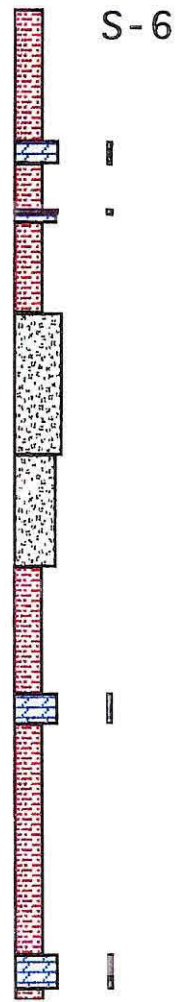
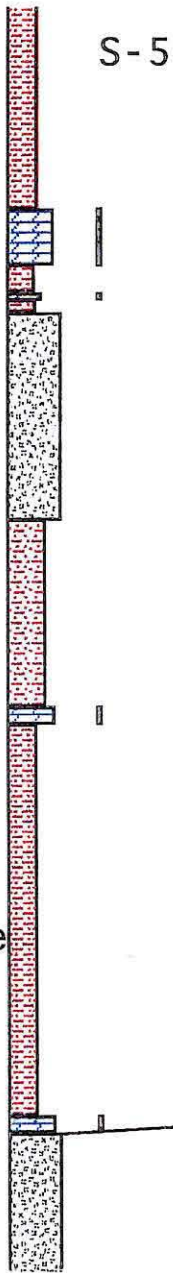


Figure 4-29. Measured sections north (domain II) and south (domain III) of the Grapevine fault. Black vertical line to right of section indicates dolostone.

4-78

North
of Grapevine fault

South
of Grapevine fault



Zjm 2

Zjm 1

KEY

- oolitic limestone
- siltstone
- quartzite
- dolomite
- dolomitic sandstone

foreland thrusts are commonly curved and steepen toward the surface (Allmendinger, 1992).

Thrusting and the fold trains in domain II

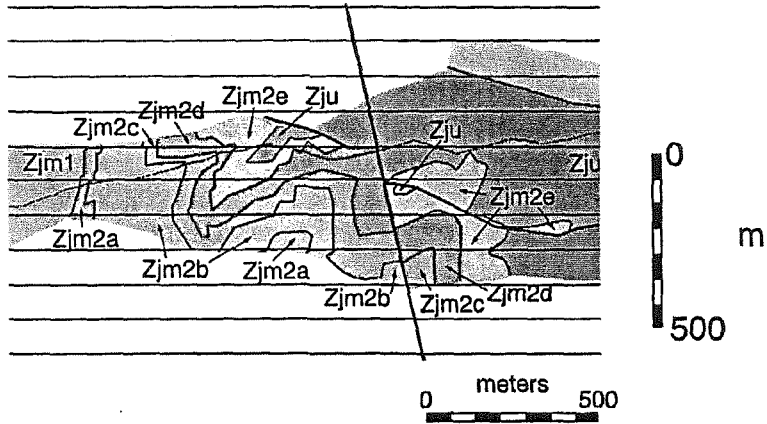
Fold trains in domain II resemble fold trains associated with thrusts in the Variscan foreland and the Helvetic nappes as shown in Figure 4-30. In the northern part of domain II (Figure 4-13), the fold train exhibits a progression from upright to overturned folds in the hanging wall of the Jaybird thrust. This progression suggests a link between shallowing of the fold axial surface and thrusting. A similar progression from upright to overturned folds is observed in the Variscan foreland in Cornwall, England (Sanderson, 1979). In the Cornwall fold train, axial surfaces shallow toward the Tintagel thrust zone. In the Alps, fold axial surfaces shallow toward the thrust fault at the base of the Morcles nappe (Ramsay and others, 1983).

In the Variscan foreland and Morcles nappe, fold axial surfaces were probably rotated by simple shear adjacent to the thrust. Shear strains are highest adjacent to the thrust, so rotation is greatest near the fault surface. Both shear strain and rotation decrease away from the fault. Rowan and Kligfield (1992) studied the kinematics of folding in the Wildhorn nappe and concluded that fold trains similar to those in domain II could form entirely through simple shear within a thrust sheet as shown in Figure 4-31.

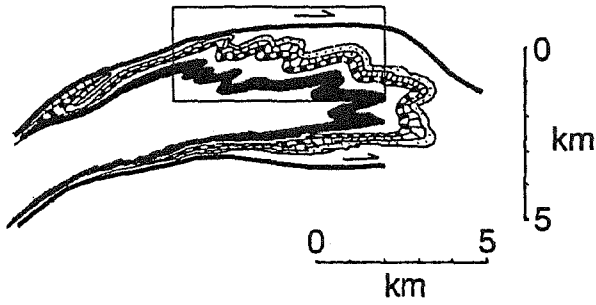
The thrust associated with the folds in domain II is not exposed at the surface. Most of the folds are probably not kinematically related to the Jaybird fault because it is a relatively minor structure (350 m of apparent displacement). In addition, the Jaybird fault cuts some of the folds in the southern part of domain II as shown in Figures 4-15 and 4-16. This cross-cutting relationship shows that at least some of the folds are older than the Jaybird fault and are not kinematically related to it. The folds in domain II are probably related to a thrust, but this thrust is not exposed at the surface in domain II. The thrust associated with these folds has probably been excised by normal faults as described below.

Figure 4-30. Fold trains in the northwestern Spring Mountains, NV, and the Morcles (Ramsay and others, 1983) and Wildhorn (Rowan and Kligfield, 1992) nappes in Switzerland. In the Morcles nappe, folds within the boxed area most resemble folds in the northwestern Spring Mountains. Note the difference in scale between the three locations.

Spring Mountains, NV



Morcles Nappe, CH



Wildhorn Nappe, CH

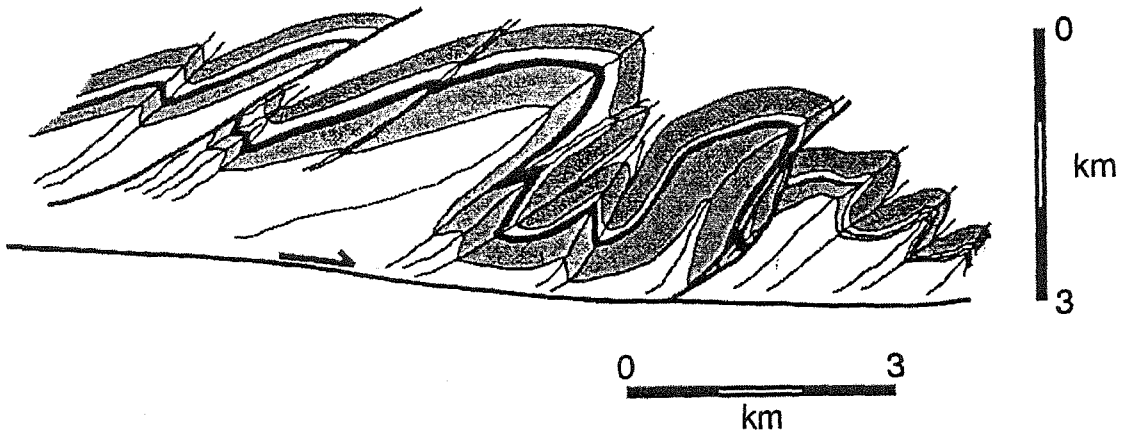


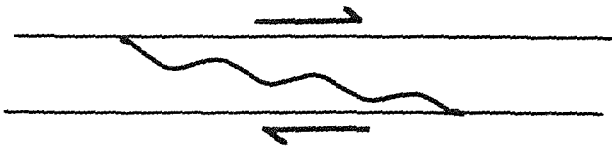
Figure 4-31. Kinematic model for the development of fold trains in the Wildhorn nappe, Switzerland after Rowan and Kligfield (1992). **Step 1:** Initially, bedding is inclined to the shear zone. Some early shortening is accommodated by the formation of pressure solution cleavage and by the tectonic thickening of beds. **Step 2:** Layers buckle to form symmetric folds. **Step 3:** The folds tighten until they lock (commonly at an interlimb angle of about 90° ; Ramsay and others, 1983). Subsequent deformation occurs by passive rotation of fold limbs. With progressive simple shear, the forelimb steepens, rotates through vertical, and overturns, while the backlimb rotates toward parallelism with the thrust surface.

Steps 1 and 2 could occur under pure shear or simple shear, while step 3 requires simple shear.

Step 1



Step 2



Step 3



Extension in domain II

After the formation of contractile structures in domain II, the domain experienced considerable extension on the Diebert, Niavi, and Point of Rocks faults. In addition, broad upright folds in this domain are probably syn-extensional. The Hill 1348T anticline folds the Diebert and Niavi faults and is cut by the Point of Rocks fault. The Hill 1274T syncline also folds the Niavi fault and is cut by the Point of Rocks fault. Cross-cutting relationships associated with the Hill 937T anticline are less clear. However, the core of the anticline exposes a window into the footwall of the Point of Rocks fault, suggesting that the anticline is, at least in part, younger than the Point of Rocks fault. Broad upright syn-extensional folds in domain II are geometrically analogous to "turtleback" folds which occur in several highly-extended areas including the Black Mountains on the east side of Death Valley (Holm and others, 1994) and the Simplonpas in the Alps (Mancktelow and Pavlis, 1994).

Syn-extensional basin deposits are exposed in a small area in the northwestern corner of domain II as shown on Figure 4-32. These deposits occur in the hanging wall of the Point of Rocks fault and include a carbonate breccia which was probably derived from the northwestern Spring Mountains during extensional unroofing. The breccia has been repeated by normal faults and is tilted. The carbonate breccia is overlain by conglomerate which is also tilted, suggesting a syn-tectonic origin. Ash beds in the conglomerate yielded biotite K-Ar ages of 12.6-13.5 Ma (Zigler and Simonds, 1992). Tertiary basin deposits were only mapped in reconnaissance in this study, but the author located a pumaceous ash that yielded plagioclase K-Ar ages of 10.9 and 12.0 Ma (Zigler and Simonds, 1992) and verified a strike of N33W and a dip of 20° NE. Together, the normal faults, upright folds, and basin deposits indicate considerable Miocene extension in domain II.

Figure 4-32. Tertiary basin deposits in the northwestern Spring Mountains, NV.

Qa	alluvium
Tp	Tertiary playa deposits
Tg	Tertiary gravel
Tb	Tertiary carbonate breccia
En	Nopah Formation
Cwc	Wood Canyon Formation
Zjm2	upper Johnnie Formation
Zjm1	middle Johnnie Formation

Contact

Dashed where approximately located
Dotted where concealed

Fault

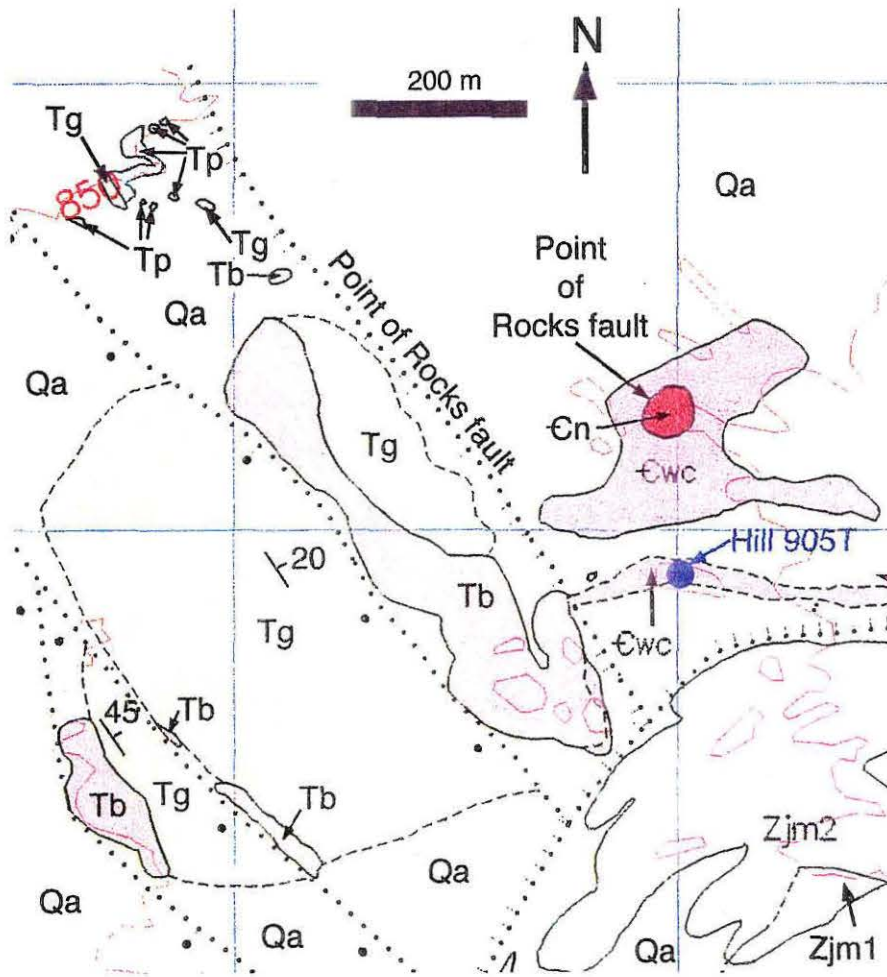
Dashed where approximately located;
Dotted where concealed

Normal Fault

Dashed where approximately located;
Dotted where concealed;
ball on downthrown side

Normal Fault

Dashed where approximately located;
Dotted where concealed;
ball on downthrown side



Thrusting and extensional reactivation in domain II

As interpreted above, the Stirling Mine fault is a major thrust in domain I and fold trains in domain II show that a major thrust was also present in that domain. The proximity of the Stirling Mine fault in domain I and the overturned folds in domain II suggests that both are manifestations of a single major thrust that was continuous through both domains I and II. This major thrust is referred to as the Kwichup Spring thrust after a hypothetical structure discussed by Snow (1992). Figure 4-33 is an interpretive cross section through the Kwichup Spring thrust as it probably appeared before it was disrupted by Neogene extension. The Stirling Mine thrust in domain I is a fragment of the Kwichup Spring thrust, and preserves the older-over-younger thrust relationship. The fold trains in domain II formed within the Johnnie Formation in both the hanging wall and the footwall of the Kwichup Spring thrust.

After thrusting, dip-slip motion on the Diebert fault reactivated and/or excised the Kwichup Spring thrust (Figure 4-34), and, as shown in Figure 4-35, juxtaposed the hanging wall fold train (west of Paddy's fault and the Diebert fault) against the footwall fold train (east of Paddy's fault and the Diebert fault). During or shortly after extension, the footwall of the Diebert fault was tilted and the Diebert fault rotated to a low angle. Analogous footwall tilting is observed along other major normal faults (Wernicke and Axen, 1988), and has been ascribed to footwall isostatic rebound (Wernicke and Axen, 1988; Buck, 1988). After movement on the Diebert fault, Paddy's fault omitted the Diebert fault in the southern and central parts of domain II.

The Rock Spring fault is interpreted as a Neogene fault which separates relatively unextended (domain I) and extended (domain II) areas. In this interpretation, major low-angle normal faults in domain II (the Diebert, Niavi, and Point of Rocks faults) terminate against the Rock Spring fault. The Rock Spring fault probably experienced two phases of motion. First, while domain II was extending, the Rock Spring fault accommodated right-

Figure 4-33. Interpretive cross section through the Kwichup Spring thrust showing the inferred relationships between section lines AB in domain I and EF and GH in domain II and the overall structure of the thrust.

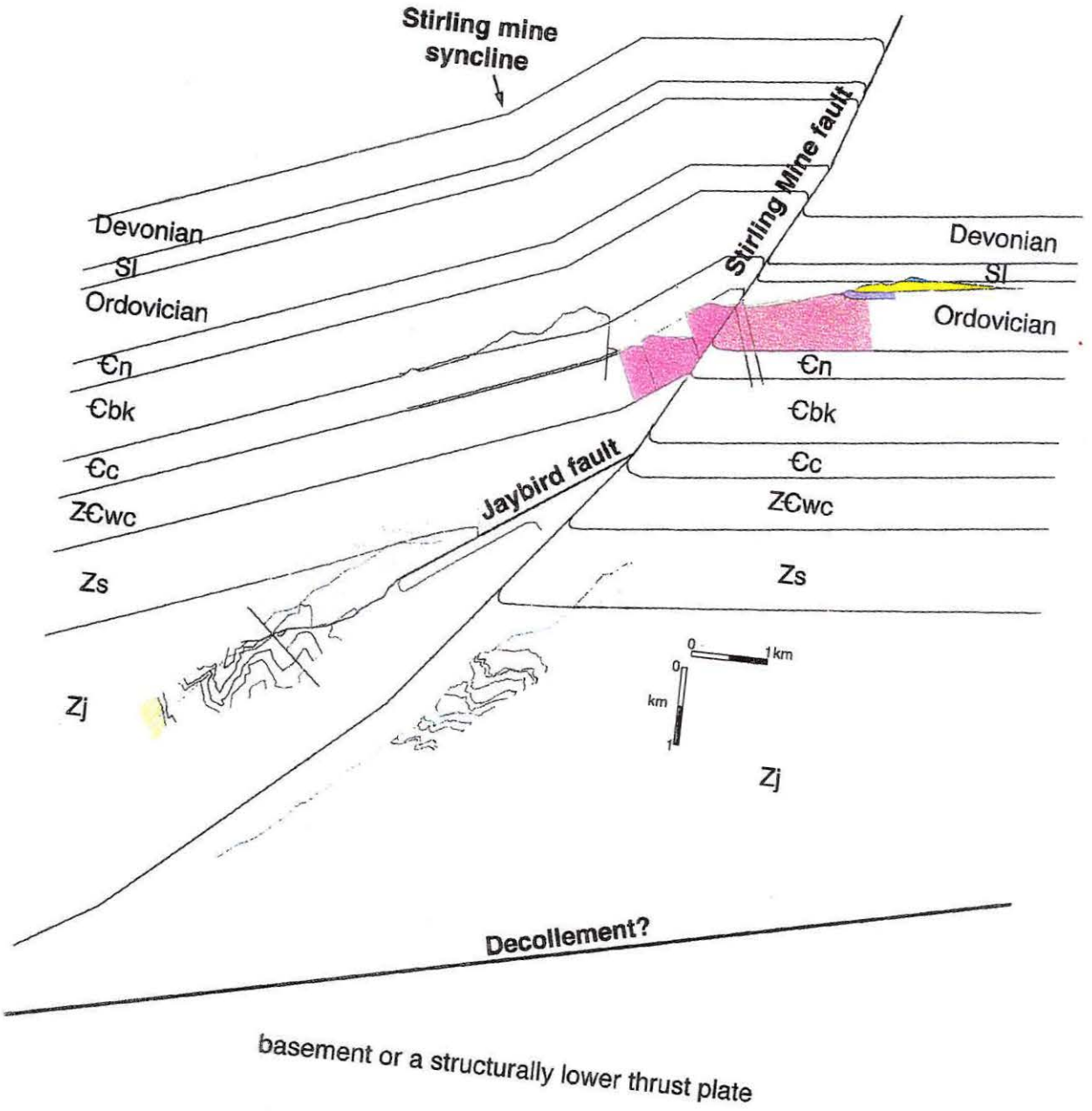


Figure 4-34. Cross section showing the future position of the Diebert fault within the Kwichup Spring thrust prior to extension. Units are as shown in Figures 4-10, 4-15, and 4-23.

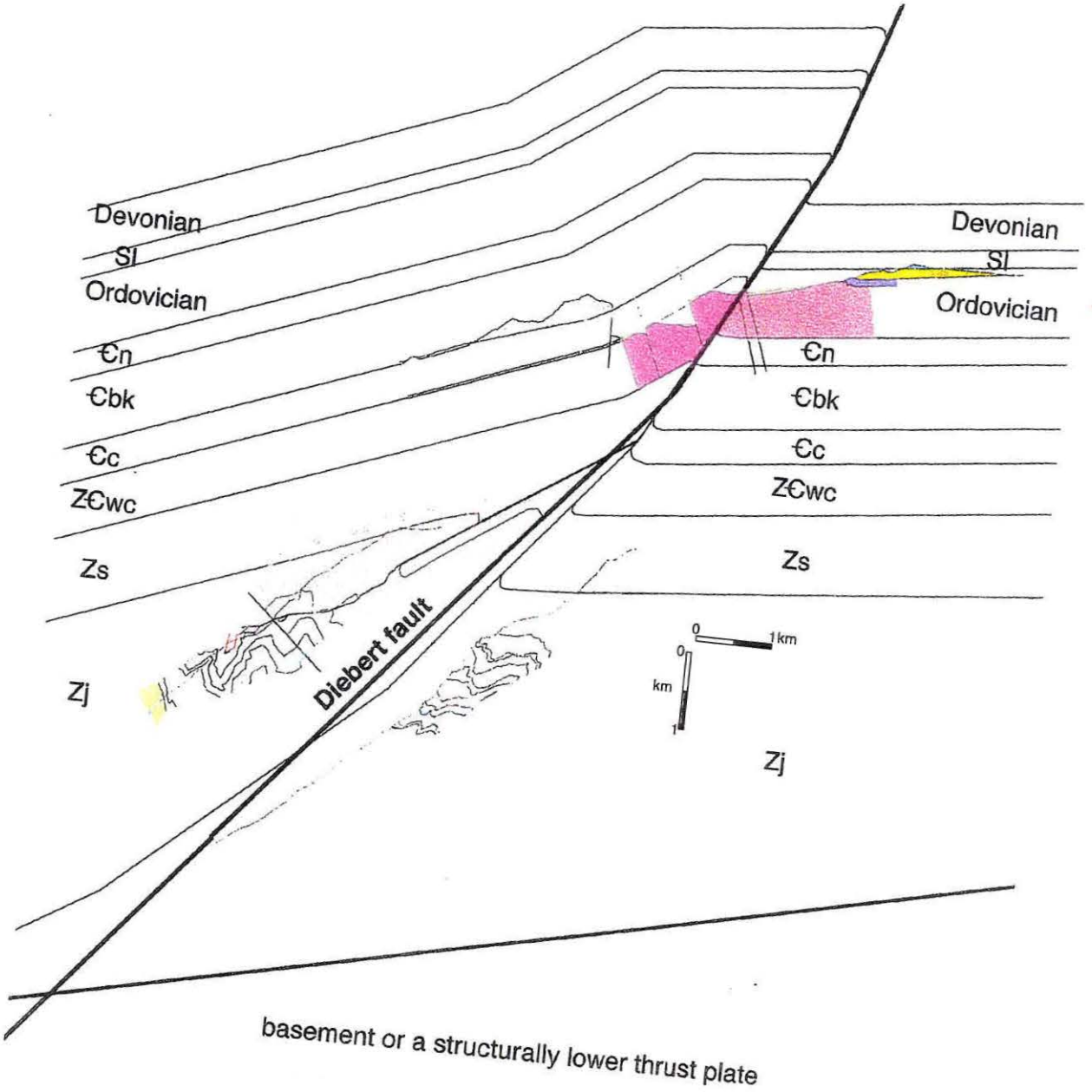
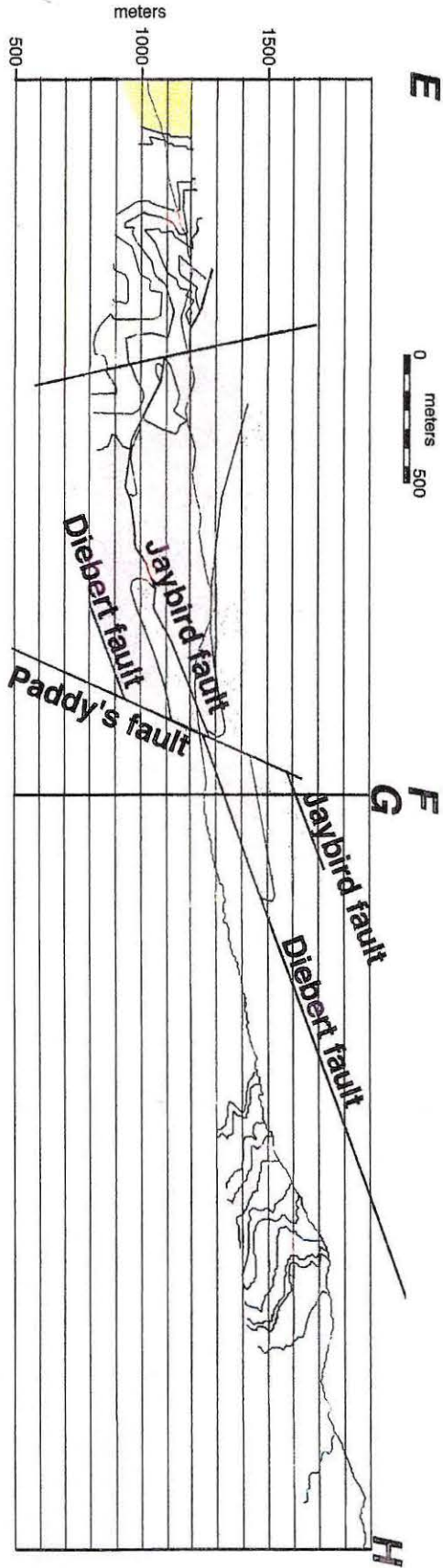


Figure 4-35. Cross section showing the inferred relationship between the Diebert fault, Jaybird fault, and Paddy's fault. Units are as shown in Figures 4-10, 4-15, and 4-23.



lateral displacement between the Diebert hanging wall and domain I. Second, the fault accommodated tilting and uplift of the Diebert footwall.

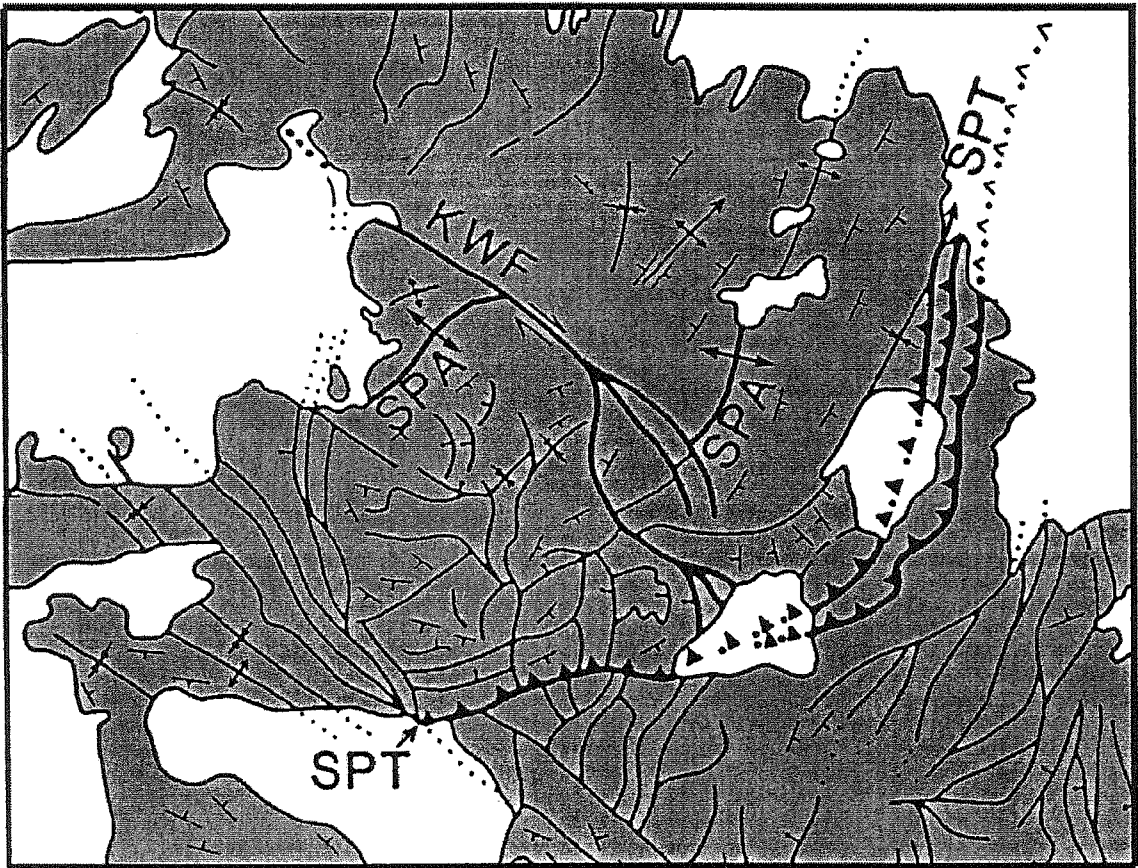
The sequence of events described above is not unique to the Kwichup Spring thrust. The Schwaub Peak thrust in the Funeral Mountains, CA, has a similar map-view geometry (Figure 4-36) and probably experienced a similar history of extensional reactivation. Like the Kwichup Spring thrust, the Schwaub Peak thrust consists of an eastern segment which is relatively unextended and a western segment in which the hanging wall of the thrust is cut by numerous normal faults (Cemen and Wright, 1990). The extended and unextended segments are separated by the Keane Wonder fault which is analogous to the Rock Spring fault. A large anticline in the hanging wall of the Schwaub Peak thrust is offset by 5 km in a right-lateral sense across the Keane Wonder fault. Similarly, the Rock Spring fault probably also experienced a phase of right-lateral motion. Normal faults in the extended hanging wall of the Schwaub Peak thrust terminate against the Keane Wonder fault. In an analogous manner, the Diebert, Niavi, and Point of Rocks faults terminate against the Rock Spring fault.

Several other thrusts are reactivated or excised by normal faults in the Death Valley region of southeastern California. In the Cottonwood Mountains, the Marble Canyon thrust is reactivated or excised as are the Baxter and Resting thrusts in the Resting Spring Range (Wernicke and others, 1993). In the Funeral Mountains, the Clery thrust has been reactivated or excised (Cemen and Wright, 1990).

*Correlation of the Kwichup Spring thrust
with the Montgomery thrust in domain III*

Stratigraphic observations in domains II and III show that the two domains have been adjacent since the Neoproterozoic. Five sections measured in the middle Johnnie Formation in domain II (Figure 4-27) show that individual dolomitic intervals can be followed along strike for distances of 3-5 kilometers. In contrast, dolomitic intervals do

Figure 4-36. Extensional reactivation of the Schwaub Peak thrust in the Funeral Mountains as envisioned by Cemen and Wright (1990). SPT: Schwaub Peak thrust; SPA: Schwaub Peak anticline; KWF: Keane Wonder fault.



not match across a comparable across-strike distance. As shown in Figures 4-28 and 4-29, the close match between dolomitic intervals, and, near the base of Zjm2, other lithologies at locations S-5 and S-6 on opposite sides of the Grapevine fault strongly suggests that these two locations have never been separated by an across-strike distance of more than ~2 kilometers.

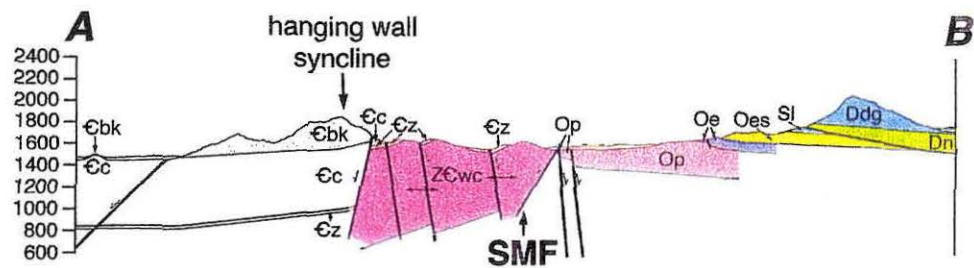
Since domains II and III were adjacent during thrusting, the Kwichup Spring thrust probably correlates with the Montgomery thrust. The Montgomery thrust has no other plausible equivalent in the northwestern Spring Mountains. Figure 4-37 presents cross sections through the Stirling Mine fault and the Montgomery thrust. Like the Stirling Mine fault, the Montgomery thrust has a syncline in its hanging wall. The cross sections differ in some other details. The Stirling Mine fault is depicted as a hanging wall and footwall ramp while the Montgomery thrust is depicted as a hanging wall flat and a footwall ramp. This difference between the two cross sections is probably not significant. Thrust geometry could vary along strike. In addition, the dip of both thrust planes is poorly constrained, the Stirling Mine fault is covered by alluvium and the Montgomery thrust has probably been reactivated or excised by a normal fault at the only location where the thrust plane is exposed.

The throw of the Montgomery thrust is about 3.5 times the throw of the Stirling Mine fault. This difference in throw could indicate that the Montgomery thrust is losing slip to the north. However, the throw on the Stirling Mine fault could have been reduced by extensional reactivation. Geologic mapping along the Stirling Mine fault shows that extensional reactivation is plausible. The thrust is cut by at least four normal faults, and variations in stratigraphic throw along the fault indicate reactivation along at least some segments. In addition, extensional reactivation would explain the omission of the footwall syncline observed below the Montgomery thrust.

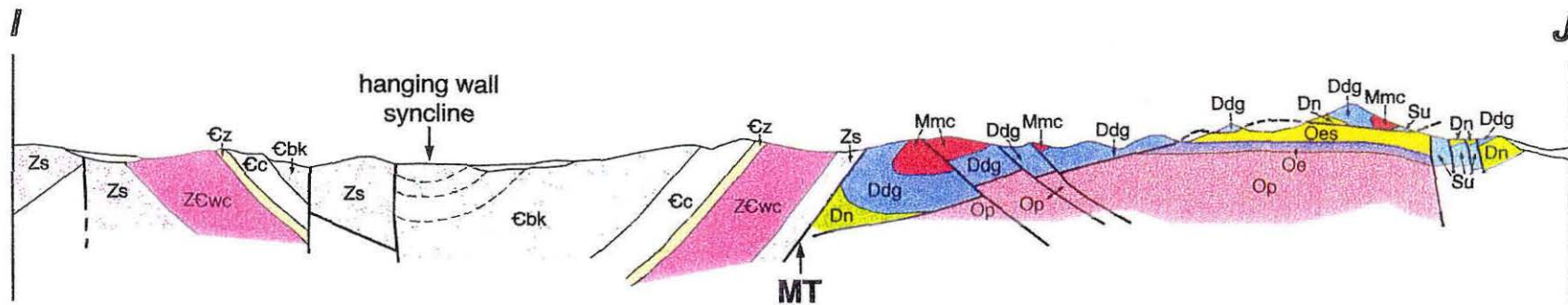
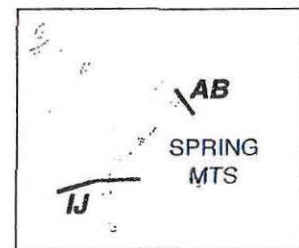
Figure 4-37. Comparison of cross sections through the Stirling Mine fault (this paper) and Montgomery thrust (Burchfiel and others, 1983). Units are as shown in Figure 4-10.

4-100

0 1 km



B



Summary

Figure 4-38 is a tectonic map summarizing the relationship between structures in the three domains. The Wheeler Pass plate is the footwall of the Kwichup Spring - Montgomery thrust and is continuous through all three domains. The Kwichup Spring thrust is also continuous through all three domains. The Niavi and Rocks plates terminate against the Rock Spring fault and are not present in domain II. The continuation of these two plates into domain III is uncertain.

Implications for thrust belt structure and large-magnitude extension in the Death Valley region

Correlation of the Kwichup Spring and Montgomery thrusts requires a reappraisal of thrust belt structure in the Death Valley region. If, as suggested by Snow (1992) and Snow and Wernicke (in press), the Montgomery thrust correlates with the Chicago Pass and Panamint thrusts, the Lemoigne thrust has no equivalent in the northwestern Spring Mountains or Specter Range. Likewise, the Wheeler Pass thrust could not correlate with the Chicago Pass and Panamint thrusts. In this scenario (Figure 4-39), the Lemoigne thrust would continue through the Funeral Mountains (as the Clery thrust of Cemen and Wright, 1990), and then end under alluvium in the Amargosa Desert. The Wheeler Pass thrust would continue south under alluvium in Pahrump Valley, and either end under alluvium or correlate with the Pachalka thrust in the Kingston Range and Clark Mountains.

The scenario outlined above would require less westward translation of the Panamint Mountains relative to the Spring Mountains during the Neogene. The amount of translation would decrease by about 30 km or 25% as shown by the purple vector in Figure 4-39. In this scenario, the breakaway zone for the Death Valley extended region would be located along the western flank of the Nopah and Resting Spring Ranges instead of along the Spring Mountains range front. Nonetheless, the amount of extension between the Nopah-

Figure 4-38. Tectonic map showing the relationship between structures in the three domains of Figure 4-6.

4-103

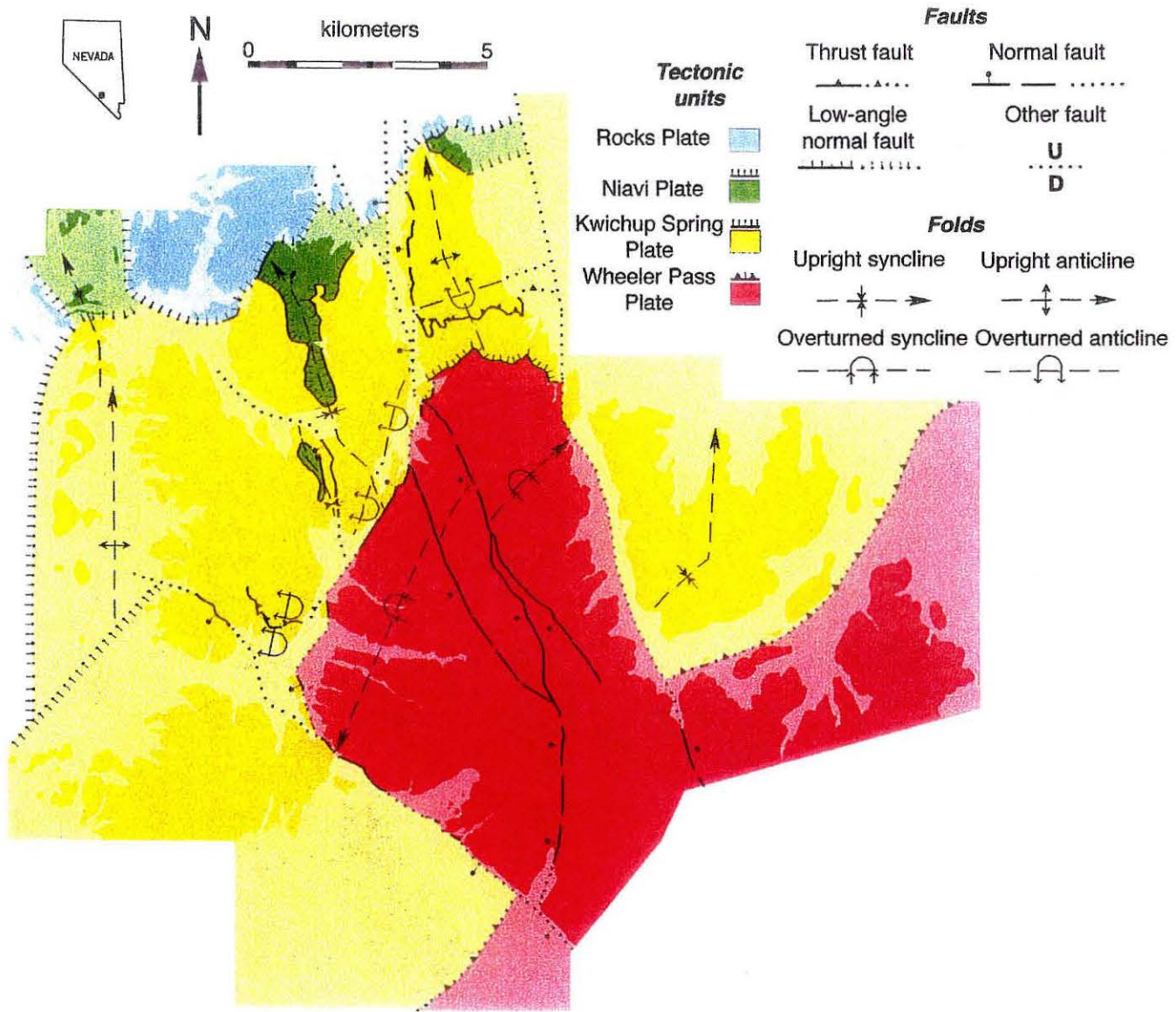
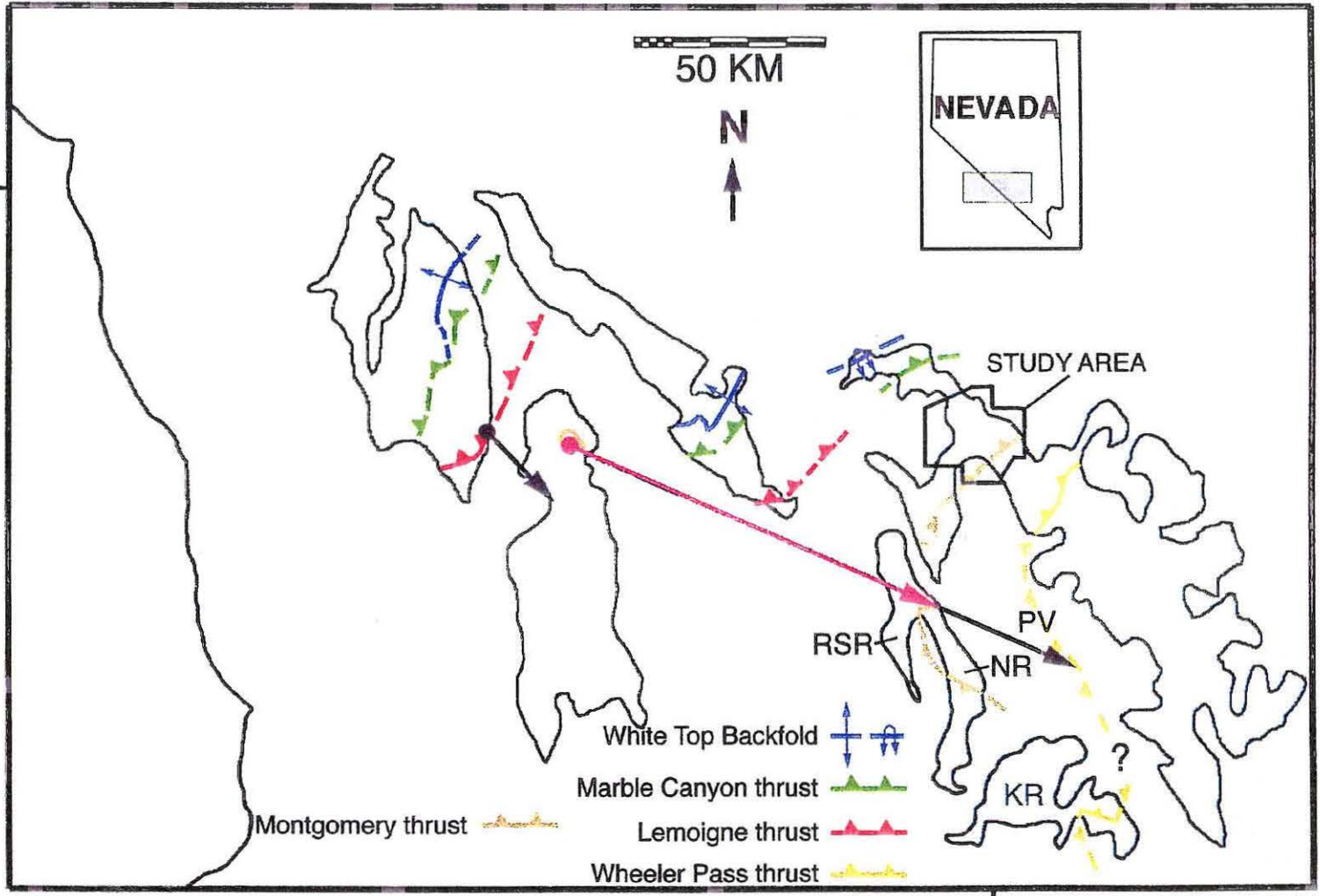


Figure 4-39. Correlation of the Montgomery - Kwichup Spring thrust with the Chicago Pass and Panamint thrusts and implications for large-magnitude extension in the Death Valley region. In this scenario, the Wheeler Pass thrust is envisioned as distinct from these three thrusts, and extension between the Montgomery-Kwichup Spring-Chicago Pass thrust and the Wheeler Pass thrust is minimal. The amount of westward translation of the Panamint Mountains relative to the Nopah-Resting Spring Range is reduced from the amount proposed by Wernicke and others (1988) to the amount shown by the purple vector.

37°



116°

Resting Spring Range and the Panamint Mountains would still be far larger (up to 500%) than the 30-50% extension envisioned by Wright and Troxel (1973).

Alternatively, the Montgomery thrust could correlate with the Clery thrust in the Funeral Mountains as suggested by Stevens and others (1991), and the Clery thrust could correlate with the Lemoigne thrust. In general, this scenario preserves the thrust belt geometry of Snow (1992) and Snow and Wernicke (in press). In this scenario, all three major contractile structures in the Cottonwood Mountains would correlate with major contractile structures in the Specter Range and northwestern Spring Mountains, providing a robust pre-extension link between the two areas. In a palinspastic reconstruction, the Panamint, Nopah and Resting Spring Ranges would have to restore a few kilometers farther south to allow the placement of the Montgomery Mountains adjacent to the northwestern Spring Mountains. However, the Wheeler Pass thrust would still correlate with the Chicago Pass and Panamint thrusts, so the westward translation of the Panamint Mountains with respect to the Spring Mountains would still be as large as the translation depicted in Figure 4-3.

The proposed correlation of the Montgomery and Clery thrusts can be evaluated by examining mapping in the Funeral Mountains by Cemen and Wright (1990). Structurally, the Montgomery and Clery thrusts both involve footwall synclines. However, the Clery thrust involves a stratigraphic throw of only 1.6 km. The thrust has been reactivated or excised along its entire length, but the throw is constrained by the Tertiary unconformity on both sides of the fault. Tertiary conglomerate sits on the Cambrian Bonanza King Formation in the hanging wall and on the Silurian Hidden Valley Dolomite in the footwall. The difference in stratigraphic throw between the Montgomery and Clery thrusts could indicate a loss of displacement along strike between the Montgomery and Clery thrusts. However, the Clery thrust could have back-slipped by some amount before erosion of the unconformity and deposition of the conglomerate. If some reactivation pre-dates the

unconformity, the throw of the Clery thrust could be comparable to the throw of the Montgomery thrust.

Implications for thrust belt structure and large-magnitude extension north of Las Vegas Valley

The Kwichup Spring thrust probably continues north from the northwestern Spring Mountains for many tens of kilometers. Elliot (1976) showed that thrusts in the Cordilleran foreland of southern Canada typically have along-strike lengths which are 10 to typically 15 times their maximum displacement. The largest displacement on the Kwichup Spring thrust and its correlatives probably occurs on the Montgomery thrust. The Montgomery thrust involves about 5 km of stratigraphic throw and probably involves about 7 km of displacement. This amount of displacement suggests a strike length of 70-105 km, so the Montgomery thrust and its correlatives probably continue for 35-50 km to the north.

As suggested by Snow (1992) and Snow and Wernicke (in press), the Pintwater thrust in the Pintwater Range is the most likely correlative of the Kwichup Spring thrust northeast of the Spring Mountains. The Pintwater Range and adjacent ranges are shown in Figure 4-40 and the Pintwater thrust is shown in Figure 4-41. As described by Guth (1990), the Pintwater thrust has a throw of at least 1 km, and has been overprinted by normal faults. The fault dips steeply, but omission of a shallowly dipping thrust by a normal fault cannot be ruled out. An upright syncline occurs in the footwall of the fault.

Correlation of the Kwichup Spring and Pintwater thrusts constrains the amount of extension between the Sheep Range and the Pintwater Range. In the Spring Mountains the Kwichup Spring and Wheeler Pass thrust ramps are about 18 km apart. The Wheeler Pass thrust continues north of Las Vegas Valley as the Gass Peak thrust, and the across-strike distance between the Pintwater and Gass Peak thrusts is about 50 km. Restoration of the Pintwater thrust along a S65E vector (Snow, 1992) to a position 18 km from the Gass Peak thrust (Figure 4-42) requires 170% extension between the two thrusts. Differential

Figure 4-40. Location of ranges discussed in text.

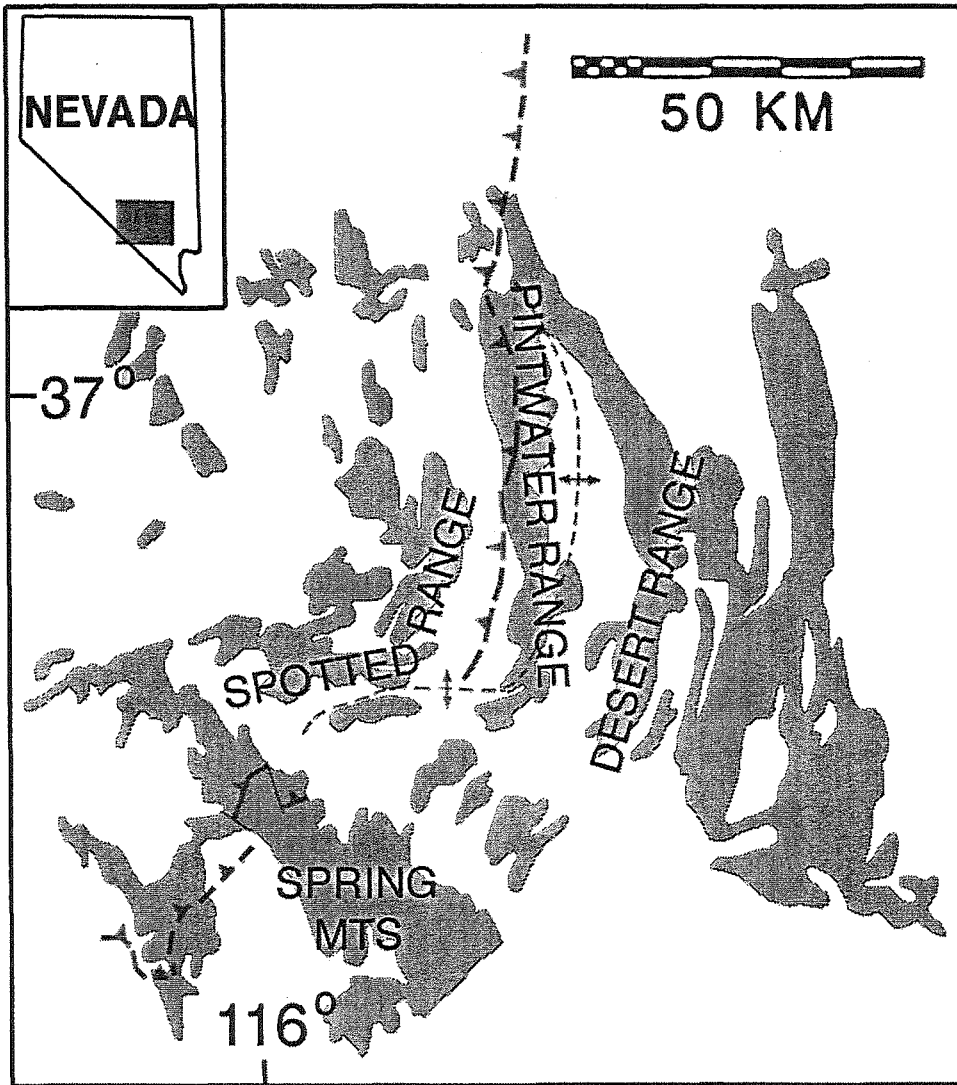


Figure 4-41. Kwichup Spring thrust and possibly correlative contractile structures. KST: Kwichup Spring thrust, MT: Montgomery thrust, PT: Pintwater thrust, PA: Pintwater anticline.

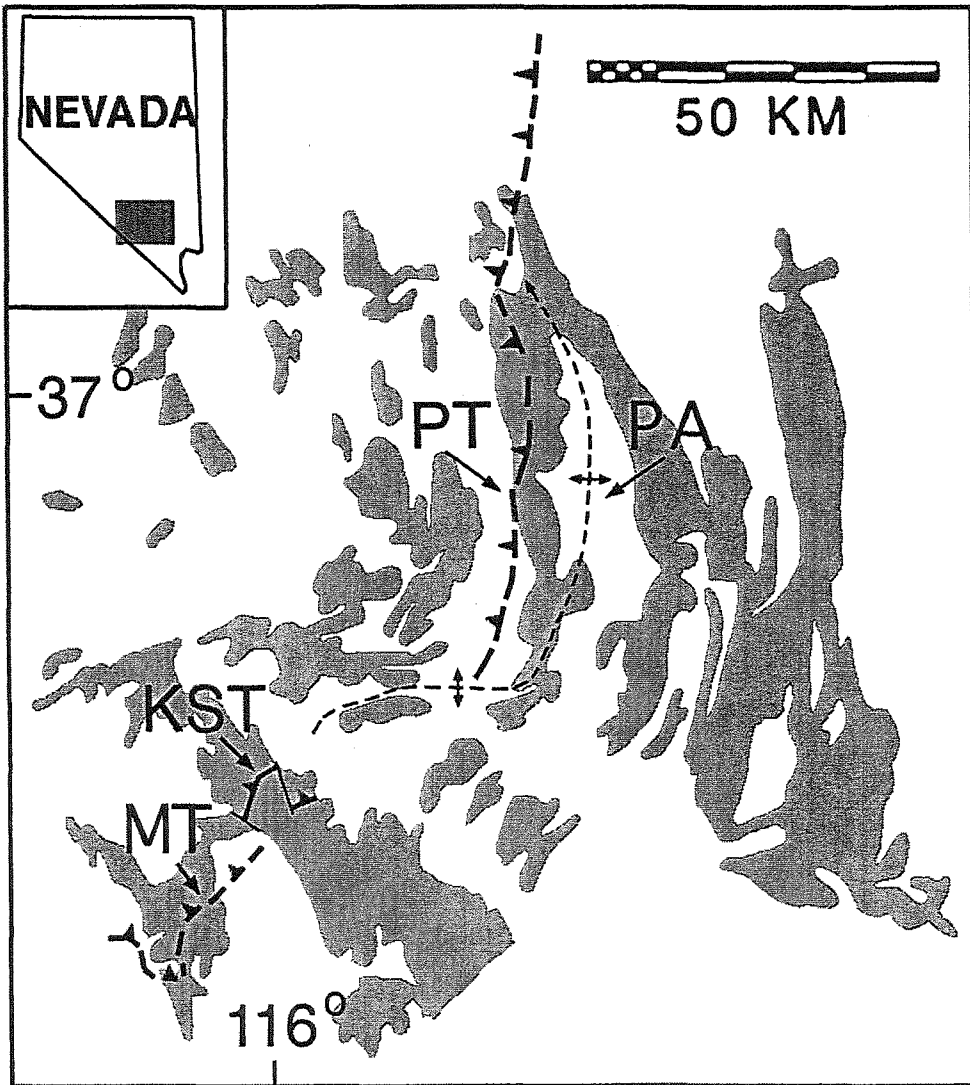
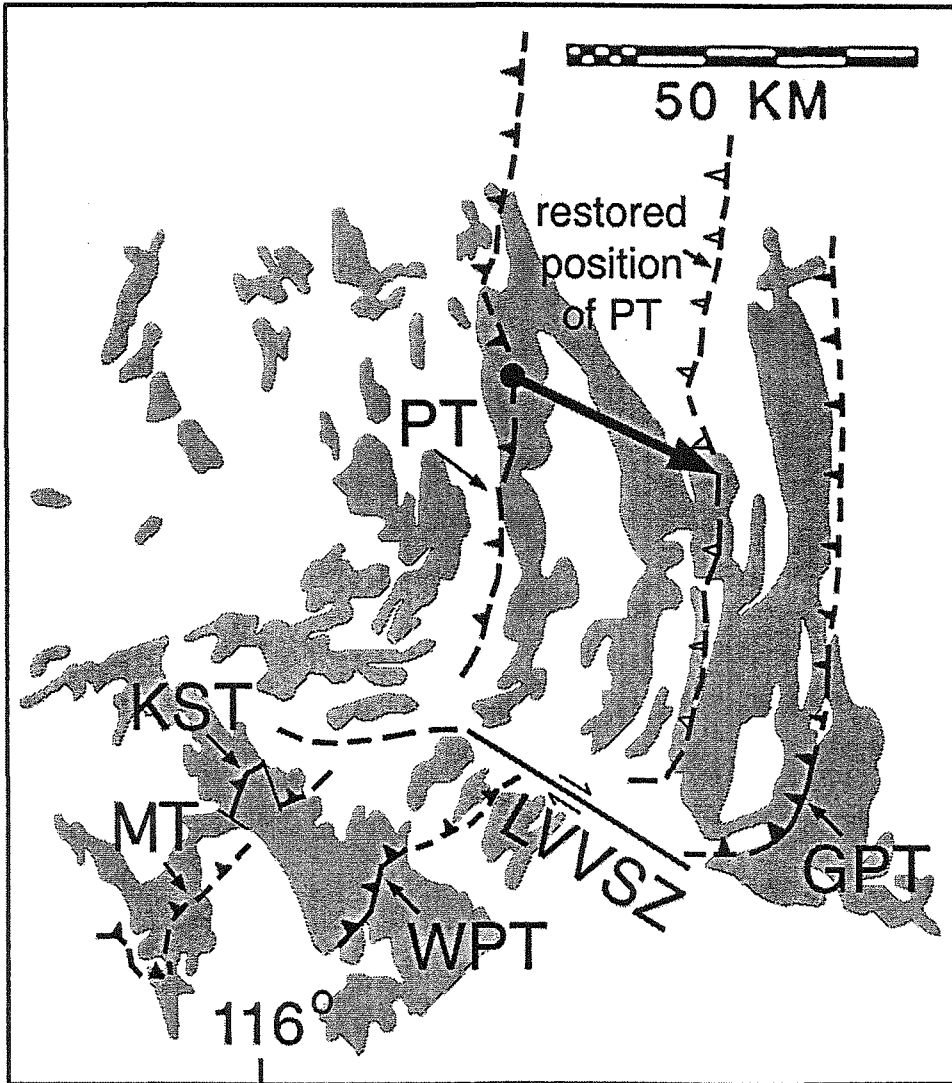


Figure 4-42. Restoration of the Pintwater thrust to its pre-extension position west of the Sheep Range stable block based on the spacing between the Wheeler Pass and Kwichup Spring thrusts.



extension between the Spring Mountains and the area to the north was accommodated by the Las Vegas Valley shear zone (Snow, 1992). The restoration in Figure 4-42 places the Pintwater thrust adjacent to the breakaway zone on the west side of the Sheep Range stable block, indicating that the area between the Sheep Range and Pintwater Range has been highly extended.

Previous estimates of extension between the Pintwater Range and the Sheep Range were based on the correlation of the overturned folds in domain II with the Pintwater anticline north of Las Vegas Valley. The folds in domain II are farther from the Wheeler Pass thrust and the Pintwater anticline is closer to the Gass Peak thrust, so estimates of extension based on this alternative correlation are substantially lower. Caskey and Schweickert (1992) and Guth (1981) proposed 24% and 80% extension, respectively, between the Pintwater anticline and the Wheeler Pass thrusts. Their estimates differ in large part because the two papers use different interpretations of the geometry of the Pintwater anticline (see discussion in Caskey and Schweickert, 1992).

In view of the evidence presented in this paper, correlation of the overturned folds in domain II with the Pintwater anticline is highly unlikely. The folds in domain II have a short-wavelength and low amplitude and are confined to the Johnnie Formation. In contrast, the Pintwater anticline is a broad upright fold which involves the entire stratigraphic section (Caskey and Schweickert, 1992). Overturned folds in domain II are almost certainly related to movement on the Kwichup Spring thrust. Correlation of the Kwichup Spring thrust with the Pintwater thrust is a much more straightforward interpretation of structural relationships across Las Vegas Valley.

Implications for Permo-Triassic foreland thrusting in the Cordillera

Both of the Death Valley thrust belt geometries discussed in this paper link Permo-Triassic structures in the Cottonwood Mountains with contractile structures in the Specter Range. In addition, the Lemoigne thrust in the Cottonwood Mountains may correlate with

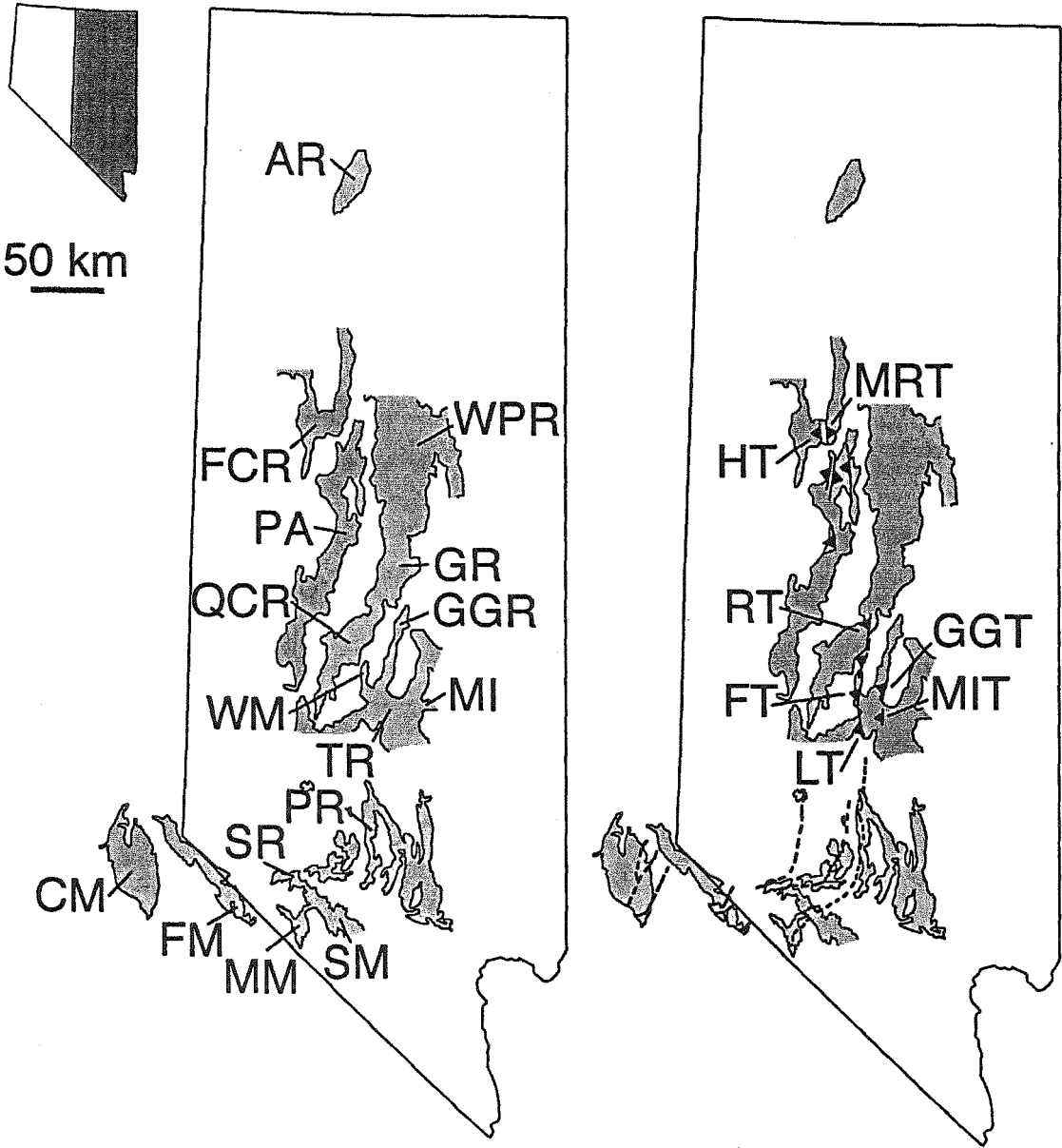
the Kwichup Spring - Montgomery thrust. These thrust correlations require the eastward restoration of the Cottonwood Mountains to a position along the southern projection of the Central Nevada thrust belt of Taylor and others (1993), suggesting that thrusts in the two thrust belts could be related. Contractile structures in the Cottonwood Mountains are of Permo-Triassic age, suggesting that the Central Nevada thrust belt may be at least partially Permo-Triassic.

Cross-cutting relationships constrain the age of contractile structures in the Cottonwood Mountains. The White Top backfold is kinematically related to the Marble Canyon thrust, and is cut by the middle Triassic White Top Stock (Snow and others, 1991). The youngest strata involved in the footwall syncline below the Marble Canyon thrust are middle Permian. The youngest strata deformed by the Lemoigne thrust are also middle Permian and the thrust is overprinted by the contact metamorphic aureole of the middle Jurassic Hunter Mountain batholith (178 Ma U-Pb baddeleyite age; Niemi and Saleeby in Niemi and others, in review). However, a Jurassic age for the Lemoigne thrust is unlikely in view of other geochronologic data from the Death Valley region. The oldest post-Permo-Triassic thrust in the region is the latest Jurassic Pachalka thrust in the Clark Mountains. As a result, the Lemoigne thrust is probably Permo-Triassic.

The largest Permo-Triassic thrust in the Cottonwood Mountains is the Last Chance thrust which may have experienced 50 km of displacement (Snow, 1992). A late Permian turbidite basin in the Darwin Plateau to the southwest of the Cottonwood Mountains may be a marine foredeep associated with emplacement of the allochthon. The allochthon is overlapped by early Triassic strata.

The age of many contractile structures in the Central Nevada thrust belt are poorly constrained, and could be Permo-Triassic. These structures are shown in Figure 4-43, and include the Hoosac and Milk Ranch thrusts in the Fish Creek Range, the Golden Gate thrust in the Golden Gate Range, the Mt. Irish thrust in the Timpahute Range, the Rimrock

Figure 4-43. Contractile structures in the Central Nevada thrust belt of Taylor and others (1993). Ranges and thrusts in southeastern California and southern Nevada are also shown, but thrusts are not labeled. Ranges- CM: Cottonwood Mountains, FM: Funeral Mountains, MM: Montgomery Mountains, SM: Spring Mountains, SR: Specter Range, PR: Pintwater Range, TR: Timpahute Range, WM: Worthington Mountains, MI: Mount Irish, QCR: Quinn Canyon Range, GGR: Golden Gate Range, GR: Grant Range, PA: Pancake Range, FCR: Fish Creek Range, WPR: White Pine Range; Thrusts - LT: Lincoln thrust, MIT: Mt. Irish thrust, FT: Freiberg thrust, GGT: Golden Gate thrust, RT: Rimrock thrust, HT: Hoosac thrust, MRT: Milk Ranch thrust.

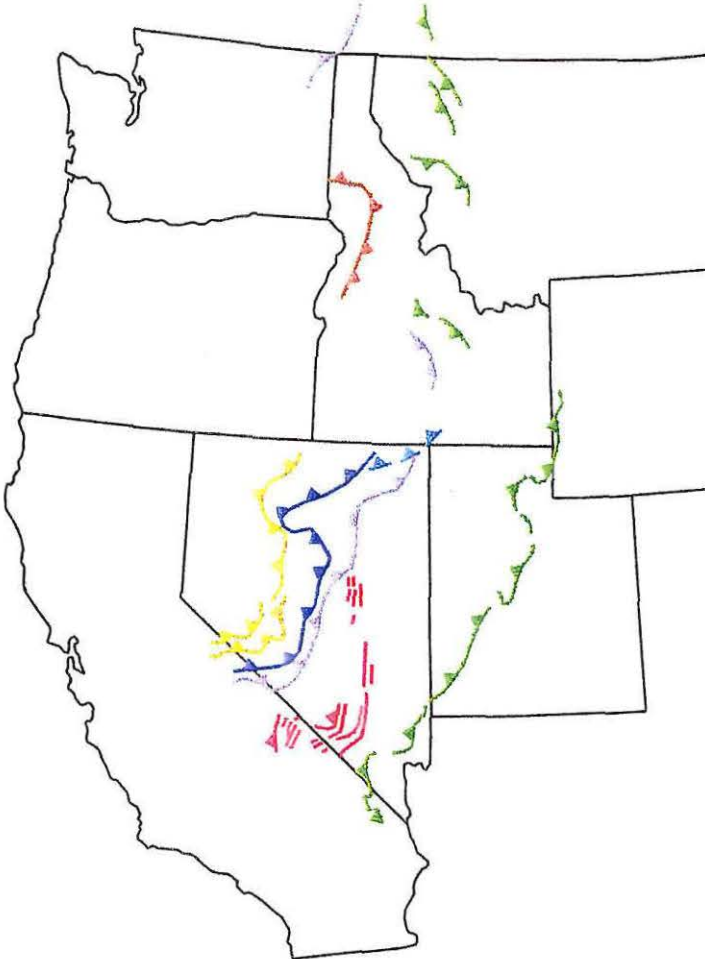


thrust in the Grant Range, and various contractile structures in the White Pine Range, Pancake Range, and the Quinn Canyon Range. The age of all of these structures is loosely constrained to between the Permian and late Cretaceous. The Pennsylvanian-Permian Ely Limestone is folded in the Timpahute Range and the 86.5 ± 4.6 Ma (U-Pb zircon, J.D. Walker unpublished data) Troy granite cuts the Timber Mountain anticline in the central Grant Range (Taylor and others, 1993). In addition, the Milk Ranch and Hoosac thrusts are overlapped by the Albian-Aptian Newark Canyon Formation.

Structurally, these thrusts resemble the Marble Canyon thrust in the Cottonwood Mountains in that they are moderate to steeply dipping ramps (35-55°) with large stratigraphic throws (2-6 km) (Taylor and others, 1993). The west-vergent Milk Ranch thrust (Taylor and others, 1993) resembles west-vergent folds in the Test Site region (Caskey and Schweickert, 1992; Snow and Wernicke, in press), and the White Top backfold in the Cottonwood Mountains (Snow, 1992). Like the Permo-Triassic thrust belt in the Death Valley region, the Central Nevada thrust belt is located immediately east of the late Jurassic to Cretaceous Sevier thrust belt. Stuart and Taylor (1997) showed that, after removing the effects of extension at latitude 38° 25' north, the Central Nevada thrust belt was less than 75 km west of the Sevier belt.

I speculate that the Central Nevada thrust belt is a foreland fold and thrust belt which developed inboard of the Golconda allochthon during emplacement of the allochthon in Permo-Triassic time. Figure 4-44 shows the position of the Central Nevada thrust belt and the Cottonwood Mountains thrusts (in red with the Last Chance thrust in black) and the Golconda allochthon (in blue). Strata deposited in central Nevada during the emplacement of the Golconda allochthon are early Triassic (Speed, 1984), suggesting that emplacement of the allochthon and thrusting in the Cottonwood Mountains are broadly contemporaneous.

Figure 4-44. Position of Permo-Triassic foreland thrusts (red) and Permo-Triassic Last Chance thrust (black) in the context of other major thrusts and thrust belts in the western United States. Major thrusts and thrust belts are adapted from Burchfiel and others (1992) and Taylor and others (1993).



- Lt. J - K eastern limit of Sevier thrust belt
- J - ea. K West Idaho suture zone
- J Elko thrust belt
- J Luning-Fencemaker thrust belt
- P - T_R Permo-Triassic foreland thrust belt
- P - T_R Golconda thrust and equivalents
- M Roberts Mts thrust and equivalents

The Central Nevada thrust belt does not continue into northeastern Nevada. As shown in Figure 4-44, northeastern Nevada contains the Golconda and Roberts Mountains allochthons as well as the Jurassic Elko thrust belt of Thorman and others (1990). The Central Nevada thrust belt appears to terminate against the Roberts Mountains allochthon under alluvium. In this area, strata of Roberts Mountains affinity were probably thrust over the Central Nevada thrust belt long after the close of Permo-Triassic thrusting. For example, in the Adobe Range (location shown on Figure 4-43), a thrust carrying allochthonous strata of Roberts Mountain affinity folds early Cretaceous strata in its footwall. Thrusting contemporaneous with the Jurassic Luning-Fencemaker (gold on Figure 4-44) and Elko (blue on Figure 4-44) thrust belts may also have involved the eastward transport of allochthonous strata.

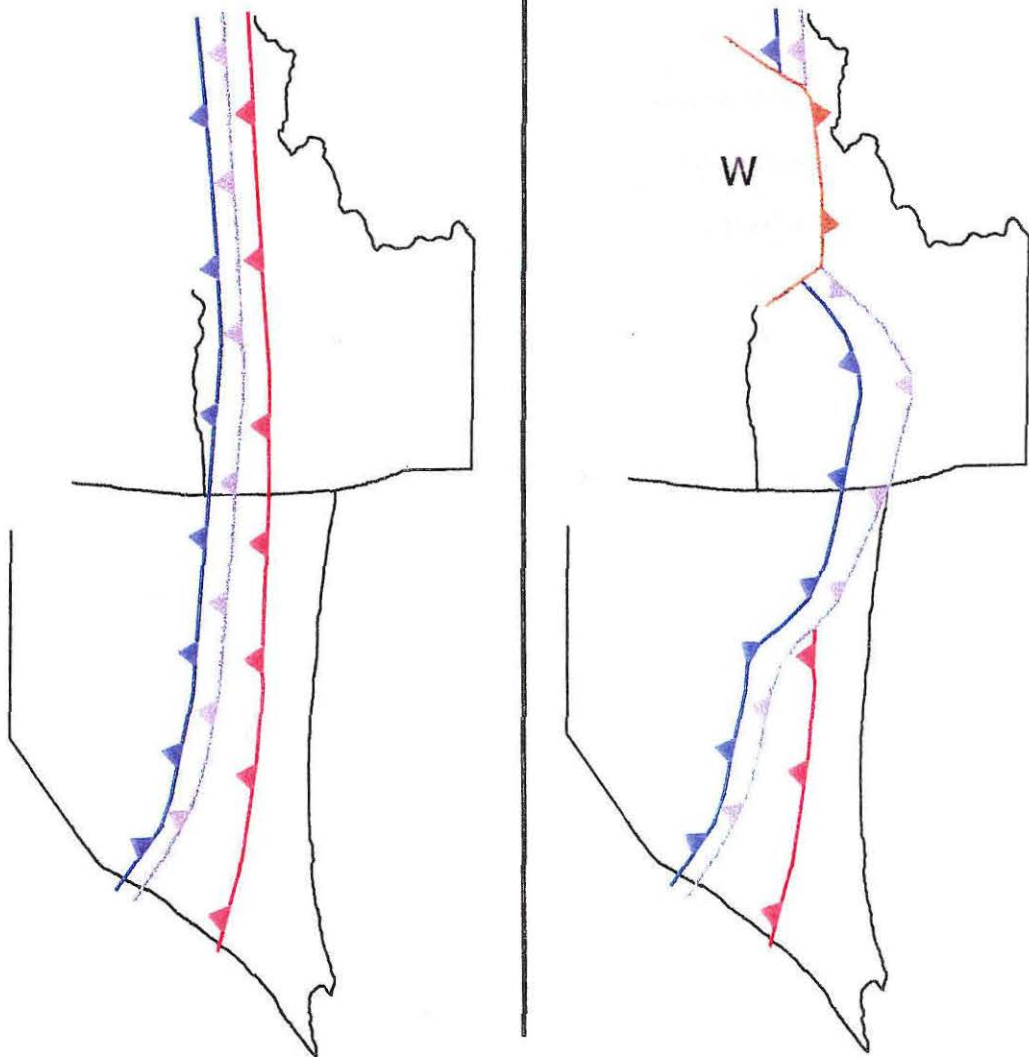
I suggest that the Central Nevada thrust belt was continuous through northeastern Nevada and Idaho at the close of Permo-Triassic thrusting, as shown schematically in Figure 4-45. In northeastern Nevada, the Permo-Triassic thrust belt was overthrust by strata of Robert's Mountains affinity during the Jurassic and/or early Cretaceous. Farther north in Idaho, both allochthons and the Permo-Triassic foreland thrust belt were probably removed along the West Idaho Suture Zone by the emplacement of the allochthonous Wallowa terrane (Wernicke and Klepacki, 1988) during Jurassic or early Cretaceous time (Selverstone and others, 1992).

The interpretation of Permo-Triassic miogeoclinal deformation presented here differs from that of Saleeby and others (1992). They do not interpret the Central Nevada thrust belt as Permo-Triassic and schematically depict the Golconda thrust and Last Chance thrusts as en echelon structures (Figure 2 of Saleeby and others, 1992). They also suggest that Permo-Triassic deformation within the miogeocline was confined to an area in southern Nevada and southeastern California where late Paleozoic truncation of the continental margin resulted in the juxtaposition of subsequent continental margin deformation against

Figure 4-45. Schematic diagram showing the proposed geometry of the Golconda and Roberts Mountains allochthons and the Permo-Triassic foreland thrust belt at the beginning of the middle Triassic and the beginning of the middle Cretaceous. Rough pre-extension palinspastic reconstruction of Nevada and Idaho from Saleeby and others (1992). The allochthonous Wallowa terrane is indicated with a W.

middle Triassic

middle Cretaceous



-  West Idaho suture zone
-  Golconda thrust and equivalents
-  Roberts Mts thrust and equivalents
-  Permo-Triassic foreland thrust belt

the miogeocline. Both the view presented here and that of Saleeby and others (1992) are consistent with known geologic data.

FUTURE WORK

New geologic mapping in central Nevada offers the best hope for resolving the relationship between the Permo-Triassic thrust belt in the Cottonwood Mountains and the Central Nevada thrust belt. This work must distinguish between two possibilities: 1) that the Permo-Triassic thrust belt in the Death Valley region is continuous with the Central Nevada thrust belt, or 2) that the Permo-Triassic thrust belt in the Cottonwood Mountains dies out to the north while the Juro-Cretaceous (?) thrust belt in Central Nevada dies out to the south.

In general, this paper shows that, with the possible exception of the Lemoigne thrust, the Permo-Triassic thrust belt in the Cottonwood Mountains probably continues at least as far north as the Nevada Test Site. In addition, this paper shows that thrust correlations based on general geologic maps from the 1950's, 60's, and 70's should be made with caution. New detailed structural and stratigraphic field studies are critical to our understanding of the Cordilleran thrust belt in areas where it has been heavily overprinted by Neogene tectonism. Field studies are particularly important in areas like central Nevada where geochronologic constraints and critical cross-cutting relationships are scarce.

In particular, new mapping should focus on the lateral continuity of the Central Nevada thrust belt. For example, the Golden Gate thrust in the Golden Gate Range terminates to the north in a fold (Armstrong and Bartley, 1993). Do other contractile structures also terminate along strike in this region, or is the Golden Gate termination an isolated phenomena? Taylor and others (1993) summarized considerable structural work in central Nevada, but their between-range thrust correlations are limited (e.g., correlation of the Golden Gate and Mt. Irish thrusts). Are more comprehensive correlations unwarranted

because of discontinuities within the thrust belt? An overall picture of the thrust belt will only emerge through continued field work in this region.

CONCLUSION

The Stirling Mine thrust and trains of folds in the northwestern Spring Mountains are manifestations of a single once-continuous fault called the Kwichup Spring thrust. The Stirling Mine segment of the Kwichup Spring thrust involves at least 1.4 km of stratigraphic throw. Fold trains in the Johnnie Formation to the west and south of the Stirling Mine fault formed during movement on the Kwichup Spring thrust. Along much of its length, the Kwichup Spring thrust was reactivated or excised by the Diebert normal fault.

Correlation of the Kwichup Spring and Montgomery thrusts is supported by the continuity of stratigraphic units between the northwestern Spring Mountains and the Montgomery Mountains as well as the overall structural similarity between the Stirling Mine and Montgomery thrusts. The correlation of these two thrusts requires modification of the thrust belt reconstructions of Snow (1992) and Snow and Wernicke (in press). However, both modified thrust belt reconstructions presented in this paper still support large (>115 km) west-northwest translation of the Panamint Mountains with respect to the Spring Mountains. Correlation of the Kwichup Spring thrust with the Pintwater thrust north of Las Vegas Valley bolsters claims of large-scale extension in that region as well.

Correlation of Permo-Triassic structures in the Cottonwood Mountains with structures in the northwestern Spring Mountains and Specter Range shows that some contractile structures in central Nevada are probably Permo-Triassic. These structures may constitute a Permo-Triassic foreland thrust belt which developed inboard of the Golconda allochthon during emplacement of the allochthon onto the continental margin.

APPENDIX 4 - A MEASURED SECTIONS

Location S-1

Spring Mountains section, measured along ridge crest 4.7 km northeast of the Johnnie mine, Mt. Schader and Point of Rocks 7.5' quadrangles, sec. 3, T. 17S., R. 53 E.

[Measured by M. J. Abolins, May 1996]

Johnnie Formation

Zju upper member (incomplete) -

15. Siltstone, purple, massive, cross-bedded from 1.25m above base to top of unit; unit capped by orange limestone which is a flat-pebble orange limestone-clast conglomerate in its uppermost part

8.5m

14. Oolitic limestone, tan, upper 20cm is reddish brown and contains pebbles and cobbles of underlying tan oolite

1.4m

Zjm2 middle member unit 2

13. Siltstone, blue gray, fissile

3.2m

12. Siltstone, blue gray, fissile, very thin bedded to medium bedded, parallel laminated; sub-millimeter goethite blebs throughout, cubic goethite pseudomorphs after pyrite are up to 2mm in places

34m

11. Quartzite, very light gray

1m

10. Siltstone, gray and brown, fissile, finely laminated

20.5m

9. Quartzite, very light gray, medium to coarse grained at base, coarse at top, sub-rounded grains, bedding obscure (thick bedded or massive); millimeter goethite blebs;

28.5m

8. Siltstone and minor sandstone; siltstone, brown, coarse, fissile and laminated in places; sandstone, very fine, 20 cm beds; unit poorly exposed

55m

7. Quartzite, very light gray, fine grained, contains goethite blebs;

13.5m

6. Mostly covered; in part, siltstone, gray, fissile, finely laminated; unit recessive

8.5m

5. Quartzite, gray

	6m
4. Mostly covered; in part, siltstone, brown, fissile; unit recessive	
	13.5m
3. Dolomitic sandstone and quartzite, dolomitic sandstone in one meter beds; quartzite, fine, 2.5m at base of unit	
	6m
2. Dolostone, gray, much of it oolitic	
	30m
1. Mostly covered; at top, siltstone, gray and reddish brown, phyllitic; at base, siltstone, brown, phyllitic	
	12m
Total of Zjm2 _____	231.7m

Location S-2

*Johnnie Wash section, measured along ridge crest 2.8 km east-northeast
of the Johnnie mine, Mt. Schader 7.5' quadrangle,
southeastern quarter sec. 16, northeastern quarter sec. 21, T. 17S., R. 53 E.*

[Measured by M. J. Abolins, April 1996]

Stirling Quartzite

A member (incomplete) -

2. Quartzite; pink-purple; medium grained; grains sub-rounded;
occasional black and red chert pebbles; thin bedded

Unmeasured

1. Quartzite; very light gray; finely crystalline; massive

28.5m

Johnnie Formation

Zju upper member (incomplete) -

22. Phyllitic siltstone; light green to tan brown
becoming more gray down-section; coarse;
very thin to thin bedded; breaks apart in slabs;
Unit contains at least one 20cm+ bed
of tan medium grained sandy limestone-clast
flat-pebble conglomerate about 40m above base;
upper 16.5m are largely buried by Stirling talus;
contact with Stirling not observed

82.5m

21. Siltstone and minor limestone;
Siltstone, purple; top of unit is a flat-pebble
limestone-clast conglomerate;
base of unit is 1.5m of parallel laminated siltstone;
thickness of individual limestone beds decreases
up-section from 40cm near base to 10cm near top;

sandy limestone beds near top of unit are clearly limestone-clast flat-pebble conglomerates	<i>22m</i>
20. Siltstone and minor quartzite; siltstone, blue gray, very thin bedded, possible rain drops; quartzite, gray, fine grained 5-30cm beds, largely in upper part of unit; 80 cm of parallel laminated fine purple-brown quartzite at base	<i>30m</i>
19. Siltstone and minor limestone; Siltstone, purple; sandy limestone-clast flat-pebble conglomerate in upper 55m of unit; only intact limestone beds in the lower 35m	<i>90m</i>
18. Siltstone, purple, massive, parallel laminated	<i>15.5m</i>
17. Oolitic limestone, coarsens upward; tan, upper 30cm is reddish brown and contains cobbles of underlying tan oolite	<i>2.2m</i>
Total of upper member _____	<i>242.2m</i>

Zjm2 middle member unit 2

16. Siltstone, blue gray, fissile	<i>3.2m</i>
15. Siltstone and minor quartzite; siltstone, brown, fissile, poorly exposed	<i>60m</i>
14. Quartzite, very light gray, fine, contains goethite blebs; unit may include some siltstone; poorly exposed	<i>16.5m</i>
13. Siltstone, brown, poorly exposed	<i>16.5m</i>
12. Siltstone, blue gray and brown; at least one 30cm dark brown gray dolostone bed 9m above base of unit; poorly exposed	<i>75m</i>
11. Quartzite, fine grained, very thin bedded; contains goethite blebs; fissile gray siltstone in uppermost meter of unit	<i>15m</i>
10. Siltstone, tan, parts irregularly (not phyllitic)	<i>3.5m</i>
9. Quartzite, medium to coarse grained; very thin bedded	<i>3m</i>
8. Dolostone, gray and in places reddish brown, coarsely crystalline, oolitic at base, thick bedded	<i>6.5m</i>
7. Quartzite and dolomitic sandstone, fine to medium grained, dolomitic in upper .5m	

6. Dolostone, tan, fine grained, bedding indistinct	3m
5. Dolostone, gray, coarse, massive	3m
4. Oolitic dolostone, reddish brown, coarse (some ooids larger than 1mm)	5.3m
3. Dolomitic sandstone and minor sandstone, dark tan to chocolate, sandstone layers up to 5cm thick, thin dark resistant lamina spaced .5 to 1cm apart	.7m
2. Quartzite and siltstone, coarsens upward from siltstone at base to fine quartzite at top, thin bedded	3m
1. Siltstone, phyllitic, tan, brown, white, and reddish brown; poorly exposed	1.5m
	22.5m
Total of Zjm2 _____	238.2m

Location S-3

*Hill 1268 section, measured in wash and along ridge crest south of 958T,
Point of Rocks 7.5' quadrangle, southeastern quarter sec. 25,
northeastern quarter sec. 36, T. 16S., R. 52 E.*

[Measured by M. J. Abolins, April 1996]

Johnnie Formation

Zju upper member -

25. Siltstone and minor limestone-clast flat-pebble conglomerate; siltstone blue-purple; poorly exposed	165m
24. Siltstone and minor limestone-clast flat-pebble conglomerate; siltstone, purple;	30m
23. Siltstone and minor limestone-clast flat-pebble conglomerate; siltstone, purple;	45m
22. Siltstone, purple; capped by 30cm orange pink-purple limestone, weathers tan, parallel laminated at base	9m
21. Oolitic limestone, 1mm ooids, 3cm reddish brown top	1.5m
Total of upper member _____	250.5m

Zjm2 middle member unit 2

20. Mostly covered; siltstone, dolomitic sandstone, and quartzite; blue siltstone in uppermost part of unit	63m
19. Quartzite, capped by 20cm tan dolostone; base of unit poorly exposed	15m
18. Siltstone, poorly exposed	3m
17. Dolostone and siltstone, interbedded dolostone and siltstone, dolostone beds each 50cm thick; unit capped by 50cm dolomitic sandstone; 1.25m of siltstone at base	7.25m
16. Siltstone capped by 50cm tan dolostone	4.75m
15. Siltstone and minor quartzite; siltstone, blue and tan, quartzite in 1m beds	52m
14. Dolostone, tan-olive, individual beds indistinct	2m
13. Quartzite, very light gray, coarse grained, cross bedded, thin bedded; goethite blebs	12m
12. Covered, recessive; siltstone?	25.5m
11. Dolostone, quartzite, and dolomitic sandstone; dolostone, tan and olive, 50cm beds; 5-10cm quartzite interbeds; 75cm of dolomitic sandstone at base and in a bed 4m above base	6m
10. Siltstone, poorly exposed	7.5m
Total of Zjm2 _____	198m

Zjm1 middle member unit 1 -

9. Quartzite and minor siltstone; quartzite fine to medium grained, laminated in places, goethite blebs; 20cm tan dolostone 47.5m above base; 15cm tan dolostone 66.5m above base	158m
8. Quartzite and siltstone; quartzite very fine, beds up to 75cm; thickly laminated; siltstone, coarse, fissile, in places reddish brown; goethite blebs	44m
7. Siltstone, 35cm very fine quartzite with goethite blebs 7.5m above base	

	<i>21m</i>
6. Siltstone, capped by 50cm of olive brown to light gray dolostone resting on 30cm of very fine sandstone	
	<i>6m</i>
5. Dolostone and sandy dolostone; from top to bottom: 1m of maroon and olive dolostone, 25cm of darkly varnished sandy dolostone, 25cm of maroon and olive dolostone 1m of sandy dolostone in 5-10cm beds; very fine sandstone	
	<i>2.5m</i>
4. Siltstone and quartzite; siltstone, fissile, white and maroon, goethite blebs; interbedded quartzite, very fine, with goethite blebs; prominent indurated 40cm coarse siltstone at base	
	<i>20m</i>
3. Siltstone, tan, coarse grained, .5cm partings	
	<i>10m</i>
2. Covered, recessive; siltstone?; 25cm tan and brown-gray dolostone at top, thickly laminated in places	
	<i>19m</i>
1. Dolostone, olive gray and tan, dark gray when fresh, finely crystalline, a few 1-5cm chert layers	
	<i>~13m</i>
Total of Zjm1 _____	<i>293.5m</i>

Location S-4

*Hill 1066 section, measured on south and southeast flank of 1066,
Point of Rocks 7.5' quadrangle, western half sec. 31, T. 16S., R. 53 E.*

[Measured by M. J. Abolins, April 1996]

Johnnie Formation

Zju upper member -

22. Grayish orange oolitic limestone
with 5cm maroon bed at top; finer at base
with .5cm pellets

1.6m

Zjm2 middle member unit 2

21. Purple-blue siltstone

3m

20. Green relatively resistant siltstone with some

maroon and white siltstone at top; quartzite has 1-2cm partings in places; cross-laminated in places	<i>27m</i>
19. Fine quartzite and dolomitic sandstone	<i>24m</i>
18. Dolomitic sandstone and light bluish gray siltstone	<i>3m</i>
17. Fine quartzite with mm-scale cross laminations; "knobby" appearance; blue-gray color; sub-mm goethite blebs	<i>4.5m</i>
16. Tan and maroon fissile siltstone; may be much thinner than measured here; brown and occasionally very light gray	<i>7.5m</i>
15. Blue-gray fine quartzite	<i>14.5m</i>
14. Blue fissile siltstone	<i>4.5m</i>
13. Maroon and very light gray fissile siltstone with some army green siltstone in middle	<i>7.5m</i>
12. Maroon and very light gray fissile siltstone with some brown fine quartzite in middle	<i>9m</i>
11. Blue gray fine quartzite with 15cm dolomitic sandstone layers	<i>2.5m</i>
10. Florescent green fissile siltstone	<i>3m</i>
9. Very light gray and maroon fissile siltstone	<i>15m</i>
8. Olive green-gray dolostone; ~75cm beds with cherty and fissile silty partings	<i>4.5m</i>
7. Olive green siltstone; fissile in places but also in 20-50cm beds; 50cm dolomitic sandstone with "swiss cheese" appearance (1cm spots) 3m below top; dolomitic sandstone underlain by at least 1m of maroon and white siltstone	<i>15m</i>
6. Tan to olive dolostone; bedding indistinct; cherty or sandy partings; dolostone overlain by 30cm dolomitic sandstone	<i>3m</i>
5. Very light gray and maroon fissile siltstone	

with abundant sub-mm goethite blebs at top of unit; 15cm orange-brown dolostone 6.5m above base of unit	25m
4. Fine quartzite	6m
3. Tan and olive gray dolostone in 30-50cm beds with 3mm laminations	4.5m
2. Very light gray siltstone; stained maroon in places; sub-mm goethite blebs	3.5m
Total of Zjm2 _____	186.5m

Zjm1 middle member unit 1 (incomplete) -

1. Poorly exposed interval; probably mostly fine sandstone with some siltstone and fine quartzite at top; 1cm goethite blobs impart "swiss cheese" appearance to some of the cleaner quartzite; 30cm dolomitic sandstone with black resistant lamina 5.5m above base; 30cm tan dolostone 6.5m above base	35m
--	-----

Location S-5

*Hill 4057 section, measured along ridge crest west of 4057,
Mt. Schader 7.5' quadrangle, southern half sec. 6 ,
northern half sec. 7, T. 17S., R. 53 E.*

[Measured by M. J. Abolins, April 1996]

Johnnie Formation

Zju upper member (incomplete) -

15. Grayish orange oolitic limestone;	1.5m
---------------------------------------	------

Zjm2 middle member unit 2

14. Light bluish gray silty fine sandstone; fissile in part but also blocky; also, very light gray fissile siltstone with maroon and purple staining siltstone, purple; 30cm of dark brown dolomitic fine sandstone with dark resistant lamina as wide as 1cm about 30cm about 50cm below top; ~10cm layer of dolomitic sandstone at top; light bluish gray siltstone separates the two dolomitic sandstones	26m
13. Fine quartzite and, in places, coarse fine quartzite;	

quartzite has 1-2cm partings in places; cross-laminated in places	10.5m
12. Siltstone and fine quartzite	3m
11. White and maroon fissile siltstone	4.8m
10. Fine quartzite with goethite blebs; 1-2cm partings	16.5m
9. Poorly exposed recessive fissile siltstone; may be much thinner than measured here; brown and occasionally very light gray	65.5m
8. At least 4 beds of dolostone separated by silty intervals; beds up to 75cm thick; lowest bed ~10cm thick; dolostone contains quartz veins and possibly some chert; dolostone laminated on the cm-scale in places	6m
7. Siltstone with 30cm of dolomitic sandstone 3.5 m above base	6m
6. Fine quartzite with 1-2cm partings	22.5m
5. Brown and light bluish gray siltstone and fine quartzite; poorly exposed	21m
4. Tan to tan-gray dolostone	1.5m
3. Tan fissile siltstone	43.5m
2. Brown and olive gray dolostone; contains sandy layers and brown laminations; individual beds 10-40cm	1.5m
Total of Zjm2 _____	228.3m
1. Quartzite	<i>unmeasured</i>

Location S-6

*Hill 3231 section, measured along ridge crest east of 3231,
Mt. Schader 7.5' quadrangle, southeast quarter sec. 12 ,
T. 17S., R. 52 E.*

[Measured by M. J. Abolins, April 1996]

Johnnie Formation

Zju upper member (incomplete)

22. Grayish orange oolitic limestone; finer at base than at top

1.6m

Zjm2 middle member unit 2 (incomplete) -

21. Very light gray fissile siltstone; stained maroon and tan in places; blue gray siltstone NOT present immediately under oolite; 1-2mm goethite blebs common

15.5m

20. Gray-green fissile siltstone with 10-30cm parallel laminated siltstone beds

9m

19. Poorly exposed brown, maroon, very light gray, and purple varicolored siltstone; fissile

14m

18. Dirty brown dolomitic sandstone and light bluish gray quartzose siltstone; light bluish gray siltstone parting on cm-scale; dolomitic sandstone in 10-30cm beds; dolomitic sandstone is quartzose at base in places

14m

17. Purple siltstone with goethite blebs and fine quartzite with goethite blebs; quartzite has .5cm-scale laminations

13m

16. Fissile siltstone with a 20cm thick fine quartzite layer near the middle

7.5m

15. Quartzite, laminated fine to medium with pinkish color; sub-rounded grains

18m

14. Fine quartzite and siltstone with fissile very light gray and yellow siltstone at top

26m

13. Siltstone and possibly some fine quartzite

15m

12. Light gray to orange gray dolostone; possibly in two beds of about equal thickness; cherty laminations near top of lower bed	<i>2.5m</i>
11. Poorly exposed and recessive; siltstone and fine quartzite?	<i>5.5m</i>
10. Tan fissile siltstone	<i>43.5m</i>
9. Darkly varnished sandy dolostone with "knobby" appearance; capped by 50 cm of tan dolostone	<i>1.5m</i>
8. Fissile siltstone with 10-30 cm interbeds of fine quartzite in middle of unit	<i>10.5m</i>
7. Fine quartzite with goethite pseudomorphs; cross-laminated in upper part	<i>16.5m</i>
6. Very fine quartzite; very light gray when fresh; numerous sub-mm goethite pseudomorphs; 1-10cm partings	<i>11.5m</i>
5. Fine quartzite with sub-mm goethite blebs; cm-scale laminations in part	<i>1.5m</i>
4. Recessive and poorly-exposed; float indicates very light gray and very fine siltstone; at top, siltstone with sub-mm goethite blebs in cm-scale beds thickening upsection to dm-scale	<i>15m</i>
3. Light gray, tan, and orange-brown dolostone bedding difficult to discern (if present at all); dark gray and finely crystalline when fresh	<i>3.5m</i>
2. Recessive and poorly-exposed; based on float, probably very light gray fissile very fine siltstone or mudstone; stained orange in places	<i>27m</i>
1. Olive gray and tan dolostone in 30cm beds; dark gray fine crystalline appearance on fresh surface; underlain by a few cm of tan dolomitic siltstone	<i>4m</i>
Total of Zjm2 _____	<i>274.5m</i>

REFERENCES

- Armstrong, Phillip A., and Bartley, John M., 1993, Displacement and deformation associated with a lateral thrust termination, southern Golden Gate Range, southern Nevada, U.S.A.: *Journal of Structural Geology*, v. 15, no. 6, p. 721-735.
- Allmendinger, Richard W., 1992, Fold and thrust tectonics of the Western United States exclusive of the accreted terranes, *in* Burchfiel, B. C., Lipman, P. W., and Zoback, M. L., ed., *The Cordilleran Orogen; conterminous U.S.*, p. 583-607.
- Buck, W. Roger, 1988, Flexural rotation of normal faults, *Tectonics*, v. 7, no. 5, p. 959-973.
- Burchfiel, B. C., 1965, Structural geology of the Spector Range Quadrangle, Nevada, and its regional significance: *Geological Society of America Bulletin*, v. 76, no. 2, p. 175-191.
- Burchfiel, B. C., Fleck, R. J., Secor, D. T., Vincelette, R. R., and Davis, G. A., 1974, Geology of the Spring Mountains, Nevada: *Geological Society of America Bulletin*, v. 85, no. 7, p. 1013-1022.
- Burchfiel, B.C., Hamill IV, G.S., and Wilhelms, D.E., 1983, Structural geology of the Montgomery Mountains, and the northern half of the Nopah and Resting Spring Ranges, Nevada and California: *Geological Society of America Bulletin*, v. 94, no. 11, p. 1359-1376.

Burchfiel, B. Clark, Cowan, Darrel S., and Davis, Gregory A., 1992, Tectonic overview of the Cordilleran Orogen in the Western United States, *in* Burchfiel, B. C., Lipman, P. W., and Zoback, M. L., ed., *The Cordilleran Orogen; conterminous U.S.*, p. 407-479.

Caskey, S. John, and Schweickert, Richard A., 1992, Mesozoic deformation in the Nevada Test Site and vicinity; implications for the structural framework of the Cordilleran fold and thrust belt and Tertiary extension north of Las Vegas Valley: *Tectonics*, v. 11, no 6, p. 1314-1331.

Cemen, Ibrahim, Wright, L. A., Drake, R. E., and Johnson, F. C., Cenozoic sedimentation and sequence of deformational events at the southeastern end of Furnace Creek strike-slip fault-zone, Death Valley region, California, *in* Biddle, Kevin T., and Christie-Blick, Nicholas, eds., *Strike-slip deformation, basin formation, and sedimentation: Society of Economic Paleontologists and Mineralogists Special Publication*, v. 37, p. 127-139.

Cemen, Ibrahim, and Wright, Lauren A., 1990, Effect of Cenozoic extension on Mesozoic thrust surfaces in the central and southern Funeral Mountains, Death Valley, California, *in* Wernicke, Brian P., ed., *Basin and Range extensional tectonics near the latitude of Las Vegas, Nevada: Geological Society of America Memoir 176*, p. 305-316.

Cornwall, Henry R., 1972, *Geology and mineral deposits of southern Nye County, Nevada: Nevada Bureau of Mines and Geology Bulletin*, v. 77, 45 p.

Dickinson, William R., and Wernicke, Brian P., 1997, Reconciliation of San Andreas slip discrepancy by a combination of interior Basin and Range extension and transrotation near the coast: *Geology*, v. 25, no. 7, p. 663-665.

Elliott, D., 1976, The energy balance and deformation mechanisms of thrust sheets: *Philosophical Transactions of the Royal Society of London, Series A; Mathematical and Physical Sciences*, v. 283, no. 1312, p. 289-312.

Guth, Peter L., 1981, Tertiary extension north of the Las Vegas Valley shear zone, Sheep and Desert ranges, Clark County, Nevada, *Geological Society of America Bulletin*, v. 92, no. 10, p. I 763-I 771.

Guth, Peter L., 1990, Superposed Mesozoic and Cenozoic deformation, Indian Springs Quadrangle, southern Nevada, *in* Wernicke, Brian P., ed., *Basin and Range extensional tectonics near the latitude of Las Vegas, Nevada: Geological Society of America Memoir*, v. 176, p. 237-249.

Hodges, K. V., Walker, J. D., and Wernicke, Brian P., 1987, Footwall structural evolution of the Tucki Mountain detachment system, Death Valley region, southeastern California, *in* Coward, M. P., Dewey, J. F., and Hancock, P. L., ed., *Continental extensional tectonics, Geological Society Special Publication 28*, p. 393-408.

Holm, Daniel K., Fleck, Robert J., and Lux, Daniel R., 1994, The Death Valley turtlebacks reinterpreted as Miocene-Pliocene folds of a major detachment surface: *Journal of Geology*, v. 102, no. 6, p. 718-727.

Holm, Daniel K., and Wernicke, Brian P., 1990, Black Mountains crustal section, Death Valley extended terrain, California: *Geology*, v. 18, no. 6, p. 520-523.

Ketner, Keith B., 1987, Post-Early Triassic, pre-middle Eocene folds and thrust faults, northern Adobe Range, Nevada, *in* Hill, Mason L., ed., *Cordilleran Section of the Geological Society of America Centennial Field Guide*, v. 1, p. 91-94.

Mancktelow, Neil S., and Pavlis, Terry L., 1994, Fold-fault relationships in low-angle detachment systems: *Tectonics*, v. 13, no. 3, p. 668-685.

Niemi, N.A., Wernicke, B.P., Brady, R.J., Saleeby, J.B., and Dunne, G.C., in review, Distribution and provenance of the middle Miocene Eagle Mountain Formation, and implications for the tectonic development of the Death Valley extended terrane, California: *Geological Society of America Bulletin*.

Ramsay, John G., Casey, Martin, and Kligfield, Roy, 1983, Role of shear in development of the Helvetic fold-thrust belt of Switzerland: *Geology*, v. 11, no. 8, p. 439-442.

Rowan, Mark G., and Kligfield, Roy, 1992, Kinematics of large-scale asymmetric buckle folds in overthrust shear; an example from the Helvetic nappes, *in* McClay, K. R., ed., *Thrust tectonics*, p. 165-173.

Saleeby, Jason B., Busby-Spera, Cathy, Oldow, J. S., Dunne, G. C., Wright, J. E., Cowan, D. S., Walker, N., 1992, Early Mesozoic tectonic evolution of the Western U.S. Cordillera, *in* Burchfiel, B. C., Lipman, P. W., and Zoback, M. L., ed., *The Cordilleran Orogen; conterminous U.S.*, p. 107-168.

Sanderson, D. J., 1979, The transition from upright to recumbent folding in the Variscan fold belt of Southwest England; a model based on the kinematics of simple shear: *Journal of Structural Geology*, v. 1, no. 3, p. 171-180.

Selverstone, Jane, Wernicke, Brian P., and Aliberti, Elaine A., 1992, Intracontinental subduction and hinged unroofing along the Salmon River suture zone, west central Idaho, *Tectonics*, v. 11, no. 1, p. 124-144.

Snow, J. Kent, Asmerom, Yemane, and Lux, Daniel R., 1991, Permian-Triassic plutonism and tectonics; Death Valley region, California and Nevada: *Geology*, v. 19, no. 6, p. 629-632.

Snow, J. Kent, 1992, Large-magnitude Permian shortening and continental margin tectonics in the southern Cordillera: *Geological Society of America Bulletin*, v. 104, no. 1, p. 80-105.

Snow, J.K., Geissman, J.W., and Wernicke, B., 1993, Paleomagnetic data from Paleozoic sedimentary rocks and Permo-Triassic intrusions, Death Valley area southeast CA; Implications for Mesozoic and Cenozoic deformation, *Eos*, v. 74, p. 206.

Snow, J. Kent, and Wernicke, Brian P., 1989, Uniqueness of geological correlations; an example from the Death Valley extended terrain: *Geological Society of America Bulletin*, v. 101, no. 11, p. 1351-1362.

- Snow, J. K., and Wernicke, B., 1994, Crustal mass balance in Central Basin and Range; geological constraints, *Eos*, v. 75, no. 44, p. 583.
- Snow, J. Kent, and Wernicke, Brian P., in press, Cenozoic tectonism in the central Basin and Range: magnitude, rate, and distribution of upper crustal strain: *American Journal of Science*.
- Speed, Robert C., 1984, Paleozoic and Mesozoic continental margin collision zone features; Mina to Candelaria, Nevada, traverse; (field trip 6), *in* Lintz, Joseph Jr., ed., *Western geological excursions*, v. 4, p. 66-80.
- Stevens, Calvin H., Stone, Paul, and Belasky, Paul, 1991, Paleogeographic and structural significance of an Upper Mississippian facies boundary in southern Nevada and east-central California: *Geological Society of America Bulletin*, v. 103, no. 7, p. 876-885.
- Stewart, John H., 1970, Upper Precambrian and Lower Cambrian strata in the southern Great Basin, California and Nevada: *U. S. Geological Survey Professional Paper 620*, 206 p.
- Stewart, J. H., 1978, Basin-range structure in western North America; a review, *in* Smith, R. B., and Eaton, G. P., ed., *Cenozoic tectonics and regional geophysics of the Western Cordillera: Geological Society of America Memoir 152*, p. 1-31.
- Stuart, Maureen A., and Taylor, Wanda J., 1997, Fragmentation of the Mesozoic Sevier orogenic belt, Utah by large-magnitude Cenozoic extension: *Geological Society of America Abstracts*, v. 29, no. 5, p. 67-68.

Summa, Catherine L., 1993, Sedimentologic, stratigraphic, and tectonic controls of a mixed carbonate-siliciclastic succession; Neoproterozoic Johnnie Formation, Southeast California, unpublished doctoral dissertation: Massachusetts Institute of Technology.

Taylor, Wanda J., Bartley, John M., Fryxell, Joan E., Schmitt, James G., and Vandervoort, Dirk S., 1993, Tectonic style and regional relations of the central Nevada thrust belt, *in* Lahren, Mary M., Trexler, James H., Jr., and Spinoso, Claude, ed., *Crustal evolution of the Great Basin and the Sierra Nevada*, p. 57-96.

Thorman, C. H., Ketner, K. B., and Peterson, Fred, 1990, The Elko Orogeny; Late Jurassic orogenesis in the Cordilleran Miogeocline: *Geological Society of America Abstracts*, v. 22, no. 3, p. 88.

Wernicke, Brian P., and Axen, Gary J., 1988, On the role of isostasy in the evolution of normal fault systems: *Geology*, v. 16, no. 9, p. 848-851.

Wernicke, Brian, Axen, Gary J., and Snow, J. Kent, 1988, Basin and Range extensional tectonics at the latitude of Las Vegas, Nevada: *Geological Society of America Bulletin*, v. 100, no. 11, p. 1738-1757.

Wernicke, Brian P., and Klepacki, David W., 1988, Escape hypothesis for the Stikine Block: *Geology*, v. 16, no. 5, p. 461-464.

Wernicke, Brian, Snow, J. Kent, Hodges, Kip V., and Walker, J. Douglas, 1993, Structural constraints on Neogene tectonism in the southern Great Basin, *in* Lahren,

Mary M., Trexler, James H., Jr., and Spinosa, Claude, ed., Crustal evolution of the Great Basin and the Sierra Nevada, p. 453-479.

Wright, L. A., and Troxel, B. W., 1973, Shallow-Fault Interpretation of Basin and Range Structure, Southwestern Great Basin, *in* de Jong, K.A., and Scholten, R., eds., Gravity and Tectonics: New York, John Wiley and Sons, p. 397-407.

Zigler, Jan L., and Simonds, F. William, 1992, A preliminary evaluation of the Point of Rocks fault, *in* Characterization of detachment faults in the Yucca Mountain region, U.S. Geological Survey Administrative Report 3GTD500M.